Role of the RNase E in the diversification and survival of mycobacteria

Anna Griego

Université de Paris

École doctorale BioSPC 562

Laboratoire Institut Pasteur - Groupe à 5 ans Individualité Microbienne et Infection

Role of the RNase E in the diversification and survival of mycobacteria

Par Anna Griego

Thèse de doctorat de Microbiologie

Dirigée par Dr Giulia Manina

Présentée et soutenue publiquement le 15/01/2021

Devant un jury composé de :

Rapporteurs:	Prof Papenfort Kai, Institute of General Microbiology, Jena, Germany
	Dr Grangeasse Christophe, Université de Lyon, France
Examinateurs :	Prof De Reuse Hilde, Institut Pasteur, Paris, France
	Prof Gomes De Pinho Mariana, Universidade NOVA de Lisboa, Portugal
Directeur de thèse :	Dr Manina Giulia, Institut Pasteur, Paris, France

Université de Paris

LISTE DES ÉLÉMENTS SOUS DROITS

Liste de **tous les éléments retirés** de la version complète de la thèse
faute d'en détenir les droits

Document à intégrer dans la version partielle de la thèse

Illustrations, figures, images...

Légende de l'image	N° de l'image	Page(s) dans la thèse
Estimated TB incidence in 2018	Figure 1	4
Estimated incidence of MDR/RR-TB in 2018	Figure 2	5
Circular map of the chromosome of *M. tuberculosis* H37Rv	Figure 3	13
Model of the mycobacterial cell envelope	Figure 4	17
Regulatory small RNAs (sRNAs) and their function	Figure 5	23
The life cycle of *M. tuberculosis*	Figure 6	27
Schematic representation of the TB granuloma	Figure 7	32
Biphasic killing kinetics of a clonal population containing persisters	Figure 8	55
Toxin Antitoxin (TA) modules promote persister formation in *E. coli* K12	Figure 9	63
Empiric measurement of the magnitude of noise in gene expression	Figure/Equation 1	71
Empirical quantification of the total noise (η_{tot})	Figure/Equation 2	73
The spatial organization of gene expression in bacteria	Figure 10	83
Three nonexclusive models explaining gene expression	Figure 11	84
Diverse localization of RNA within a bacterial cell	Figure 12	85

Schematic summary of known ribonucleases and their function	Figure 13	93
Structure of the RNase E in *E. coli*	Figure 14	102
RNase E pathways of substrate recognition	Figure 15	109
Sequence of the RNase E promoter	Figure 16	111
Secondary structure of the RNase E 5'UTR	Figure 17	113
Model of rRNAs precursors in *M. smegmatis*	Figure 19	123

Rôle de la RNase E dans la diversification et la survie des mycobactéries

Mycobacterium tuberculosis est un pathogène aéroporté à croissance lente et l'agent causal de la tuberculose (TB). En raison de sa grave implication sociale et du nombre de victimes revendiquées, *M. tuberculosis* demeure l'un des agents pathogènes microbiens les plus meurtriers de l'histoire humaine. L'infection à *M. tuberculosis* commence lorsqu'un individu non infecté inhale une gouttelette contenant les bacilles, atteignant les voies respiratoires inférieures. Bien que le *M. tuberculosis* puisse se propager dans différentes niches à l'intérieur de l'hôte (c.-à-d. plèvre, ganglion lymphatique, foie, rate, os et articulations, cœur, cerveau, système génito-urinaire, méningis, péritoine et peau), les poumons représentent le site principal de infections. Dans 95% des cas, l'infection à *M. tuberculosis* établit avec succès une primo-infection, soit éliminée par la poussée de l'immunité à médiation cellulaire, soit contenue à l'intérieur du granulome, la caractéristique de la tuberculose. Cette dernière cause une forme de tuberculose asymptomatique de longue durée, également connue sous le nom de tuberculose latente (ITL). Actuellement, la meilleure estimation suggère qu'environ un quart de la population mondiale est porteuse de la LTBI, qui se caractérise par la présence de bacilles persistants et vivants chez l'hôte. La tuberculose active survient soit en raison de l'incapacité du système immunitaire de l'hôte à éliminer l'infection primaire, soit à la suite de la réactivation de l'infection latente. La tuberculose présente un large spectre de formes cliniques et subcliniques, dans lesquelles les formes actives et latentes représentent les deux extrêmes de l'infection. La progression vers la tuberculose active délimite la formation de cavités à proximité des espaces des voies respiratoires permet l'excrétion (c'est-à-dire la toux) des bacilles par les voies respiratoires, une étape de transmission. Par la suite, de manière cyclique, les bacilles de la tuberculose sont transmis à d'autres individus pour établir une primo-infection (M. Pai et al., 2016). Les bacilles tuberculeux peuvent survivre chez l'homme pendant de longues périodes, et les outils diagnostiques et thérapeutiques à notre disposition sont encore sous-optimaux. Ceci est principalement dû au fait que la population de *M. tuberculosis* est hétérogène et peut se diversifier davantage au sein de l'infection et du traitement. Cette hétérogénéité phénotypique donne lieu à des sous-populations plus susceptibles de persister chez l'hôte humain, difficiles à détecter et à traiter. Bien que les mécanismes sous-jacents à la variation phénotypique restent insaisissables, l'accumulation d'observations expérimentales démontre que cette diversité de cellule à cellule dans l'expression génique pourrait aider les mycobactéries à supporter l'environnement hostile difficile. Il est bien établi que les différences phénotypiques unicellulaires dans le taux de croissance et l'état métabolique peuvent influencer la décision de devenir de la bactérie dans des conditions stressantes (Dhar et al., 2016). Parmi le

mécanisme putatif influençant la variation phénotypique de cellule à cellule, nous émettons l'hypothèse que l'influence du renouvellement de l'ARN dans la variation de l'expression génique pourrait représenter l'un des les principales sources de diversification phénotypique bactérienne (Baudrimont et al., 2019; Eldar & Elowitz, 2010). La désintégration de l'ARN dépend principalement de l'activité des ribonucléases (RNases).

Les bactéries Gram-positives et négatives possèdent divers mécanismes de dégradation de l'ARN, en fonction des RNases présentes dans le micro-organisme et de leur interaction avec d'autres partenaires moléculaires (Durand et al., 2015). L'un des exemples les plus significatifs est le complexe multi-enzymatique de dégradosome d'ARN, découvert initialement dans *E. coli* (Mackie, 2013). La RNase E est l'enzyme de base du complexe de dégradosome ARN, c'est une enzyme essentielle, étroitement régulée au niveau de l'ARN et des protéines, ainsi que subcellulairement compartimentée, et sa dérégulation est préjudiciable aux cellules (Jain et Belasco, 1995; Tejada- Arranz et al., 2020a). L'activité catalytique combinée de tous les composants du dégradosome d'ARN est cruciale pour une régulation post-transcriptionnelle efficace de l'expression génique dans différentes espèces bactériennes, où le clivage endonucléolytique initial de la RNase E sur son ARN cible peut être considéré comme l'étape limitant la vitesse (Belasco, 2010). Les bactéries Gram-positives n'ont pas d'orthologue RNase E, mais elles sont toujours capables d'assembler un complexe de type ARN dégradosome, en utilisant comme enzyme de base soit la RNase J ou la RNase Y, qui initient la dégradation des transcrits, similaire à la RNase E (Cho, 2017; Tejada-Arranz et al., 2020, Galtier, et al., 2020). *M. tuberculosis* et le modèle de tuberculose non pathogène *M. smegmatis* possède des orthologues à la fois de la RNase E et de la RNase J, mais ne possède pas d'orthologue RNase Y. Cependant, la fonction et l'interaction de la RNase E et de la RNase J dans des conditions homéostatiques et stressantes, et comment les mycobactéries assemblent un complexe de dégradosome d'ARN sont encore des questions ouvertes. Une étude récente, visant à clarifier le protéome mycobactérien associé à l'ARN, a proposé que la RNase J et la RNase E participent à l'assemblage possible de deux complexes de dégradosomes d'ARN non mutuellement exclusifs, qui pourraient coexister. Alternativement, la RNase E, la RNase J, la PNPase et la RhlE pourraient former un seul complexe qui exclut structurellement une interaction directe entre la RNase E et la RNase J (Płociński et al., 2019). Basé sur une analyse transcriptionnelle préliminaire des cellules mycobactériennes Sur la base d'une analyse transcriptionnelle préliminaire des cellules mycobactériennes exposées à différentes conditions mimétiques de l'hôte, nous avons postulé que l'activité de la RNase E peut contribuer à la variation phénotypique et favoriser l'adaptation à des conditions stressantes. Par conséquent, nous nous concentrons sur la RNase E mycobactérienne à la fois au niveau des cellules en vrac et unicellulaire, sondons ses interactions moléculaires et sa dynamique cellulaire,

et étudions sa contribution à la remise en forme unicellulaire dans des conditions stressantes liées au médicament et à l'hôte.

Au niveau de la cellule unique, nous avons généré des souches de reporter fluorescentes de RNase E dans les mycobactéries non pathogènes et pathogènes, et analysé leur dynamique spatio-temporelle unicellulaire par microscopie microfluidique time-lapse. Nous avons surveillé le comportement des reporters fluorescents RNase E au cours du temps de génération de cellules de réplication uniques et découvert que chez *M. smegmatis* et *M. tuberculosis*, la RNase E présente une distribution inégale dans toute la cellule et forme des foyers plus brillants de courte durée au cours de la vie des cellules individuelles. De plus, la formation de foyers RNase E a été observée dans une fraction inférieure de la population de *M. tuberculosis* (40%) par rapport à *M. smegmatis* (60%). Alors que dans l'organisme modèle à croissance rapide *M. smegmatis*, la présence de foyers RNase E a entraîné une réduction de la taille des cellules et un taux de croissance plus rapide, nous n'avons pas observé de différence significative dans les paramètres liés à la croissance entre les sous-populations de *M. tuberculosis*, sur la base de la présence ou absence de foyers RNase E. En outre, nous avons constaté que des grappes de RNase E mycobactériennes dans des foyers plus lumineux qui pourraient correspondre à des locus hautement transcrits, tels que le locus ribosomal, sont également compatibles avec les grappes de localisation d'ARN polymérase identifiées dans E. coli (Weng et al., 2019). Bien que le rôle réel de l'occurrence des foyers RNase E ne soit toujours pas clair, ils pourraient correspondre à des centres transcriptionnels actifs, cohérents avec leur colocalisation avec un colorant spécifique de l'ARN. Nous pouvons émettre l'hypothèse de deux rôles opposés pour la RNase E au sein de ces clusters. D'une part, la RNase E pourrait exercer sa fonction endonucléolytique, et d'autre part, elle pourrait être séquestrée dans ces foyers, pour affiner sa fonction et réduire la toxicité possible pour la cellule (Tejada-Arranz et al., 2020a). De plus, nous avons constaté que l'inhibition chimique spécifique de la RNase E entraînait une disparition progressive des foyers, et aussi que l'inhibition transitoire du site catalytique de la RNase E est préjudiciable pour les cellules, en ce que les cellules subissent des événements de division réductrice jusqu'à l'arrêt de la croissance. Ces résultats confortent l'hypothèse d'un rôle actif de la RNase E au sein de ces foyers de localisation. Collectivement, ces données suggèrent que le ciblage de l'expression et / ou de l'activité de la RNase E affecte considérablement la physiologie des cellules mycobactériennes, ce qui se traduit principalement par une perturbation de l'homéostasie de la croissance et de la division.

Au niveau des cellules en vrac, nous avons effectué une analyse par spectrométrie de masse (MS) d'une souche surexprimant la RNase E. En effet, en analysant le protéome associé à la RNase E de *M. smegmatis*, nous avons démontré que la RNase E interagit non seulement avec des protéines impliquées dans le traitement de l'ARN, mais aussi avec d'autres enzymes impliquées dans les dommages à l'ADN, la réponse rigoureuse et la virulence. En particulier, nous avons

généré un tableau de souches rapporteurs à double fluorescence et vérifié la colocalisation cellulaire de la RNase E par rapport à ses interacteurs putatifs. Nous avons également généré une souche inductible CRISPRi knock-down de rne, ce qui nous permet de souligner l'interaction possible entre la RNase E et HupB, une protéine associée aux nucléoïdes de type histone.

La RNase E et HupB sont des déterminants clés du transcriptome des cellules mycobactériennes, et nous avons constaté qu'ils agissaient en coopération pour réguler la physiologie des cellules mycobactériennes dans des conditions de croissance optimales. Depuis la RNase E et HupB, ils régulent l'expression de KatG, une catalase-peroxydase impliquée dans l'activation de l'isoniazide (INH), avec des mécanismes inverses mais éventuellement complémentaires (Taverniti et al., 2011; Niki et al., 2012; Gupta et al. ., 2014; Sakatos et al., 2018), Donc, nous avons décidé de surveiller l'expression et la localisation unicellulaires des deux protéines fusionnées à des marqueurs fluorescents également lors de la transition de la croissance optimale au traitement par INH. Nous avons pu démontrer qu'en présence d'INH, RNase E et HupB subissent des événements de condensation corrélés, et qu'une variation préexistante de cellule à cellule dans l'expression de la RNase E peut en partie prédire le sort unicellulaire de *M. tuberculosis*. De plus, nous avons constaté que la survie unicellulaire se produisait exclusivement lorsque les bacilles étaient capables d'ajuster les deux niveaux de RNase E et de HupB pendant et après le traitement à l'INH, et qu'une expression trop faible ou excessive des deux protéines était propice à la mort dans les cellules exposées à INH. Par conséquent, nous pensons que la régulation à la hausse préexistante et / ou induite par le stress de la RNase E pourrait être nécessaire pour déclencher des mécanismes adaptatifs associés à la fois au ralentissement métabolique et les réponses au stress.

On en sait moins sur le rôle joué par la RNase E lors d'une infection des cellules hôtes par des bactéries pathogènes. Son caractère essentiel et l'absence de phénotype viable suite à l'épuisement de la RNase E n'ont abouti qu'à un lien indirect entre la RNase et la virulence chez différentes bactéries pathogènes (Lodato et al., 2017 ; Sharp et al., 2019 ; Viegas et al., 2007; Yang et al., 2008). Ici, nous fournissons la première analyse unicellulaire directe de la dynamique de *M. tuberculosis* RNase E en conjonction avec HupB au cours de l'infection des macrophages. Nous avons montré que les niveaux de RNase E et HupB diminuent au début de l'infection, alors que leurs niveaux augmentent conjointement à mesure que l'infection progresse et au stade tardif de l'infection des macrophages. En outre, l'augmentation de la variation phénotypique de l'expression de la RNase E et de HupB dans des cellules uniques de *M. tuberculosis* est cohérente avec nos observations passées sur l'augmentation de la variation phénotypique de l'expression de l'ARNr pendant l'infection macrophagique et dans le modèle d'infection de la souris (Manina et al., 2015). Bien qu'il ne soit pas clair si la variation phénotypique mycobactérienne est directement induite par des conditions stressantes qui interfèrent avec les processus cellulaires

vitaux, ou si elle résulte d'une réponse adaptative qui vise à favoriser la survie unicellulaire, une interprétation faisable de nos observations est que la RNase et HupB pourraient participer à l'amélioration de la diversification bactérienne de cellule à cellule pendant l'infection, pour finalement favoriser la survie d'au moins une fraction de la population. De plus, conformément à notre observation *in vitro* de cellules mycobactériennes à croissance exponentielle et traitées avec des médicaments, également au cours d'une seule infection macrophagique, la RNase E et HupB présentent un comportement plutôt synchronisé, corroborant l'association étroite de ces deux protéines en réponse à un large éventail de stress conditions. Cependant, compte tenu du rôle crucial de HupB dans la promotion de l'entrée et de la survie des mycobactéries dans les cellules hôtes, nous ne pouvons pas exclure que la RNase E puisse agir de manière dépendante de HupB pendant l'infection. Cela décrirait un scénario dans lequel les deux protéines pourraient se coordonner mutuellement en fonction du stress auquel les bacilles doivent faire face.

Avec ce travail, nous avons découvert que la RNase E présente une variation phénotypique au niveau de la cellule unique, nous avons dévoilé l'interaction entre la RNase E et HupB et leur pertinence pour la tolérance au stress, et nous avons commencé à étudier les conséquences d'un déséquilibre de ces deux facteurs pléiotropiques pour *M. tuberculosis* aptitude. A l'avenir, nous envisageons de clarifier davantage les mécanismes moléculaires régulant ces deux enzymes, que nous considérons comme cruciaux pour la diversification et la persistance des mycobactéries.

Rôle de la RNase E dans la diversification et la survie des mycobactéries

La tuberculose reste la principale cause de mortalité dû à un seul agent pathogène, Mycobacterium tuberculosis, qui provoque des infections pulmonaires persistantes et récalcitrantes aux médicaments qui peuvent se propager à d'autres organes. La capacité des populations bactériennes clonales à se diversifier, appelée variation phénotypique, a des implications majeures pour leur survie dans des conditions défavorables. Les mycobactéries présentent une variation phénotypique à la fois en tant que trait inhérent et en réponse aux changements environnementaux. Ce potentiel de diversification aide les cellules mycobactériennes uniques à faire face à l'hôte et aux antimicrobiens, contribuant éventuellement à la persistance de la tuberculose, mais les mécanismes sous-jacents restent insaisissables. Le renouvellement de l'ARN influence grandement la variation de l'expression des gènes et représente l'une des principales sources de variation phénotypique bactérienne. Les ribonucléases (RNases) sont des enzymes clés impliquées dans le renouvellement de l'ARN, agissant seules ou dans des complexes multi-enzymatiques. Les génomes mycobactériens codent pour un orthologue de la RNase E, qui est impliquée dans la plupart des aspects du traitement et de la dégradation de l'ARN chez les bactéries à Gram négatif. Donc nous avons postulé que l'activité de la RNase E peut contribuer à la variation phénotypique et favoriser l'adaptation à des conditions stressantes. Par conséquent, nous avons entrepris une approche interdisciplinaire, pour sonder le rôle de la RNase E dans les mycobactéries.

Au niveau de la cellule unique, nous avons généré des souches de reporter fluorescentes de RNase E dans les mycobactéries non pathogènes et pathogènes, et analysé leur dynamique spatio-temporelle unicellulaire par time-lapse microscopie microfluidique. Chez les deux espèces, nous avons constaté que les cellules à croissance exponentielle présentent deux sous-populations, qui diffèrent par la présence ou l'absence de foyers de localisation de la RNase E. Nous avons également observé des modèles spécifiques de re-localisation de la RNase E en altérant les processus essentiels, spécifiquement, la réplication, la transcription, la traduction et la division. Ces données suggèrent une contribution probable de la RNase E à l'homéostasie des cellules mycobactériennes.

Au niveau des cellules en vrac, nous avons effectué une analyse par spectrométrie de masse (MS) d'une souche sur-exprimant la RNase E. Cela nous a permis d'identifier des interacteurs putatifs de RNase E et nous avons validé ces données protéomiques soit au niveau de l'ARNm soit au niveau des protéines. En particulier, nous avons généré un tableau de souches rapporteurs à double fluorescence et vérifié la colocalisation cellulaire de la RNase E par rapport à ses interacteurs putatifs. Nous avons également généré une souche inductible CRISPRi knock-down de l'rne, ce qui nous permet de souligner l'interaction possible entre la RNase E et HupB,

une protéine associée aux nucléotides de type histone. Cela nous a conduit à émettre l'hypothèse que la RNase E et HupB pourraient agir de concert pour réguler les enzymes cruciales pour l'adaptation bactérienne aux médicaments antituberculeux de première ligne. Pour mieux caractériser l'interaction fonctionnelle entre RNase E et HupB, nous avons analysé la dynamique subcellulaire de la RNase E et HupB dans les cellules mycobactériennes exposées à l'isoniazide et lors de l'infection des macrophages. Nous avons prouvé la régulation concertée de la RNase E et HupB soit au niveau de l'ARN soit au niveau des protéines et leur association moléculaire. Nous avons aussi démontré la contribution de ces deux facteurs à la survie de M. tuberculosis, notamment en ce qui concerne la tolérance à l'isoniazid et la persistance intracellulaire

Mots clés : *Tuberculose, hétérogénéité phénotypique, microscopie microfluidique, microbiologie unicellulaire, persistance bactérienne.*

Role of the RNase E in the diversification and survival of mycobacteria

Tuberculosis remains the leading cause of death from a single pathogen, *Mycobacterium tuberculosis*, which causes persistent and drug-recalcitrant lung infections that can disseminate to other organs. Better understanding of the mechanisms underlying mycobacterial survival could lead to new strategies to tackle this global health problem. The ability of clonal bacterial populations to diversify, referred to as phenotypic variation, has major implications for their survival under adverse conditions. Mycobacteria exhibit phenotypic variation both as an inherent trait and in response to environmental changes. This diversification potential helps single mycobacterial cells to cope with the host and antimicrobials, possibly contributing to tuberculosis persistence, however the underlying mechanisms remain elusive. RNA turnover greatly influences variation in gene expression and represents one of the main sources of bacterial phenotypic variation. Ribonucleases (RNases) are key enzymes involved in RNA turnover, acting alone or in multi-enzymatic complexes. Interestingly, mycobacterial genomes encode the main RNases of both gram-positive and -negative bacteria, including an orthologous of the RNase E, which is implicated in most aspects of RNA processing and degradation in gram-negative bacteria. Based on a preliminary transcriptional analysis of mycobacterial cells exposed to different host-mimetic conditions, we postulated that RNase E activity may contribute to phenotypic variation and foster adaptation to stressful conditions. Therefore, we undertook an interdisciplinary approach, to probe the role of RNase E in mycobacteria.

At the single-cell level, we generated fluorescent reporter strains of RNase E in both non-pathogenic and pathogenic mycobacteria, and analyzed their single-cell spatiotemporal dynamics by time-lapse microfluidic microscopy. In both species we found that exponentially-growing cells exhibit two subpopulations, which differ for the presence or absence of RNase E localization foci. RNase E foci disappear upon exposure to a specific RNase E inhibitor and cells undergo reductive division, implying a functional role of RNase E foci. We also observed specific patterns of RNase E re-localization by impairing essential processes, namely, replication, transcription, translation and division. These data suggest a likely contribution of RNase E to the mycobacterial cell homeostasis.

At the bulk-cell level, we carried out Mass Spectrometry (MS) analysis of a strain over-expressing the RNase E. This enabled us to identify putative RNase E interactors, involved in RNA processing, DNA damage, stringent response and virulence. We validated these proteomic data both at the mRNA and at the protein level. In particular, we generated an array of dual-fluorescent reporter strains, and checked the cellular colocalization of RNase E with respect to its putative interactors. We also generated an inducible CRISPRi knock-down strain of *rne*, enabling us to point

out the possible interplay between RNase E and HupB, a histone-like nucleoid-associated protein. By either overexpressing or by knocking-down *rne*, we checked the patterns of re-localization of our HupB fluorescent variant. This led us to hypothesize that RNase E and HupB may act in concert to regulate enzymes crucial for bacterial adaptation to frontline antitubercular drugs. For instance, the catalase peroxidase KatG, which is implicated in response to peroxide stress and in tolerance to isoniazid. To better characterize the functional interaction between RNase E and HupB, we carried out comparative analysis of a strain expressing different levels of RNase E, by using microscopy approaches, and during macrophage infection. By analyzing the subcellular dynamic of RNase E and HupB in mycobacterial cell exposed to INH and during macrophages infection, we proved that the concerted regulation of RNase E and HupB both at the RNA and protein level and their molecular association in the tubercular pathogen, but also demonstrate the contribution of these two factors in *M. tuberculosis* survival, particularly with regard to INH tolerance and intracellular persistence

Keywords: *Tuberculosis, phenotypic heterogeneity, microfluidic microscopy, single-cell microbiology, bacterial persistence.*

“And once the storm is over,

you won’t remember how you made it through,

how you managed to survive.

You won’t even be sure whether the storm is really over.

But one thing is certain, when you come out of the storm,

you won’t be the same person who walked in.

That’s what this storm’s all about”.

- Haruki Murakami

Acknowledgements

Usually, the acknowledgment writing should be the easiest part of any manuscript; actually, it was the hardest for me. At the end of this incredibly everchanging, bumpy, reshaping experience, I cannot be more grateful to all the persons that contributed to this work.

First of all, I want to thank Giulia. She actually made all of this work possible. For generating the CRISPR systems, for all the work she did in BLS3 with the pathogen and for all her help during each step of this work. For giving me the possibility to discover and appreciate how complex and still unknown *M. tuberculosis* is. To have taught me so much and to have never shut down any idea I had. To have taught me how to reframe an intuition into a proper and structured experimental design. Most importantly, although the bumpy roads, to have been a fantastic mentor. To have always pushed me to grow as a scientist and person and to have been there all the time doubts and crisis (to be honest, there were many) were along the way. Although I was never able to show it properly, I have constantly appreciated and felt grateful for the opportunity I had, during these four years, to work with her.

To the IMI squad, Nicolas, Lalit, Mena, Maxime, and Crispin. To have always been supporting all along the way. Also, thanks to Jean-Philippe Tosiani and Delphin Vergoz. To have contributed during their internship to this project. I couldn't have asked for a better lab.

To Nicolas, for his help in the lab and for his availability, especially during the first months. I have always overwhelmed you with 100 questions a day.

To Mena, for always knowing when it was the right moment to remember me to breathe, for reminding me that "une choce à la fois" is the best way to reach the end.

To Maxime, I could be filling pages about the reasons why I am so grateful to have had the possibility to work with you and become friends. We shared the constant frustration of failed experiments and the happiness (too-short) of moments of the successful ones. Above all, I am immensely happy to have had you along the way because of yours always and spontaneously being there when I needed the most. When I was so lost in myself that I couldn't even see a palm from my noise.

To Crispin, the last arrived in the lab, for his incredible and useful help during the thesis writing. For his always constructive curiosity, comments, and encouragement.

Thanks to the Proteomic Platform of the Institute Pasteur for the Mass Spectrometry part, for their support with the statistical analysis and for part of the functional analysis.

Thanks to the Hub of Bioinformatic and Biostatistics for their support in the development of image post-processing tools. They really made my life easier.

Because Paris was not only about ending tuberculosis, to my amazing friends. To Mariano, Adria, Crispin, Borja, Laura, Maria, Oliver, Surya, Livia, and Nacho. For all the incredible memories we built together. Each one of you, in such a special and different way, flavored my time in Paris in way that it is impossible to forget and that I will always bring with me. Love you guys!

Especially to Maria, Mariano, Crispin and Surya. Because I have never felt luckier to have met all of you along the way. Because I couldn't have never reached the end without all your support, love, and sense of perspective. Because all of you were and are one of the best gifts I could have ever wished and hoped for from Paris.

To the "No rep Squad". To have shown me that the right persons around you can always push you a step further. For all the lightmindedness, happy, sweaty moments we shared together.

To the two best flatmates I could have ever asked for, Maria and Silke. To Maria, to have been my calm place and for remembering me all the time that slowdown is necessary along the way. To Silke, to have been patience with my papers house invasion and with my constant moments of crisis during my home writing. Also, for reading and helping me with the thesis and for her unconditional support during the last crazy weeks of the writing.

To Frederic, because in each situation he has always helped me to see the light at the end of the tunnel and to have remembered me that a decision taken is never something to look back at and feel regret for.

To Rishi, to have remember me that during every stressful moment and “when everything around you is running faster than you, staying static can be the best solution”. For reminding me that the writing of a thesis it is not only a stressful time, but a moment to enjoy all along the way. Thanks Einstein!

To my since forever friends. To Cecilia, Daniele, Giacomo, Maurizio, Marta, Thomas, Riccardo, Antonella, Nicolas and Debora. Because it didn't never really matter how many kilometers, differences in time and countries were dividing each other. Because you always reminded me who I was when I was lost and to have constantly been my compass. Because you never made me feel alone, and for have been such an important and constant presence in every single step of this journey.

To my incredibly amazing parents and sister. Because I would say that 90%, if not all, of what I have reached so far wouldn't have been possible without them. To have never complained about my constant moving around and for just getting along with it. To have always been my greatest fans, to have always always encouraged me to follow my ambitions and to be my safest place to always come back to.

Lastly, to all the people I met along the way.

Disclaimer

I hereby declare that I composed this dissertation. All sources and aids used have been indicated as such. All texts either quoted directly or paraphrased have been indicated by in-text citations. Full bibliographic details are given in the reference list which also contains sources containing URL and access date. This work has not been submitted to any other examination authority.

Abbreviation List

Tuberculosis (TB)
Latent Tuberculosis Infection (LTBI)
Mycobacterium tuberculosis (*M. tuberculosis*)
World Health Organization (WHO)
Direct observed treatment, short-course (DOTS)
Rifampicin-resistant tuberculosis (RR-TB)
Multidrug resistant tuberculosis (MDR-TB)
Extensively drug resistant tuberculosis (XDR-TB)
Restriction fragment length polymorphism (RFLP)
Bacillus Calmette-Guérin (BCG)
Variable number tandem repeat (VNTRs)
Mycobacterial interspersed repetitive units (MIRUs)
Base pair (bp)
Megabase Mb)
Transfer RNA (tRNA)
Non-coding RNA (ncRNA)
Ribosomal RNA (rRNA)
Miscellaneous (miscRNA)
Open reading frame (ORFs)
Guanine-Cytosine (GC)
Adenine – Thymine (AT)
Ribosomal RNA gene (rrn)
Toxin-Antitoxin systems (TA systems)
Two Component System (TCSs)
Transcriptional factor (TFs)
Small RNA (sRNA)
3'/5' Untranslated region (3'/5'UTR)
Clustered Regularly Interspaced Short Palindromic Repeats (CRISPR)
Ribosomal Binding Site (RBS)
RNA-sequencing (RNA-seq)
Nucleotide (nt)
Dehydroepiandrosterone (DHEA)
T helper cell 1 (Th1)
6 kDa early secretory antigenic target (ESAT6)
Matrix metallopeptidase 9 (MMP9)
Early secretory antigenic target 6 system 1 (ESAT6/ESX1)
Oxygen/Nitrogen Reactive Species (ROS/RNS)
Viable but not culturable (VBNC)
Non-growing but metabolically active (NGMA)
Enduring hypoxic response (EHR)
Sputum smear microscopy (SSM)
Ultraviolet radiation (UV)
Isoniazid (INH)

Rifampicin (RIF)
Pyrazinamide (PZA)
Ethambutol (EMB)
Fluoroquinolones (FQ)
Kanamycin (KAN)
Streptomycin (STR)
Para-Aminosalicylic Acid (PAS)
Biosafety level 3(BSL3)
Tuberculin skin test (TST)
Recombinant Bacillus Calmette-Guérin (rBCG)
Nucleoid-Associated protein (NAPs)
Non-coding/small non-coding RNA (nc/snRNA)
Ribonuclease (RNase)
Polynucleotide phophorylase (PNPase)
arginine and proline residue (RP-rich)
Amino acid (aa)
Sodium dodecyl sulfate (SDS)
Ribonucleoprotein (RNP)
Adenine/Uracil (A/U)
Genomic DNA gDNA)
Anhydrotetacycline (ATC)
Mass Spectrometry (MS)
Endoribonuclease (endoRNA)
Exoribonuclease (exoRNAse)
LFQ (Label Free Quantification)
FDR (False Discovery Rate)
Guide RNA (sgRNA)

Index

INTRODUCTION **- 1 -**

CHAPTER 1. TUBERCULOSIS **- 1 -**

1.1 THE HISTORY OF TUBERCULOSIS - 1 -

1.2 TB EPIDEMIOLOGY - 2 -

1.3 DIVERSITY IN TB EPIDEMIOLOGY - 6 -

1.4 MOLECULAR EPIDEMIOLOGY OF TB - 9 -

1.5 *MYCOBACTERIUM TUBERCULOSIS* PHYSIOLOGY - 11 -

1.7 DIAGNOSIS - 42 -

1.8 VACCINES - 47 -

1.9 TREATMENT - 49 -

1.10 HIV AND TB: AN AMPLIFIED GLOBAL BURDEN - 51 -

CHAPTER 2. MYCOBACTERIAL PERSISTENCE **- 53 -**

2.1 OUTLINING BACTERIAL PERSISTERS - 54 -

2.2 THE METABOLIC STATUS OF PERSISTERS - 55 -

2.3 PUTATIVE MECHANISMS BEHIND THE FORMATION OF PERSISTERS - 58 -

2.4 BACTERIAL PHENOTYPIC HETEROGENEITY AS A MECHANISM OF SPONTANEOUS PERSISTENCE - 67 -

CHAPTER 3. BACTERIAL RNA TURNOVER **- 81 -**

3.1 BACTERIAL RNA SPATIAL ORGANIZATION - 82 -

3.2 BACTERIAL MRNA DEGRADATION - 86 -

3.3 MRNA DECAY IN GRAM-POSITIVE AND GRAM-NEGATIVE BACTERIA - 93 -

CHAPTER 4. THE ENDORIBONUCLEASE E **- 99 -**

4.1 PHYLOGENETIC DISTRIBUTION OF THE RNASE E - 100 -

4.2 THE RNASE E STRUCTURE - 101 -

4.3 RNASE E PROTEIN INTERACTIONS - 104 -

4.4 RNASE E SUBSTRATE RECOGNITION AND CLEAVAGE - 106 -

4.5 REGULATION OF THE RNASE E ACTIVITY - 110 -

4.6. RNASE E CELLULAR LOCATION - 118 -

4.7 MYCOBACTERIAL RNASE E - 119 -

AIM OF THE WORK **- 125 -**

MATERIALS AND METHODS - 127 -

CHAPTER 5 - 127 -

5.1 MICROBIOLOGY AND MOLECULAR BIOLOGY - 127 -

5.2 PROTEIN EXPRESSION ANALYSIS - 130 -

5.3 MICROSCOPY - 132 -

5.4 DATA ANALYSIS AND STATISTIC - 134 -

RESULTS - 137 -

CHAPTER 6 - 137 -

6.1 *M. SMEGMATIS* P*RNE*-MKATE2 REPORTER STRAIN EXHIBITS DYNAMIC LOCALIZATION EVENTS THAT ARE ASSOCIATED WITH CELLULAR HOMEOSTASIS. - 137 -

6.2 THE MYCOBACTERIAL RNASE E INTERACTOME INCLUDES PROTEINS INVOLVED IN RNA TURNOVER AND STRESS-RESPONSE PATHWAYS - 141 -

6.3 RNASE E AND HUPB ARE MOLECULAR PARTNERS AND RESPOND JOINTLY TO STRESSFUL CONDITIONS - 146 -

6.4 DYNAMIC EXPRESSION OF RNASE E IN *M. TUBERCULOSIS* POSITIVELY CORRELATES WITH HUPB AND AFFECTS THE FATE OF INDIVIDUAL CELLS STRESSES WITH ISONIAZID - 150 -

6.5 RNASE E AND HUPB JOINTLY ASSISTS *M. TUBERCULOSIS* SURVIVAL DURING BOTH ISONIAZID TREATMENT AND INFECTION - 155 -

DISCUSSION - 160 -

BIBLIOGRAPHY I

ANNEX 1. XXV

Introduction

Chapter 1. Tuberculosis

1.1 The history of tuberculosis

Tuberculosis (TB) is a communicable infectious disease caused by *Mycobacterium tuberculosis* (*M. tuberculosis*). Because of its severe social implication and the number of victims claimed, *M. tuberculosis* endures as one of the deadliest microbial pathogens of human history. It infects around 10 million people worldwide, and almost 23% of the world's population (1.7 billion people) is estimated to have a latent TB infection (WHO, 2019).

The genus *Mycobacterium* presumably originated more than 150 million years ago (Hayman, 1984). The low mutation rate and the genome sequencing of several strains of *M. tuberculosis* allowed a more rigorous estimation of its origin. As early as 3 million years ago, an early progenitor of *M. tuberculosis* was already present in East Africa. However, all modern members of the *M. tuberculosis* complex originated from a common ancestor around 35 000-15 000 years ago (M Cristina et al., 2005). East Africa was the ancestral home of both pathogen and its human host. Archeological evidence demonstrated signs of TB both in Egyptian and in Peruvian mummies (Thomas M. Daniel, 2000; Morse et al., 1964). In classical Greece, TB was known as phthisis. Isocrates was the first to claim TB as an infectious disease, and Hippocrates accurately described its symptoms and the tubercular lung lesions. In Roman times, Galen, the personal physician of Emperor *Marcus Aurelius*, reported fever, sweating, coughing, and blood-stained sputum as TB symptoms (Daniel, 2000).

During the Middle Age, the written records of TB, also known as the "king's evil", became rare, and the royal touch was believed to cure infected persons (Murray et al., 2016). In 1679, in the *Opera Medica,* Francis Sylvius thoroughly described the illness, and in 1699 the first official reference of TB infectious nature appeared in an editorial issued by the Republic of Lucca. Being conscious of the severity of the disease, the Health Board of the Republic of Lucca declared as mandatory the notification and isolation of the consumptives. Their admission to public hospitals was forbidden, establishing specific places for their treatment (Barberis et al., 2017).

In the 18th century, TB claimed 900 deaths each 100 000 individuals per year. The society started to romanticize about it, and the extreme whiteness of consumptives rename TB as the "white plague." At the beginning of the 19th century, medical practitioners and scientists struggled to understand the underlying roots of TB etiology. Northern Europe described TB as a heritable

disease, and Southern Europe stated its infectious origin (Daniel, 2006). The infectious nature of TB was only proved in 1865 by Jean-Antoine Villemin. Villemin inoculated a rabbit with "a small amount of purulent liquid from a tuberculous cavity" (Villemin, 1865). Although the animal survived, after its autopsy clear signs of TB were evident (Villemin, 1865). Towards the end of the 19th Century, the first sanatoria were founded to cure TB patients with continuous exposure to fresh air, sun, and proper nutrition. Patients' care in sanatoria represented the first successful remedy against TB in the pre-antibiotic era (Daniel, 2011).

In 1882, Hermann Heinrich Robert Koch, in *Die Aetiologie der Tuberculose*, demonstrated both the infectious etiology and the bacterial origin of the disease (Daniel, 2005a). Shortly after, Koch isolated a substance from tubercle bacilli. He claimed that this substance, known as tuberculin, was able to "render harmless the pathogenic bacteria that are found in a living body and do this without disadvantage to the body" (Robert Koch, 1890). At the begging of 1900, Clemens Freiherr von Pirquet and Charles Mantoux introduced the subcutaneous injection of tuberculin as a diagnostic tool. Moreover, Pirquet also coined the term latent tuberculosis infection (LTBI), which reflected the observation of children positive to the tuberculin test, but not manifesting the symptoms of the disease (Pirquet, 1909).

Starting from the early 19th century until the present time, we assist to a decline in the mortality rate of TB. The reason for its decline can be conceivably associated with three main factors (Davies RPO et al., 1999), namely, the introduction of better hygienic and healthcare measures, the production of a vaccine, and the discovery of antibiotics. The creation of a vaccine against *M. tuberculosis* was the first more direct approach undertook to fight TB. Albert Calmette and Camille Guérin succeeded in attenuating a strain of *Mycobacterium bovis* causing the disease in cattle by serial laboratory passages until the virulence potential was lost but immunogenicity preserved. In 1921, they tested their vaccine on an infant born from a mother dying of pulmonary TB. The child survived without developing the disease afterward (Daniel, 2005b). From the name of their fathers, the vaccine Bacille-Calmette-Guérin, commonly known as BCG, remains the most effective vaccine, although its protective effect is mainly exerted in infants. In 1948, the World Health Organization (WHO) carried out the first program for TB control. The program was based on tuberculin testing, followed by BCG mass vaccination for nonreactors (Altink, 2014).

In 1974, the WHO Expert Committee in Tuberculosis issued its Ninth Report, providing the guidelines for TB control. Since then, the WHO has been continuing its TB control program.

1.2 TB epidemiology

M. tuberculosis remains the world's leading infectious killer, representing a significant public health concern worldwide. The WHO has published annual TB estimates of incidence (new

cases per 100 000 population per year) and mortality (deaths per 100 000 population per year) for all member countries.

Globally, the TB prevalence is declining since the early 1990s. To further foster the burden of TB, WHO established two programs: the Sustainable Development Goals (SDGs) and the End TB Strategy. While SDG targeted ending the worldwide TB epidemy by 2030, the End TB Strategy aims a 90% reduction in TB death and an 80% reduction in TB incidence rate between 2015 and 2030, placing a 35% reduction in TB deaths and a 20% reduction in TB incidence rates by 2020. In the European region, the cumulative TB incidence rate for the period 2015-2018 was 15%, and the TB death declined by 24%. In high TB burden countries, such as in the African region, TB incidence and mortality have been declining, reducing the TB incidence cumulatively at 12%, and the TB death of the 16% within the same timeframe. A more significant concern is the increasing burden of TB-drug resistant cases, which, globally, represent around 3.4% of new TB cases.

Despite the positive declining trend in TB incidence, prevalence, mortality, and drug resistance, all these parameters together are not in line with the 2020 milestones and to reach the global targets for 2020-2035 of the End TB Strategy (WHO, 2019).

1.2.1 Global epidemiology

In 2018*, M. tuberculosis* killed 1.2 million people, including 251 000 HIV-positive individuals. Overall, the TB deaths showed a 27% reduction from the 1.7 million total death reported in 2000 and a 60% reduction of the mortality among HIV-positive people. Despite the general decline in TB incidence and mortality, TB remains the leading cause of death due to a single infectious agent, ranking above HIV/AIDS. The severity of the national epidemic varies widely. TB still mainly remains a poverty-related disease. Indeed, in most high-income countries, there were fewer than ten new cases for 100 000 population, 150-400 in most of the ten high TB burden countries (South-East Asia and Africa). In 2018, the Region of Americas and Europe only accounted for around 3% of the total cases, respectively, a smaller proportion of the cases were reported in the WHO Eastern Mediterranean Region (8.1%), with the highest number of cases in the WHO South-East Asia Region (44%) and African Region (24%) (**Figure 1**) (WHO, 2019).

Content removed for copyright

Figure 1. Estimated TB incidence in 2018*. The map displays countries with at least 100 000 incident cases. The 87% of the total TB cases worldwide are geographically restricted to the 30 high TB burden countries. Among them, two thirds of the global total is accounted by eight counties: India (27%), China (9%), Indonesia (8%), the Philippines (6%), Pakistan (6%), Nigeria (4%), Bangladesh (4%), and South Africa (3%) (WHO, 2019).*

World Health Organization (WHO) reported an estimated 10.0 million new cases (a 1.8% decline from 2016), corresponding to 132 cases per 100 000 population. TB differentially affects people in all age groups and gender. The WHO estimated that around 90% of the case were adults (aged ≥ 15 years), with a high rate of infection among adult men. Data collected through prevalence surveys show that TB affects men more than women. In 2018, adult men accounted for 57% of all cases, while adult women only represent 32%. Children represent 11% of the total cases of TB infections. For all ages, the M: F ratio of incident TB cases varies depending on the geographic area. In the WHO Eastern Mediterranean Region, the M: F ratio is 1.3, 2.0 in the European and Western Pacific regions. The M: F ratio in children is close to 1.

Drug-resistance TB continues as a public health crisis. Overall, an estimated 484 000 incident cases of rifampicin-resistant TB (RR-TB) or multi-drug resistant TB (MDR-TB), resistant to both rifampicin and isoniazid occurred in 2018, representing 5.6% of all TB cases, 3.4% of newly diagnosed TB cases, and 18% of previously treated cases. Among the reported cases of MDR-TB, 8.5% were estimated to have extensively drug-resistant TB (XDR-TB)[1] (**Figure 2**).

[1]*Defined as MDR-TB showing resistance to at least one drug, fluoroquinolones and/or second-line injectable agents, used in the treatment of MDR-TB*

Content removed for copyright

Figure 2. **Estimated incidence of MDR/RR-TB[a] in 2018.** *The map displays countries with at least 1000 incident case. Three countries accounted for almost half of the world's cases of MDR/RR-TB: India (27%), China (14%), and the Russian Federation (9%).* [(a)] *MDR-TB represents a subset of RR-TB) (WHO, 2019).*

About 23% of the global population (1.7 billion people) is estimated to have a latent TB infection, with the risk of developing active TB disease during their lifetime (WHO, 2019).

1.2.2 WHO TB Management

TB incidence shows a yearly decline of 1.5% (WHO, 2019). Despite the decline of TB incidence in Europe and North America, TB remains endemic in low-income countries, and it is reemerging in high-income countries, mainly due to the massive increase in drug resistance, comorbidities, and aging (Daniel, 2006).

The WHO has set up an active surveillance program to define the course of the epidemic and to assess the impact of control measures on the disease. Yearly, the 194 WHO's member states report the TB data to WHO, which are then reviewed and validated in collaboration with reporting entities. Each country estimates the disease incidence and confidence intervals depending on 1) TB prevalence surveys; 2) notifications adjusted by a standard factor to account for underreporting, overdiagnosis, and underdiagnosis; 3) results from national inventory studies that measured the level of underreporting of detected TB cases combined with capture-recapture analysis, and 4) case notification data combined with an expert opinion about case-detection gaps (WHO, 2019).

To enhance the control of the TB pandemic, the WHO has introduced global control programs, such as the Directly Observed Treatment, Short-course (DOTS), and the End TB Strategy.

DOTS represents the strongest and most successful strategy for the control of TB. It is a cost-effective program summing up all the best practices, clinical trials, and operations to control the diffusion of TB infection over the past two decades. The pillars behind the DOTS program include: (i) the commitment of the government in sustaining TB control activities; (ii) the detection through sputum smear microscopy (SSM) of self-report of symptomatic individuals; (iii) six to eight months standard chemotherapy for SSM-positive individuals directly monitored for at least the first two months; (iv) constant supply of all the essential anti-TB drugs and (v) standard reporting system for the chemotherapy follow-up of each patient (WHO, 1999).

In 2014, the World Health Assembly adopted the End TB Strategy, which aims to eradicate the global TB pandemic by 2035. To reach this goal, the TB-related deaths and the actual TB incidence should fall by 95% and 90%, respectively, compared to the 2015 statistics. The End TB Strategy stands on three principles: (i) TB early detection, treatment, and prevention in patient-centered fashion (ii) engagement of government, communities, and public and private care providers to implement health coverage and social protection, with particular regard to vulnerable groups (*i.e.,* poor, HIV-positive individuals, refugees, and prisoners), and (iii) support the required technological progress. To reach the fixed target, WHO considers it necessary to establish programs for interventions, diagnosis, treatment, management, prevention, research, and innovation. Also, the institution of universal health systems and policies, social and final protection, and a significant engagement of all health care providers, are thought of as essential policies to eliminate TB.

Collectively these measures have led to a moderate but constant decline in TB incidence and mortality. However, further reduction of these parameters is needed to reach the goals set by the End TB Strategy. To this aim, it is mandatory to implement the existing intervention measures further, to optimize the available tools, to develop original diagnostic methods, and to implement universal drug susceptibility screening of high-risk populations and universal coverage and social protection (WHO, 2015a). In conclusion, only a comprehensive and integrated approach would enable to reach a 10% annual reduction of TB incidence, getting close to target the eradication of TB infection by 2050 (WHO, 2019).

1.3 Diversity in TB epidemiology

The burden of TB is gradually declining and thus masks the diverseness in its distribution. TB epidemiology relies on multiple parameters, such as the wide variation in the disease burden

within and between countries and individual-level factors associated with the risk of disease. Those parameters are unevenly scattered across space or social network and define the diverseness of TB epidemics (Trauer et al., 2019). The drivers at the base of this diverseness include the characteristics of both the host (*i.e.,* susceptibility to infection, progression to disease after infection, impaired immune system) and the pathogen (*i.e., M. tuberculosis* strains diversity and virulence), and of the environment (*i.e.,* sociodemographic factors). Furthermore, the possible interaction between those three parameters might enhance or reduce the degree of diversity of TB epidemiology (Trauer et al., 2019).

The main drivers contributing to the TB epidemiological diverseness in the host are linked to the individual features predisposing to the susceptibility and outcome of the infection, and the rate of infectiousness. Host characteristics (*i.e.,* age; comorbidities such as HIV, type-2 diabetes, and immune disorders; poor living conditions; malnutrition and alcohol and tobacco abuse) considerably impact human susceptibility to TB infection. They also enhance the likelihood of disease progression and the risk of reactivation (Trauer et al., 2019). The susceptibility of the host to the progression of the infection also depends on previously treated infections and the establishment of LTBI. Indeed, it has been shown that latently infected individuals have a lower risk of developing active TB after reinfection. Hence people carrying LTBI might be partially protected against *M. tuberculosis* reinfection. Interestingly, the observed protective effect might not be entirely dependent on the immune response established upon latent infection. Nevertheless, that acquired immunity might confer a protective effect upon repeated exposure to the pathogen (Andrews et al., 2012). On the contrary, previously treated individuals are more likely to be reinfected due to repeated exposures, incomplete treatment, or immunological vulnerability (Gomes et al., 2012). Differently from other respiratory pathogens (*i.e.,* measles, influenza), TB shows a lower rate of infection. The lower rate of infection can be explained by accounting the critical role of additional factors, such as the cough characteristics, the quality and the ability to form aerosols, and environmental factors in affecting the occurring of the infection. Currently, the most widespread and affordable diagnostic technique of tubercular infection is smear microscopy in conjunction with Ziehl-Neelsen acid-fast staining[2], which enables to directly identify tubercular bacilli in the sputum of patients with active infection. Smear-positive adults with cavity pulmonary TB result to be more infectious than those with only extrapulmonary involvement (Melsew et al., 2018). Lastly, despite the less likely ability of HIV-positive individuals

[2] *Ziehl_Neelsen (ZN) method of Acid-Fast staining technique is used to stain Mycobacterium species. The stain (carbol fuchsin combined with phenol) binds to the mycolic acid in the mycobacterial cell wall, which is only retained by mycobacteria within a sputum smear. The sputum smear is counterstained with malachite green or methylene blue. This last step stains the background material, creating a contrast colour against which the red bacilli can be observed.*

and children to transmit the disease, their level of infectiousness can be variable, and children (> 10 years old) often show the adult form of TB (Trauer et al., 2019).

M. tuberculosis shows a complex interaction with its human host. This interplay shows a co-evolution between the host and the pathogen. Seven major *M. tuberculosis* lineages have evolved and adapted to specific human host populations (Gagneux, 2012). Different lineages exhibit diverse clinical and epidemiological behavior. Indeed, molecular epidemiology studies demonstrated that the genetic diversity of *M. tuberculosis* lineages is associated with the outcome of infection (Barnes and Cave, 2003).

In contrast to other pulmonary pathogens, such as *Pseudomonas aeruginosa* (Gagneux, 2018), a strain of *M. tuberculosis* infecting an individual tends to remain genetically homogeneous or clonal during infection. Whereas drug resistance represents the most obvious form of genetic diversification shown by *M. tuberculosis*. Mutations enabling the bacillus to sustain drug exposure might be the result of physiological impairments caused by the drug. Often drug-resistant strains exhibit a fitness defect in the absence of the drug, but compensatory mutations can be selected to promote their fitness. Other mutations do not affect bacterial fitness and are more likely to be selected in the clinical setting (Gagneux, 2018). Furthermore, the infectiousness of drug-resistant TB (DR-TB) differs from drug-susceptible TB due to the diagnostic limitation in determining the drug resistance, the longer duration of DR-TB treatment, and the clustering of DR-TB patients. Altogether, these factors may prolong the infectious period and promote their transmission (Gagneux et al., 2006).

The environmental setting also plays a critical role in modifying the transmission of TB. It is well known that crowded environments, poor ventilation, and a high level of indoor pollution might facilitate airborne transmission. Locations with these features (*i.e.,* prison, public transit, mines) are often frequented by high-risk individuals. Hence these settings and the presence of high-risk categories further foster the enhancing of the transmission and the fueling of the epidemic (Trauer et al., 2019). While the association between indoor pollution and TB transmission has been easily assessed, fewer data are available regarding outdoor pollution and the spreading of TB. Although still limited studies have been done in this context, it starts to be demonstrated that the outdoor air pollution might be playing an effect on TB infection and/or in the progression of the disease (Rajaei et al., 2018).

Lastly**,** factors such as migration, urbanization, and demographic transitions are some distal determinants that might be driving heterogeneity in the TB burden (Lönnroth et al., 2009). Pockets of poverty, unhygienic behavior, and a weak health system represent critical factors for TB spreading. Moreover, social factors also influence the spreading of the disease. The airborne transmission of *M. tuberculosis* cancels the need for direct person-to-person contact for its transmission, hence modifying social settings (*i.e.,* household, workplace, general community).

Those social determinants might delay the diagnosis, prolonging the duration of the infection, and, in consequence, enhancing the disease heterogeneity (Lin et al., 2008).

To date, the extent of the TB infection is estimated by merging data obtained from treated and/or reported cases, cases that received a diagnosis, and cases registered during surveillance systems or local studies. Nevertheless, a substantial number of cases are not reported. For instance, from report surveys, it emerges that adult males are more susceptible to TB infection, but at the same, they seek or access care at a lower rate than women. An additional bias in the interpretation of the epidemiological data is linked to the socioeconomic status or the geographic location considered. Hence, epidemiological studies relying on these biases data (aged categories, geographic regions, drug resistance profile, and latent infection) might not reflect the reality of the infection and often hide the diverseness within the TB epidemic. Therefore, a better understanding of the diverseness of the TB epidemic can result in a more efficient intervention that will differ depending on the targeted individuals and on the distribution of risk factors, such as transmission, the incidence of infection, and mortality. For more accurate modeling of the TB infection and the relevance of the diverseness within it, it is essential to (1) analyze the data in a context-specific situation, (2) use epidemiological research to elaborate critical factors for the estimation of the infection, (3) highlight uncertainty in the predictive model, (4) use operational research to summarize the effectiveness/cost ratio of targeted intervention, and (5) account for inequities in health status (Trauer et al., 2019).

1.4 Molecular epidemiology of TB

The tracking and identification of individual strains of *M. tuberculosis* play a prominent role in enhancing the understanding of TB transmission within populations. The development of molecular techniques established a new discipline, molecular epidemiology, which bases its expertise on the genome sequencing of *M. tuberculosis*. It aims to provide new tools for probing the epidemiology of TB.

Genotyping can be used to confirm cross-contamination in the laboratory, which represents about 3% of positive patient isolates. Cross-contamination is likely to occur when the acid-fast smears are negative, and only one specimen is culture-positive. Indeed, laboratory cross-contamination due to the concurrent handling of other *M. tuberculosis* strains and the absence of clinical TB symptoms finally results in the end of the anti-TB treatment for the misdiagnosed patient. Genotyping is also used to discriminate between drug susceptibility and drug resistance in clinical isolates. Therefore, genotyping is a very useful tool to guide clinicians in their therapeutic choices in different phases of a patient's infection and during therapy. Lastly, genotyping can detect the occurrence of a TB outbreak. The molecular evaluation of the outbreak

will not only determine if the event is just due to a large number of cases, but it will also guide the public health measure to reduce TB transmission. The study of TB transmission at the molecular level shows a vast geographic variation. To gain more insights into the dynamics of TB spread, genotyping data must be considered together with epidemiologic information (Barnes and Cave, 2003).

1.4.1 Epidemiological markers

Epidemiological biomarkers serve to characterize the genetic profile of an epidemic strain and to assess the genetic variation among different bacterial isolates during an outbreak. The most commonly used genotyping techniques and epidemiological markers in the TB field are described below.

1.4.1.1 IS6110 restriction fragment length polymorphism.

IS*6110* marker comprises 1355 base pairs (bp) and belongs to the IS*3* family of insertion sequences. It has two open reading frames encoding for transposons. IS*6110* copies range from 0 to 25, and their location in the *M. tuberculosis* genome is highly variable between isolates (Van Soolingen et al., 1991). IS*6110*-based typing is the gold standard method of comparison with other techniques. Nevertheless, the not random distribution of the IS*6110* locus within the genome represents its limitation (van Embden et al., 1992). This limitation, together with the presence of less than five IS*6110* hybridizing bands, accounts for the need for secondary markers to determine epidemiological links of transmission (Burgos et al., 2004).

1.4.1.2 Polymorphic guanine-cytosine-rich repetitive sequence (PGRS) restriction fragment length polymorphism typing

PGRS is a second restriction fragment length polymorphism (RFLP)-typing method, which shows a discriminatory power close to the IS*6110* one. PGRS regions are present in multiple chromosomal clusters and comprise many imperfect repeats, which code for the C-terminal end of a novel class of proteins of unknown function. The limitation of this secondary markers is the complexity in the RFPL pattern, due to the properties of the PGRS locus (Burgos et al., 2004).

1.4.1.3 Spoligotyping

All the RFLP-based analyses require to culture the bacillus and are technically demanding and costly. On the contrary, PCR-based methods permit to carry out the analysis directly on clinical samples and to fingerprint multiple *M. tuberculosis* strains simultaneously (Xet-Mull et al., 2001). One example of this secondary marker technique is spoligotyping. The spoligotyping method examines a direct repeat (DR) sequence comprising a repetitive 36-bp element separated by a short nonrepetitive sequence. *M. tuberculosis* strains are differentiated depending on the presence or absence and the number of spacers.

Spoligotyping has the advantage of being cost-effective and easy to perform. Moreover, it is specific for typing the *M. tuberculosis* complex, albeit its lower discriminatory power compared with the IS*6110* typing (De La Salmonière et al., 1997).

1.4.1.4 Mycobacterial interspersed repetitive unit variable number of tandem repeats and other polymerase chain reaction-based techniques.

Other examples of PCR-based techniques with significant discriminatory power and reproducibility are the mixed-linker PCR and the variable number of tandem repeats (VNTRs). Between these two new techniques, only the mixed-linker PCR is comparable with the IS*6110* typing. The mixed-linker PCR method relies on IS*6110*-generated polymorphism, therefore limiting its use against low-band-number isolates (Kremer et al., 1999).

Mycobacterial interspersed repetitive units (MIRUs) identify novel polymorphic loci used to develop a new PCR-based system independent from the IS*6110* typing method (Supply et al., 1997). MIRUs are a specific class of VNTRs, and each comprises strings of short repetitive sequences (<100 bp). PCR amplification across each MIRU yields fragments of different sizes from different strains. The analysis of 12 of the most hypervariable loci shows a discriminative power similar to the IS*6110* typing. The MIRUs profile assigned a 12-digit number for each strain typed, making it suitable for interlaboratory comparison. The main limitation of this method is the technical difficulty in the sizing of multiple small PCR fragments (Mazars et al., 2001).

1.5 *Mycobacterium tuberculosis* physiology

Mycobacterium genus includes 60 known species, including some prominent pathogens that cause severe diseases in humans and other mammals. Among these species are the aetiological agents responsible for leprosy (*Mycobacterium leprae*), buruli ulcer (*Mycobacterium*

ulcerans), and TB (mainly *M. tuberculosis,* but also *Mycobacterium bovis, Mycobacterium africanum*, and M*ycobacterium Canetti)*. *M. tuberculosis* is a rod-shaped Gram-positive bacterium with a complex and lipid-rich cellular envelope. However, the presence of waxy mycolic acids in the cell wall prevents efficient penetration of the Gram stain, whose outcome is often ambiguous to interpret. Therefore, the preferred differential staining technique is a so-called acid-fast staining technique, referred to as Ziehl-Neelsen staining. The bacillus width and height range between 0.3 to 0.6 μm and 1 and 4 μm, respectively. *M. tuberculosis* is an aerobic-to-facultative-anaerobic intracellular pathogen capable of entering into a dormant state. It shows high genetic stability and significantly slow growth, with a generation time spanning between 18 and 24 hours under optimal growth conditions *in vitro* (Ducati et al., 2006).

1.5.1 General features of M. tuberculosis genome

The organization of the mycobacterial genome started to be deciphered in 1998 when the first *M. tuberculosis* genome (H37Rv strain) was entirely sequenced (Cole et al., 1998). The size of the *M. tuberculosis* reference genome is 4.4 megabase pairs (Mb) (**Figure 3**) (Cole et al., 1998), and it codes for 401 proteins (~91% of the potential coding capacity), 13 pseudogenes, 45 tRNA genes, 30 ncRNA, 3 rRNA, and 2 miscRNA genes (Waman et al., 2019).

The identification and attribution of specific functions were possible only for approximately 40% of the identified open reading frames (ORFs) thanks to the availability of the sequence of the *M. tuberculosis* genome combined with comparative genomics approaches. Fragmentary information or similarities were determined for 44% of the putative ORFs, and an unknown role was attributed to the remaining 16%, which may exert a function specific to mycobacteria (Ducati et al., 2006).

In bacteria, gene transcription in the same polarity as the replication commonly correlates with a more efficient expression. For example, in *Bacillus subtilis,* around 75% of genes display this property. On the contrary, in mycobacteria, gene transcription and polarity of replication coincide only for ~59% of the genes. This more even distribution, a unique mycobacterial feature, might be one of the possible sources of the slow growth of *M. tuberculosis* and its infrequent replication cycle (Cole et al., 1998).

The *M. tuberculosis* genome shows a very high (65.6%) but relatively constant guanine and cytosine (GC) content. Indeed, the GTG initiation codons are more frequent (35%) than in model organisms, such as *B. subtilis* and *Escherichia coli*, although ATG remains the most common start codon (61%). Furthermore, mycobacterial proteins are particularly rich in amino acids encoded by GC-rich codons, *i.e.,* alanine, glycine, arginine, and tryptophan, than amino acids

encoded by adenine and thymine (AT)-rich codons, *i.e.,* asparagine, isoleucine, lysine, phenylalanine, and tyrosine (Cole et al., 1998).

Content removed for copyright

Figure 3. Circular map of the chromosome of M. tuberculosis H37Rv. *The external circle reports the scale in Mb, in which 0 indicates the origin of replication. The ring below details the location of stable RNA genes (blue and pink indicate tRNAs and others, respectively), and direct repeat region (pink cube). The coding sequence for both strands is described by the second ring inwards (clockwise and anticlockwise in dark and light green, respectively). The third ring indicates the location of insertion sequences (in orange) and 13E12 REP family (in dark pink), and prophage (in blue). The fourth and fifth ring displays the location of PPE family members (in green) and PE family member (purple, excluding PGRS), respectively. The sixth ring reports the location of PGRS sequences (dark red). In the center, the histogram displays the G + C content (G + C <65% in yellow, G + C >65% in red (Cole et al., 1998).*

1.5.1.1 M. smegmatis as a model to study M. tuberculosis

M. smegmatis is a fast-growing saprophytic mycobacterial species isolated in 1885 by Lustgarten from a syphilitic chancre. Although it can rarely be infectious, several human infections (*i.e.,* skin and soft tissue infections, osteomyelitis, localized abscesses, and infections due to the installation of catheters and pacemakers, and cardiac operations) have been reported (Singh and Reyrat, 2009). It is a bacillus shaped bacterium, with a length ranging from 3.0 to 5.0 μm. It has a similar cell wall as the human pathogen *M. tuberculosis*, and for this reason, it can be stained with

the Ziehl-Neelsen method. Under optimal conditions *in vitro*, *M. smegmatis* has a generation time of around 3 hours. Depending on the used media, it forms visible colonies between 3 to 5 days (Singh and Reyrat, 2009). It does not present any flagella or pili; however, it can move through sliding motility. Lastly, *M. smegmatis* can also form biofilms (Martínez et al., 1999; Recht and Kolter, 2001)

The Institute of Genomic Research fully sequenced the *M. smegmatis* mc^2155 genome in 2004, which is hypertransformable and isolated from the reference strain ATCC 607 (Snapper et al., 1990). Its circular genome is around 6.9 Mb (1.7 times bigger than *M. tuberculosis* genome) with a high GC content (67%), coding for 6938 genes (~90 % of the potential coding capacity) (Deshayes et al., 2007).

A comparative genomic analysis showed that *M. smegmatis* and *M. tuberculosis* genomes share at least 2000 highly conserved genes (70%) (Catanho et al., 2006).

Hence, this non-pathogenic mycobacterial species has been proposed as a useful, simple, and attractive model to study the pathogenic species, as *M. tuberculosis*. The use of *M. smegmatis* as a model to study *M. tuberculosis* enabled to discover plasmids, phages, mobile elements, and the generation of genetic tools, such as specific gene-inactivation and gene-reporter systems (Singh and Reyrat, 2009). The difference in the genome size between these two mycobacterial species, their different growth rates, and the absence in *M. smegmatis* of all the pathogenic features described for *M. tuberculosis* can lead to arguing that these two mycobacterial species are probably too evolutionary distant, which might imply that *M. smegmatis* could not represent a proper model to study TB. Although the use of *M. smegmatis* can contribute to elucidate genus-specific or species-specific genes, their real functions, particularly true for the study of virulence factors, must be confirmed in *M. tuberculosis.* Indeed, *M. smegmatis* represent a more accessible genetic model to manipulate to unveil the tubercle bacilli's biology. However, it should be noted that *M. tuberculosis* displays a complex interaction with its human host, which has to be accounted for in understanding the biology of this successful pathogen (Barry, 2001).

1.5.2 Mycobacterial rrn operon

Slowly growing mycobacteria have a single ribosomal RNA (rRNA) operon (*rrn*). In contrast, faster-growing mycobacteria have two *rrn* operons (Bercovier et al., 1986). Phylogenetic analysis of the 16S rRNA locus supports the hypothesis that *Mycobacterium* ancestral strain owned two rRNA operons, namely, *rrnA* and *rrnB*. The *rrnA* operon is located downstream of the *murA* gene, while *rrnB,* if present, is found downstream of the *tyrS* gene (Cook et al., 2009). The loss of the *rrnB* operon originated two clusters of mycobacteria having either the *rrnA* operon, including *M. leprae* and *M. tuberculosis,* or both *rrn* operons, including *M. smegmatis*,

Mycobacterium abscessus, and *Mycobacterium chelonae* (Stadthagen-Gomez et al., 2008). Sander and colleagues proved that there is no association linking the number of operons per genome and the growth rate. Thus, the presence of a second *rrn* operon shows to have a redundant function (Sander et al., 1996). Unlike most eubacteria in *M. tuberculosis*, the *rrn* operon is located about 1500 kilobase pairs (kb) far from the origins of replication (*oriC*), which was also proposed as one of the possible causes of the slow growth of *M. tuberculosis* (Cole et al., 1998). Nevertheless, to date, there is no clarity as to the causes of the slow growth rate of *M. tuberculosis*, and whether one or more factors are concerned. For instance, also the reductive evolution and the presence of a very high number of genetic modules encoding toxin-antitoxin (TA) systems (more than 80) are among the alleged causes of this typical characteristic of *M. tuberculosis* and other pathogenic mycobacteria.

1.5.3 Mycobacterial cell envelope

Mycobacteria exhibit a unique cell envelope (**Figure 4**), which serves as an interface with the host. The composition of the mycobacterial cell envelope and its immunoregulatory capacity are critical determinants for the outcome of TB infection. Interestingly, the cell envelope dynamically changes, both structurally and functionally, across the all infection steps, and its dynamic variation may enable *M. tuberculosis* to manipulate the host immune response, adapt to the host environment, and tolerate antitubercular chemotherapy (Dulberger et al., 2020).

Differentially from *E. coli* and *B. subtilis,* mycobacteria deposit cell wall asymmetrically at the cell pole. Mycobacteria divide asymmetrically, which results in two daughter cells with different growth rates, sizes, and distributions of macromolecules. This diversity among the daughter cells might drive a differential response to host immunity and drugs. The biosynthesis on the mycobacterial envelope is tightly regulated both in space and time. Spatially, the molecular machinery necessary for mycobacterial cell wall growth act coordinately and are either anchored in the inner membrane or localized in microdomains in the growing cell pole (Hayashi et al., 2016). Temporally, the mycobacterial envelope's biosynthesis followed a sequential order at the septal side, where the peptidoglycan is laid down first, followed by the mycomembrane (Zhou et al., 2019).

While the biochemistry and the structure of the mycobacterial envelope start to be understood more in-depth for bacilli in the logarithmic phase of culture, its remodeling during the *M. tuberculosis* infection is more challenging to investigate. The current understanding about mycobacterial remodeling during infection relies upon data gathered from *in vitro* and *in vivo* studies, which cannot completely mirror the heterogeneity of the *M. tuberculosis* infection in its natural host. *In vitro* and the early phase of infection, *M. tuberculosis* displays a rapid growth,

which shifts to a growth stasis when the bacillus undergoes to stress conditions *in vitro* and during the establishment of chronic infection. Moreover, the term growth stasis does not involve a complete arrest of *M. tuberculosis* growth, but a dynamic equilibrium between growth and death, in which the tubercle bacillus is exposed to adaptive immunity, lower oxygen tension, detergents, and oxidative and osmotic stress (Dulberger et al., 2020).

The mycobacterial cell envelope (**Figure 4**) is composed of four different layers: (i) cytoplasmic membrane, (ii) cell wall, (iii) surface lipid, and (iv) capsule. The cytoplasmic membrane is composed of canonical membrane lipids, such as glycerophospholipids, phosphatidylinositol mannosides (PIMs), lipomannans (LMs), and lipoarabinomannans (LAMs) (Bansal-Mutalik and Nikaido, 2014). The presence of PIMs, LMs, and LAMs results is critical for both the maintenance of the membrane integrity and the manipulation of the host's immune system. Furthermore, PIMs are responsible for the low permeability of the membrane (Bansal-Mutalik and Nikaido, 2014). Hence, it has been hypothesized that the impermeability could operate in synergy with intrinsic resistance mechanisms as the activation of efflux pumps or enzymatic defense systems (Nguyen & Thompson, 2006). PIMs are predominantly present in rapid growth, and, contrarily to the LMs and LAMs, are downregulated in stasis. The PIMs, LMs, and LAMs differential presence in the rapid growth and stasis phase appear to be critical for the infection outcome. Indeed, while PIMs in the early phase of the infection might promote the infection's progression, the high level of LAMs, in the chronic stage of infection, might protect the formed granuloma from the sterilizing action of the immune system (Dulberger et al., 2020). The cell wall is formed by the peptidoglycan, which preserves the cell shape. It has a layered, honeycomb structure formed through the crosslinking by peptides of alternating linear strands of N-acetylmuramic acid and N-acetylglucosamine (GlcNAc) sugar (Meroueh et al., 2006). Although the peptidoglycan can stimulate both the innate and adaptive immunity, its chemical structure is believed to not change in both the active and static phase of the infection. Also, if, from one side, its high level during the active phase of the infection can activate the innate immune response, promoting, in some cases, the clearance of the infection, on the other side, it can induce the maturation of the granuloma recruiting lymphocytes in the ongoing infection (Dulberger et al., 2020). In the middle layer of the cell wall, the peptidoglycan, with a rhamnose-GlcNAc linker disaccharide, is connected to arabinogalactan (Alderwick et al., 2015). The covalent bond between the arabinogalactan and the peptidoglycan suggests that its metabolism follows the peptidoglycan dynamic during active growth (Dulberger et al., 2020).

The use of biochemical fraction and electron microscopy approaches showed that a typical feature of the third layer of the mycobacterial cell envelope is the presence of mycolic acids (Brennan & Nikaido, 1995) and proteins. This third layer is also known as mycomembrane, and it can be divided into two leaflets.

Content removed for copyright

Figure 4. Model of the mycobacterial cell envelope. *The four layers of the mycobacterial envelope and the proteins participating in their formation are here reported. In the bottom lower layer structural information of the proteins involved in the biosynthesis of the mycobacterial cell envelope are indicated. The dashed line indicates portions of the proteins for which there are not crystal structure resolved. PknB (Protein Data Bank (PDB) entries 2KUI and 1MRU) regulator of peptidoglycan metabolism during active growth, GlfT2 (PDB entry 4FIY) arabinogalactan glycosyltransferase, KasA (PDB entry 4C6X) β-ketoacyl synthase, FtsZ (PDB entry 4KWE) cytokinetic protein involved in the formation of a contractile ring, PonA1 (PDB entry 5CXW) a bifunctional penicillin-binding protein (PBP), EmbC (PDB entry 3PTY) an arabinotransferases, Mvin-FhaA forkhead-associated (FHA) domain complex (PDB entry 3OUN) a lipid II flippase (Mvin) and its putative inhibitor (FhaA), CmaA2 (PDB entry 1KPI) a trans-cycopropanase, LDT2 (PDB entry 3TUR,5DUJ) a L,D-transpeptidase 2, and MspA (PDB entry 1UUN) a porin. PIMs are indicated in purple (inositol) and light purple (mannose). Mannose residue in a lighter purple indicates LMs. LAMs display branched, light green arabinose chains. Peptidoglycanes are in blue. D-D and D-L crosslink are respectively indicated in dark blue and light blue. Arabinogalactan (galactan) and arabinan are indicated in dark and light green, respectively. Trehalose is represented as two hexagons (in dark orange). Trehalose is linked to the mycolic acids in TMM and TDM. For the mycolic acids, modifications are as followed reported: α-cis/cis-cyclopropane (light yellow), keto, trans-cyclopropane (dark yellow), keto, cis-cyclopropane (light orange), metoxy, trans-cyclopropane (orange), metoxy, cis-cyclopropane (dark orange). PDIM are colored in red. In the reported model, several classes of surface and cytoplasmic membrane lipids are not reported. Modified from Figure 1 of Dulberger et al. (Dulberger et al., 2020).*

The outer one is mostly composed of mycolic acids. Mycolic acids are 60-90 carbons long-chain fatty acids with short (22 to 24 carbons) and long (40 to 64 carbons) branches, composing up to 60% of the mycomembrane. They can be either free or attached to trehalose sugar (forming either trehalose monomycolate (TMM) or trehalose dimycolate (TDM))(Marrakchi et al., 2014). In the inner leaflet, the mycolic acids are covalently attached to the arabinogalactan of the mycobacterial envelope's inner lower layer (Minnikin et al., 2015). Lastly, due to its physical properties, the mycomembrane limits molecules' passage by passive exclusion and guarantees resistance to the most common antibiotics. The mycomembrane does not only serve as a physical barrier but also to modulate host cell behavior. Indeed, the biosynthesis of mycolic acid not only correlates with the growth of the bacteria, but mycolic acids can also undergo chemical modifications (*i.e., cis*- or *trans*-cyclopropanation, esterification) and influence the course of the *M. tuberculosis* infection. These mycolic acid modifications have been shown to modulate, for instance, the production of tumor necrosis factor and virulence (Dulberger et al., 2020).

Moreover, in the mycomembrane, there are many molecules with potent modulating activity on the innate and immune responses, which demonstrates the ability of *M. tuberculosis* to have an active role in influencing the progression of infection (Cook et al., 2009b). Among them, the phthiocerol dimycocerosate (PDIM) plays a critical role during the infection. Indeed, PDIM might also promote phagosomal rupture and promote a type I interferon-mediated immune response. Furthermore, *M. tuberculosis* can mask pathogen-associated molecular patterns (PAMPs) of the cell wall from the innate immune systems. This mechanism would allow the pathogen to recruit naive and not microbicidal macrophages (Cambier et al., 2014). The mycobacterial envelope's outer structure is the capsule, described as a loose matrix of glucans and secreted proteins. It has been shown that the capsule can influence both the interaction with the host and modulate the bacillus virulence. In this respect, some glycans in the capsule mediate the bacilli's adhesion to the cell's host. Also, in the capsule, secreted enzymes, such as catalase/peroxidase and superoxide dismutase, may help *M. tuberculosis* to resist the host's microbial mechanisms. Lastly, the capsule might also represent a passive physical barrier and limit macromolecules' diffusion towards the inner parts of the envelope (Daffé and Etienne, 1999).

1.5.4 Cellular metabolism

The analysis of the *M. tuberculosis* genome revealed a prototroph microorganism. It can synthesize all the essential amino acids, vitamins, and enzyme cofactor required for its survival (Cole et al., 1998). The ability of mycobacteria to use a wide variety of carbon sources contributes to their high metabolic flexibility, which is essential for the survival of *M. tuberculosis* inside the

host. Little is known about how mycobacteria sense the carbon availability and adjust their metabolism within the host. However, fatty acids constitute the primary carbon source (Cook et al., 2009). It is still an open question whether the bacillus catabolizes host lipids or its own during chronic persistence (Glickman and Jacobs, 2001). Several studies demonstrated that *M. tuberculosis* metabolizes host-derived cholesterol, odd-chain fatty acid, methyl-branched fatty acids, and amino acids. The oxidation process of these molecules funnels into propionyl-CoA, a three carbon atoms intermediate, with a toxic effect if present in excess. However, *M. tuberculosis* can overcome its toxicity, directing it in the 2-methylcitrate cycle. In this process, both Icl-1 and Icl-2 enzymes play an essential double role. On the one hand, they help the bacillus to overcome carbon loss, and on the other hand, they prevent the accumulation of propionyl-CoA (Gengenbacher and Kaufmann, 2012).

1.5.5 Regulation and signal transduction

The adaptive potential of *M. tuberculosis* is conceivably associated with its highly integrated and coordinated gene expression. *M. tuberculosis* genome encodes for around 190 defined and putative transcription regulators: 13 sigma (σ) factors, 11 paired two-component regulatory systems, 5 unpaired homologous regulators, 11 protein kinase, and more than 140 other putative transcriptional regulators (Flentie et al., 2016; Manganelli et al., 2004).

1.5.5.1 Sigma factors and promoter organization

Sigma factors in association with the RNA polymerase fine-tune transcription initiation. Variation in sigma factor activity may serve as a strategy to modulate gene expression and overcome the host defense. The mycobacterial genome displays the highest ratio of sigma factors to genome size and only codes for sigma factors belonging to the σ^{70} family. It exhibits one essential housekeeping sigma factor (SigA), one stress-responsive (SigB), and 11 alternative sigma factors. In optimal growth conditions, *M. tuberculosis* expresses all the 13 sigma factors, integrating stress-associated transcriptional regulators into essential cellular processes. A global change in the sigma factor expression takes place under stress conditions, and SigE and SigG play a crucial role during the infection process (Flentie et al., 2016). The regulation of sigma factors activity not only depends on their mRNA level but also by the regulation of the protein activity, which relies on their binding to anti-sigma factors. Anti-sigma factors recognize specific sigma factors inactivating them. They can then be released and activated upon precise stimuli (Manganelli et al., 2004).

The formation of a specific RNA polymerase holoenzyme with a sigma factor determines the recognition of a specific promoter. The σ^{70} factors recognize the -10 and the -35 consensus elements of promoters. In *M. tuberculosis,* the -35 element is not conserved and appears not to be essential for gene transcription. In contrast, the -10 element is highly conserved and is essential and, in some circumstances, sufficient for transcription (Newton-Foot and Gey Van Pittius, 2013).

In *E. coli,* the -10 region or Pribnow box has the canonical TATAAT motif, which is less stringent in mycobacteria. In the study of the mycobacterial promoter, Cortes and colleagues identified a TANNNT -10 conserved motif (in the 73% of promoter sequenced), which is centered 7-12 bp upstream of the primary Transcriptional Start Sites (TSSs). A more in-depth analysis of the motif demonstrates that while the NNN internal region does not display any base preference, the three nucleotides preceding the TANNNT element influence the promoter activity. In the 49% of promoters containing the TANNNT motif showed the 3 base pair sequence [G/C][A/G]N, reporting the CGN sequence 45% of cases. Moreover, when the TGN sequence precedes the TANNNT motif (in 7% of the cases), an extended consensus element with an enhanced promoter activity is identified (Agarwal and Tyagi, 2003; Cortes et al., 2013) The absence of the TANNNT motif in 27% of cases could identify promoters bound by alternative sigma factors. Interestingly, Cortes and colleagues also proved that the *M. tuberculosis* transcriptome contains a high number of leaderless transcripts. The functional characterization of those leaderless transcripts showed a lack of mRNA coding for growth function, such as energy generation and ribosomal proteins, and in mycobacteria-specific gene families (type VII secretion systems and PE/PPE proteins). On the contrary, leaderless transcripts are abundant in the TA modules and might play an essential role in nonreplicating *M. tuberculosis* cells (Cortes et al., 2013).

1.5.5.2 Two-component systems and transcription factors

Two-component systems (TCSs) are bacterial signal transduction systems that sense and respond to stressful conditions and changes in the outside environment. A typical TCS includes at least one membrane-bound histidine kinase, acting as a sensor and a response regulator. The histidine kinase senses specific environmental stimuli, autophosphorylates, and phosphorylates the cognate response regulator. In turn, the response regulator binds and activates a specific regulon. *M. tuberculosis* encodes 12 complete TCSs, among which MtrAB and PrrAB are essential. The MtrAB TCS colocalizes with the cell division machinery, allowing the bacilli to abort cell division under stress conditions. PrrAB TCS has not been fully characterized yet, but might have a role in intracellular growth. Specific stresses induce non-essential TCS, such as DosRST, SenX3/RegX3, and PhoPR (Flentie et al., 2016). The DosRST system, which plays a role in nonreplicating persistence, contains two histidine kinases, DosS and DosT, which act as redox and

hypoxia sensor, respectively, and both can activate the DosR response regulator (Kumar et al., 2007)

The SenX3/RegX3 TCS acts as a critical sensing system in response to low phosphate levels encountered by *M. tuberculosis* during the infection. Its activation controls the expression of several genes, such as genes coding for proteins involved in the phosphate uptake, lipid metabolism, translation, DNA replication, and repair, which are essential in promoting *M. tuberculosis* growth under this condition (Flentie et al., 2016).

Lastly, another important and non-essential TCS is PhoPR. Although it is induced under low pH conditions, it is considered necessary for the physiological growth of *M. tuberculosis* under all growth conditions. PhoPR also plays a role in the virulence of the pathogen. Indeed, *M. bovis* and *M. africanum* strains carrying mutations in *phoPR* display a reduced virulence. It is involved in regulating several pathways involved in lipid biosynthesis, *dosR, dosS*, and gene related to the ESX1 secretion systems (Flentie et al., 2016).

M. tuberculosis also encodes several essential and non-essential transcription factors (TFs). Essential TFs are the 7-member family of WhiB iron-sulfur (Fe-S) TFs, which are involved in redox sensing and iron availability. However, the *M. tuberculosis* genome-wide characterization of the transcriptional network showed the presence of a high number of non-essential TFs, which have not been fully characterized (Flentie et al., 2016).

1.5.5.3 Post-transcriptional regulation and RNA metabolism

The ability of *M. tuberculosis* to remodel its transcriptome as a primary means of adaptation requires balancing the synthesis and the degradation of transcripts. Transcriptome remodeling relies on alterations in transcription efficiency, mainly due to promoter strength, RNA polymerase affinity to promoters, operators, regulatory elements, and transcription termination, as well as on mRNA stability, which is often mediated by RNA regulators, such as small regulatory RNA (sRNA), 5' and 3' untranslated regions (UTRs), and riboswitches.

sRNAs have already been described in *E. coli, Listeria monocytogenes,* and *Staphylococcus aureus.* They act by base-pairing with the target mRNA, and their regulatory activity has been associated with stress responses, bacterial cell-cycle, and virulence (Oliva et al., 2015). sRNA regulation provides an intermediate control over the gene expression, acting between the control of the transcription and the protein turnover. Hence, sRNA regulation results in a rapid mechanism that bacteria can exploit under environmental changes. Furthermore, it is also hypothesized to enhance bacterial cell-to-cell phenotypic variation (Komorowski et al., 2009).

There are two main known classes of sRNAs: *cis*-encoded and *trans*-sRNAs (**Figure 5**). *Cis*-encoded sRNAs (**Figure 5a**) are encoded on the opposite strand of the target RNA, which are

highly complementary, and are transcribed in the antisense orientation. For instance, antitoxins often belong to this category. *Trans*-encoded sRNAs (**Figure 5b**) are usually in a chromosomal location far from the target mRNAs, with which they share low complementarity. They act mainly by occluding the ribosome binding site (RBS) and inhibiting translation or by mRNA degradation, which happens in an RNase E-dependent manner (Morita and Aiba, 2011). sRNAs range between 50 and 400 nucleotides and act by generating sRNA-mRNA duplex molecules either with the coding mRNA or with the 5'UTR. The formation of these duplex structures cannot only repress translation and alter mRNA stability, ultimately inhibiting gene expression, but in some cases, it can also lead to the disruption of RNA secondary structures and activate gene expression (Waters and Storz, 2009). The deep sequencing of the whole transcriptome (RNA-seq) and other experimental approaches (*i.e., cloning approaches, Northern Blot, qRT-PCR, and computational predictions*) has been widely used to identify sRNAs in many bacterial species, including *M. tuberculosis.* Arnvig and colleagues were the first to prove the presence of nine putative sRNAs experimentally. The two *cis*-encoded sRNAs named ASdes and ASpks target *desA1* and *pks*, respectively, which are known to regulate lipid metabolism (Arnvig and Young, 2009). Following this pioneering study, several other groups have identified other sRNAs, such as the starvation-induced ncRV12659, the PhoP sRNA regulator Mcr7; the DosR regulated 109-nt long sRNA DrrS and the iron-starvation induced MsrI (ncRv11846) (Gerrick et al., 2018; Houghton et al., 2013; Solans et al., 2014),

Trans-encoded sRNAs necessitate the presence of Hfq to form a stable sRNA-mRNA pairing. Moreover, chaperone proteins also have a role in protecting sRNAs from the degradosome activity. Interestingly, mycobacteria genome does not encode the Hfq chaperone, the questions of how mycobacteria stabilize sRNAs, how *trans*-sRNAs recognize their targets, and lastly, of how the fate of sRNA-mRNA duplex is determined, arise (Taneja and Dutta, 2019).

A second *cis*-acting regulatory element is the 5'UTR region. Its regulatory activity relies on the formation of the secondary structure, which can enhance transcription or inhibit translation of the mRNA. For example, it is known that long bacterial 5'UTRs interact with RNA, proteins, or small molecule ligands regulating mRNA stability, as in the case of the long 5'UTRs of *infA* and *infC,* where the extensive homology is suggesting that these genes could share some post-transcriptional regulation (Arnvig et al., 2011). Interestingly, *M. tuberculosis* transcripts show long 3'UTRs, which could influence mRNA half-life and the efficiency of translation. Long 3'UTRs formation depends on the presence of an I-shaped terminator without a poly-U stretch, which determines an inefficient termination in the transcription. The long 3' UTRs (more than 50 nt-long) have the function of connecting adjacent genes for regulatory purposes. Interestingly, genes showing long 3'UTRs regions are not randomly distributed in the genome (Arnvig and Young, 2012).

Content removed for copyright

Figure 5. Regulatory small RNAs (sRNAs) and their function. *(**a**) cis-encoded antisense sRNAs (in red) share high complementarity with their target RNAs (in blue). In (**a**), two possible configurations are indicated. The left panel outlines an sRNA encoded in an antisense manner respect its target mRNA. This sRNA-RNA base-pairing will inhibit the ribosome binding and most likely induce the degradation of the transcript. The right panel shows the regulatory effect of a cis-sRNA encoded in a sequence dividing two genes located in an operon. In this case, the base-pairing of the sRNA within this sequence can lead to different outcomes: (i) causes the cleavage of the mRNA, and (ii) induces transcriptional termination and reduces the expression of the downstream gene. (**b**) outlines the regulatory activity of trans-encoded antisense RNA (in red) on their target RNA (in blue). Differently from cis-sRNAs, trans-sRNAs have a limited complementarity with their target. The base-pairing of a trans-sRNAs with its target leads to three possible outcomes: (i) it can base-pair with the 5' UTR and block the binding of the ribosome (bottom, left panel), (ii) it can form a sRNA-mRNA duplex and induced RNA degradation (bottom, middle panel), and (iii) it can sequester ribosome-binding site (RBS) and prevent the formation of inhibitory secondary structure* (Waters and Storz, 2009).

Other elements having a widespread role in the regulation of *M. tuberculosis* gene expression are riboswitches. For instance, a cobalamin riboswitch was identified and validated to affect translation by generating truncated 5'UTR transcripts. It has been hypothesized that the cobalamin riboswitch can repress the expression of downstream genes in the presence of vitamin B12. A second identified riboswitch, not fully characterized yet but conceivably relevant during infection, is the *ykok* leader or Mbox. This riboswitch is duplicated in *M. tuberculosis* and responds to magnesium starvation, which might occur during infection, due to the low magnesium concentration found in macrophages (Arnvig and Young, 2012).

While post-transcriptional regulation begins to emerge in mycobacteria, we still have a less clear understanding of RNA turnover. A first step in unveiling mycobacterial mRNA stability was done by Rustad and colleagues (Rustad et al., 2013).

In their study, they measured the mRNA half-life in both *M. smegmatis* and *M. tuberculosis*. *M. smegmatis* shows an mRNA half-life of about 5 minutes, on average closer to the values reported for model microorganism, namely, *E. coli* and *B. subtilis. M. tuberculosis* has a longer mRNA half-life, spanning between 8 and 12 minutes. This experimental evidence raised the hypothesis of a possible correlation between the slow growth of the bacillus and mRNA stability. Indeed, Rustad and colleagues demonstrated that mRNAs coding for ribosomal protein, subunits of ATP synthetase, Clp protease, and *sigA*, have a shorter half-life, as compared with genes involved in replication, recombination, metabolism, and stress response are more stable (Rustad et al., 2013).

The longer mRNA half-life of genes involved in the DNA repair and recombination processes might contribute to maintaining *M. tuberculosis* genome stable and repairing mutations accumulated during its slow replication cycle and even during dormancy. Although the host's immune response is thought to reduce or cease the bacteria replication dramatically, the duplication of *M. tuberculosis in vivo* is uncertain. Currently, the generation time of *M. tuberculosis* remains unknown in humans and nonhuman primates. Despite that, Ford and colleagues demonstrated that *M. tuberculosis* genome undergoes to mutations (Ford et al., 2011). By using high-density whole-genome sequencing (WGS), they showed that *M. tuberculosis* presents a similar mutation rate during latency as during active disease or *in vitro* exponentially growing culture. A possible explanation of the mutational burden observed *in vivo* might depend on the oxidative DNA damage (Ford et al., 2011), which might explain the longer mRNA half-life of genes involved in DNA repair.

A second study on the mRNA turnover and metabolism in non-culturable (NC) cells reported a remarkable reshaping of *M. tuberculosis* transcriptome (Ignatov et al., 2015). In this study, NC cells were generated inducing a K^+ deficiency, which can trigger the mycobacterial cell to enter a dormant state. Moreover, to reduce the intrinsic heterogeneity of the NC bacterial

population, the authors treated the 15-day K^+-starved *M. tuberculosis* culture with rifampicin to eliminate the dividing cells (namely, 'zero-CFU'). As a result, they obtained a dormant NC *M. tub* population induced by K^+ deficiency, further characterized by a 'zero-CFU' phenotype, and used to perform a transcriptional analysis by RNA-seq. The transcriptional profile of NC cells showed a significant decrease in the total mRNA content, suggesting global repression of the protein-coding genes during dormancy. This observed reduction in the protein-coding pool of mRNAs is hypothesized to reduce the metabolic activity of the bacteria while maintaining the dormant state. If from one side, NC mycobacteria cell were characterized by a dramatic reduction in their transcriptional activity, on the other side, they were capable of conserving a low-abundance but stable transcriptome for at least ten days after reaching the 'zero-CFU' state. Functional analysis of this low-abundance but stable pool of transcripts displayed mRNA molecules coding for biosynthetic enzymes, proteins involved in adaptation and repair mechanisms, detoxification, and the control of transcription initiation. A second interesting feature of NC mycobacterial cells is the increase in non-coding RNAs (ncRNAs). In particular, the transcriptional analysis of NC cell revealed the upregulation of two small RNAs, MTS0997 and MTS1338, already known to be induced under starvation, suggesting the role of these regulatory molecules in the maintenance of dormancy. Altogether, these data raise the hypothesis that dormant mycobacterial cells might conserve crucial RNA molecules necessary for resuscitation (Ignatov et al., 2015).

Although a more profound reshape of the transcriptome was observed comparing NC cells to exponentially growing cells, Arnvig and colleagues already reported significant difference comparing the transcriptional profile of exponentially growing and stationary mycobacterial cultures. In exponentially growing cells, the coding transcriptome represents 78.4% of the annotated genome. Contrarily, for mycobacteria in the stationary phase, the pool of protein-encoding transcripts only represents 11% of the genome. Moreover, while in exponentially growing mycobacteria, mRNA encoding for proteins involved in energy metabolism, ESX type VII secretion system, PE and PPE family protein, and Type II toxin and antitoxin (TA) are over-represented, in stationary cells, the coding transcriptome was highly enriched by genes belonging to the DosR regulon (Arnvig et al., 2011).

These first studies started to shed light on mycobacterial RNA metabolism and turnover. Indeed, while the transcription regulation is better understood, the potential molecular mechanisms behind the *M. tuberculosis* ability to reshape its transcriptome by modulating mRNA stability has yet to be identified. One emerging hypothesis possibly explaining the modulation of mycobacterial RNA stability is that the enzymes involved in the degradation could limit the rate of mRNA decay. In 2019, Płonciński and colleagues proved the presence of degradosome machinery, where the RNase E and PNPase play a significant role in reshaping the transcriptome

on *M. tuberculosis* acting on the RNA turnover (Płociński et al., 2019). The role of the RNA degradosome and the RNase E will be extensively described later on.

1.6 From the host to the pathogen: a TB panorama

1.6.1 A glance at the M. tuberculosis infection cycle

The infection begins when airborne droplet nuclei (1 to 5 μm size), each one containing a few tubercular bacilli (estimated at 1 to 10), are coughed up in the air and inhaled by individuals nearby (**Figure 6**). The bacilli surviving to the innate immunity of the upper respiratory tract reach the alveoli where they can establish the infection. In the lower respiratory tract, the host develops an early innate immune response to the pathogen. This early immune response is characterized by the progressive accumulation of alveolar macrophages, inflammatory monocytes, dendritic cells (DCs), and neutrophils infected by *M. tuberculosis* and can be either immediately killed or survive. The release of intracellular bacteria from the killed cells results in the subsequent uptake from the freshly recruited cells and the expansion of the bacterial population. The innate immune stage of *M. tuberculosis* infection is considered a highly dynamic phase of infection, in which the expanding bacterial population keeps on infecting freshly recruited cells, including DCs that can initiate the adaptive immune response. The establishment of an adaptive immune response to *M. tuberculosis* is characterized by a long delay in its onset, which is approximately observed 42 days post-infection in humans. The initiation of the adaptive response requires the transport of the bacilli to the draining lymph nodes by the myeloid DCs from the lungs. In the draining lymph node, antigens against the bacilli are produced and used to activate naïve CD4+ cells, which differentiate and migrate to the side of the lung infection. At this stage of the infection, the host's adaptive immune response can arrest the progressive growth of the mycobacterial population (Ernst, 2012). After the onset of adaptive immunity, most of the infected individuals become asymptomatic. Indeed, only 10% of infected individuals will develop active TB over a lifetime, which, in most cases, occurs within 18 months from the infection. Late insurgency (>10 years) of active TB is considered rare (Esmail et al., 2014). These asymptomatic infected individuals are deemed to carry latent TB infection. The progression toward active TB remains to be fully elucidated, but a 'weakened' immune system is hypothesized to play a significant role in it. Currently, two mechanisms (CD4+ T cell depletion and Tumor Necrosis Factor (TNF) blockade) are known to promote the progression of the infection. However, they only contribute to a minority of cases (Ernst, 2012). The last stage of TB infection is the transmission, which occurs when bacteria are expelled by coughing from an individual with active disease. In

particular, most infectious individuals show cavitary TB. Cavitary TB is characterized by the destruction of the lung tissue, allowing the mycobacteria to reach a bronchus and creating an optimal environment for bacilli proliferation and dissemination into the air through coughing.

Content removed for copyright

Figure 6. The life cycle of M. tuberculosis. *The bacillus is transmitted by inhalation of aerosolized microdroplets coughed in the air by infected individuals showing cavitary TB. When the tubercle bacilli reach the lower respiratory trait, the host initiates an innate immune response, which is followed the establishment of a primary infection. This primary infection is either cleared by a cell-mediated immune response or contained inside the granuloma, leading the latent form of TB. The progress of TB can be stalled at this stage and this state might last for the lifespan of the infected individual. The progression to active TB by reactivation of the existing infection, within a lifetime, only accounts for 5–15% of the cases. The risk of progression is enhanced especially in individuals with immune-compromising factors (i.e., HIV-AIDS, diabetes, indoor air pollution and tobacco smoke). Reactivation of TB is shown to occur at the upper and more oxygenated lobe of the lung. Although active TB can be cured with drug therapy, untreated or poorly treated TB might lead to the cavities in the lungs, which allow shedding (e.g. coughing) of the bacilli through the airway. Subsequently, in a cyclic manner, the TB bacilli are transmitted to other individuals. Modified from* (Porcelli and Jacobs, 2019).

Pulmonary TB remains the majority of active cases. It leads to gradual debilitation and physical fatigue due to fever, weight loss, respiratory insufficiency (in the most advanced cases hemoptysis), and cough. Less than 2% of all TB cases describe individuals affected by disseminating TB, known as miliary TB, while up to 20% represents all extrapulmonary TB cases. Disseminating TB may occur when after the progression of the primary infection or reactivation of a latent focus, the bacilli enter in the systemic circulation and start to multiply, affecting several

organs (*i.e.,* pleura, lymph node, liver, spleen, bones and joints, heart, brain, genital-urinary system, meningis, peritoneum, and skin) (Khan, 2019). The death rate for untreated TB cases is estimated to be around 45% for HIV-negative individuals, and nearly all HIV-positive people with active TB will die (WHO, 2019).

1.6.2 Factors determining the outcome of TB

The host-pathogen interplay can result in four possible scenarios: (i) complete eradication of infection, (ii) development of active TB, (iii) a cyclic waxing-waning course alternating disease progression and control phases, and (iv) the establishment of a commensal state where the host and the pathogen coexist in an asymptomatic state (Esmail et al., 2014).

Within this interaction, both host predisposing and precipitating factors play a critical role. For instance, the integrity of the immune system and the presence of comorbidities inevitably impact TB evolution.

One determinant negatively influencing the outcome of the infection is either a too aggressive or weak immune response (known as "Goldilocks effect"). A too aggressive immune response in the early stages of the infection might extensively enhance the tissue damage and be beneficial for the bacteria. Contrarily, a too weak immune response might fail to contain the spreading of the infection, promoting bacterial proliferation in the late stages of the disease. Thus, both cases would provide a favorable environment for bacilli survival. The maintenance of the balance between pro- and anti-inflammatory factors has been recently linked, in the human population in Vietnam, to the presence of polymorphisms in the leukotriene A4 hydrolase (LTA4H). Indeed, the lipid mediator by-product of LTA4H, leukotriene B4, impairs the anti-inflammatory activity of lipoxins and promote a balanced synthesis of Tumor Necrosis Factor α (TNFα), which, in turn, limits the bacterial proliferation and necrosis of the infected immune cells (Tobin et al., 2010). Hence, a balanced immune response has a more host-beneficial TB progression promoting the clearance of *M. tuberculosis* infection, especially during the early stage of the formation of the granuloma (Kiran et al., 2016).

Age has also been considered as another critical predisposing factor. Infants, adolescents, and young adults have a higher risk of developing TB as opposed to children between 5-10 years of age (Donald et al., 2010). A possible explanation is a different balance between the dehydroepiandrosterone (DHEA - a precursor of sex steroids) and glucocorticoids. Hence, DHEA acts as an antagonist of glucocorticoids. DHEA levels increase during childhood, peak in early adulthood, and decline in the elderly. During TB infection, DHEA affects the efficiency of dendritic cells to promote the T helper type 1 (Th1) response after *M. tuberculosis* stimulation, enhancing T cell proliferation and IFN-γ production (Angerami et al., 2013).

Hence, the design of novel intervention strategies should also consider host predisposing and precipitating determinants. Their identification can help to predict high-risk subpopulations more likely to develop active TB.

1.6.3 From the early to the late stage of M. tuberculosis infection

1.6.3.1 M. tuberculosis journey in the phagosome

The full understanding of the TB infection is far to be complete. Nevertheless, the use of small mammals, such as mice, guinea pigs, and rabbits, and non-human primates, have helped to reconstruct the main steps during primary infection and the progression towards active TB.

Once *M. tuberculosis* reaches the alveoli, it is phagocytized by the alveolar macrophages through various receptor-mediated pathways (Pai et al., 2016). Indeed, the bacilli present several and diverse ligands on their surface. The type of receptor mediating the internalization of the pathogen, the receptor availability, and the antibody opsonization influence the downstream endocytic pathway, the endosome fate, and ultimately *M. tuberculosis* intracellular survival (Kumar et al., 2015). *M. tuberculosis* can also hijack the phagocytosis step to its advantage. For instance, mycobacterial membrane molecules might undermine the clustering of the receptors, and consequently alter the endocytosis process (Bussi and Gutierrez, 2019).

M. tuberculosis internalization within a phagosome, named *Mycobacterium*-containing vacuoles (MCVs), is followed by its maturation. Usually, this process includes a series of interactions with several early and late endocytic organelles ending with the fusion of the mature phagosome with the lysosomes, with the final aim of limiting bacterial growth. In 1995, Clemens and Horwitz demonstrated that *M. tuberculosis* manipulates the phagosomal maturation for its survival. They showed that in human monocytes, phagosomes containing *M. tuberculosis* do not fuse with late endosomes/lysosomes (Clemens and Horwitz, 1996). Since then, several efforts have been made to shed light on the mechanisms behind the ability of *M. tuberculosis* to block the phagosomal maturation and to survive in a non-acidic compartment. Although the escaping mechanisms of *M. tuberculosis* are not fully elucidated yet, it has been demonstrated that *M. tuberculosis* can arrest the phagosomal maturation secreting two proteins, SapM and Ndk, an acid phosphatase and a nucleoside diphosphate kinase, respectively. These two factors affect MCVs maturation through two different mechanisms. While SapM blocks MCV maturation interacting with the phosphatidylinositol-3-phosphate, PI(3)P, and removing it from the phagosome, at the same time, NdK limits their fusion with the lysosomes and the production of reactive oxygen species (ROS) (Martinez et al., 2018). Furthermore, also the early secreted antigen 6 SS1(ESX-1)

type VII secretion system (T7SS) appears to play a critical role in phagosomal rupture and bacteria escape into the cytosol at a late stage of the infection (Martinez et al., 2018). Interestingly, it was shown that infecting bacilli exhibit phenotypic variation in the activity of ESX-1, which may affect the fate of the phagosome (Ohol et al., 2010).

Also, infected macrophages attempt to respond to endosomal rupture. Schnettger and colleagues proposed that ESCRT-III (a component of the endolysosomal repair machinery) could act on the damaged phagosome. ESCRT-III would restore the endosomal integrity by promoting the fusion with other endosomal membranes. A later study proposed that ESCRT-III is recruited in a T7-secreted protein ESAT-6 (EsxA)-dependent manner into the *M. tuberculosis* phagosome. This led to the hypothesis of a dynamic balance between bacterial damage and the host repairing. In conclusion, several physiological events taking place in both the host and the pathogen, as well as the chronological progression of these events, contribute to determine the fate of *M. tuberculosis* in the host phagosome (Mittal et al., 2018; Schnettger et al., 2017).

1.6.3.2 M. tuberculosis into the cytosol

M. tuberculosis survival inside the host relies on the ability of the pathogen to modulate the immune response of the host immune system. Thus, its access to the cytosol is crucial for modulating downstream signaling pathways. However, the precise mechanism(s) *M. tuberculosis* uses to access to the cytosol, its spatial and temporal location, and how the host recognizes the pathogen in the cytosol are still open questions. Although the still debated cytosolic location of the bacillus, recent evidence strongly suggests that *M. tuberculosis* can be localized in functionally different intracellular locations, such as membrane-bound compartment, transiently damaged phagosome, and freely in the cytosol (Bussi and Gutierrez, 2019).

Currently, whether *M. tuberculosis* replicates in the cytosol of the host cell after its release from damaged phagosomal structures is still unclear. Nevertheless, experimental evidence suggests that this facultative intracellular pathogen might promote MCVs rupture to disseminate the infection (Martinez et al., 2018). The MCVs rupture consequently leads to release into the cytoplasm of the infected cell of bacterial components, like DNA and RNA, and even a few bacteria (van der Wel et al., 2007). These bacterial components can gain access to the cytosol either by ESX-1-mediated secretion, spontaneous release due to bacterial lysis, or by the permeabilization of the outer membrane of MCVs. It has also been shown that the *M. tuberculosis* DNA is a critical signaling factor for the activation of the innate immune response. Indeed, it can be sensed by DNA receptor IFNγ-inducible 16, activating the STING-TBK-IRF3 signaling pathway (Martinez et al., 2018). The outcome of this signaling cascade is the production of type 1 interferon (IFN) and interleukin-1β (1L-β), which result to be beneficial both for the pathogen and the host. While the

pathogen will benefit of type I IFN response, which can promote *M. tuberculosis* intracellular growth, on the host side, this signaling cascade will induce the death of the infected macrophages (either by apoptosis or necrosis), resulting in the onset of the adaptive immune response (Pai et al., 2016).

1.6.4 The onset of the primary infection

1.6.4.1 From phagosomal escape to granuloma formation

M. tuberculosis encounter with alveolar macrophages can end with the killing of the pathogen and the clearance of infection. Nevertheless, this first line of defense against the tubercle bacilli might fail. The latter case paves the way for *M. tuberculosis* to invade the interstitial lung tissue. *M. tuberculosis* could access to the lung interstitium either directly, infecting the alveolar epithelial cells, or through transmigration across the tissue of infected macrophages. The bacilli presence in the parenchyma settles the establishment of the primary infection and the organization of TB hallmark: the granuloma (Pai et al., 2016; Stek et al., 2018).

The initiation of the primary infection, and in particular, the priming of naive CD4+ T cell, is actively delayed by the pathogen. As compared to other bacteria, such as *Salmonella enterica* or *Listeria monocytogenes*, *M. tuberculosis* infection requires a prolonged incubation time before the manifestation of an adaptive immune response, which arises in about 5-6-week post infection

This longer interval may depend on the host incapability of actuating an adaptive immune response until *M. tuberculosis* reaches the draining lymph nodes, in which the cellular immune response initiates. The migratory step is considered to be essential for the evolution of the infection. In the early stages of TB, the intracellular localization of the bacilli prevents the antigen presentation to naive CD4+T cells. Together with the macrophages, also myeloid dendritic cells can be infected in the lungs, and either cell type can transport the pathogen to the lymph nodes. Interestingly, the transport of live *M. tuberculosis* to the local lymph node by myeloid dendritic cells is essential for the next step in the host immune response. In the lymph nodes, CD4+ T cells are primed and ready to migrate to the lungs to resolve the infection. *M. tuberculosis* can hijack this phase, lagging it. This lag phase allows the expansion of the bacterial population, which can elude the host response and install a chronic infection.

The migration of the dendritic cells to the local lymph node and the activation of the cellular immune response undergo host-to-host variations, which may explain the different outcomes of TB in different individuals (Wolf et al., 2008).

1.6.4.2 The granuloma formation

The host activation of the cellular immune response ends with the establishment of lesions known as granuloma, considered as the hallmark of TB.

The granuloma, by definition, it is an aggregation of several immune cells (*i.e.,* macrophages, monocytes, dendritic cells, neutrophils, epithelioid cells, foamy macrophages, and multi-nucleated giant cells surrounded by lymphocyte) in an organized structure in response to persistent stimuli of infectious or non-infectious nature (Williams and Williams, 1983).

The TB granuloma formation (**Figure 7**) is a dynamic process, where both host cells and *M. tuberculosis* itself modulate its formation. Newly and not infected macrophages continuously migrate to the site of infection to avoid *M. tuberculosis* spread by the phagocytizing dying infected cell. *M. tuberculosis* exploits this process to its benefit, through the ESX-1/RD1 virulence locus and the ESAT-6 induced metalloproteinase-9 (MMP-9) (Davis and Ramakrishnan, 2009).

During the formation of the granuloma, many macrophages fuse and specialize into epithelioid and foamy macrophages and multi-nucleated giant cells constructing its central part.

The primary granuloma can act as a dissemination means of the infection. After the establishment of the primary granuloma, infected macrophages can detach from it and migrate, resulting in the appearance of secondary granulomas. The propagation of the infection through macrophage migration may be an additional example of how *M. tuberculosis* manipulates the host to its own benefit (Davis and Ramakrishnan, 2009). The discovery of the expansion of the lesions inside the lungs has clinical relevance for the TB treatment, as different lesions in the same individual may respond differently to the therapy (Lenaerts et al., 2015; Ramakrishnan, 2012).

Figure 7. Schematic representation of the TB granuloma. *The formation of the granuloma is a prominent features of TB. The formation of the granuloma in the lungs of infected individuals is driven by both host and bacterial factors. A granuloma can be described as a compact, organized, and immunologically rich structure, in whch different immune cells (i.e., macrophages, monocytes, dendritic cells, neutrophils, epithelioid cells, foamy macrophages, and multi-nucleated giant cells) participated in its formation. The center of the granuloma is rich with macrophages, which can differentiate into other cell types, such as epithelioid cells, multi-nucleated giant cells, and foamy macrophages. The outher layer of the granuloma is formed by a lymphocytic cuff, including both B and T cells. Picture from* (Ndlovu and Marakalala, 2016).

Lastly, the arrival of T and B lymphocytes determines the production of the periphery cuff, which compact the granuloma structure. The lymphocyte's occupation of the infection site, around 14-21 days post-infection, restricts the bacterial proliferation and enhances their macrophages-mediated killing (Ndlovu and Marakalala, 2016).

1.6.4.3 Granuloma remodeling and TB progression

From an evolutionary point of view, the granuloma formation is considered an immunological response towards persistent elements whose dimensions are too large to be phagocytized by a single macrophage, with the final aim of containing the infection. Hence, granuloma formation has often been considered a self-protective mechanism beneficial for the host (Williams and Williams, 1983).

The granuloma can be considered as a dynamic environment, which undergoes constant remodeling. In infected individuals, three types of granulomas can be found: (a) solid granuloma (mostly in the latent phase of the infection), (b) necrotic granuloma (marks of an early stage of active TB), and (c) caseous granuloma (for end-stage or severe TB). All these types of lesions can also coexist in the same infected individual. This coexistence can either represent the development of the same lesion through a continuum of different forms or can be specific to the lung location (Gengenbacher and Kaufmann, 2012). Moreover, host-specific factors, such as pro- and anti-inflammatory eicosanoids, can contribute to the lesion fate (Lenaerts et al., 2015). Indeed, each granuloma is a distinct lesion with a separate fate, reflecting a heterogenous immune response within the host. Ultimately, the collective fate of several granulomas dictates the clinical course of infection (Lin et al., 2014).

TB progression towards the active form starts when the caseum is formed within the granuloma. The caseum is a cheese-like structure accumulating after the necrosis of macrophages. Molecular characterization of the caseous granuloma also shows a hypoxic environment rich in lipids, where pro-inflammatory pathways are highly abundant (Marakalala et al., 2016).

During granuloma remodeling, infected macrophages die either by necrosis or apoptosis. Interestingly, both processes can facilitate and inhibit bacterial growth under different conditions. Hence, if, on the one hand, the granuloma is a crucial structure to restrict *M. tuberculosis* proliferation, on the other hand, *M. tuberculosis* can turn the granuloma environment to its own advantage (Ramakrishnan, 2012).

Necrosis. The necrotic process results in the loss of membrane integrity. Thus, the macrophages, undergoing this type of death, release *M. tuberculosis* in the extracellular environment. Here, *M. tuberculosis* finds a milieu favorable for its proliferation, in particular in the so-called 'soft' caseum. Within this niche, bacilli assume the typical cording phenotype, a multicellular bundle compacted by mycobacterial lipid molecules, and harder to be phagocytized (Ndlovu and Marakalala, 2016; Ramakrishnan, 2012). Both the host and *M. tuberculosis* can induce macrophage necrosis. On the one hand, the host production of TNFα causes macrophage necrosis. Both TNFα excess and absence negatively affect the host response to the infection. On the other hand, *M. tuberculosis* modulates and induces necrosis through the production of lipoxin A4 (LXA4), which, in turn, suppresses the activity of TNFα (Tobin et al., 2010).

Apoptosis. In contrast to necrosis, apoptotic macrophages show nuclear collapse and cellular fragmentation, which produces spherical membrane structures wherein the bacteria are trapped. These membranous structures are further engulfed by non-infected macrophages and recruited to the site of infection through the ESAT6-MMP9 pathway. As already discussed above, *M. tuberculosis* might be exploiting this step to disseminate the infection throughout healthy macrophages (Ndlovu and Marakalala, 2016; Ramakrishnan, 2012).

It is still unclear which of these two processes, necrosis or apoptosis, are more detrimental to the host, and whether they are activated independently or if there is cross-talk between them.

Necrosis is essential for the progression of active TB. The breakdown of necrotic areas of the granuloma liquifies the caseum inducing its cavitation. Whenever a cavitary lesion forms, it can undergo opposite fates: rapidly grow and resolve, continue to expand, or encounter a wax and wane cycle (Ihms et al., 2018).

It has been widely accepted that cavitary lesions arise preferentially at sites of high ventilation: perfusion ratio, anatomically represented by the apices of the lung. These regions not only would favor bacterial growth and dissemination but also show the highest mechanical stress. Ihms and colleagues proposed a model whereby the mechanical stress induced by the inhalation-expiration process would favor the formation of a tear within the structure of the cavitary granuloma. During the inspiration step, the cavitary lesion withstands a negative pressure due to external tension. Both the application of these physical forces and the non-elastic nature of the external fibrotic tissue of the granuloma create a tear. The tear will then enlarge the cavitation and the release of the bacteria into the airways. Inversely, expiration will temporarily

induce the closure of the tear (Ihms et al., 2018). Whenever *M. tuberculosis* reaches the airways, it is coughed out in droplet nuclei, and the cycle of infection can restart in a new host.

1.6.5 Latent tuberculosis infection: the hidden side of TB

1.6.5.1 A summary of the current views on LTBI

The host immune system is capable to effectively control the spread of TB infection in about 90-95% of the cases, and LTBI could be established. LTBI is defined as a persistent immune response to *M. tuberculosis* stimulation without the manifestation of clinical symptoms. Asymptomatic TB carriers are not able to spread the infection but are considered a reservoir of the pathogen, with a 5-10% risk of developing active TB over their lifetime. However, the fact that LTBI can reactivate later in life, after many years of primary infection, and how often this happens remains controversial and is still a matter of debate (Behr et al., 2018). The absence of reliable diagnostic tools for the evaluation of the LTBI status has made it difficult to concretely assess its global burden and possible consequences (WHO, 2004). Currently, the most accurate estimation of LTBI burden counts between a third and a quarter of the worldwide population latently infected by *M. tuberculosis,* which has a potential negative impact on the WHO End TB Strategy by 2050 (Houben and Dodd, 2016).

The classic view of LTBI infers that *M. tuberculosis* experiences a state of dormancy or quiescence within the microenvironments of the host. A more recent view has proposed LTBI as a more dynamic state, which spans from active bacterial replication and killing to asymptomatic forms, up to complete clearance of infection (Barry et al., 2009). Taken into account the more complex view of LTBI and also the heterogeneity of single granulomas within the same host, these two factors are questioning the mere binary clinical distribution in latent or active TB. Indeed, the interaction between the host and the pathogen manifests itself rather in a continuum of forms, ranging from active infection to complete eradication across a broad spectrum of clinical and subclinical conditions (Drain et al., 2018). A better understanding of the different clinical states of TB infection and their pathophysiological characterization could foster a better diagnosis and treatment and prevent its progression. From a clinical point of view, it is challenging to attribute a patient into a specific category, considering that the infected individuals might transit from one state to another. Also, it can be complex to assign a specific duration to each status, considering the high variability in TB progression (Drain et al., 2018).

Drain and colleagues proposed a division of the pathophysiological spectrum of TB into five discrete stages. Besides the complete clearance of the infection, LTBI, and active TB, they

suggest two other states, referred to as incipient and subclinical. Incipient TB indicates a state of infection with viable *M. tuberculosis* without any clinical symptoms, likely to progress to the active form in the absence of intervention. Radiological and microbiological assays cannot detect incipient TB. Subclinical TB indicates viable *M. tuberculosis*, responsible for non-specific clinical symptoms. Subclinical TB, contrarily to incipient TB, can be detected by the existing diagnostic assays (Drain et al., 2018).

Although several studies affirm the relevance of the latent status of TB infection and its association with a continuum of clinical forms, Behr and colleagues claim the contrary. According to their vision, TB should be exclusively defined with the terms TB reactivity, primary infection, and active TB. They strengthen the irrelevance of LTBI, on the evidence that epidemiological studies do no support the hypothesis of the different physiology of the bacilli during the asymptomatic period. Furthermore, the fact that active TB typically occurs within two years from the contact with the pathogen, and its later insurgency is rare points out the absence of bimodal distribution between what they define as primary progressive disease and reactivation. Summing up their vision, a more attentive look to individuals with active TB and their contacts might better help to eradicate TB, rather than focusing on a less convincing status such as LTBI (Behr et al., 2018).

Although the absence of a universal agreement about LTBI, the most accepted assumption is that TB is a more complex and dynamic process, where both host and pathogen have an active role. Hence, the dichotomy between latent and active has been reviewed versus a more heterogenous and continuum spectrum of conditions (Barry et al., 2009).

1.6.5.2 The physiology of M. tuberculosis during LTBI: Still more questions than answers

The physiology and metabolic status of *M. tuberculosis* during LTBI are still far from being entirely explained. The prevailing belief is that *M. tuberculosis* enters in a state of non-replicating quiescence, yet maintaining the ability to resuscitate under favorable conditions. According to the definition of LTBI, *M. tuberculosis* can be considered as dormant and persistent (Gideon and Flynn, 2011). Both concepts will be extensively discussed in the next chapter.

The triggering factors behind *M. tuberculosis* phenotypic shift towards a persistent and dormant status are the hostile host microenvironments, including the granuloma. *M. tuberculosis* is confronted with several host-induced stresses, such as nutrient limitation, low oxygen tension, the presence of oxygen and nitrogen reactive species (ROS, RNS), and shifts in pH. In response to these challenges, *M. tuberculosis* can respond by changing its growth and division rates and gene expression of pathways involved in DNA damage repair, metabolic rearrangement, neutralization of oxidants, redox modulation, and expulsion of antimicrobial molecules (Delogu

and Goletti, 2014). As a consequence, persistent bacilli are generally characterized by low metabolic activity and are difficult to isolate and study. When isolated or identified, persistent bacilli are often challenging to be cultured *in vitro*, and have been defined in several ways that indicate their state of dormancy, including viable but not culturable (VBNC) (Pai et al., 2000) and non-growing but metabolically active (NGMA) (Manina et al., 2015).

Although increasing evidence points out to a VBNC or NGMA state of *M. tuberculosis* during LTBI, we are still far away to line up its actual metabolic status. The current view supports the hypothesis that *M. tuberculosis* experiences a transition to anaerobic and alternative metabolism, including upregulation of the glyoxylate cycle and the triacylglycerol biosynthesis. Besides reshaping its energy metabolism, also modification of *M. tuberculosis* cell wall has been observed, including cell-wall free bacilli, leading to questioning the efficacy of isoniazid (INH) monotherapy proposed by the WHO to eradicate LTBI (Velayati et al., 2016).

Other factors that could contribute to the dormant state of persistent bacilli are TA systems. *M. tuberculosis* has a large number of TA systems, which exert a bacteriostatic effect during the harsh environmental conditions encountered by the bacilli during LTBI (Korch et al., 2009).

Moreover, low oxygen tension is a crucial factor thought to shape *M. tuberculosis* latency. *M. tuberculosis* copes with the hypoxia condition in the inner part of the granuloma, and in response to oxygen limitation, by fine-tuning the expression of approximately 100 genes (Rustad et al., 2009). General repression occurs in genes involved in protein, DNA, lipid, and amino acid synthesis, cell division, and aerobic metabolism, confirming the transition towards an altered metabolic activity (Rustad et al., 2009). Among 47 induced genes, there are some coding for uncharacterized proteins, but also several coding for proteins implicated in adaptation to hypoxia, such as the chaperone protein Acr; NarX, Nark2, and FdxA involved in nitrogen and energy metabolism; proteins involved in lipid metabolism and universal stress protein family. In the early stage of hypoxia, the DosS/DosT-DosR TCS is induced. The dormancy survival regulon, or DosR regulon, helps *M. tuberculosis* to shift from an aerobic to an anaerobic environment. DosR can trigger *M. tuberculosis* dormancy and is considered essential during the establishment of LTBI, and for this reason, its transcriptional response has been deeply analyzed. The general understanding, though, is that the DosR regulon is only weakly linked to *M. tuberculosis* dormancy. Indeed, the DosR regulon expression was also reported during exponential growth, and its loss only mildly affects *M. tuberculosis* dormancy (Rustad et al., 2009). A more recent view supports the hypothesis that DosR may have a more central function in the survival of extended respiratory, nitrosative, or redox stress. The weak connection of the DosR regulon with *M. tuberculosis* dormancy during hypoxia raised the hypothesis of a second mechanism downstream DosR. Rustad and colleagues analyzed the intersection of the mycobacterial transcriptome

(around 230 genes) induced between 4 and 7 days of exposure to a hypoxic environment. Their analysis showed the activation of a complex and probably redundant network of transcriptional regulators, which they named enduring hypoxic response (EHR) (Rustad et al., 2009). EHR is considered a more powerful DosR-independent induced response in a hypoxic environment. This experimental observation led Rustad and colleagues to conclude that the DosR response is not essential to establish a dormant state (Rustad et al., 2009).

Non-replicating bacilli can also undergo a process, referred to as resuscitation, where they resume an active metabolism and growth. The resuscitation mechanism was presumably attributed to a bacterial cytokine, named resuscitation-promoting factor, and initially studied in *Micrococcus luteus* (Gengenbacher and Kaufmann, 2012). Resuscitation-promoting factors promote bacterial growth by inducing the digestion and modification of peptidoglycan and triggering the metabolism activation (Chao and Rubin, 2010). *M. tuberculosis* genome encodes 5 putative resuscitation-promoting factors, which could be redundant. *Ex vivo* studies proved their role in promoting mycobacterial growth, also of bacilli present in the sputum of individuals with active TB (Mukamolova et al., 2010). An attractive model proposes that resuscitation-promoting factors would promote the resuscitation of a few dormant *M. tuberculosis* cells, so-called 'scouts' that would sense the environment. If the 'scouts' sense hostile conditions, they would die and induce dormancy of the remaining bacterial population; if the 'scouts' sense a favorable setting, they would cause the resuscitation of the entire dormant population. Such scenario, may explain the long duration of the antitubercular therapy (6–24 more months), where the activity of drugs must be exerted continuously to kill metabolic active bacilli that regularly resuscitate from the dormant status (Gengenbacher and Kaufmann, 2012).

The hypothesis of a dynamic balance between dormant and replicating *M. tuberculosis* during LTBI, in its broadest meaning, raises critical questions about the plasticity of the pathogen in response to the host defense mechanisms and the action of drugs. A deeper understanding of the molecular mechanisms underlying mycobacterial dormancy will be necessary to design more targeted and effective TB containment measures.

1.6.5.3 In vitro, in vivo, and in silico investigation of TB and LTBI

The limitations of accessing human-derived samples and the experimental impossibility of working on bacilli directly isolated from asymptomatic individuals carrying LTBI led researchers to use model systems to reproduce different stages of infection. These systems include *in vitro* tools and cell lines, different mammals as models of infection, *i.e.,* mice, guinea pigs, rabbits, and non-human primates and *in silico* approaches.

In vitro models. The *in vitro* models attempt to reproduce the adaptive *M. tuberculosis* behaviors mainly by inducing starvation to essential nutrients (carbon, nitrogen, or phosphate), and by subjecting bacilli to hypoxia and/or other stressful conditions, such as antimicrobials and host effectors and high concentration of nitric oxide (NO). Hypoxia and lower oxygen tension were the first two characterized elements of the granuloma microenvironment (Gengenbacher and Kaufmann, 2012). For this reason, *in vitro* models recreating a hypoxic environment are more widely diffuse and characterized to study *M. tuberculosis* adaptation to the host. The first model created to replicate hypoxia was the Wayne model. The Wayne model reproduces the initial steps of mycobacterial adaptation to low-oxygen tension and not the late dormant state. It is generated by sealing standing culture and incubating them until bacteria consume the available oxygen (Wayne and Hayes, 1996). A second Wayne-based model, which combines a hypoxic environment and a high throughput phenotypic screening (HTPS), is the Hypoxic Resazurin Reduction Assay (HyRRA). The final aim of this model is to identify new active antimicrobials. In the HyRRA model, hypoxia is achieved following the Wayne model. After that, the selected drugs are aseptically added, and the culture incubates for 96 hours. To finally evaluate the drugs' activity, a resazurin cell viability assay is performed (Gibson et al., 2018). An alternative model to perform HTPS under hypoxic conditions is the Low Oxygen Recovery Assay (LORA). The LORA model, similar to HyRRA one, is a Wayne-based model to recreate hypoxia. The peculiarity of the LORA model is that it uses a luciferase reporter (*luxAB* gene) to monitor the metabolic activity of hypoxic mycobacteria. The last *in vitro* model reproducing hypoxia and used for HTPS is the Red Fluorescent Protein (RFP) model. This model uses an RFP fluorescent reporter to determine the growing status (exponential, static, and culture treated with a bactericidal drug) (Gibson et al., 2018).

Although the before-mentioned models represent a proxy to simulate the granuloma microenvironment, they can only evaluate mycobacterial adaptation to one stress factor the bacilli face during the progression of the infection. The role of nutrient starvation in the reshaping of mycobacterial biology in the granuloma microenvironment was only acknowledged later on, and, hence, the effect of nutrient starvation has been less studied than hypoxia. The first *in vitro* model attempting to reproduce the mycobacterial adaptation during the induced host-starvation is the Loebel nutrient starvation model (Betts et al., 2002). The Loebel model provokes mycobacterial starvation in an oxygen-rich media. In this model, the bacilli are grown in rich media for a week, at which point they are pelleted and resuspended in phosphate saline buffer (PBS). Under these conditions, bacilli have been shown to keep low but constant intracellular ATP levels (Süel et al., 2006). As the described models inducing hypoxia, the main limitation of this model is the possibility to look at only one environmental factor (*i.e.,* nutrient starvation). Another model aiming to reproduce and investigate the effect of nutrient deprivation on *M. tuberculosis* is the

stationary chemostat model. This model includes using a chemostat to tightly control factors such as pH, temperature, and dissolved oxygen. In this model, mycobacteria are cultured in rich media with a defined concentration (50%) of dissolved oxygen until all the nutrients have been depleted. The primary advantage of this model is the rigid control of several environmental parameters through the use of a chemostat (Betts et al., 2002).

Another factor, even less studied, that mycobacteria face during the infection is NO, which is produced by the activated macrophages as both signaling molecules and antimicrobial (Delogu and Goletti, 2014). Currently, there is not yet a fully developed model to study the physiological reshape of mycobacteria in the presence of NO. Nevertheless, a first attempt has been made cultivating the bacilli in rich media to which a low, non-toxic concentration of NO has been added. The researchers hypothesized that this low, non-toxic concentration of NO could inhibit bacterial respiration and trigger a similar metabolic status the bacilli assume in the granuloma (Gibson et al., 2018). Lastly, to explore the mycobacterial metabolic response and drug susceptibility also 100 days-old and unshaken cultures have been used (Hu et al., 2003).

In vivo models. The use of *in vivo* animal systems has been an enormous asset, helping the researchers to unveil the biology behind TB and LTBI. Hence, the possibility of infecting the animal by the aerosol route and the development of both the innate and adaptive immune response to control the spreading and progression of the infection are key factors that contribute to accelerating vaccine evaluation, chemotherapeutic treatment, and predict TB relapse. These models are mice, and guinea pigs, among the most widely used for pulmonary TB, provided a valuable framework to understand the human response to TB. However, they cannot mimic the human process behind the latent infection entirely due to *M. tuberculosis* being a natural human pathogen(Gideon and Flynn, 2011).

The simple handling, low cost, less space requirement, presence of immunological tools, and the availability of both inbred, outbred, and transgenic strains affirm the mouse's use as one of the most widely and preferred animal model. Among the first mouse models used, there are the Cornell (Mccune et al., 1956) and the low-dose chronic (or untreated) (Sever, 1957) mice models, which both fail to mimic LTBI optimally. The mice's inability to mimic LTBI is due to the absence of pathological hallmarks after establishing the infection, such as the caseating granuloma and lung cavitation. Although considerable progress has been made to fine-tune the mice's immune system, they cannot reproduce mycobacterial latency (Chao and Rubin, 2010).

Only recently, a study performed in C3HeB/FeJ showed that this mouse model could develop necrotic granulomas after infection with *M. tuberculosis*. The lesions observed are reported to be more similar to the one developed in infected humans (Irwin et al., 2015). To overcome the lack of similarity in the immunological response between the mouse model and the humans, researchers have developed humanized mice for TB. Although this model can recreate

the same pathological lesions, the humanized mouse model for TB displays impairment in controlling the bacterial burden and an abnormal T-cell response after *M. tuberculosis* infection (Singh and Gupta, 2018).

A second model often employed is the guinea pig. They are highly sensitive to *M. tuberculosis* and can recreate several aspects of human infection, such as primary necrotic granulomas. Similar TB physiopathology between guinea pigs and humans have been determined using this animal model to evaluate further drugs and vaccine candidates, which performed well in mice. Moreover, their bigger size also helped the researchers to perform multiple analyses over the same animals. They still represent the gold standard animal model to progress towards clinical trials. The opposing sides in using this model are related to their difficult maintenance and the restricted availability of immunological tools. Lastly, despite their similarity to humans with respect to *M. tuberculosis* infection, this animal model is still not fully able to recreate all the features of human TB (Singh and Gupta, 2018). To achieve that, a new protocol that can reproduce LTBI in guinea pigs was developed. However, although it might closely mimic a wild-type *M. tuberculosis* infection, it still requires to infected the animals with a streptomycin-dependent *M. tuberculosis* strain, (Kashino et al., 2008).

Another interesting model for TB research is the rabbit, which can closely reproduce the human features of human LTBI. Rabbits infected with *M. tuberculosis* undergo initial exponential growth of the bacilli to reduce the bacteria load around ten weeks after infection. Still, it is unclear how well they can reproduce human latency and, thus, the bacilli's dormant status (Manabe et al., 2008). Even though rabbits can closely reproduce human TB, they do not represent a widely used model because of their size and the advanced biocontainment. Moreover, there is a lack of immunological reagents, and TB clinical symptoms are not obvious. Lastly, another problem is the presence of *M. tuberculosis* in the urine, representing a significant biocontainment concern (Singh and Gupta, 2018).

To date, the most attractive models to study LTBI are the non-human primates due to their immunological similarity with the human immune system. *Cynomolgus macaque* infected with a low-dose of *M. tuberculosis* shows a heterogeneous progression of the disease, showing both active TB and LTBI (Magombedze et al., 2013). Reactivation is frequent, and it does not need immunosuppression as reported for rabbits. Moreover, TB lesions resemble human granuloma. Still, it is uncertain if the response of the macaque to the chemotherapeutic treatment correlates with the human one. The downside of this model comprises the restricted number of potential experiments that can be performed, the limited number of available reagents, the high cost, the difficulty in handling the animals, and ethical considerations (Magombedze et al., 2013).

An emergent and exciting model to study TB is the zebrafish. The close homology of the immune system of the zebrafish with the human one and the presence of essential and critical

virulence factors in *M. marinum* allow to reproduce several aspects of the human infection. Moreover, the use of optically clear zebrafish larvae permits the real-time following of the infection and specific immune cell-type contribution to the infection process. On the bacterial side, the use of *M. marinum* adds the convenience of using fast-growing mycobacteria (its generation time is around 4 hours with respect to the 24 hours of *M. tuberculosis*). Finally, several zebrafish genetic manipulations tools are available and well-characterized, allowing its easy manipulation (Cronan and Tobin, 2014).

In silico models. In 1994 Antia and Koella firstly attempted to model the bacterial evolution and its virulence (Antia and Koella, 1994). This study paved the way for other research groups, which have been investing effort in increasing our understanding of *M. tuberculosis* physiology under host-mimicking conditions generating *in silico* models. The *in silico* models allow the prediction of mycobacterial determinants and host immune response leading to either LTBI or active TB, but cannot unmask the mechanism(s) behind LTBI development and persistence (Magombedze et al., 2013). *In silico* and mathematical models can bypass the biological restrictions of the adopted *in vitro* and *in vivo* models, even though their predictions still require experimental validation. Computational models are not only inexpensive experiments but also concurrently enable the study of multiple parameters and their interaction, processing of a large amount of data, and allow for predictions that can be tested experimentally. Mathematical approaches find application in (i) creating LTBI to active TB transition model (Ruggiero et al., 2017), (ii) comprehending the impact of pharmaceutical interference over TB activation (Marino et al., 2007), (iii) modeling the different stages of TB infection, (Fallahi-Sichani et al., 2011; Hao et al., 2016), and, finally, (iv) identifying putative new vaccine candidates (Wang et al., 2013).

1.7 Diagnosis

TB is a multifaceted disease, and several aspects still necessitate experimental studies. Hence, to date, it is still not available a one fits all test for its. Indeed, the main determinant behind the choice of the diagnostic test performed depends on either the sole identification of the pathogen or for the identification of MDR-TB infection (Pai et al., 2016).

1.7.1 Diagnostic tools for active TB

1.7.1.1 Sputum smear microscopy (SSM)

SSM is a standard test that does not require sophisticated instruments and delivers results in a few hours. For these reasons, it can be easily implemented for the diagnosis of pulmonary TB also in low-income and middle-income countries, where the TB burden is high. SSM is performed over a thin layer of stained sputum (smear) on a glass slide, which is then analyzed under a light microscope. It has a sensitivity ranging between 50-60%, and high specificity (99-100%) (Mase et al., 2007). The main limitations of SSM are a lower detection in patients carrying HIV-TB coinfection, due to the low number of mycobacteria in these patients and the not good quality of the sputum. Also, SSM shows a high percentage of false-negative in children and older people. Moreover, it only detects pulmonary TB (Mase et al., 2007). Starting from 2011, the WHO recommended conducting SSM on two sputum specimens collected at the same time (WHO, 2011).

1.7.1.2 Loop-mediated isothermal amplification (TB-LAMP) for the diagnosis of pulmonary TB

TB-LAMP is a commercial molecular essay developed by Eiken Chemical Company Ltd. (Tokyo, Japan). This manual assay is based on a loop-mediated isothermal amplification of nucleic acid. TB-LAMP specifically targets the *gyrB* and *IS* regions of the *M. tuberculose* genome (WHO, 2016). It can be performed in less than one hour, with the results readable under ultraviolet (UV) light. TB-LAMP is a robust test detecting TB, which does not require expensive instruments. The WHO does not recommend the use of the TB-LAMP to detect drug resistance. Indeed, among populations at risk of MDR-TB, TB-LAMP cannot replace rapid diagnostic tests for antibiotic resistance, such as Xpert MTB/RIF, which is described below (WHO, 2016). The WHO recommends the use of TB-LAMP as a replacement of SSM for pulmonary TB in adults. It is also advised as a follow-up assay for adults with pulmonary TB symptoms and negative SSM negative (WHO, 2016).

1.7.1.3 Gene Xpert MTB/RIF assay

This automated semi-quantitative nested real-time PCR allows both the rapid detection of TB and rifampicin (RIF) resistance. It uses unprocessed sputum as a specimen, and the results are

delivered within two hours (Chao and Rubin, 2010). The WHO recommends its use to test HIV-positive or with unknown HIV-status individuals showing TB symptoms, and for people showing TB within a population at high risk of MDR TB regardless of the HIV status. Although the Gene Xpert MTB/RIF test is a critical step toward TB diagnosis, it presents several drawbacks. Among them, the short shelf life of the cartridge (18 months), the need for a very stable power supply, and its cost, including of the disposable cartridges (Trébucq et al., 2011). An upgrade of the Gene Xpert MTB/RIF was launched in 2017 under the name of GeneXpert Ultra (Ultra). It shows a higher sensitivity for TB detection in children, HIV-positive individuals, and patients with extrapulmonary TB. On the contrary, GeneXpert Ultra shows a lower specificity than MTB/RIF assay. Since their introduction, these tests have contributed to simultaneously detecting TB and RIF resistance (WHO, 2016a).

1.7.1.4 Lipoarabinomannan urine strip test (LF-LAM) for TB diagnosis in HIV-infected patients

LF-LAM test is a commercial assay developed by Alere Determine™ TB LAM Ag, for the detection of mycobacterial lipoarabinomannan (LAM) antigen in the urine. The WHO advises the LF-LAM test for HIV-positive individuals and children showing symptoms of either pulmonary or extrapulmonary TB. In particular, it applies for HIV-positive individuals with CD4+ T cell counts equal to 100 cell/µl or HIV-positive individuals seriously ill regardless of the CD4+ T cell count. LF-LAM test has the advantage of using urine as a specimen, which can be easily obtained also from very ill patients. However, for still unknown reasons, the LF-LAM test is suitable only for people showing HIV-TB coinfection with low CD4+ T cells (WHO, 2015b).

1.7.2 Diagnostic tools for multidrug resistance testing

1.7.2.1 Culture for TB diagnosis and drug resistance testing

The WHO considers commercial liquid culture systems and molecular line-probe the gold standards for the detection of MDR-TB. All commercial liquid systems (*i.e.,* BACTEC, MGIT, VersaTREK, and MBBACT) detect mycobacterial growth within 4-14 days, intending to predict the mutations responsible for resistance to given drugs. The main limitation of them is the obligation of being performed in specialized biosafety level 3 (BSL3) laboratories, using costly instruments and with well-trained staff. Since 2011, the WHO also advises the use of non-commercial culture and drug sensitivity testing (DST) methods for MDR-TB patients, including (i) microscopic

observation of drug susceptibility; (ii) colorimetric redox indicator, and (iii) nitrate reductase assay. All these non-commercial tests can only be executed in reference laboratories and have the main drawback of the impossibility of detecting XDR-TB (WHO, 2008).

1.7.2.2 Molecular line-probe assays (LiPA) for diagnosis of TB and detection of drug resistance

The appearance of MDR- and XDR-TB strains is raising the need for rapid tests for antibiotic resistance identification. Currently, the only MDR- and XDR-TB tests based on nucleic acid amplification are the INNO-Lipa Rif.TB (LiPA, Innogenetic, Ghent Belgium) and the Genotype MTBDR (MTBDR, Hain Life Science, Gmbh, Nehren Germany) (Morgan et al., 2005).

The LiPA test presents a high sensitivity for the detection of RIF resistance. It requires the amplification of the RIF resistance-determining region of the *rpoB* gene by PCR, but more confirmations are required before its application in clinical practice (Rossau et al., 1997).
MTBDR, instead, can detect mutations on the gene responsible for both RIF (*rpoB*) and INH (*katG*) resistance. MTBDR has high precision in the detection of RIF resistance, while INH resistance sensitivity is less accurate and variable (Ling et al., 2008).

In the last years, two others commercial LiPAs, Nipro TM + MDRTB detection kit 2 (Tokyo, Japan) and Hain version 1 and version 2, have become available. Nipro TM, following WHO requirements, can concurrently detect *M. tuberculosis*, RIF, and INH resistance, using a mutation probe for *rpoB* (RIF resistance), *katG* (for high-level INH resistance), and *inhA* (for low-level INH resistance) (WHO, 2016b).

The first version of MTBDR (Hain Life Science) can assess genotypic resistance to fluoroquinolones (FQ) and second-line injectable drugs, especially aminoglycosides, including kanamycin (KAN), amikacin, and capreomycin (Theron et al., 2016)). The FQ resistance is detected probing the *gyrA* gene, while second-line injectable drug (SLID) via *rrs*. The Hain version 1 test can also detect ethambutol (EMB) resistance targeting *embB*, which is absent in the Hain test version 2. Hain version 2 also includes assays for *gyrB* (FQ resistance) and the *eis* promoter region (SLID resistance) (Hain Lifescience, 2016).

The WHO does not recommend using the LiPA test as only DST diagnostic method for MDR-TB, but combining them with the more classical culture-based assays (WHO, 2016b).

1.7.3 Latent TB detection

1.7.3.1 Tuberculin test

The TB Skin test (TST) was developed in the 19th century, and it is still the most common test used to detect TB. The Mantoux test (TST standard) consists of an intradermal injection of a 100 µl solution containing purified protein derivative (PPD) in the top layer of the forearm, with the results obtained after 48-72 hours post-injection (Nayak and Acharjya, 2012). The most used antigenic proteins in PPD are the heat shock proteins GroES, GroEL, HspX, and DnaK (2016). The TST test has several limitations as it cannot discriminate between latent and active TB. Moreover, false negatives and mainly false-positive TST are not rare. In particular, TST is unable to discriminate between *M. tuberculosis* infection and infection caused by nontuberculous mycobacteria, and by BCG vaccination. Moreover, the TST output can be further confounded by incorrect administration, wrong interpretation, recent TB infection (within 8-10 weeks of exposure), previous TST, individual's age, and recent live-virus vaccination (American Thoracin Society, 1999).

Currently, the WHO suggests the TST in high- and upper-medium income countries with low TB burden for specific groups (*i.e.,* HIV-positive individuals, patients on dialysis, adult, and children in contact with pulmonary TB, patients on anti-TNF treatment) (WHO, 2004).

1.7.3.2 Interferon-gamma release assay (IGRA)

The IGRA measures the release of IFN-γ from T lymphocytes after their stimulation with *M. tuberculosis*-specific antigens. To date, two commercial IGRA are available: the QuantiFERON-TB Gold (Cellestis Ltd, Australia) and the T-SPOT-TB (Oxford Immunotec, United Kingdom). QuantiFERON-TB Gold evaluates the concentration of IFN-γ release by the T lymphocytes contact with the early-secreted ESAT-6 and the culture filtrate protein 10 (CFP-10). T-SPOT-TB assay checks the level of IFN-γ produced by peripheral blood mononuclear cells when stimulated with ESAT6 and CFP10 through an ELISPOT assay (Oxford Immunotec,). The IGRA offers the advantage of being rapid, with results are available within 24 hours, and not to cross-react with a prior BCG vaccination. However, these are expensive tests that require quick processing of the blood specimen collected. Moreover, the test is only used to diagnose LTBI, with a high risk of interpretation errors, mainly in HIV-positive individuals. The WHO advises the use of IGRAs in high-income and upper-middle-income countries with low TB incidence (lower than 100 per 100,000 individuals) (Santin et al., 2012).

1.7.4 Chest radiography

Chest X-rays cannot be considered a standard test for TB diagnosis but can be a valuable adjunct at the beginning of the medical evaluation. In particular, the WHO recommends the use of chest X-rays for TB diagnosis in HIV-positive individuals SSM-negative. In 2016 the WHO suggested the use of chest X-rays also for TB diagnosis of childhood pulmonary TB, extrapulmonary TB and to rule out the possibility of active TB before LTBI treatment. Chest X-rays are particularly useful in the determination of active TB and routinely can be offered as a preliminary guide to clinicians and to reduce the number of further testing. Only in case of abnormal chest X-rays, in the presence of specific symptoms and based on the patients' condition and risk of transmission, additional bacteriological and molecular tests are appointed for confirmation. The main limitations of chest X-rays are the need for equipped healthcare facilities and the difficulty in the interpretation of the results, which can be confounded with other lung pathologies, such as cancer (WHO, 2016c).

1.8 Vaccines

1.8.1 The Bacillus Calmette-Guérine vaccine

The BCG vaccine is the most widely-used vaccine to prevent the development of active TB, especially in children (Orme, 2015). Calmette and Guérin cultivated the *M. bovis* strain for 11 years at the Institut Pasteur in Lille (carrying out 230 subcultures) before obtaining a bacillus which failed to cause active TB. The safety of the BCG vaccine depends on the region of difference 1 (RD1) deletion and the loss of the ESX-1 secretion system, which guarantees sufficient strain attenuation as compared to the original strain (Nieuwenhuizen and Kaufmann, 2018). The BCG vaccine was first tested in humans in 1921 by the oral route. The introduction of the BCG vaccine immediately showed a drop in TB mortality among vaccinated children (Luca and Mihaescu, 2013). The arising confidence in the efficacy of the BCG vaccine was questioned after the "Lübeck disaster". On this occasion, within a scheme to vaccinate newborn babies, a large number of newborns developed TB after four to six weeks from the vaccination. Of 250 newborns, 73 died of TB, and 135 were infected but recovered from the infection. An inquiry set up by the German government attributed the cause of the disaster to negligent contamination of the vaccine by an *M. tuberculosis* virulent strain used in the Lübeck laboratory. Hence, the Lübeck (1930, Germany) incident led to a gradual change from the oral to the intradermal administration route (Ducati et al., 2006).

Several strains derived from the original BCG strain, *i.e.,* the BCG Russia, Japan, Copenhagen, and BCG Pasteur, having additional genetic variations, which did not account for changes in the vaccine efficacy (Dockrell and Smith, 2017). Nowadays, different BCG vaccine variants are used worldwide. Pasteur-Merieux-Connaught, the Danish Statens Serum Institut, and the Japan BCG Laboratory in Tokyo are the leading producers, whose vaccines differ in various characteristics, such as the production and the number of viable cells per dose (Milstien and Gibson, 1990).

According to each country's public health policies, the BCG vaccine is administered immediately or shortly after birth. It represents a very cost-effective protection against pulmonary TB in children, especially in countries where TB is endemic. One of the main weaknesses of the BCG vaccine is its highly variable protection (0 to 80 %) in adolescent and adult populations. Moreover, the BCG vaccine shows more significant protection against pulmonary TB in both children and adults at a higher latitude and those previously sensitized by environmental mycobacteria (Orme et al., 2001).

To conclude, the BCG vaccine remains, the only available vaccine offering protection against pulmonary TB. Despite the numerous studies carried out to understand how and when the BCG vaccine protects and why it fails in certain circumstances, the immunological and molecular underlying is not fully understood. This lack of understanding severely limits the possibility of modifying and improving the characteristics and, therefore, the protection of this vaccine.

1.8.2 Alternative approaches for the development of new TB vaccines

The variable protection offered by the BCG vaccine in adults prompted a generalized effort to research new vaccines or boost the existing one. In order to guarantee more extended protection across populations and over time against TB infection, several approaches have been undertaken. Among them, the search for new vaccine candidates with a preventive effect or able to reduce the severity of the infection. Attractive approaches are the search for targets acting on preventing the establishment of the infection, boosting the BCG vaccine to more than 80% worldwide coverage, the use of therapeutic and post-exposure vaccines, and, lastly, preventing TB relapse (Orme, 2015)

The preferred strategy has been hitherto to try improving the existing BCG vaccine. The first improved BCG version was a recombinant BCG (rBCG) strain (Tice), which overexpresses the antigen 85B (Ag85B) and offered better protection in guinea pigs. However, it was abandoned because of the presence of an antibiotic resistance marker. In the same direction, a more

successful BCG modification is the VPM1002 (rBGC Prague strain). The concept behind this candidate was to enhance the T cell response. This candidate and its subsequent modifications produced by Aeras were also abandoned due to some adverse outcomes during the initial safety studies (Orme, 2015).

Another approach used to produce several potential new vaccine candidates consisted of the construction of fusion proteins. Among them, the M72 fusion construct showed encouraging results, and it is in clinical trials, phase IIb. M72 is a recombinant fusion protein of two *M. tuberculosis* antigens, *Mtb*32A and *Mtb*39A, coupled with the AS01e adjuvant system. It protects from TB progression towards the pulmonary active form in about 50% of cases for three years in HIV-negative TB-infected individuals. Nevertheless, M72 needs to be tested in a larger population, including individuals from different geographic locations, ethnic background, and age groups (Tait et al., 2019).

A second vaccine based on a new rational is RUTI®, and it is in clinical trials, phase IIb. It is conceived as a therapeutic vaccine to boost the primary immune response, control the spread of infection, and reduce treatment duration (Prabowo et al., 2019).

To get closer to the WHO's aim to eradicate TB by 2050, a successful new TB vaccination should prevent the progression of active TB from LTBI and, ideally, prevent its establishment. Despite multiple challenges in obtaining a TB vaccine significantly better than BCG, additional studies are ongoing, and several vaccine candidates are clinically tested (Pai et al., 2016).

1.9 Treatment

While TB is a severe condition that can be fatal if left untreated, deaths are rare if treatment is completed. The current TB chemotherapy usually involves a cocktail of antibiotics administrated for several months, with the final goal of clearing the whole bacterial load and any potential reservoir from patients (Petrini B., 1999).

For individuals with active pulmonary TB, the WHO advises chemotherapy with isoniazid (INH), rifampicin (RIF), pyrazinamide (PZA), and streptomycin (or ethambutol) for the first two months. Due to a possible primary mycobacterial resistance to INH, a fourth drug, either ethambutol (EMB) or streptomycin (STR), is added to the treatment (Pai et al., 2016). After these first two months of chemotherapeutic treatment, providing that the bacilli are still sensitive to both INH and RIF, while EMB or STR and PZA can be discontinued, the treatment with INH and RIF is continued for additional four months. INH, RIF, PZA, EMB, and STR are classified as first-line drugs with a bactericidal effect. They combine high efficacy and relative low toxicity towards the patients. The combination of multiple drugs and a long-term treatment aims to kill all the

metabolically active bacteria through first-line drugs initially, to eradicate drug-persistent bacilli, and to prevent the onset of resistance.

MDR-TB is defined as an infection caused by strains that are resistant to INH and RIF. In this case, the standard regimen foresees an elongation of the treatment and the employment of second- or, in most severe cases, third-line drugs. TB second-line drugs exhibit a lower efficacy, mainly because of their bacteriostatic effect and higher toxicity. This category includes para-aminosalicylic acid, ethionamide, cycloserine, aminoglycosides, polypetides, and FQ. XDR-TB is defined as an infection caused by strains that are resistant not only to INH and RIF but also to at least three of the six main classes of second-line drugs. Individuals affected by MDR- and/or XDR-TB are more difficult to treat. The treatment is prolonged up to 12-24 months, and, in the most severe cases, surgical removal of the lesions may be necessary for a better outcome of the treatment (Telenti A., 2000).

For the treatment of LTBI, the WHO advises several treatments with similar efficacy, such as 6-9 months of isoniazid, three months of rifapentine, 3-4 months of isoniazid and rifapentine, or 3-4 months of rifampicin alone (WHO, 2009). Treatments including rifampicin alone are generally shorter, which depends on the well-tolerability of the drug. The shorter treatment will also result in diminishing compliance issues and lower cost of the treatment (Rothstein, 2016).

The massive side effects of the antitubercular drugs, including skin rash, liver damage, gastrointestinal intolerance, neuropathy, arthralgia, renal failure and hemolysis, and the long duration of their administration cause low patients' compliance in completing the chemotherapy. The introduction of the DOT program by the WHO aimed at reducing the number of patients abandoning the treatment. Sputum smears, microbiology cultures, and X-rays are routinely used to evaluate the status of the treatment (WHO, 2009).

The early diagnosis and establishment of a correct pharmacological treatment are essential for reducing the onset and spread of MDR and XDR-TB infection.

In 2016, the WHO updated its MDR/XDR TB treatment guidelines with a seven-drug regiment to be used under particular conditions. This regimen includes the use of new drugs with new mechanisms of action, bedaquiline, and delamanid, even though the effectiveness of this therapy still requires more evaluation (Tweed et al., 2019). In around 40 years, only two new molecules with new mechanisms of action have been approved for MDR-TB treatment. In 2012, the US Food and Drug Administration (FDA) approved bedaquiline, which inhibits the activity of ATP synthase (Cox and Laessig, 2014). In 2014 the European Commission introduced both bedaquiline and delamanid, which inhibits the synthesis of the mycolic acid, as news compounds in the TB chemotherapy (Zumla et al., 2015).

The increase of MDR- and mainly XDR-TB infections and the absence of an appropriate and fast-acting treatment heralds an era in which TB is incurable if new and more effective drug

combinations are not introduced soon. This situation is being extensively reported in countries as India, eastern Europe, and sub-Saharan Africa, which raises legal, ethical, and logistic concerns (Dheda et al., 2014).

Considering the length of the chemotherapy and the side effects associated with the currently available drugs, the need for a new, shorter, and more efficient treatment is emerging. The use of intermittent regimens, the prescription of drugs never widely used against TB or repurposed drugs, and the increase in the dose of usually prescribed TB drugs are among the proposed solutions to bypass the major hurdle of TB drug resistance (Pai et al., 2016), until new drugs with new mechanisms of action are discovered and proven effective and safe.

Besides the design of new chemotherapeutic approaches, in the last years, researchers have also pointed their interest in developing new strategies targeting host factors instead of the pathogen. These approaches, known as host-directed therapy, have as a target the identification of any compound able to modulate the immune defense of the host, either by enhancing it or by improving the clinical treatment, and having as an outcome reduced morbidity, mortality, and long-term functional recovery (Ndlovu and Marakalala, 2016). To date, it is well known the host factors, such as the intact T cell response, the production of INF-γ and TNF, are critical elements in the assembly of a proper anti-*M. tuberculosis* immune response (Ndlovu and Marakalala, 2016). Hence, the understanding of their critical role in the immune response to *M. tuberculosis* infection generates a growing number of host-directed therapies, which not only aim to improve the treatment outcomes and shorten the duration of the therapy but also act on the physiopathology of the infection caused by both drug-sensitive and MDR-TB strains. The currently developed host-directed therapies against TB infection include cellular therapy using bone marrow-derived mesenchymal stromal cells, repurposing of drugs used to treat other pathologies (*i.e.,* diabetes, epilepsy, peptic ulcers, hypercholesterolemia, asthma, cancer, and arthritis), the administration of micronutrients and immune-modulators, antimicrobial peptide inducers and checkpoint inhibitors, targeted immune-based therapies, and lastly, therapeutic vaccines (Ndlovu and Marakalala, 2016).

1.10 HIV and TB: An amplified global burden

Another major issue associated with TB infection control is its prevalence in HIV-positive individuals, which are 30-fold more likely to develop active TB with high severity and poor outcome. In 2017, 370,000 deaths were claimed by TB-HIV coinfection (Fry et al., 2019).

HIV and TB coinfection affects the function of CD4+ T cells, facilitating TB progression from latent to active due to an impairment of the innate immune response. However, these

individuals are not necessarily more contagious than HIV-negative TB infected individuals (Fry et al., 2019). Indeed, people carrying both HIV and TB show a reduction in the cavitary formation, a lower mycobacterial load in the sputum, and the infection mostly develops in the lower lobes of the lungs. The WHO advises a regular TB screening for HIV-positive individuals, especially if they show active TB-like symptoms, *i.e.,* cough, fever, weight loss, and night sweat. HIV-positive patients asymptomatic for TB are recommended to follow the treatment for LTBI, depending on the TB burden of the country they come from (Getahun et al., 2011).

Another critical parameter to consider when treating HIV-positive individuals against TB is the interaction between anti-mycobacterial drugs and antiretroviral therapy. In these circumstances, the WHO recommends treating TB by daily treatment with RIF and INH for six months, including PZA and EMB in the first two months, regardless of whether the infection is caused by sensitive or drug-resistant strains. Moreover, TB treatment should be started within two months from the diagnosis of TB regardless of the CD4+ T cell count (WHO, 2009). Furthermore, the design of the treatment for HIV-TB coinfection must also consider restoring the activity of the immune system, since the antiretroviral therapy can induce the immune reconstitution inflammatory syndrome. Such a syndrome defines a condition where the host response to an infection is unbalanced and detrimental for the patient, and significantly increases the risk of mortality (Uthman et al., 2015).

In conclusion, the HIV-TB co-infection poses a significant challenge for the global control of TB infection and its part of the WHO End TB strategy. Although both the diagnosis and treatment of HIV-TB positive individuals have improved, additional effort is needed to achieve the WHO objectives.

Chapter 2. Mycobacterial persistence

The invasion of pathogenic bacteria and the resulting establishment of the infection can result in either the complete clearance of the infection by the host's immune system or by the formation of a persistent infection (Fisher et al., 2017). A persistent infection, which can be either asymptomatic or symptomatic, is defined as the host immune system's resulted failure to eliminate the pathogen in the absence of antibiotic treatment (Fisher et al., 2017). Pathogens responsible for persistent asymptomatic infections, such as *M. tuberculosis*, *Helicobacter pylori*, *Salmonella* Thypi, and *L. monocytogenes*, establish persistent infection adapting to and modulating the host immunes system of the host. For instance, *M. tuberculosis* and *L. monocytogenes* can hijack the immune system, inhibiting the production of factors (*i.e.,* INFγ response) restricting bacterial growth. Furthermore, other pathogens, such as *M. tuberculosis*, *Legionella pneumophila,* and *Salmonella* spp, can survive phagocytosis by altering phagosomal maturation or influencing the host T cell response (Fisher et al., 2017). Contrarily to persistent asymptomatic infection, individuals carrying symptomatic one exhibit a clinical manifestation of the infection, which might be associated with variation in the host's physiology (Grant and Hung, 2013). A notorious example of symptomatic infections is the nosocomial infections and infections in patients with cystic fibrosis (CF). Indeed, infections due to *P. aeruginosa, S. aureus, Burkholderia cepacia,* and *Haemophilus influenza* are difficult to clear in CF patients, and generally leading to their death (Grant and Hung, 2013).

The recalcitrant nature of persistent infections contributes to their difficult eradication, in which both host and bacterial factors play an important role. Three contributing factors that can explain persistent infection are the pathogen sequestration from the immune system, antibiotic treatment, and the presence of both phenotypic and drug persisters (Grant and Hung, 2013). Thus, the pathogen establishes chronic infection within a protected niche. This niche can be either a physical structure, which can obstacles the action of the immune system, or the ability of bacteria to form biofilm or modulate their gene expression, or, as in the case of the granuloma in *M. tuberculosis* infection, it might be the immune system of the host to create this protective niche (Grant and Hung, 2013). The second important factor influencing the formation of persistent infection is the action of the antibiotic. The inefficient action of antibiotic(s) has been linked to various factors, such as patient's poor compliance, the pharmacokinetic dynamics of the drug at the site of the infection, and the presence of both drug-tolerance and resistance (Fisher et al., 2017), which aspects will be treated at the end of this chapter. Lastly, the establishment of chronic infection also relies on the plasticity of bacteria to alter their biology in the response to the host immune defense and the antimicrobials (Grant and Hung, 2013).

M. tuberculosis is a well-known pathogen able to establish persistent, chronic infection (Gomez and McKinney, 2004). To possibly succeed in its clearance, it requires at least six months of multidrug therapy. This lengthy treatment combines multiple drugs with different mechanism of action, which are required to tackle *M. tuberculosis*'s ability to persist in the host. The selective pressure exerted by the host's immune system has forced *M. tuberculosis* to develop mechanisms to maintain its viability under stressful conditions. To date, it is known that this successful pathogen can hijack the host defenses for its benefit. In turn, the resulting host responses can restrict *M. tuberculosis* replication and virulence, thus enhancing its long-term persistence (Gomez and McKinney, 2004).

2.1 Outlining bacterial persisters

Persisters are individuals belonging to the antibiotic-persistent subpopulation (typically between 0.001% and 1%) capable of temporary survive, through different mechanisms, to the exposition of antimicrobials. Albeit the nature behind a chronic infection has different layers of complexity, emerging evidence supports the role of persisters in either causing persistent infection or being selected via long-term antibiotic treatments (Claudi et al., 2014; Kaiser et al., 2014). Therefore, these experimental observations support the hypothesis that the persister phenotype might participate in promoting bacterial survival during the infection (Gollan et al., 2019).

The term "persisters" was coined by Bigger in 1944 when he observed the failure of complete sterilization of a staphylococcal culture treated with penicillin (Bigger, 1944). The presence of drug-persistent cells within a bacterial population determines a killing curve that follows a biphasic kinetic (**Figure 8**). As shown in **Figure 8**, when an isogenic bacterial population is exposed to an antibiotic, all drug-sensitive bacteria are rapidly killed, resulting in an initial fast killing rate, which then slows down due to the presence of the drug-tolerant subpopulation, resulting in a plateau phase. Once the drug is removed, the surviving subpopulation recreates a population still sensitive to the treatment, which is killed with the same kinetics as the original population upon second drug exposure. These kinetics of mortality and survival demonstrate the transient nature of drug tolerance (or persistence) and the absence of genetic-based drug resistance.

Persisters have been first reported after antibiotic treatment, making them clinically relevant due to emergence of antibiotic resistance. Nonetheless, the stationary phase, oxidative stress, starvation, the presence of DNA-damaging agents, and biofilm formation are all factors that

promote the formation of persisters. Thus, all the data collected so far denote a more sophisticated bacterial adaptation (Khlebodarova and Likhoshvai, 2018).

Figure 8. Biphasic killing kinetics of a clonal population containing persisters. *The presence of persisters within a bacterial population (I) produces a characteristic biphasic killing curve in presence of an antimicrobial. The sensitive population's rapid death characterizes the initial phase of the curve (II). However, the infection is not entirely cleared due to the presence of persister (III). In the absence of the selective pressure of the antimicrobial, persisters start to regrow (IV), giving rise to a still drug-sensitive population (Cohen et al., 2013).*

2.2 The metabolic status of persisters

Since the early discovery of persisters within a clonal population, several groups have been trying to unveil their nature and metabolic features. The initial hypothesis deemed that persisters are in a dormant state, but, to date, there are controversial assumptions about their metabolic activity (Balaban et al., 2013).

The rationale behind the dormant state of persisters was formulated by Bigger. In his study, he demonstrated that the reduction of either growth rate or temperature increased the formation rate of persisters (Bigger, 1944). Despite the mounting literature, the metabolic status of persisters is still an open question. However, it can be asserted that persisters are cells genetically susceptible to a specific antibiotic (or any environmental fluctuations), but able to endure to it (Balaban et al., 2013). The bacterial transition from an active to a dormant phenotype is supposed to not only depend on responsive diversification but also on stochastic processes (Verstraeten et al., 2015). Furthermore, the hypothesis supporting dormancy as a metabolic

characteristic of persisters relies upon the idea that in bacteria with low metabolic activity, antimicrobials can still interact with their target, but they cannot exert their toxic effect because of the low functioning of cellular processes (Lewis, 2010). The association of persisters with dormancy (defined as a state in which cells are metabolically inactive) resulted from two observations: (i) metabolically inactive cells were more tolerant to antibiotic treatment (Shah et al., 2006), and (ii) that more dormant cells were corresponding to a higher number of persisters (Kim and Wood, 2016). In fact, in *E. coli*, time-lapse fluorescence microscopy, single-cell analysis, and flow cytometry demonstrated that persisters could originate from a preexisting dormant subpopulation, which is also non-growing and displays a low levels of protein synthesis. However, since these data indirectly prove a reduced bacteria metabolic activity, it remains unclear whether dormancy is a persisters' feature or drug tolerance requires growth inhibition. Contrarily, other studies claim that persisters cells might also arise from metabolically active bacteria (Orman and Brynildsen, 2013; Pu et al., 2016). For instance, a study investigating the role of the efflux pump in *E. coli* demonstrated that although dormant bacteria generally display a slow-down in most biological processes, they actively induce the activity of the efflux pump, which, in turn, enhances antibiotic persistence (Pu et al., 2016). Indeed, a controversial picture of the metabolic status of persisters is emerging: if persisters are dormant bacteria, a metabolic status which excludes active efflux, it remains unknown how these cells can selectively decide to switch on the activity of the efflux pump (Pu et al., 2016). Furthermore, a second study trying to address if dormancy is a sufficient and necessary feature of persisters showed that bacteria with a lower reductase activity prior to the antimicrobial treatment increased the likelihood of the cell becoming a persister. However, only a lower metabolic activity was insufficient to determine persisters, leading to the conclusion that persisters can arise from cells in different metabolic states (Orman and Brynildsen, 2013).

Hence, persisters might be defined as a bacterial subpopulation phenotypically tolerant to a specific environmental fluctuation showing a gradient of metabolic activity. However, to persist, they clearly must reduce their metabolic activity (J. S. Kim & Wood, 2016; Manina et al., 2015).

2.2.1 Metabolic changes in mycobacterial persisters

In mycobacteria, metabolic pathways have evolved in concert with the pathogen's complicated lifestyle, adjusting its replication according to the host immune response. *In* vivo, *M. tuberculosis* resides in heterogenous niches, either intracellularly or extracellularly, whose nutrient availability is limited. Hence, to potentially survive inside the host, *M. tuberculosis* needs to reshape its metabolism. The bacillus' metabolic plasticity allows the pathogen to utilize a wide

range of carbon sources, which permit *M. tuberculosis* to withstand the immune and drug pressure, and finally to persist. Thus, metabolic enzymes are arising as new putative and attractive factors promoting *M. tuberculosis* persistence (Ehrt et al., 2018).

During the establishment of chronic infection, *M. tuberculosis* undergoes a metabolic shift, characterized by the use of C_2 carbon substrates produced by β-oxidation of fatty acid. In other words, *M. tuberculosis* reduces its glycolysis, but continue to assimilate carbon source *via* gluconeogenesis, which permits the maintenance of the activity of the TCA cycle (Sharma et al., 2000). Pioneering studies performed by McKinney and colleagues investigating this metabolic shift demonstrated the pivotal role of the isocitrate lyase (Icl) in this process (Sharma et al., 2000). A more complex picture about the role of Icl in mycobacterial biology is emerging, in which Icl functions both as a detoxifying and odd chain fatty acid assimilating enzyme. Thus Icl significantly participates in enhancing mycobacteria persistence (Ehrt et al., 2018). Indeed, the currently collected data (Sharma et al., 2000; Upton and McKinney, 2007) support the possibility of using Icl inhibitors to treat TB infection at the chronic stage. Thus, considering the role of Icl in mycobacterial persistence, it is enticing to hypothesize that the coupling of Icl inhibitors with frontline antitubercular drugs (*i.e.,* isoniazid and rifampicin) might reduce the lengthy TB treatment.

Also, the relevance of metabolic enzymes in persisters hinges on the regulation of chemically reactive or biologically toxic intermediates (Ehrt et al., 2018). One example is the inhibition of the fructose bisphosphatase (present in the gluconeogenesis cascade) by accumulating propionyl-CoA and its derivates. These intermediates derive from cholesterol and odd-chain fatty acids catabolism, and their presence in increasing quantity may be toxic for *M. tuberculosis* (Gengenbacher and Kaufmann, 2012). Surprisingly, *M. tuberculosis* can avoid these molecules' toxicity, redirecting them in the 2-methylcitrate cycle, where both Icl-1 and Icl-2 are essential (Upton and McKinney, 2007). Thus, another attractive strategy for drug development stands on targeting enzymes involved in the metabolism of toxic intermediates or reactive species, with the final aim to reduce their detoxifying activity.

Altogether, this experimental evidence proves that the high plasticity of *M. tuberculosis* metabolism is essential for mycobacterial survival and the establishment of chronic infections. Hence, the functional activity of metabolic enzymes commences holding a critical role for *M. tuberculosis* persistence. Nonetheless, their specific function remains to be explained thoroughly.

Consistent with the idea that persisters are dormant cells exhibiting a low metabolic activity, it was hypothesized that mycobacteria cells able to persist display a dormant phenotype. However, several studies (Manina et al., 2015, Manina et al., 2019; Richardson et al., 2016; Ueno et al., 2019; Wakamoto et al., 2013) proved that persistent drug-tolerant mycobacterial cells do not necessarily correlate with a dormant phenotype. For instance, in the study of Wakamoto and

colleagues, the fate of *M. smegmatis* exposed to INH was depending on the cell-to-cell differential and stochastic expression of KatG (the INH-activating enzyme catalase-peroxidase) and not on the single bacteria growth rate prior to drug exposure (Wakamoto et al., 2013). The absence of correlation between the single bacteria growing state and the rare persister phenotype is also supported by a study performed by Manina and colleagues (Manina et al., 2015). In this study, the single-cell analysis of *M. tuberculosis*'s ribosomal activity revealed a wide range of non-genetic variation, which was observed already at the steady-state level and even enhanced under pressure of the host immune response. This increase in the cell-to-cell variation might be due to either the direct interference of the host immunity with essential processes of mycobacterial biology or, more indirectly, by enhancing an adaptive response and promoting phenotypic diversity to ensure the survival of few cells (Manina et al., 2015). However, despite the *in vitro* putative role of phenotypic heterogeneity in promoting *M. tuberculosis* drug tolerance, the single-cell analysis of the bacterial grow-rate showed the absence of correlation between the single bacterial growing state and persistence variation of the ribosomal activity within the clonal *M. tuberculosis* population (Manina et al., 2015). Thus, further confirms the hypothesis that persisters can arise among bacteria with different metabolic states.

Another interesting study coupled single-cell analysis and D_2O Raman imaging spectroscopy to understand the correlation between dormancy and persistence (Ueno et al., 2019). In this study, using the model organism *M. smegmatis*, they showed that rifampicin-tolerant *M. smegmatis* persisters display a range of metabolic status and growth inhibition is not required for persistence (Ueno et al., 2019).

Altogether, these results further confirm that dormancy alone is not an essential feature of bacterial persistence. Thus, mycobacterial persistence might rely on diverse mechanisms, which can be differently activated depending on the induced stress that mycobacterial cells have to overcome.

2.3 Putative mechanisms behind the formation of persisters

The initial hypothesis of the stochastic formation of persisters under standard conditions has been revisited over time. Indeed, several recent studies have proved that starvation, changes in carbon source, oxidative stress, quorum sensing, SOS response, and antibiotics cause persister formation (Helaine and Kugelberg, 2014). Although, the molecular processes behind persister formation are still controversial and not fully understood, strong experimental evidence supports the hypothesis that both stochastic and deterministic factors are responsible for controlling this phenomenon (Lewis, 2010). Here, we report some of the general molecular mechanisms

suggested in the formation of persisters, with particular attention to their role in mycobacterial persistence.

2.3.1 (p)ppGpp signaling

Bacterial survival to harsh environmental fluctuations depends on the aptitude of reshaping their cellular physiology, which relies on the activation of a wide variety of molecular mechanisms. Of them, the ubiquitous second messenger (p)ppGpp, also known as 'alarmone', has a critical role in bacterial adaptation during starvation, known as stringent response, and heat shock (Hauryliuk et al., 2015).

In *E. coli*, the regulation of the cellular levels of (p)ppGpp hinges on the synthetic and/or degrading activity of two enzymes, namely RelA and SpoT, which appear to be differentially activated upon diverse starvation stimuli (Hauryliuk et al., 2015). Despite the fact that changes in (p)ppGpp levels appear to influence the persister formation in *E. coli* and *P. aeruginosa*, the role of this alarmone still requires further understanding. The level of (p)ppGpp has been demonstrated to induce persistence in Gram-positive bacteria, such as *Enterococcus faecalis* and *S. aureus*, but the magnitude of this phenotype appears to be highly context-depending, thus, supporting the hypothesis that complementary pathways might participate in persistence (Harms et al., 2016). Furthermore, it cannot be excluded a stochastic activation of the (p)ppGpp signaling pathways in rare cells in optimal conditions, which might generate a pool of preexisting persisters (Harms et al., 2016). The mechanisms behind the (p)ppGpp-dependent alteration in gene expression have been extensively studied in the two model organisms, *E. coli* and *B. subtilis.* Although the outcome of (p)ppGpp level deregulation is a change in gene expression, *E. coli* and *B. subtilis* exhibit a divergent molecular aspect of the stringent response. While in *E. coli* (p)ppGpp destabilizes the RNAP-promoter open complex interacting with the RNA polymerase (Zuo et al., 2013), in *B. subtilis,* (p)ppGpp indirectly influences transcription modulating the intracellular level of GTP (Kriel et al., 2012).

A link between mycobacterial persistence and stringent response as a critical survival mechanism has also been investigated in *M. tuberculosis.* Contrary to *E. coli,* the *M. tuberculosis* genome owns only one gene (*relA, Rv2583c*) encoding for a dual-functional enzyme, RelA, involved in both the synthesis and hydrolysis of (p)ppGpp (Bhaskar et al., 2018). Interestingly, even in unstressed conditions, *M. tuberculosis* requires a low concentration of (p)ppGpp, which is deemed to provide a growth advantage and maintain mycobacterial homeostasis (Primm et al., 2000). Indeed, the pathogen can regulate the level of (p)ppGpp modulating the synthetic/degrading activity of RelA. Whenever an increase (*i.e.,* starvation, hypoxia, and oxidative stress) or decrease

(unstressed condition) in (p)ppGpp level are required, RelA undergoes a conformational change, which only allows either its hydrolytic or synthetic activity (Hogg et al., 2004).

Similar to other bacteria, the variation in the intracellular levels of (p)ppGpp finally results in a transcriptional change. Similarly to *E. coli* and *B. subtilis,* also in *M. tuberculosis* the mechanism underpinning the (p)ppGpp function finally results in downregulation of rRNA and ribosomal protein biosynthesis and upregulation in pathways involved in the biosynthesis of amino acids (Prusa et al., 2018). Moreover, (p)ppGpp also acts as a key regulator of polyphosphate (polyP) metabolism through the *mprAB-sigE-relA* signaling cascade, facilitating mycobacterial endurance (Sureka et al., 2007). Thus, poly(P) acts as a phosphor donor to the histidine kinase MprB, resulting in phosphorylation of the regulator MprA. The activated form of MprA can then promote the transcription of *relA* through SigE, finally positively regulating the production of (p)ppGpp and poly(P) (Sureka et al., 2007). Contrarily, mycobacterial persistence with respect to antibiotics seems to be independent of the mechanism mentioned above. Bhashar and colleagues hypothesize that while this signaling cascade might regulate mycobacterial growth and survival, it indirectly affects antibiotic persistence without playing a central role in drug tolerance. This would imply that mycobacteria might dispose of different mechanisms to induce persister formation, further supporting the contribution of multiple pathways to it (Bhaskar et al., 2018).

2.3.2 Persisters and biofilms

Within the environment, bacteria can be found in surface-associated multicellular structures known as biofilms. Biofilms composition protects bacteria from hostile conditions, such as immune response and antimicrobials (Harms et al., 2016). One key feature of biofilm is that bacteria are embedded in an extracellular matrix, which, on one side, protects the bacteria from environmental stresses; on other one, it lowers the oxygen tension, limits the nutrients, and promotes the accumulation of metabolic waste. Altogether these factors are hypothesized to enhance bacteria antibiotics tolerance and the formation of persisters (Dhar and McKinney, 2007). Indeed, both their drug-tolerance and their propensity to relapse have been ascribed to a large number of persisters present in the biofilm (100- to 1000-fold more than a planktonic culture). Although further studies are required to fully understand the nature behind the formation of a high number of persisters within the biofilm, one possible explanation was ruled out by using a mathematical model. In this model, the surface and the more accessible regions of the biofilm would be populated by normal growing bacteria, which would be continuously killed by the presence of stress(es). Contrarily, more internal regions of the biofilm, characterized by substrate limitation and low oxygen, would favor persisters' formation. Hence, the biofilm's internal region, crowded with persisters cells, would then, in the absence of the stress(es),

repopulate the biofilm (Roberts and Stewart, 2005). Thus, the local accumulation of persister cells in biofilm areas where no or little cell growth occurs would determine the higher bacterial resistance to hostile external conditions (*i.e.,* immune response and presence of antimicrobial). Lastly, the biofilm's recalcitrant nature would be associated with the lower grow-rate and reduced biology activity of the persistent population populating the biofilm.

As mentioned before, the high ratio of persisters makes the biofilm a critical setting for establishing recalcitrant and relapsing infections, such as in the case of TB infection (Harms et al., 2016). Nonetheless, the role of biofilms in *M. tuberculosis* pathogenesis is still not defined entirely. Biofilms structures are hypothesized to form during TB infection, with the final aim of protecting *M. tuberculosis* from the immune system and antimicrobials (Prusa et al., 2018). Although further experimental observations are required, several extracellular *M. tuberculosis* cells have been observed within the necrotic core of the granuloma. These bacilli are thought to be embedded in an extracellular matrix of polymers. It had been shown that a fraction of these extracellular *M. tuberculosis* clustered in the necrotic core of the granuloma in guinea pigs could survive antimicrobial treatment (Chakraborty and Kumar, 2019). However, to finally demonstrate the presence of *M. tuberculosis* biofilm *in vivo*, the presence of an extracellular matrix needs to be proved (Chakraborty and Kumar, 2019)

In conclusion, even though further studies are required, these observations push to speculate about *M. tuberculosis*'s ability to form biofilms *in vivo* as a survival strategy (Chakraborty and Kumar, 2019).

2.3.3 Persistence and toxin antitoxin (TA) systems

The molecular mechanisms behind the formation of persisters are still far from being completely understood. However, a more accurate molecular description of persisters began with analyzing the transcriptome of persister cells (Harms et al., 2016). The transcriptomic analysis highlighted a prominent and consistent up-regulation of the TA system, leading to the hypothesis that TA systems might modulate persister formation (Harms et al., 2016).

The Toxin-Antitoxin systems are genetic modules encoding for two elements, a stable toxin and a labile antitoxin. While the toxin targets essential bacterial processes, the antitoxin interacts with the toxin to abrogate its function and regulate the TA expression (Page and Peti, 2016). The nature of the antitoxin (RNA or protein) and the mechanism of action of the toxin (inhibition of toxin synthesis or activity) discriminate the TA systems into six different classes. Among them, only type I and II TA systems likely function in promoting the formation of persisters under stresses (Page and Peti, 2016). Briefly, while type I antitoxins are antisense RNAs capable

of neutralizing the toxins, which act through several mechanisms, such as collapsing the bacterial membrane or affecting adenosine triphosphate (ATP) synthesis, type II antitoxins are proteins directly interacting with their respective toxins to restrain their function. Respect type I toxins, type II toxins show high variability, even though they are all classified as translational inhibitors (Page and Peti, 2016).

Although the upregulation of TA systems has been reported and associated with antibiotic tolerance, this phenomenon shows high functional redundancy and often produces separate persisters phenotypes, which is explained by the different mechanisms of action of the involved toxins (Harms et al., 2016). The molecular basis behind the formation of persisters due to the activity of TA has been widely investigated in the model organism *E. coli* K12, and it can be summed up on three pathways reported in **Figure 9.** Furthermore, the formation of persisters due to the action of type II TA systems has also been shown in several other bacteria, such as *M. tuberculosis, Salmonella enterica* serovar Typhimurium, and recently also in several strains belonging to the genus *Pseudomonas* (Pandey and Gerdes, 2005; Vogwill et al., 2016).

2.3.3.1 Polyphosphate/Lon/mRNA endonuclease pathway

This signaling cascade's activation strictly depends on the bacterial intracellular level of (p)ppGpp (**Figure 9**). In *E. coli,* it has been demonstrated that the polyphosphate/Lon pathway regulates around ten mRNA endonucleases, also known as RNA interferases, which belong to the type II TA systems. The formation of persisters promoted by this pathway depends on the stochastic or induced increase in (p)ppGpp intracellular levels. The augmented cellular levels of (p)ppGpp results typically in the repression of the action of PPX, a polyphosphate hydrolase. PPX inhibition determines, in consequence, an enhancement in the production of the cellular polyP level through the enzymatic activity of PPK, a polyphosphate kinase. The high cellular levels of polyP finally stimulate the protease Lon to degrade the antitoxin of the HipAB type II TA module. The Lon-induced degradation of the antitoxin HipB induces the release of HipA, which, once free, phosphorylates and inactivates the aminoacyl-tRNA synthetase GtlX (Germain et al., 2013; Hansen et al., 2012). Lastly, the GtlX inactivation results in the binding of the ribosomal subunits A with uncharged tRNA, which further activates the (p)ppGpp synthesis through RelA. Interestingly, this signaling cascade includes two feedback loops: a positive-feedback loop, which keeps activating HipA, and the other connected ten mRNA endoribonucleases (Germain et al., 2015); and a negative-feedback loop, by which the released mRNA toxins limit the entry of uncharged tRNA into the ribosome through degradation. This, in turn, regulates the amplitude and the duration of the (p)ppGpp signaling (Tian et al., 2016).

Content removed for copyright

Figure 9. Toxin Antitoxin (TA) modules promote persister formation in E. coli K12*. The schematic represents the three primary molecular mechanisms by which the TA systems induce (in red) or counteract (in blue) the formation of persisters. The Obg/HokB pathway (A), the polyphosphate/Lon/mRNA interferases (B), and (C) TisB pathways are detailed. The Obg/HokB and the polyphosphate/Lon/mRNA interferase pathways are under the control of (p)ppGpp. Contrary, the TisB pathway is activated upon SOS induction. HokB and TisB belong to the type I TA systems and enhance the formation of persisters by abrogating the cellular proton-motive force (PMF). The other toxins participating in the formation of persisters are mRNA endoribonuclease, or RNA interferases, belonging to the type II TA. The latter interferes with ribosomal translation, Figure from (Harms et al., 2016).*

Altogether these studies supported the hypothesis that TA dysregulation transiently enhances dormancy and cell tolerance to stress. However, this signaling cascade's implication in the formation of persisters has been questioned based on several contradictory observations. Firstly, *lon* deletion does not induce ampicillin persistence (Chowdhury et al., 2016), and in the strain depleted of *lon*, the bacterial survival to ciprofloxacin depended on *sulA* (Theodore et al., 2013). Secondly, serine hydroxamate (SHX) upregulation of RelE antitoxin appears in a (p)ppGpp-independent fashion (Christensen et al., 2001). Moreover, *in vitro* accumulation of polyP has an inhibitory effect on Lon (Osbourne et al., 2014). Lastly, the deletion of the *hipAB* TA module does not affect persistence (Hansen et al., 2008). Finally, this model, claiming the role of type II TA systems in persistence, was entirely and finally rejected in 2017 when the Gerdes group retracted all the previous publications due to phage contaminations (Harms et al., 2017b, 2017a).

The model mentioned above, and the high number of TA systems in *M. tuberculosis* suggested a putative role of TA systems in mycobacterial persistence. *M. tuberculosis* H37Rv genome encodes for 79 type II TA systems (Sala et al., 2014), which are mostly absent in other mycobacterial species, such as *M. smegmatis* and *M. marinum,* and, of this, 30 encode for functional TA systems (Ramage et al., 2009). Thus, the surprisingly high number and variety of TA systems in *M. tuberculosis* are deemed to help the pathogen to stabilize its genome and provide endurance within the harsh infection environment (Ramage et al., 2009). Although the biological function of most of the TA modules encoded by *M. tuberculosis* remains poorly understood, one of the best characterized TA systems is MazEF. *M. tuberculosis* encodes 10 MazEF systems, which have been described to be upregulated under several *in vitro* and host-mimicking conditions (Slayden et al., 2018). MazEF belongs to the type II TA system, and the same promoter regulates both toxin and antitoxin transcription. The MazEF locus encodes for MazF, the toxin, a stable RNA interferase that acts altering mRNA translation, and MazE, the antitoxin, which is rapidly degraded by cellular proteases as those belonging to the Clp family. The Clp protease family is transcriptionally regulated by ClgR, which is also known to regulate the activation of the SOS response (Manina et al., 2019). Hence, in the presence of DNA damage, Clp proteases might induce MazF-mediated slow-down of the mycobacterial cellular function, enhancing the degradation of MazE. Thus, the reduced cellular activity induced by the toxin action of MazF might promote mycobacterial endurance under several stress conditions, such as in the presence of antimicrobials or during infection. A first pivotal study aiming to prove the MazEF TA module's role in mycobacteria biology demonstrated that changes in the intracellular level of MazF might influence the single-cell fate (Burgess Tornaletti and Manina, 2020). Although further studies are required to corroborate the link between the biological function of the MazEF TA system and mycobacterial endurance, this first experimental observation starts to shed light on the critical pathway required for *M. tuberculosis* survival under fluctuating environment.

Furthermore, another study trying to unveil the role of the type II TA systems in mycobacterial persistence investigated the role of (p)ppGpp and polyP regulatory network in *M. smegmatis* (Bhaskar et al., 2018). Contrary to *E. coli*, in mycobacteria, the changes in the intracellular level of both (p)ppGpp and polyP do not appear to influence the formation of persisters against unrelated antibiotics (Bhaskar et al., 2018). Hence, these data suggest that mycobacterial persistence against antimicrobial might be differently regulated, and the mechanisms behind this phenomenon are highly heterogeneous depending on different bacterial species.

2.3.4 Type I TA systems and persistence

Although the type II TA systems have been primarily related to persistence, type I TA systems deregulation has also been described in persister formation (Harms et al., 2016). As previously mentioned, type I antitoxins are RNAs that, under physiological conditions, inhibit the toxin, small hydrophobic proteins, by inhibiting its translation. Under specific environmental fluctuations, the toxin's mRNA levels can increase and overcome the antitoxin action. The high abundance of the toxin's mRNA determines the toxins' production, usually targeting the inner membrane. Hence, the high level of type I toxin would disrupt the proton motive force (PMF) and, finally, induce persistence by depolarizing the inner membrane and depleting the ATP intracellular level. Altogether, the type I toxin's action aims to slow-down the cellular metabolic activity, which can foster bacterial endurance under stress conditions (Edelmann and Berghoff, 2019). In *E. coli*, TisB, DinQ, and HokB are hypothesized to regulate type I TA-mediated persistence, upon different environmental stimuli. While TisB and DinQ are induced upon the SOS response, HokB is controlled by the essential GTPase Obg and (p)ppGpp (Harms et al., 2016). TisB and DinQ induce bacterial persistence by modulating the ROS production upon DNA damage. More interestingly, a recent study linked the TisB-dependent membrane depolarization, ROS production with the cells' ability to persist. The proposed model suggests that a weak membrane depolarization with a low ROS level would induce the formation of persisters, while a cell strongly depolarized with a high level of ROS would lead to the death of the cell or the VBNC phenotype (Edelmann and Berghoff, 2019). Although the biological function of Obg is still not fully understood, a recent study proved that Obg, in *E. coli* and *P. aeruginosa*, can mediate persisters formation under starvation in the presence of antimicrobial by promoting the overexpression of HokB. However, the bacteria to initiate this pathway requires that (p)ppGpp binds Obg causing the increase in the cellular level of HokB, which ultimately induce membrane depolarization and the switch to a persistent state. (Verstraeten et al., 2015)

Despite the high number of TA systems encoded by *M. tuberculosis*, only type II TA modules have been identified (Sala et al., 2014). Hence, the mechanisms described above do not apply to mycobacterial persistence. Nevertheless, the essential GTPase Obg (*Rv2440c*) has proved necessary for *M. tuberculosis* survival under stress conditions (Kumar et al., 2017). Contrarily, to its ortholog in other bacteria, mycobacterial Obg (i) is preferentially associated to the membrane, (ii) interacts with all the three ribosomal subunits (30S, 50S, and 70S), and (iii) binds to UsfX, an anti-sigma factor, rather than RelA (Sasindran et al., 2011). In a recent study, Kumar et al. speculate that under stress conditions, Obg upregulation might promote SigF (a late-stage sigma factor) activity by phosphorylating UsfX, reported to inhibit the SigF expression (Kumar et al., 2017).

Hence, identifying a different molecular cascade for Obg in mycobacteria enhances the idea that in *M. tuberculosis,* stress response pathways described to be involved in persistence might be more heterogeneous and differ from those described in other bacteria.

2.3.5 SOS response and persistence

Bacteria are exposed continuously to DNA damaging agents and intra- and extracellular factors that trigger the SOS response. The SOS response is an inducible DNA damage repair pathway, required for bacterial diversification, adaptation, and pathogenesis (Podlesek and Žgur Bertok, 2020). The SOS response is controlled by the inducer RecA and its repressor LexA. In the presence of DNA damage, either due to endogenous or exogenous factors, the activated form of RecA bind to single-stranded DNA (ssDNA) and promotes the self-cleavage of LexA, which finally determines the derepression of a pool of genes involved in the SOS response pathway (Manasherob et al., 2012).

Bacteria with DNA damage have to arrest their growth for activating the SOS regulon and the DNA repair mechanisms (*i.e., sulA, recABCD, uvrABC,* and *ruvABC*), thus possibly enhancing tolerance to antibiotics (van den Bergh et al., 2017). Accumulating evidence suggests that the role of the SOS response in bacteria plays a much broader role. Indeed, the SOS response has also been shown to promote diversification through the SOS-error-prone polymerase activity and promote the formation of persisters by the regulation of TA systems.

Interestingly, persisters only originate in bacteria that are able to trigger a mild SOS response and with efficient DNA repair mechanisms (van den Bergh et al., 2017). Moreover, the SOS response's activation level and the DNA repair mechanisms' efficiency are not the only factors contributing to bacterial survival within the DNA damage stress. In *E. coli,* the persister phenotype was also proven to depend on the timing of molecular events following fluoroquinolone (FQ) treatment (Mok and Brynildsen, 2018). In their study, Mok and colleagues showed that the survival of the *E. coli* non-growing subpopulation before FQ treatment depended on the timing of both DNA repairs and the reactivation of the growth, which lastly has been linked to RecA functional availability (Mok and Brynildsen, 2018).

Among different bacterial species, the SOS response pathway is highly conserved. Although the SOS response in mycobacteria is not fully elucidated yet, it is known that the SOS response in mycobacteria is mediated by both a RecA-dependent inactivation of LexA and by a LexA-independent mechanism (Manina et al., 2019). However, as in *E. coli*, a similar role of the SOS response in promoting bacterial diversification and persistence has also been recently reported in mycobacterial (Manina et al., 2019). The single-cell analysis of the RecA dynamic by

using a fluorescent reporter, in both mycobacterial pathogenic and non-pathogenic strains, proved that already at the steady-state level, in a clonal population, two subpopulations could be identified upon stochastic pulses of RecA. These two subpopulations, namely pulsing and not-pulsing, exhibit differential susceptibility to FQ treatment. Thus, showing that the pulsing population prior to and during drug exposure is more susceptible to antibiotic treatment (Manina et al., 2019). Moreover, this study supports the hypothesis that persisters can arise only from cells able to mount a mild SOS response. Lastly, from the same study, it also emerges that *M. tuberculosia* cells most likely to survive drug exposure display a moderate variation in their growth, supporting the idea that persisters can arise from cells with different metabolic states (Manina et al., 2019)

Lastly, within this work context, it is of particular interest to notice that *E. coli* cells deficient in RNase E are incapable of correctly activating and maintaining a physiological SOS response (Manasherob et al., 2012). Therefore, it is conceivable to believe that RNase E's global role in RNA turnover might affect the cellular abundance of the molecular factor involved in the SOS response and, hence, bacterial survival.

2.4 Bacterial phenotypic heterogeneity as a mechanism of spontaneous persistence

Bacteria regularly face abrupt environmental fluctuations, which cause a selective pressure that bacteria have to withstand. The survival of an isogenic microbial population to those relies on cell-to-cell phenotypic variations. Thus, the presence of a non-genetic diverse subpopulation could reflect a fitness cost paid by the bacterial community to overcome detrimental circumstances, without incorporating long-term alterations in the genome (Vincent and Uphoff, 2020). Respect genomic alteration, phenotypic variation is not a committed cell state. The same bacterium can switch between different phenotypes, modulating its survival (Kussell, 2013). This bacterial strategy, called bet-hedging, might influence persister formation, exploiting both stochastic and deterministic mechanisms (Kussell and Leibler, 2005). Several factors contribute to phenotypic variation, including the cells' mechanical features, epigenetic modifications, availability of nutrients, and the noise gene expression (Kussell, 2013). Overall, the determinants driving phenotypic heterogeneity can be divided into three categories: (i) molecular memory, (ii) molecular partitioning and cellular aging, and (iii) molecular noise.

2.4.1 Molecular memory

Phenotypic variations do not establish mutations in the genome. However, the progeny can inherit cell-to-cell variation and, in some cases, it can be maintained even for several

generations (Rando and Verstrepen, 2007). The inheritance of the ancestor's molecular state is known as 'molecular memory' and can represent a fitness advantage (Veening et al., 2008).

During cell division, the offspring inherit not only the genomic information but also part of the mother cells' cytoplasmic content. The proteins and RNA molecules inherited will influence the phenotype of the offspring dictating their future life-history decision. One example can be summarized in a simple genetic network containing a positive feedback loop in which a positive regulator enhances its expression in the presence of an external signal. In this example, the regulator's degradation rate and the growth rate of the cells are the critical parameters influencing the molecular memory of the cells. One of the first examples describing such a genetic network is the *lac* operon in *E. coli* (Lambert and Kussel, 2014). The genes involved in the uptake and metabolism of lactose, such as the *lac* permease *lacY*, are induced in the presence of lactose or lactose analog in the environment. Hence, in the presence of the stimulus, *E. coli* cells express the *lac* permease (*lacY*) and are considered in an ON state for this specific pathway. At low concentrations of the inducer, the previously not induced cell, defined in an OFF state, will not respond to the exogenous signal. However, due to the positive feedback loop in the network, cells in an ON status would still be sensitive to the inducer. This would determine the presence of two coexisting subpopulations, either in ON or OFF state, known as a bistable process. The offspring can epigenetically inherit the ON and OFF state of the cells in the presence of a low level of inducer through several generations. Thus, in conclusion, the offspring's phenotype reflects the physiological state of its ancestor (Lambert and Kussel, 2014). A second example of a bistable process inherited through generation is the propagation of the sporulation signal in *B. subtilis.* Briefly, the sporulation process relies on the activation of Spo0A, which genetic circuit displays a positive feedback loop. Thus, within a clonal population, the level of activation of Spo0A would determine a bistable population, namely an ON/OFF state, which, lastly, will determine spore or not phenotype. Like the *lac* operon, also the sporulating ON/OFF state, it can be inherited through several generations, which, in turn, can help the progeny to respond to harsh environmental conditions (Aguilar et al., 2007).

Furthermore, heritable cell-to-cell variation also applies to epigenetic modifications, such as promoter methylation (Lim and Van Oudenaarden, 2007) and posttranslational modification (Sakatos et al., 2018). With reference to mycobacteria, Sakatos and colleagues proved that posttranslational modifications of HupB, a histone-like nucleoid-associated protein, in *M. smegmatis*, are heritable and semi-stable. HupB posttranslational modifications (*i.e.,* methylation and acetylation) specify two mycobacterial subpopulations, large and small colony variant (LCV and SCV), which exhibit discrete transcriptional profiles and growth features. LCV and SCV phenotypes display a different tolerance to isoniazid (INH), a first-line antitubercular drug, which depends on both the methylation and/or acetylation of the lysine in position 86 (K86) of HupB

(Sakatos et al., 2018). Although further studies are required to prove if the LCV and SCV are preexisting to the drug exposure or induced in its presence, the inheritance of diverse phenotypic states may be critical for bacterial adaptation and pathogenesis, which can spatially depend upon the pressure withstood by the bacterial community.

2.4.2 Molecular partitioning and cellular aging

The partitioning of the genomic material is strictly regulated during cell division. This tight regulation assures its equal inheritance among the two daughter cells. Contrarily, other molecular components, such as proteins, RNA molecules, and other cytoplasmic macromolecules, are partitioned either randomly or depending on their cellular localization (*i.e.,* membrane or cell pole) (Van Boxtel et al., 2017). Generally, each offspring will receive a similar concentration of the cytoplasmic content of the mother cell. However, the low number of the molecules present and the absence of a coordinating segregation mechanism determine a large partitioning error, which, in turn, enhances the cell-to-cell phenotypic variability of the offspring (Van Boxtel et al., 2017). The effect of the molecular partitioning coupled with cellular aging further enhances the cell division's phenotypic diversity. Rod-shaped bacteria, after each division, generate two daughter cells differing in their pole age. They inherit, from the mother, a new and an old pole, in which the number of old poles inherited determines the final ages of the cells (Stewart et al., 2005). For instance, *E. coli,* a symmetric-dividing bacterium, exploits the aging and the asymmetric partitioning to generate a young and an old daughter cell, in which the older cells accumulate the higher number of damaged proteins. As a rule, the accumulation of damaged proteins in the older offspring is often translated with a slower growth rate, a decreased generation of offspring, and lower sensitivity to antibiotics (Van Boxtel et al., 2017; Russell, 2017). Thus, this strategy, meant to be a rejuvenating step for only one of two daughter cells, results in diverse chronological ages and cellular physiology, which might dictate a diverse life-history decision and further enhance the phenotypic heterogeneity of the population (Kussell, 2013). Another experimental observation demonstrating the role of the asymmetric partitioning of the cellular content and the associated phenotypic heterogeneity results from the investigation of the main multidrug efflux pump AcrAB-TolC in *E. coli* (Bergmiller et al., 2017). The single-cell tracking of a fluorescent reporter for AcrAB-TolC inside a microfluidic device showed a biased partitioning of the AcrAB-TolC ternary complex towards old cell poles. Hence, the older offspring displays an increased drug efflux activity with respect to the young daughter cells, resulting in a differential drug sensitivity of the individual cells (Bergmiller et al., 2017).

Mycobacteria are characterized by an asymmetric division, which adds a further level of complexity to the cellular aging and molecular partitioning. In each division event, mycobacteria

divide into an older and younger offspring, which differs not only in age but also in size. However, single-cell level analysis, aiming to outline the putative difference in the older and younger offspring, proved that although the two daughter cells differ in birth length and elongation velocity, they still display a similar elongation rate and antibiotic sensitivity (Aldridge et al., 2012; Santi et al., 2013). Surprisingly, while several works (Aldridge et al., 2012; Manina et al., 2019; Santi et al., 2013) demonstrated that the pole age does not influence mycobacterial survival to antimicrobials, many others have done so (Rego et al., 2017; Manina et al., 2015; Wakamoto et al., 2013). For instance, Manina and colleagues showed that at the single-cell level, *M. tuberculosis* survivors to INH treatment only include new-pole cells, even though the old -pole offspring appeared to be more resistant to cytolysis (Manina et al., 2015). Contrarily, Wakamoto and colleague's work revealed a weak positive correlation between old-pole mycobacteria and INH survival (Wakamoto et al., 2013). Lastly, Rego and colleagues show that cells inheriting the old-pole have a lower sensitivity to rifampicin with respect to the new-pole cells (Rego et al., 2017). Although these controversial data cannot be fully explained, it is widely accepted that cell aging and molecular partitioning enhance cell-to-cell variation. It might be interesting to deem that mycobacterial offspring might differentially respond to the action of diverse antimicrobials and/or external stimuli to which they are exposed. Thus, it might be deemed that in *M. tuberculosis,* multiple factors linked to the pole age can weigh in the mycobacterial survival under antimicrobials or not stress. However, whether the inheritance of the pole age in mycobacteria can have a role in promoting their survival under antimicrobial treatment remains an open question.

2.4.3 Molecular noise

The cell-to-cell phenotypic variation has been revealed as a critical factor for bacterial adaptation and survival in an ever-changing environment (Uthman et al., 2015). Several determinants, such as growth rate, molecular partitioning, cellular age and division, and gene expression contribute to it. Among all of them, noise in gene expression is the primary driver. Monod and Jacob already presumed molecular noise's role in enhancing bacterial phenotypic heterogeneity in 1961(Monod and Jacob, 1961). However, only with the development of more advanced technologies, such as single-cell microscopy and microfluidics, it started to be possible to clarify its role in bacterial physiology (Elowitz et al., 2002).

The relevance of stochasticity in gene expression relies on the finite number of molecules or infrequent interactions involved in transcription, RNA degradation, and translation. Hence, even a small difference can further enhance the non-genetic variability (Veening et al., 2008). In sum, molecular noise describes stochastic fluctuations within the biochemical processes due to

molecules' discreteness and random collision. Empirically, noise in gene expression (**Equation 1**), $\eta(t)$, can be quantified as the grade of protein fluctuations, $P(t)$, with respect to their mean concentration.

Content removed for copyright

Equation 1. Empiric measurement of the magnitude of noise in gene expression. $P(t)$ represent the protein concentration at the time *t* and $\eta(t)$ *the protein noise. The angled brackets indicate an averaged probability distribution of* P *at the time t (Swain et al., 2002).*

In detail, molecular noise is shaped by three central mechanisms: the bursty expression of the mRNA, the buffering effect of the longer half-life of the proteins, and its downstream propagation in the signaling cascade (Eldar and Elowitz, 2010). The mRNA transcription depends on the promoter transcriptional efficiency, which varies over time. Thus, the mRNA production cannot be considered constant, resulting in a random burst of mRNA production, which will enhance even more protein fluctuations (Eldar and Elowitz, 2010). Despite that, proteins longer half-life can average their intermitting synthesis. This outcome is known as the finite-number effect. Although both protein and mRNA fluctuations contribute to the molecular noise, the finite-number modeling predicts that the variability observed for mRNA abundance variation is mightier than the one of protein molecules. Moreover, the finite-number effect also accounts that the noise positively correlated with the dimensions of the studied systems (Kærn et al., 2005). Interestingly, noise significantly increases in response to fluctuations in translational efficiency than to the rate of transcription. The influence of translational efficiency over the noise may represent a bacterial defense mechanism against the damaging effect of protein fluctuations (Ozbudak et al., 2002).

Summing up, it is evident that transcriptional bursts can determine fluctuation in protein levels, large enough to modulate the downstream signaling cascade. Hence, such events might trigger stochastic switches leading to cell-to-cell phenotypic variability that can be exploited by the bacterial population to overcome environmental stresses.

In prokaryotes, it is deemed that the limiting step causing protein fluctuations is the RNA-dependent degradation of the transcript with respect to the start of the transcription. Thus, the number of proteins synthesized to one molecule of mRNA has to correlate with the number of ribosomes bound to the transcript positively. Moreover, in bacteria where the RNA metabolism is controlled by the endoribonuclease E, RNase E (Mackie, 2013), the ribosomal binding site (RBS)

is known to be located in the proximity of the RNase E binding site (Mcadams and Arkin, 1997). The RNase E and ribosomal binding sites' close location generates a direct competition between the RNase E and the ribosome binding of the transcript. Therefore, whenever a ribosome occludes the RNase E's binding side, the mRNA can be translated and the protein synthesized. Contrary, the binding of the RNase E will promote mRNA degradation. Furthermore, in this model, since each binding event is considered an independent, the efficiency of translation of the transcript directly depends upon the RNase E-ribosome binding competition (Mcadams and Arkin, 1997).

The rate of RNA synthesis, due to the promoter activity, chromatin remodeling, and cell division, has been widely studied as one of the main stochastic factor influencing the variability in gene expression, and, in consequence, cell-to-cell phenotypic variation (Baudrimont et al., 2019). However, although it is still unclear, the rate by which RNA molecules are degraded is also known to affect gene expression's molecular noise. A recent study developed a two-reporter method coupled to FISH to measure the contribution of the mRNA degradation in stochastic variations of the gene expression (Baudrimont et al., 2019). This study demonstrated that unstable transcripts are more susceptible to noise than stable ones and that the cells tightly control this by exploiting low-noise degrading pathways. Nevertheless, the mild alteration in the RNA degrading network is sufficient to induce macroscopic cell-to-cell variations (Baudrimont et al., 2019).

2.4.3.1 Intrinsic and extrinsic noise and its functional role

The molecular noise of a system results from the sum of both extrinsic and intrinsic stochasticity. By definition, intrinsic variations are the random biochemical reactions occurring during gene expression. On the other side, extrinsic fluctuations describe the system's state and its interaction with the external environment (Elowitz et al., 2002). Elowitz's landmark study demonstrated that both noise sources control the heterogeneous expression (η_{tot}) of two fluorescent reporters in the same system, like *E. coli*, under the control of the same inducible promoter (Elowitz et al., 2002). These experimental data have been elegantly modeled and empirically quantified by Swain and colleagues (**Equation 2**) (Swain et al., 2002). Furthermore, while intrinsic noise (η_{int}) can describe the variation in expression of a single gene in a known moment, extrinsic noise (η_{ext}) must be considered as an alteration of the gene in different cells in response to the environmental stimuli, which can potentially affect all the genes within the examined system (Swain et al., 2002).

Content removed for copyright

Equation 2. Empirical quantification of the total noise (η_{tot}). *The square of the experimentally measurable noise (η_{tot}) of a system results from the sum of both extrinsic (η_{ext}) and intrinsic (η_{int}) stochastic contribution. The η_{int} is directly proportional to the variance of the intrinsic, if calculated for a determined value of the extrinsic variable and then averaged on all the putative values of the considered variables. η_{ext}, instead, vanishes as the extrinsic distribution increases (Swain et al., 2002).*

Stochastic phenotypic switches due to the molecular noise are considered an ingenious mechanism used by bacteria to overcome environmental clues. They have to be considered metastable and probabilistic cell states, which vary over time and rely on positive and negative feedback loops (Eldar and Elowitz, 2010). A more in-depth analysis of positive and negative feedback mechanisms showed a more elaborate role in regulating the molecular noise. Negative feedbacks are deemed to reduce molecular noise (Becskel and Serrano, 2000). Nonetheless, negative feedback can also have a destabilizing effect, such as the one reported in the DNA-damage response mediated by the p53-MDM2 genetic circuit (Lahav et al., 2004). Contrarily, positive feedbacks have been associated with the amplification of phenotypic oscillation, determining a bimodal distribution of the gene expression, which is generally referred to as bistability and previously described in this chapter (Veening et al., 2008).

The molecular noise's functional role in promoting non-genetic phenotypic diversity has also been proved for pathogenic bacteria. The best-studied example is the formation of persister cells in the presence of antimicrobials (Balaban et al., 2004). However, phenotypic heterogeneity has been reported as a critical aspect also in other pathogens such as *Salmonella* (Avraham et al., 2015; Claudi et al., 2014), *Yersinia pseudotuberculosis* (Weigel and Dersch, 2018), and *M, tuberculosis* (Dhar et al., 2016).

2.4.3.2 Example of the functional role of molecular noise in mycobacteria

Over the last decade, the advancement in single-cell technologies allowed to unveil molecular mechanisms hidden within a clonal microbial population's bulk behavior. The possibility to closely look at the fate of a single cell over time and in the presence or absence of an environmental strain highlighted the relevance of the cell-to-cell phenotypic variability. This cell phenotypic heterogeneity has only been recently appreciated and investigated in mycobacteria

(Dhar et al., 2016). Although we are still far from comprehending the molecular mechanisms behind its origin, it is clear that the cellular phenotypic variation plays a critical role in promoting mycobacterial survival during infection. Indeed, it is hypothesized that the mycobacterial phenotypic heterogeneity might help this successful pathogen fine-tune its expression profile in response to the harsh conditions faced in the host, such as the immune response and the presence of antimicrobials (Dhar et al., 2016).

In 2015, an *in vitro* single-cell study demonstrated that a mycobacterial isogenic population exhibits, already in steady-state conditions, highly phenotypic variation (Manina et al., 2015). Although its molecular origins were not investigated, this study suggested that the bacilli might exploit this gene expression's heterogeneity to overcome environmental cues. Accordingly, it was shown that this non-genetic diversity is further enhanced whenever the bacilli face the host's immune response during the infection process or in the presence of antimicrobials (Manina et al., 2015). During the infection, mycobacteria have to withstand the immune system's pressure, which can further enhance the phenotypic heterogeneity of the bacteria. This pressure exercised by the host immune system might induce bacterial diversification in different subpopulations with distinct phenotypic characteristics, as recently demonstrated by Mishra and colleagues (Mishra et al., 2019). They showed that infected macrophages aiming to clear the phagocytized bacilli through the acidification of the phagosome could promote the formation of *M. tuberculosis* subpopulations displaying redox heterogeneity. This induced-redox physiological diverse subpopulation, named EMSH-reduced, displays an increased antioxidant potential that favors the bacterial adaptation both in response to macrophage activation and the presence of antimicrobials (Mishra et al., 2019).

Single-cell analysis of the mycobacterial behavior in the presence of antimicrobials showed that the stochastic fluctuations in gene expression, and the consequent cell-to-cell variability, also play a critical role in promoting the bacilli's endurance and survival to antibiotics (Manina et al., 2019; Wakamoto et al., 2013). For instance, it has been shown that the stochastic pulsatile expression of the catalase-peroxidase KatG in *M. smegmatis* positively correlates with the single-cell fate of the bacilli under INH treatment. In other words, bacteria, which before the INH treatment, displayed a pulse in KatG expression are more likely to die due to the higher amount of INH activated. Although the KatG pulses determined the single bacterial fate, the molecular mechanism(s) provoking KatG pulsing remains unknown. However, the authors speculate about three putative causes for the KatG pulsing: (i) a random burst in its mRNA transcription, (ii) a stochastic switch of the *katG* promoter between an "on" and "off" status, and (iii) a random production of reactive oxygen species (ROS) that could enhance KatG transcription. Altogether, the collected data suggest that the pulsatile expression of KatG might allow a nonresponsive adaptation to INH (Wakamoto et al., 2013).

Furthermore, mycobacterial phenotypic diversity, as a means of adaptation, has also been proved for rifampicin and fluoroquinolones (Rego et al., 2017; Javid et al., 2014; Manina et al., 2019; Zhu et al., 2018). The collected experimental observations outlined that the non-genetic drug tolerance to rifampicin relies upon various and complex mechanisms accountable for cell-to-cell variation. For instance, it has been shown that the depletion of LamA, a member of the mycobacteria division complex, in *M. tuberculosis* can reduce the heterogeneity of the bacterial population, which were killed more rapidly in the presence of rifampicin (Rego et al., 2017). In this case, the reduction of the population heterogeneity can be attributed to the LamA-dependent inhibition of the cell wall synthesis at the new pole within the division and elongation switch, which usually generates asymmetric growth between the two cellular poles (Rego et al., 2017). Similarly to the stochastic KatG pulses and the single bacteria fate in INH's presence, it has been recently shown that the random RecA pulsing state of a single bacillus before the antimicrobial exposure correlates with the mycobacterial survival to FQ (Manina et al., 2019). In more detail, in both *M. smegmatis* and *M. tuberculosis*, the presence/absence of a RecA pulsing phenotype, outlining the extent of DNA integrity within the cell, results in a bistable phenotype of the clonal population. The single-cells analysis of the pulsing or non-pulsing subpopulations revealed that bacteria with a higher expression of RecA, before the drug treatment, are more susceptible to the drug's action. Contrary, the non-pulsing population was more tolerant of the drug. However, this more drug-tolerant subpopulation still died at the second exposure of FQ, and only a limited fraction of them will become genetically resistant to the drug. Hence, these data prove that cell-to-cell variation regarding the preexisting cellular level of DNA damage influences mycobacteria fate under drug treatment (Manina et al., 2019).

Although the role of phenotypic diversity still necessitates further studies, it starts to be widely accepted as an elaborated strategy in promoting mycobacterial survival and persistence. Therefore, it can be envisaged that a more profound comprehension of its molecular nature and its driving mechanisms might typify new putative targets to tackle mycobacterial persistence in an alternative manner. Lastly, another emerging hypothesis deems that the reduction of the phenotypic heterogeneity within the mycobacterial population might reduce the bacilli's endurance to the negative selective pressure exercised by both the host immune response and the action of antimicrobials. Thus, it would result in both the shortening of the treatment and in its increased efficiency in the clearance of the mycobacteria population.

2.5 Mapping and fighting bacterial drug persistence

The origin of drug persistence is a major conundrum both for researchers and clinicians, and many efforts are invested in understanding, describing, and tackling this phenomenon.

Balaban and colleagues first used single-cell approaches to study drug persistence and directly observed the cell-to-cell heterogeneity at the root of drug persistence. They also classified persisters into two types: type I persisters, arising in response to an external stimulus, and type II persisters, intrinsically present and continuously formed within the bacterial population (Balaban et al., 2004). Both types of persisters preexist in the initial bacterial population but type I persisters are defined as non-growing cells, and type II persisters are a small fraction of slowly growing bacteria. The abundance of type I persisters is determined by the inoculum size from the stationary phase, whereas type II persisters are proportional to the growing bacteria (Balaban et al., 2004).

Understanding the nature of antimicrobial persisters is further complicated by both the transient and reversible physiological state of persisters and their finite number in the population. The initial studies about drug persisters, or more in general persisters, consisted in genetical and environmental alteration of the bacterial population to unveil the impact of this fluctuation on the persister levels (Gollan et al., 2019). Although these studies allowed to shed light on some of the molecular mechanisms behind (drug)-persister formation, only with the use of single-cell research, such as time-lapse microfluidic microscopy and flow cytometry, it has been possible to comprehend the biology of persisters. The employment of time-lapse microfluidic microscopy allowed to track the behavior of single isolate bacteria over time, enabling to examine persister cells' history. However, one of the limitations of this technique consists of the number of cells that can be imagined simultaneously. A complementary and alternative technique is flow cytometry, by which coupling the cell sorting and using fluorescent reporter permits to analyze single-cells in a high-throughput fashion. Altogether, these studies have suggested that persisters are responsible for the chronic nature of some infections. However, they might also be selected by the pressure exercised by long-term antibiotic treatment, finally causing the failure of the complete clearance of the infection (Gollan et al., 2019).

The abundance and presence of persisters inside a clonal population varies accordingly to the considered pathogen, the pathogen's physiology, and the environmental features of the site of the infection. However, even though the molecular bases of drug persistence have not been fully mapped yet, several converging hypotheses have emerged to explain persisters' ability to protect themselves from antibiotics. Among them, the specific phase of the cell cycle and metabolic state in which bacteria are prior drug exposure, the bacterial ability to turn on/off stress-response genes, the cellular efflux or chemical modification of the drug, and lastly, the changes or reduction in the drug targets (Fisher et al., 2017).

The constant adaptive nature of persisters acts as a reservoir of microorganisms constantly hampering our effort in treating bacterial infections. The arising hypothesis of a connection between drug persistence and drug resistance underscores the relevance of

developing methods to eliminate this phenotypic drug-refractory subpopulation (Cohen et al., 2013). Although this area is still in its infancy, new strategies aiming to specifically target these cells or promote their susceptibility to the action of already known antimicrobial are being developed. One approach proposes to target the stress response(s) that modulate the persister formation. For instance, in this direction, several experimental observations have shown that the inhibition of the SOS response, either by genetic manipulation of the factors involved (*i.e.,* LexA and RecA) or by the use of RecA inhibitors enhance the bacterial susceptibility to different classes of antibiotics, such as quinolones, aminoglycosides and β-lactams (Cohen et al., 2013). Another attractive strategy interferes with persister survival by targeting the residual metabolic activity of the persisting organism. For instance, in *M. tuberculosis,* the block of the mycobacterial proteasome or ATP synthase has been shown to promote the death of non-growing bacteria (Andries et al., 2005; Gandotra et al., 2007). Other mechanisms targeting drug persisters also consider disaggregating existing biofilm structures, altering the detoxification mechanisms, potentiating the antimicrobial toxicity by enhancing the drug uptake, and using adjuvants that promote the antibiotic-induced production of ROS (Cohen et al., 2013).

In conclusion, the complex picture of persistence in response to the antimicrobial pressure highlights the existence of a dynamic network of pathways that modulate bacterial phenotypic adaptation. Hence, a more profound comprehension of these molecular processes and their role in promoting persistence in pathogenic organisms can yield to the identification of new drug targets and the development of more effective antimicrobial strategies to prevent the establishment of recalcitrant infection and the development of drug resistance.

2.6 Genetic resistance versus persistence

Persisters represent a small portion of a bacterial population able to survive, but non-replicate in an antimicrobial presence. Their presence or formation, notably in pathogenic bacteria, is associated with antimicrobial tolerance, which causes chemotherapy failure and the establishment of recalcitrant infections. However, *de novo* mutations or horizontal gene transfer can also promote genetic drug resistance. Drug resistance is defined as the heritable capacity of bacteria to replicate in the presence of high concentrations of antibiotics. It relies on different mechanisms, such as the use of efflux pumps, the antibiotic inactivation or degradation, and mutations in the drug target(s), with the intent to reduce the binding between the antibiotics and its molecular targets (Balaban et al., 2019).

Although the appearance of drug resistance started shortly after the antibiotics "golden era" (1940-1960), the high and diverse number of active molecules against bacteria reduced the initial concern regarding its insurgency. However, in the last years, the decreasing discovery of

new active compounds, the overuse, and misuse of antimicrobials resulted in the spread of (multi)drug-resistant infections, which The Infectious Diseases Society of America (IDSA) defines as "one of the greatest threats to human health worldwide" (Spellberg et al., 2011).

The identification of persisters enhanced the hypothesis that their antimicrobial tolerance might facilitate genetic resistance. Indeed, it has been proved both experimentally and by mathematic modeling that tolerant bacteria are a critical trait for the emergence of drug resistance (Windels et al., 2019). For example, whenever *M. tuberculosis* undergoes a short exposure to sublethal concentration of antibiotics, such as rifampicin, persisters will arise. Thus, persistent cell formation might represent an evolutionary reservoir from which resistant bacteria, to the same or another antibiotic, will form (Sebastian et al., 2017).

To date, the appearance of MDR- and XDR-TB strains represents one of the principal obstacles for TB eradication. **Table 1** summarizes the mutations in *M. tuberculosis* genes responsible for TB drug resistance. Generally, *M. tuberculosis*'s resistance depends on known mechanisms, such as the acquisition of spontaneous chromosomal mutations and intrinsic determinants (Smith et al., 2013). Interestingly, the newly introduced genetic mutations, contributing to drug resistance, are often associated with a fitness cost (Andersson and Hughes, 2010). The introduced mutation's fitness cost has been demonstrated to be often reduced by the appearance of compensatory mutations. Hence, compensatory mutations might correct the earlier mutations' cost and promote the stabilization of the resistant phenotype (Smith et al., 2013). Although the molecular mechanisms behind the insurgency of compensatory mutations have not been fully elucidate yet, the use of whole-genome sequencing starts to shed some light on it. Whole-genome analysis of rifampicin-resistant *M. tuberculosis* strains demonstrated that *M. tuberculosis* strains carrying specific mutations in *rpoA* and *rpoC* lead to the insurgency of MDR strains with higher fitness. Interestingly, these mutations are most likely to occur in the hotspot regions of the mycobacterial genomes (Comas et al., 2012). Moreover, new evidence reveals that the molecular bases of resistance might have a more complex origin since it can also occur in the absence of know mutations. In this direction, a whole-genome sequencing study proved that intergenic regions might intervene in promoting *M. tuberculosis* drug resistance (Zhang et al., 2013).

The appearance of mutations due to antimicrobial pressure is only one of the several aspects influencing mycobacterial resistance. For instance, *M. tuberculosis* endows intrinsic resistance mechanisms, such as the high impermeability of mycobacterial cell wall to antibiotics and the cytoplasm's active drug detoxification (Smith et al., 2013). The latter relies upon the pathogen's different methods to inactivate the drugs, such as modification of the drug targets, chemical modification of the drugs, or its enzymatic degradation, and finally, the action of efflux pumps. The primary function of efflux pumps is to transport nutrients, toxins, wastes, or signaling

molecules through the cell wall. Thus, the role of efflux pumps in drug resistance might represent a secondary and nonspecific transport mechanism (Smith et al., 2013). To date, 18 drug-related transporters have been characterized in mycobacteria, which confer low-level antibiotics resistance (Viveiros et al., 2012). Interestingly, the regulation of some efflux pumps has been coupled with antibiotic responsive regulatory systems, such as the transporters encoded by the *iniBAC,* which expression is regulated by the histon-like nucleoid-associated protein Lsr2 (Colangeli et al., 2007).

To conclude, current evidence demonstrates that *M. tuberculosis* withstands the selective pressure of antibiotics using different mechanisms, such as genetic and non-genetic tolerance. In particular, it has been shown that mycobacterial resistance relies on both passive and active mechanisms and the fitness cost of genetic mutations can be corrected with compensatory mutations, which can further promote the transmission of drug-resistant strains. Nevertheless, a deeper understanding of the molecular determinants behind the emergence of drug resistance is required to shorten the current chemotherapy for drug-resistant TB.

Table 1. Genes responsible for genetic resistance to the principal drugs used to treat M. tuberculosis.
The table has been built following the literature reported in Katoch 2019.

Drug	**MIC (μg/mL)**	**Gene(s) involved in resistance**	**Mechanism of action**
Isoniazid	0.02 - 0.2	*KatG inhA*, intergenic region of *kasA, oxyR-ahpC* and *furA-katG*	Inhibition of the mycolic acid biosynthesis
Rifampicin	0.05 - 1	*rpoB, rpoA, rpoC*	Inhibition of transcription
Pyrazinamide	16 - 50 (pH 5.5)	*pncA, rpsA*	Depletion of membrane potential
Ethambutol	1 - 5	*embB*	Inhibition of arabinogalactan synthesis
Streptomycin	2 - 8	*rpsL, rrs, gidB*	Inhibition of translation
Amikacin Kanamycin, Capreomycin	2 - 4	*Rrs, thyA*	Inhibition of translation
Quinolone	0.2 - 2.5	*gyrA, gyrB, parC* and *parE*	Inhibition of DNA gyrase
Ethionamide	2.5 - 10	*ethA, katG, ethR, mshA, ndh,* and *inhA*	Inhibition of the mycolic acid biosynthesis
Para-Aminosalicylic acid (PAS)	1 - 8	*thyA*	Inhibition of folic acid synthesis and iron metabolism
Bedaquiline	0.125 – 0.5	*atpE, mmpR*	Block of the ATP synthesis

Chapter 3. Bacterial RNA turnover

Prokaryotic gene expression was thought to follow relatively simple regulation, mostly controlled at the transcriptional level (Belasco, 2010). The transcription of bacterial genes relies on the formation of the RNA polymerase holoenzyme that recognizes specific promoter motifs, on the related promoter strength or binding affinity, and transcription initiation, elongation, and termination. In response to environmental stimuli, specific transcription factors use different mechanisms, such as steric hindrance, looping, protein-protein binding, and promoter conformational changes to either repress or activate transcription initiation (Belasco, 2010). Notably, the different transcription steps are also dominated by intrinsic molecular noise, described in more detail in the second chapter, due to the inherent stochasticity of biochemical processes. Indeed, intrinsic molecular noise prevails in the intracellular environment where the number of molecules is relatively low, and where even minor changes in the number of molecules can have significant consequences within small compartments acting on small timescales (Kærn et al., 2005). Also, the compaction/relaxation of DNA, mediated by nucleoid associated proteins (NAPs), can fine-tune the efficiency of transcription; the more the DNA is compacted, the less efficient transcription is (Browning and Busby, 2016).

Although gene regulation at the transcriptional level represents a key determinant of bacterial cellular homeostasis and in response to environmental stimuli, the introduction of -omics technologies has brought about a revolution in RNA biology over the past twenty years. As a consequence, the mere notion of direct linearity between transcription and translation has been surpassed by the rapid discovery of a plethora of regulatory RNA molecules, associated with several post-transcriptional control mechanisms, which affect the structure, stability, and function of cellular RNAs (Hör et al., 2018). These mechanisms can be embedded in the 5'UTR and 3'UTR of RNA molecules, associated with sRNAs, molecule-sensing riboswitches, ncRNA thermosensors, and can also be related to the RNA spatial organization (Hör et al., 2018; Llopis et al., 2010). Most sRNAs act stoichiometrically through mechanisms of mRNA degradation or competitive inhibition of translation, whereby the relative concentration of the sRNA with respect to the mRNA around a critical threshold is instrumental to the regulation of gene expression and may also help to filter out transcriptional noise (Waters and Storz, 2009).

Untangling the complex network of post-transcriptional regulation in prokaryotes represents a new major challenge in bacteriology. It will help to understand better gene regulation in a holistic manner and the ability of bacteria to adapt to environmental challenges.

3.1 Bacterial RNA spatial organization

The absence of membrane-enclosed organelles in prokaryotes, notably of a nuclear membrane spatially differentiating the nucleoid and the cytoplasm, led to the assumption that mRNA synthesis and translation are strictly coupled. However, thanks to the implementation of cutting-edge imaging techniques over the past two decades, original experimental datasets have been collected that brought to reconsider this assumption (Campos and Jacobs-Wagner, 2013). Indeed, despite their small size and the absence of membrane boundaries, bacteria have a remarkably intricate subcellular organization, with macromolecules and macromolecular complexes located within specific cellular compartments or positions. This compartmentalization hinges on dynamic processes that contribute to regulating the RNA infrastructure (Surovtsev and Jacobs-Wagner, 2018).

Fluorescence in situ hybridization (FISH) helped visualize the subcellular localization of RNA in fixed cells (Russell and Keiler, 2009). Additionally, the pioneering use of highly sensitive fluorescence imaging techniques, based on specific fluorescent protein binding of aptamer sequences fused to the RNA of interest, such as the RNA-binding coat protein of the MS2 phage fused to GFP (MS2-GFP) (Golding and Cox, 2004) and the fluorescence protein complementation assay, enabled to visualize the dynamic movement of RNA molecules inside living cells (Valencia-Burton et al., 2007). Collectively these techniques contributed to the conception of two models (**Figure 10**), describing the spatial distribution of DNA and RNA within the bacterial cell and the associated organization of gene expression (Surovtsev and Jacobs-Wagner, 2018).

The first model, or prevailing model (**Figure 10**), proposed by Jacobs-Wagner group, claims that the chromosome acts as a template for the newly transcribed RNA, which stays in the proximity of their transcription site in the nucleoid (Campos and Jacobs-Wagner, 2013). In this model, proposed for rod-shaped bacteria such as *E. coli, B. subtilis,* and mycobacteria, the ribosomes can freely diffuse through the nucleoid, located in a centered position, bind the nascent mRNA to form polysomes and initiate the translation during the transcription. In turn, polysomes would exit the nucleoid, causing a partial dissociation between transcription and translation (Surovtsev and Jacobs-Wagner, 2018). Lastly, accordingly to this model, mRNA degradation would also be spatially dissociated from the nucleoid. For instance, some RNA-degrading machinery was found to be associated with the membrane, accordingly to different spatial distribution models, namely, throughout the membrane, at the cell poles, or in a helicoidal pattern, presumably to orchestrate the RNA degradation process better, so as to not harm the cell (Khemici et al., 2008; Miczak et al., 1991).

Content removed for copyright

Figure 10. The spatial organization of gene expression in bacteria. *The experimental determination of the partitioning of ribosomes and DNA suggested that transcription and translation might be segregated in space. This spatial separation has been identified in several bacterial species and summarized in the upper panel (prevailing model) of the figure. Additionally, other bacteria, such as C. crescentus, exemplify another type of organization (lower panel). In this second model, the chromosomal DNA is spatially located throughout the cytoplasm, in which also the ribosomes are dispersed. In this second model, the ribosomes and the DNA share the same space* (Surovtsev and Jacobs-Wagner, 2018).

Based on the first model, three scenarios (**Figure 11**) were also proposed to explain gene expression despite the spatial distancing between DNA and ribosomes (Campos and Jacobs-Wagner, 2013). In the first scenario (**Fig. 11a**), naked mRNA would diffuse through the nucleoid towards the ribosomes located in the cytosol. Even though the high instability of naked mRNA does not support this first scenario, the spatial distancing of the RNA-degrading machinery, located at the membrane, would preserve the naked mRNAs' stability. In the second scenario (**Fig. 11b**), highly expressed genes would be found in the nucleoid's outermost part towards the region where the ribosomes are abundant. In contrast, non/poorly-expressed genes would remain far from the ribosomes in the nucleoid's innermost portion, from where they would migrate in response to induction, referred to as gene relocation. In the third scenario (**Fig. 11c**), a minority of ribosomes can start translation even inside the nucleoid, and polysomes could then exit the nucleoid towards the areas mostly populated by ribosomes, by means of entropic forces.

The second model (**Fig. 10**) originated following the observation in some bacterial species, such as *Caulobacter crescentus* and *Agrobacterium tumefaciens*, the localization of DNA and ribosomes, and RNA-degrading machinery appears to be more disordered and dispersed throughout the cell (Llopis et al., 2010).

Content removed for copyright

Figure 11. Three nonexclusive models explaining gene expression. *The proposed models reconcile the cooccurrence of transcription and translation with the spatial partitioning of DNA and ribosomes described for the prevalent model* (Campos and Jacobs-Wagner, 2013)

Although the two models display very different RNA spatial organization, an intriguing hypothesis is that gene expression preferably occurs close to the cellular space where the product of gene expression performs its function. (**Figure 12**). Hence, the RNA can localize in (i) a non-homogenous fashion following a helicoid path in the cytoplasm (**Figure 12C**), (ii) a discrete distribution at the membrane level (**Figure 12D**), (iii) at the foci near the poles (**Figure 12E**) and (iv) at the septum during cell division (**Figure 12F**) (Buskilay et al., 2014).

This hypothesis was experimentally proven, for instance, in the case of the *cat* gene, a cytoplasmic chloramphenicol acetyltransferase, and *lacY*, a membrane-anchored lactose permease, mRNAs in *E. coli* (Nevo-Dinur et al., 2011). The uneven distribution of *lacY* and *cat* within the cell was detected adding six copies of the MS2 coat protein fused with GFP upstream of these genes. The imaging of both fluorescent variants of *cat* and *lacY* transcript displayed a different pattern. Indeed, while the *cat* transcript showed a helix-like pattern, *lacY* mRNA is preferentially located in the proximity of the inner cell membrane (Nevo-Dinur et al., 2011). An additional experimental observation supporting the differential mRNA location based on the protein encoded function is illustrated by studying the polycistronic *bglGFB* mRNA (Nevo-Dinur et al., 2011). The *bglGFB* transcript encodes three proteins: BglF, a membrane-bound sugar permease, BglF, a soluble transcription factor, and BglB, a soluble phosphor-β-glucosidase. The visualization of an MS2-GFP tagged variant of the *bglGFB* mRNA showed its enrichment at the cell membrane, which suggests that the envelope-targeting peptide might predominantly influence the transcript's localization. This hypothesis was confirmed by analyzing the *bglG* and *bglB* mRNAs' spatial location alone, which respectively localize at the cell poles and in the cytoplasm (Nevo-Dinur et al., 2011).

Content removed for copyright

Figure 12. Diverse localization of RNA within a bacterial cell. *Schematic drawing of diverse RNA localization in bacteria. RNA molecules are colored in green and the nucleoid in gray. (A) Distributed throughout the cytoplasm, (B) Localization at site of the transcription in the nucleoid. (C) Helical localization. (D) Enrichment at the inner membrane. (E) Localization at the cell poles and (F) at the septum* (Fei and Sharma, 2018)

Although these datasets are increasing the understanding of the mRNA biology in bacteria, they are mainly limited to analyzing the localization of a single or a small number of transcripts. However, a more profound comprehension of the spatial organization of RNA at the transcriptomic scale in *E. coli* has been recently published by Zhuang and colleagues (Moffitt et al., 2016). By designing FISH probes in conjunction with super-resolution imaging, they were able to visualize that about 27% of all *E. coli* mRNA was associated with their encoded proteins' subcellular location, entailing a genome-wide spatial distribution of the mRNA based on the ultimate function of the gene product. The labeling of a certain subpopulation of the transcript as a function of their loci's genomic position proved that the genome-wide spatial organization of the mRNA does not influence transcript distribution. Thus, the transcripts' spatial location is preferably controlled by the subcellular location and function of the encoded proteins (Moffitt et al., 2016).

The post-transcriptional activity of trans-acting factors achieves an additional level of complexity in the RNA spatial organization. One relevant example is ComN, a post-transcriptional regulator of competence gene expression in *B. subtilis*. In *B. subtilis*, ComN is generally enriched at the septum and the pole of the cell. This discrete spatial distribution of ComN within the bacillus depends on its interaction with DivIVA, a general pole-marking protein, known to play a crucial

role in the spatial organization of several cellular processes (*i.e.,* division, chromosome segregation, gene expression, and /or protein segregation). Hence, although ComN activity is not essential for the complete assembly of the competence DNA uptake machinery at the pole, the delocalization of ComN resulted in a decrease in competent efficiency (dos Santos et al., 2012). This result might be explaining considering that the ComN delocalization from the pole could be induced to a delocalized production of ComEC, an integral membrane protein forming a DNA transport pore, and post-transcriptionally regulated by ComN. Thus, the ComN-depend relocation of ComEC might preclude ComEC in participating in the assembly of the polar DNA uptake complexes and with the consequent reduction of competent efficiency (dos Santos et al., 2012).

The discovery of bacterial sRNAs prompted researchers to investigate the subcellular localization by the use of FISH coupled with super-resolution microscopy. Unlike mRNA, sRNAs show lower spatial compartmentalization and a more homogenous cytoplasmic distribution (Fei and Sharma, 2018). Interestingly, the broad spatial distribution of sRNAs is consistent with the possibility of sRNAs acting on multiple targets, which are located in diverse subcellular locations. Indeed, a mathematical model predicts that the spatial location of the mRNA can influence sRNA-mediated regulation. This effect is particularly accentuated when a single sRNA acts on multiple targets. In this particular situation, the transcripts' differential spatial location might determine a hierarchy among the targets, which in turn could influence the spatio-temporal dynamic of their expression (Teimouri et al., 2017). Experimentally, this model was confirmed by examining the sRNA SgrS, a regulator of the glucose PTS transporter gene *ptsG* in *E. coli*. The efficiency of SgrS in repressing *ptsG* expression depends on the *ptsG* localization in close proximity to the membrane. For instance, the SgrS-mediated degradation of *ptsG* mRNA significantly decreases with the depletion of the PtsG transmembrane domain (Kawamoto et al., 2005). Albeit, it is still unclear whether it is Hfq inducing the SgrS localization or the formation of the SgrS-*ptsG* complex to localize Hfq, the inner membrane location of SgrS, and in consequence, efficient regulation of PtsG expression, appears to be influenced by the presence of Hfq presence (Kawamoto et al., 2005). Moreover, the membrane Hfq localization might also depend upon its interaction with the degradosome. Therefore, the interaction of the sRNAs with a specific mRNA target could be ascribed to other factors, such as the Hfq and RNase E localization, and the binding affinity between the target and the sRNA (Teimouri et al., 2017)

3.2 Bacterial mRNA degradation

Prokaryotes live in environments that require constant adaptation. This implies that the control of gene expression needs to be efficient and tightly controlled. Among the significant

mechanisms regulating gene expression, the modulation of mRNA lifetime represents a crucial step in bacterial adaptation (Laalami et al., 2014).

The half-life of bacterial mRNA varies from a few seconds to over an hour, depending on the microorganism. However, their half-life is generally shorter than the doubling time of the bacteria. Under the tightly controlled laboratory setting, where bacterial growth conditions are thought to be optimal, the mRNA average half-life tends to scale with the growth rate. In particular, for fast-growing bacteria, with a doubling time slower than 1 hour, the mRNA average half-life is estimated between 2 and 10 minutes (2.1 – 6.8 minutes in *E. coli,* and 2.6 – 5 minutes in *B. subtilis*) (Bernstein et al., 2004; Hambraeus et al., 2003). For slow-growing bacteria, as mycobacteria, the mRNA average half-life is longer than in fast-growing species. However, while the fast-growing *M. smegmatis* (doubling time ~ 3 hours) has an mRNA average half-life of about 5.2 minutes, similar to the fast-growing model microorganisms mentioned above, *M. tuberculosis* transcripts have a longer half-life of about 9.5 minutes, which might depend on its slow growth-rate (doubling time ~ 20 hours) (Rustad et al., 2013). The different mRNA stability reported in different microorganisms might also be linked to their evolutionary adaptation to given environments.

The metabolic control of the mRNA stability has to be efficient in order to (i) enable the microorganisms to timely adapt to environmental changes, (ii) synthesize the needed concentration of a given protein, and (iii) recycle the ribonucleotides for the synthesis of new RNA molecules (Laalami et al., 2014). Thus, bacteria efficiently regulate mRNA stability by tightly controlling the initiation step of transcript decay following first-order kinetics, which is characterized by a single exponential rate constant dictated by a rate-limiting initial step, so that degradation occurs according to an all-or-none model (Laalami et al., 2014).

Ribonucleases (RNases) are key enzymes involved in RNA turnover, and they can be divided into endoribonucleases and exoribonucleases depending if the degradation step starts with internal cleavage of the transcript or at the 5'- or 3'-end of the transcript. Interestingly, Gram-positive and -negative bacteria display very distinct major RNases responsible for the initial step of mRNA turnover. However, the presence or absence of a specific RNase in the considered organism will define the mechanism by which the transcripts are degraded (Laalami and Putzer, 2011).

The initiating nucleolytic decay of an mRNA can hypothetically follow three paths: the first two hypothesize the mRNA attack by either a 5-' or 3'- exoribonuclease, and the latter a cleavage within the transcript by an endoribonuclease. Despite the presence in all bacteria of 3'-exoribonuclease, the 3'- mRNA degradation is considered biologically inefficient. Indeed, the almost ubiquitous presence of a stem-loop at the 3'- end of the mRNA suggests the block of the nucleolytic action of the 3'-exoribonuclease (Hui et al., 2014). Therefore, the molecular mechanism behind the mRNA decay initiation suggested that the first rate-limiting step had to

rely upon the nucleolytic action of an endoribonuclease. This suggested model was demonstrated with the discovery of the RNase E (Babitzke and Kushner, 1991).

Bacteria own a wide number of ribonucleolytic enzymes that they employ in regulating the mRNA turnover, here briefly described with the only exception of the RNase E. A detailed understanding of the biological role played by the RNase E within the bacterial physiology is outlined in chapter four.

3.2.1 Endoribonucleases

Endoribonucleases (endoRNases) are nucleolytic enzymes that can cleave an RNA molecule internally and release fragments of various sizes. They can either be highly specific, recognizing one or few binding sites in the transcript, or non-specific, which will result in extensive degradation of the substrate (Li and Deutscher, 2004).

Endoribonuclease Y. The RNase Y is a membrane-bound RNase, which can substitute the RNase E in bacteria species lacking a homolog of the RNase E (Lehnik-Habrink et al., 2011). For instance, a critical role of the RNase Y in the regulation of the RNA metabolism has been shown in *B. subtilis* (Durand et al., 2012a), and in the control of virulence factor in *Streptococcus pyogenes* and *S. aureus* (Hui et al., 2014). The RNase Y includes a transmembrane domain, essential for its function, a disordered coiled-coil domain, an RNA-binding KH domain, and a catalytic HD domain (Lehnik-Habrink et al., 2011). Furthermore, similarly to the RNase E, the RNase Y is a not specific endoribonuclease preferentially binding to single-stranded RNA AU-rich region (Shahbabian et al., 2009).

Endoribonuclease III. The RNase III, differently from the RNase E and RNase Y, has a more limited regulatory function in controlling gene expression. It is only essential in *B. subtilis*, where it is involved in the chromosomal defense against the encoded toxins (Durand et al., 2012). It specifically acts on double-stranded RNA regions, and although it is generally involved in the maturation of the ribosomal RNA, the RNase III also selectively participate in the processing and degradation of mRNAs, sRNAs, and CRISPR RNAs (Hui et al., 2014). Structurally, the RNase III is a homodimer, and each monomer includes an endonucleolytic domain and a double-stranded RNA-binding domain. The two catalytic domains present in the monomer acts independently, generating products with a 2 bp overhang at the 3'-end. It is a non-specific endoribonuclease, but the presence of distinctive characteristics in and out of the cutting site influence the efficiency of the bond cleavage (Pertzev and Nicholson, 2006).

Minor endoribonucleases. This category includes other endoRNases primarily involved in the tRNA maturation, although they might also participate in the degradation of some mRNAs, such as the RNase P and the RNase Z (also known as RNase BN). The RNase P is a ribonucleoprotein complex involved in the maturation of the 5'-end of tRNAs and the processing of non-coding regions present inside some transcripts (Li and Altman, 2003). In *E. coli*, the RNase Z seems to display both an endonuclease and a 3'- exonuclease activity. It is primarily implicated in the elimination of tRNA with an aberrant 3'-end, but it can also participate in the decay of few mRNAs (Perwez and Kushner, 2006)

3.2.2 Exoribonucleases

The exoribonucleases (exoRNases) exert their nucleolytic activity degrading the RNA molecules from either the 3'- or the 5'-end. ExoRNases can act on the substrates following different mechanisms. They can processively cleave the substrate without dissociating from it, continuously releasing nucleotides. Moreover, the digestion of the substrates might be stopped by presence of a secondary structures in the transcript. ExoRNases can also distributively degrade the substrate. In this model, the exoRNases dissociate and rebind the substrate after one or a few catalytic events. For a long time, it was hypothesized that bacteria only owned exoRNAses starting the cleavage of the transcript at the 3-terminus of the mRNA. The absence of 5'-exoribonuclease was explained, accounting for the lack of a 5'- cap structure in the mRNA to protect the transcript from unwanted degradation initiation (Li and Deutscher, 2004). This belief was overturned by discovering RNase J as a 5'-exoribonuclease (Mathy et al., 2007).

Phosphorolytic 3'-exoribonuclease. This type of exoRNases, which belong to the PDX family, use orthophosphate as a nucleophile to irreversibly produce nucleoside diphosphate. The polynucleotide phosphorylase (PNPase) and the RNase PH belong to this group, and while the first one is known to be deeply involved in mRNA turnover, the second one principally acts in the context of tRNA maturation and only partially participate in the mRNA turnover (Jain, 2012). PNPase usually assembles as a homotrimer, and each monomer displays two homologous but non-identical PH domains. Generally, only one domain (the second) is active, a KH domain, and an S1 domain. The three monomers are structurally arranged in a ring-shaped fashion. This structural orientation locates the KH and S1 domain, essential for binding the substrate, to surround one end of the central channel. The 3'-5' exoribonuclease activity of the PNPase processively degrades the substrate until it encounters a stem-loop. To overcome the presence of stable secondary structure in the substrate, in *E. coli*, PNPase works in association with the DEAD

box ATP-dependent RNA helicase RhlB. Thus, in the presence of stem-loop, RhlB would unwind these secondary structures and allow the PNPase to almost completely degrade the substrate, releasing at the end a 5'-terminal dinucleotide. Interestingly, *in vivo*, the PNPase shows both a 3'-5' degradative and synthetic activity. The latter activity allows the PNPase to add a poly(A) tail at the 3'-terminus of the transcript, which can facilitate the 3' exonucleolytic cleavage of RNA containing secondary structure (Symmons et al., 2000).

Hydrolytic 3' exonucleases. Hydrolytic exoribonucleases irreversibly catalyze the substrate's degradation, and for this reason, they can only work as a degradative enzyme. In *E. coli*, as other γ-proteobacteria, two hydrolytic exoRNases are present: the RNase II and the RNase R. The depletion of either of these enzymes or PNPase individually is not lethal, but the combined elimination of the PNPase together with either RNase II or RNase R results in a non-viable bacterial phenotype. The RNase II is present in the cell as a monomer, which structurally contains one catalytic RNB domain flanked on both sides by the RNA-binding domain. It binds 3'- single-stranded substrates, and the processivity of this exoRNase is stalled in the presence of a stable stem-loop. Contrarily to the PNPase, the presence of a secondary structure determines the dissociation of the RNase II few nucleotides downstream (Spickler and Mackie, 2000). Unlike the RNase II, the RNase R has the intrinsic property of unwinding the secondary structure present on the target and completely degrading the mRNA. However, similarly to the RNase II, it still requires a 3'- single-stranded binding with the substrate (Vincent and Deutscher, 2009).

5'- exonucleases. The only known 5'- exoribonuclease in bacteria is the RNase J (Durand et al., 2012a). The RNase J is absent in *E. coli*, and in *B. subtilis,* it has been demonstrated that the RNase J plays a critical role in the regulation of the mRNA decay. *B. subtilis* encode for two paralogs of the RNase J, the RNase J1 and RNase J2, which *in vivo* assemble as heterotetramer. Although both the RNase J1 and RNase J2 participate in the mRNA turnover, only the RNase J1 has a 5'- exonuclease activity, and its depletion profoundly influences mRNA decay. Moreover, while Firmicutes generally encoded for two RNase J, other bacterial species have only one single RNase J. Structurally, an RNase J monomer exhibits a metallo-β-lactamase domain, a β-CASO domain, and a carboxy-terminal domain. The RNA-binding domain's spatial distribution determines the formation of a channel where only a 5'- monophosphorylated transcript can enter. Moreover, the structural organization of the catalytic site explains the ability of the RNase J to act both as a 5'-exoribonuclease and endoribonuclease (Durand et al., 2012b).

Oligoribonuclease. Oligoribonuclease (Orn) is an exoribonuclease that, differently from other exoRNAs, bind RNA no longer than 5 nucleotides. Orn acts on the 5'-terminal oligonucleotides

products generated by the degradation of a longer RNA transcript by PNPase, RNase II, and RNase R. It has the critical role of preventing the misincorporation of these oligonucleotides into new transcript and to restore the pool of RNA precursors. Due to its critical role in maintaining the bacterial physiology, in *E.* coli, Orn is an essential RNase. Orn is not present in all bacterial species, but bacteria lacking Orn encode a diverse ribonuclease (NrnA/B or NrnC), displaying similar properties (Hui et al., 2014).

3.2.3 Ribonuclease toxin

The Toxin-Antitoxin (TA) system, already described in chapter two, represents a continuously growing reservoir for new ribonucleases. TA systems, depending on their mechanism of action, can be classified into five different types. RNases are known to regulate the translation of type I toxins; which activity is inhibited by small antisense RNA acting as an antitoxin. However, several toxins are classified as RNases themselves and are known as RNA interferases. By accounting for their mechanism of action, RNA interferases can be divided into two classes: they can cleave the substrate in (i) a ribosome-dependent manner (*i.e.,* RelE) or (ii) absence of ribosome (*i.e.,* MazEF, VapBC, and ToxN) (Cook et al., 2013). The RNA interferases acting in a ribosome-dependent manner exhibit only a weak endoribonucleolytic activity, and the best-characterized one is RelE, a component of the RelBE TA system. Molecularly, RelE binds to the site A of the ribosome, the mRNA target is significantly relocated, which, in the end, results in a 2'-OH-dependent hydrolysis. This type of toxin preferentially cleaves the transcripts upstream of purines between the second and third positions of codons (Goeders et al., 2013). RNA interfaces acting in the absence of ribosomes display a wider range of molecular mechanisms used to cleave the mRNA. Interestingly, they also display a sequence specificity. For instance, with particular reference to mycobacteria, the mycobacterial VapC toxin specifically targets transcripts containing a -AUA(U/A)-hairpin-G- sequence. Furthermore, in this case, the presence of a secondary structure in the mRNA determines the specificity of the toxin's nucleolytic cleavage (McKenzie et al., 2012).

3.2.4 Other enzymes involved in mRNA decay

The mRNA decay is a complex molecular process, and to carry out these processes, bacteria employ a large variety of endoRNase and exoRNases. However, these nucleolytic enzymes' action is often coupled with the activity of other proteins, such as RNA helicases, poly(A) polymerase, Hfq (Bandyra et al., 2013).

RNA helicase. RNAs are transcribed as single-stranded molecules. However, they can fold themselves to form secondary structures essential for their proper functioning and stability (Belasco, 2010). The presence of these secondary structures within the transcript might block the nucleolytic activity of RNases. Hence, it is not surprising that bacteria exploit the ATP-depended unwinding function of the helicases to alter RNA molecules' secondary structure. The helicases participating in RNA metabolism are characterized by the DEXD/H amino acid motif and are usually referred to as DEAD-box helicase. In *E. coli*, there are five well-characterized DEAD-box helicases (*rhlB, rhlE, srmB, dbpA,* and *csdA*), which participate in several aspects of RNA decay, such as mRNA degradation, ribosome biogenesis, and/or stress response (Mohanty and Kushner, 2018).

Poly(A) Polymerase I (PAP I). The role played by PAP I in bacterial RNA decay was not wholly understood until it was proved that the addition of poly(A) tail to the transcript enhances their 3'-exonucleolytic degradation (Belasco, 2010). Interestingly, while many Gram-negative bacteria encoded for a PAP I, there is no orthologous in *B. subtilis.* Lastly, in *E. coli*, PAP I interacts with other RNA-binding proteins, such as PNPase and Hfq forming a multienzymatic complex, known as PAPI polyadenylation complex (Mohanty and Kushner, 2016).

Hfq. Hfq is a small RNA-binding protein, which preferentially interacts with sRNA and mRNA. It assumes a hexameric ring-like structure, which shows three RNA binding surfaces (Künne et al., 2014). A proximal face with a preference for U-rich region (*i.e.,* sRNAs displaying a 3' poly U tail), a distal face selectively binding A-rich sequence, and a lateral side (Künne et al., 2014). The role of Hfq in mRNA turnover is most likely indirect. Indeed, Hfq is primarily involved in forming sRNA-mRNA duplex by facilitating the pairing of most *trans*-acting sRNAs to their mRNA targets (Künne et al., 2014). Surprisingly, Hfq is absent in several bacterial species, and few species, such as *B. anthracis,* even own two Hfq proteins (Brantl, 2012). However, while the role of Hfq in regulating the activity of sRNAs is well established in Gram-negative bacteria, its role in Gram-positive bacteria encoding for an Hfq orthologous is more controversial. For instance, to date, the LhrA sRNA in *L.* monocytogenes is the only example of Hfq-dependent *trans*-acting sRNA regulation (Nielsen et al., 2009). Whereas in other Gram-positive bacteria, such as *S. aureus*, no influence of Hfq has been demonstrated for the sRNA-mRNA interaction. Considering that several Gram-positive bacterial species, such as mycobacteria, lack for an Hfq orthologous, an interesting hypothesis suggests that these bacteria might use a not-yet identified RNA-binding protein able to substitute Hfq (Brantl, 2012).

3.3 mRNA decay in Gram-positive and Gram-negative bacteria

Over the years, mRNA turnover has been extensively studied in the Gram-negative *E. coli* and Gram-positive *B. subtilis.* These studies highlighted that the genome of both model microorganisms encodes for diverse RNases (**Figure 13**). RNA degradation has been attributed to the activity of 21 RNases in *E. coli* (Deutscher, 2015) and 15 RNases in *B. subtilis* (Durand and Condon, 2018). Interestingly, the key RNases driving RNA degradation in these two microorganisms are different. In *E. coli,* the endoribonuclease E (RNase E) was reported to be the main enzyme regulating RNA stability and essential for cell viability. Orthologs of the RNase E are usually absent in Gram-positive bacteria. In contrast, RNA turnover was mainly associated with the enzymatic activity of the RNase J1/J2 and RNase Y in *B. subtilis* (Laalami et al., 2014).

***Figure 13**. **Schematic summary of known ribonucleases and their function.** Known RNases in E. coli, B. subtilis and in mycobacteria. The essential RNases are indicated in red (Durand et al., 2015)*

More in-depth phylogenetic examination of the RNases encoded in the genome of Gram-positive bacteria revealed a certain degree of species-to-species variation (Durand et al., 2015). In particular, the main RNase regulating RNA decay in low-GC Gram-positive bacteria is the endoribonuclease Y (RNase Y), which is absent in GC-rich Gram-positive bacteria, such as *M. smegmatis*, *M. tuberculosis,* and *Streptomyces coelicolor.* In contrast, an ortholog of the RNase E has been reported as one of the essential RNases controlling RNA processing in both non-pathogenic and pathogenic mycobacterial strains (Durand et al., 2015).

In both Gram-positive and Gram-negative bacteria, the initiation of bulk mRNA degradation depends on the assembly of a multienzymatic complex, referred to as the RNA degradosome. Although its composition varies depending on the species, at least one RNase and a DEAD-box RNA helicase are the core components of the degradosome complex. However, more than one RNase is usually part of the complex, where often, an exoribonuclease is also reported. The presence of a helicase ensures the proper unfolding of possible secondary structures on the transcript, making it accessible to one or more RNase action. Furthermore, in some instances, the RNA degradosome interacts with a glycolytic enzyme, such as enolase, aconitase, or a phosphofructokinase. Even though the role played by this metabolic enzyme has not been clarified yet, in *E. coli,* the interaction of the enolase with the RNA degradosome has been hypothesized to couple the metabolic status of the cell with the rate of mRNA degradation (Tejada-Arranz et al., 2020a).

However, similarly to Gram-negative bacteria, the initial and limiting step in Gram-positive bacteria is the cut of the transcript by endoribonuclease to enable RNA degradation by an exoribonuclease action of a second endoribonuclease. This step can overcome the presence of a triphosphate group at the 5'-end of the bacterial transcripts, which, together with Rho-independent terminator at the 3'-end, functionally protect the transcript from the RNase attack. The transcript's internal cleavage by an endoribonuclease will generate a 5'-monophosphate ending transcript, which can be ulteriorly degraded. Another way to overcome the 5'-triphosphate protection of the mRNA is through RNA pyrophosphohydrolase (RppH). The Rpph-induced formation of the 5'-monophosphate end can stimulate the catalytic activity of the critical bacterial RNases, such as the RNase E, RNase J1/J2, and RNase Y (Deana et al., 2008; Hsieh et al., 2013)

3.3.1 RNA degradosome in Gram-negative bacteria

The RNA degradosome of *E.coli* has been the first RNA-degrading machinery described in detail, in which the RNase E acts as both catalytic and structural core of the complex, preferentially binding 5'-monophosphate single-stranded RNA molecules (Bandyra et al., 2013). RNase E includes two domains, an N-terminal catalytic domain for RNA binding and cleavage, and a C-terminal unstructured domain. The C-terminal domain contains intrinsically disordered regions necessary for the binding with the other components of the complex: the DEAD-box helicase RhlB, the 5'-3' exoribonuclease polynucleotide phosphorylase (PNPase), and the glycolytic enzyme enolase (Bandyra et al., 2013).

The *in vitro* reconstitution of the canonical RNA degradosome showed that the stoichiometry of assembly of the complex was 1:2:1:1 (RNase E: PNPase:Eno:RhlB) for bacteria growing in rich medium. In contrast, bacteria cultured in minimal medium experienced a downregulation of RhlB expression, resulting in its absence from the complex. These findings concluded that changes in bacterial growth conditions alter the stoichiometric composition of the RNA degradosome complex (Aït-Bara and Carpousis, 2015). Furthermore, RNase E was also reported to interact with non-canonical enzymes involved in the RNA metabolism, such as Hfq (Ikeda et al., 2011), the ribosomal protein S1, L4, and L17, and the chaperon proteins DnaK and GroEL (Mauri and Dehò, 2008). Although the nature of these interactions needs further elucidation, they are likely to be essential for the post-transcriptional regulation of bacterial gene expression.

The structural analysis of the RNase E C-terminal domain revealed the presence of a membrane-anchoring sequence, known as segment A, which has been proved to locate the RNase E and the degradosome at the inner part of the cellular membrane (Khemici et al., 2008). Due to this RNase's essentiality, the RNase E catalytic site is highly conserved in different bacterial species, but alterations in other domains of the protein are not uncommon. For instance, the RNase E, encoded by *C. crescentus,* does not exhibit segment A. The absence of the segment A may justify the patchy distribution of RNase E inside the cell, with clusters localizing at the two subcellular chromosomal loci encoding for the highly expressed rRNA genes (Bayas et al., 2018). In contrast, the diverse location of the RNase E and the RNA degradosome inside the cell in relation to the absence or presence of segment A needs further validation. Irrespective of the segment A, a viable hypothesis is that the spatial organization of the RNA degradosome could be a mechanism exploited by the bacterial to control the RNase E activity and to limit the toxic effect of RNA degradation on cell fitness (Al-Husini et al., 2018). Differences in the composition of the enzymes participating in the assembly of the RNA degradosome have been reported in Gram-negative bacteria, such as *H. pylori.* Although the *H. pylori* genome does not code for an RNase E ortholog, an RNase J-based minimal degradosome has been identified (Redko et al., 2013).

In conclusion, although RNases can act alone, the formation of a multienzymatic complex, such as the RNA degradosome, efficiently facilitates the complete turnover of the attacked substrate. Also, considering the wide variability in both the structure and sequence of the RNA, it is likely that the assembling complex exhibits high flexibility to accommodate different substrates. Indeed, the complex's intrinsic flexibility is hypothesized to allow the scanning of the degradosome along the polysomes and promote the recognition of suitable transcript to initiate the degradation. Furthermore, while a more complex picture regarding the presence, in different bacterial species, of diverse RNA degrading machinery, is emerging, we still do not fully comprehend how the composition of the RNA degradosome can affect its action over the target(s).

Thus, further studies are required to understand the molecular mechanism governing the RNA degrading machinery and how they finely regulate the bacterial homeostasis.

3.3.2 RNA degradosome in Gram-positive bacteria

Whereas the RNA degradosome in *E. coli* has been extensively studied and detailed molecular information regarding its structure and function are known, understanding the RNA degradosome in Gram-positive bacteria has been only recently investigated. The existing knowledge about the structure and function of the enzymes participating in the RNA decay control in Gram-positive derives from studies performed in *B. subtilis* and *S. aureus.* Nevertheless, the molecular mechanisms behind the regulation of the RNA turnover in Gram-positive bacteria are still poorly understood (Cho, 2017). Generally, Gram-positive bacteria do not have a homolog of the RNase E, which acts as a scaffold protein for the RNA degradosome. However, they encode for a new set of endoribonucleases, absent in *E. coli*, namely the RNase Y and exo- and endo-ribonuclease RNase J1 and RNase J2, which have been proved to be the key RNases regulating the RNA decay in Gram-positive bacteria. RNase Y, RNase J1, and RNase J2 are known to interact with each other, forming RNA-degrading complexes that might differ from those described in *E. coli.* Like RNase E, RNase Y is hypothesized to act as a scaffold for a "degradosome-like" complex.

Moreover, RNase Y displays an intrinsically unstructured domain with a predicted putative membrane-anchor motif at its N-terminal domain (Durand and Condon, 2018). Shahbabian and colleagues demonstrated that by depleting the RNase Y in *B. subtilis*, the half-life of bulk RNA increased more than 2 folds, suggesting that RNase Y has a role equivalent to that of RNase E in *E. coli*, acting as the key endoRNase regulating RNA decay in *B. subtilis* (Shahbabian et al., 2009). Afterward, it was shown that RNase Y is not an essential enzyme in *B. subtilis* (Figaro et al., 2013). Indeed, *B. subtilis* mutant strains devoid of RNase Y were viable, although they grew at a slower rate and failed both to sporulate and to become competent. Despite the non-essentiality of RNase Y, the whole-transcriptome analysis of strains devoid of RNase Y showed significant downregulation of about 20% of genes encoding single proteins and many ncRNA, entailing a vital role of this enzyme in RNA turnover (Figaro et al., 2013). Contrarily, RNase Y appears to regulate only about 4% of mRNAs and sRNAs in *S. aureu*s, indicating some functional redundancy with other endoribonucleases' activity. Interestingly, in *S. aureus,* the SaeRS transcript, an uncharacterized general virulence regulatory system, is processed and stabilized by the RNase Y (Marincola et al., 2012).

In order to prove the existence of a "degradosome-like" complex in *B. subtilis* and *S. aureus,* a bacterial two-hybrid assay was used to probe the interactions of the RNase Y with other known degradosome components. While in *B. subtilis,* interactions of the RNase Y with glycolytic

enzymes, such as the enolase and phosphofructokinase, PNPase, the DEAD-box helicase CshA and RNase J1 were detected, in *S. aureus* RNase Y was shown to interact only with the enolase and helicase CshA. Although the formation of an RNase Y "degradosome-like" complex is attractive, all the experimental approaches failed in purifying a coherent degradosome in both *B. subtilis* and *S. aureus.* One possible explanation is that the reported interactions of RNase Y with other putative partners are only transient and occur exclusively when RNA degradation is required but disassociated shortly after (Redder, 2018).

RNase J1 and J2 are two 5'-3' exoribonucleases deemed to play a significant role in mRNA degradation in both *B. subtilis* and *S. aureus.* RNase J1 and RNase J2 are highly conserved at the protein levels and do not show any significant structural difference. They are located in two separate operons on the genome. While the RNase J2 is hypothesized to be in a monocistronic transcript, the RNase J1 is encoded in a bicistronic operon located downstream of the *rpoY* locus, which codes for the firmicute-specific RNA polymerase (Redder, 2018). However, *in vivo,* it is hypothesized that while the RNase J1 provides most of the activity, the RNase J2 regulates or stabilizes RNase J1 activity (Durand et al., 2015). It was demonstrated that RNase J1 and J2 strongly interact with each other forming heterodimers, but the interaction of RNase J1 with RNase Y in the hypothetic degradosome complex remains to be clarified (Durand et al., 2015).

Surprisingly, mycobacteria genome encodes for the crucial RNases of both Gram-positive and Gram-negative bacteria. Indeed, the presence of functional orthologs of both RNase E (Zeller et al., 2007) and RNase J (Taverniti et al., 2011) have been observed. However, the interplay between these two RNases is still not understood fully in mycobacteria. While the functional activity of the mycobacterial RNase E will be extensively described in chapter four here, significant attention will be given to the role of the mycobacterial RNase J. The generation of the conditional mutant for both the RNase E and RNase J proved that in *M. smegmatis*, only RNase E is essential, suggesting that the 5'-3' exonucleolytic activity of the RNase J is dispensable (Taverniti et al., 2011). In more detail, both the *rne* and *rnj* genes were put under the control of a Tet-Off pristinamycin inducible systems, and while in the absence of the inducer, the *rne* mutant was not viable, growth was still observed for the *rnj* mutant (Taverniti et al., 2011). The same study also demonstrated that both RNase E and RNase J are involved in rRNA maturation. Indeed, while conditional depletion of RNase E proved to affect the 16S rRNA's maturation significantly, RNase J knock-out significantly affected the maturation of the 23S rRNA. In *M. smegmatis*, mutant strain depleted of the RNase J exhibit no mature 23S rRNA. Nevertheless, the absence of mature 23S rRNA appears not to compromise the viability of the bacteria. This can be explained by accounting that the precursors of the mature 23S rRNA are only 14 nucleotide longer at the 5', and they can still be able to efficiently assemble a functional ribosome (Taverniti et al., 2011).

The presence of both RNase E and RNase J raised the hypothesis that more than one RNA-degrading complexes might be assembled in mycobacteria. Thus, a recent study, aiming to characterize the RNA-degrading complex(es) in mycobacteria at the transcriptomic and proteomic level, reported that in *M. tuberculosis,* both RNase E and J contribute to the formation of one of two distinct RNA degradosome complex(s). However, it is unlikely that they interact with each other (Płociński et al., 2019). By using pull-down experiments, the authors proved that the RNase J strongly interacts with the PNPase and the DEAD-box helicase RhlE, but not with the RNase E. In conclusion, in mycobacteria, it has been recently proposed either the presence of a single RNA degradosome complex, including RNase E, PNPase, RhlE, and RNase J, where RNase E and RNase J do not directly interact with each other or in the alternative, two separate complexes, each including only one of the two ribonucleases (Płociński et al., 2019).

Moreover, the use of a CRISPR/dCas9 inducible system to downregulate the mRNA level of the RNase E and PNPase showed that the deregulation of the mRNA level of these two proteins deeply affects mycobacterial biology. Thus, the depletion of either PNPase or RNase affected around 35 transcripts encoding for essential genes, such as for protein implicated in cell division, response regulators, and transcription factors. Interestingly, the depletion of PNPase and RNase E also resulted in changes in the pool of mycobacterial sRNAs, such as MTS2823 sRNA. MTS2823 sRNA is a 6S RNA-like molecule hypothesized to deregulate the RNA polymerase and finally influence how the bacilli respond to the environment. Lastly, the downregulation of the mRNA level of PNPase resulted in deregulation of the RNase P, which led to the alteration in the maturation of tRNA and rRNA (Płociński et al., 2019)

In conclusion, although this study set the ground for the molecular characterization of the RNA decay in mycobacteria, further studies are still required to comprehend better the function of all the players in the mycobacteria physiology.

Chapter 4. The endoribonuclease E

Cellular mRNA levels depend on the balance between synthesis and degradation rates. Since the 1960s, it is known that mRNA is an unstable molecule, whose degradation process has been intensively studied over the years, given its importance for the bacterial cell physiology (Kennell, 2002). RNases catalyze the cleavage of phosphodiester bonds on RNA molecules. While endo-RNases cut the RNA substrate internally, yielding RNA fragments, exo-RNases degrade the RNA substrate from either the 5′- or 3′- end, one nucleotide at a time. RNases are crucial enzymes in various aspects of RNA metabolism. They are not only involved in RNA degradation and turnover but also RNA processing and maturation. Consequently, RNases are implicated in crucial bacterial cell functions, such as DNA replication, gene regulation, and certain immune defenses against foreign DNA (Aït-Bara and Carpousis, 2015).

Historically, the model of mRNA degradation in prokaryotes grounded on studies carried out in model microorganisms. For instance, numerous endo-RNases and 3'- exo-RNases were found in *E. coli*, where, due to the presence of typical protective hairpin loops at the final 3'-end of mRNA molecules, the RNA substrate was first thought to be attacked from the inside and then progressively degraded from the 3'-end (Belasco, 2010). In the 1970s, the first evidence was found of a gene that affected mRNA's stability, referred to as *ams*, later renamed *rne,* and coding for the low-specificity endo-RNase E. The discovery of the role of RNase E in degrading mRNA *in vivo* was supported by the isolation of thermosensitive mutant strains, carrying the mutation *rne-3071*. The decay rate of the total pulse-labeled mRNA and the accumulation of 5S rRNA precursors varied in these mutant strains depending on the growth temperature (Ono and Kuwano, 1979; Taraseviciene et al., 1991).

E. coli genome encodes for at least 21 RNases. Among them, only three are essential: the RNase P, the oligo-RNases, and the RNase E. The RNase P acts on generating mature 5' terminus of all tRNAs and catalyzing a limited cleavage of a few mRNAs. The oligo-mRNA functions as an mRNA scavenger converting oligonucleotide products from the late stages of mRNA decay into mononucleotides. Interestingly, the reasons behind its essentiality are still not understood. RNase E was initially discovered as the endoribonuclease responsible for processing rRNA precursors to mature 5S rRNA (Mackie, 2013).

For about half a century, RNase E has attracted scientists' attention for its essentiality and conservation in different microorganisms. Because of its involvement in several aspects of RNA metabolism, namely, the processing and maturation of the 5S rRNA and 16S rRNA precursors, the activity on different mRNAs and several tRNA precursors, RNase E gained a central role in both spatial and temporal regulation of the RNA turnover in prokaryotes (Mackie, 2013).

4.1 Phylogenetic distribution of the RNase E

The RNase E encoding gene *rne* and its paralog non-essential gene *rng*, encoding the RNase G, are the founding member of a widespread family of protein in bacteria and chloroplast. The analysis of the primary sequence of the RNase E identified two structurally separated regions. While the N-terminal region carries the catalytic site and the domain responsible for the homotetramer assembly, the highly disordered C-terminal domain is responsible for the interaction with the membrane, RNA, and protein (Callaghan et al., 2005). In accordance with the primary structure of the RNase E/G homologs, they can be classified into five groups (type I, II, III, IV, and V). Moreover, the characterized RNase E/G homologs display activity and function similar to the RNase E of *E. coli,* which could be justified by the considerable sequence conservation (Aït-Bara and Carpousis, 2015).

Type I enzymes share a similar primary structure with the RNase E of *E. coli* and exhibit the same canonical interactions with proteins belonging to the degradosome (Aït-Bara and Carpousis, 2015). Type I homologs have been identified in several γ-proteobacteria, including *Yersinia pseudotuberculosis* (Yang et al., 2008), *Vibrio angustum* S14 (Erce et al., 2010), *Pseudoalteromonas haloplankis* (Aït-Bara and Carpousis, 2010), *Pseudomonas syringae* LzW4 (Purusharth et al., 2005), and it is ubiquitous in cyanobacteria (Aït-Bara and Carpousis, 2015).

Type II enzymes are ubiquitous in α-proteobacteria and have been characterized in diverse organisms, including *C. crescentus, Rhodobacter capsulatus,* and *Rhizobium leguminosarum.* Unlike type I, type II enzymes contain a string of amino acids (60-180 aa) rich in arginine and proline residues (RP-rich), enclosed in the RNA binding domain (S1). Although the RP-rich stretch function has not been fully understood yet, the presence of a negatively-charged *α*-helix may hinder RNA binding (Aït-Bara and Carpousis, 2015).

Type III enzymes are typical of actinobacteria and exhibit a catalytic domain flanked by N- and C-terminal extensions. Mycobacterial RNase E belongs to type III but shares a higher similarity with the RNase G, although it can form a multienzymatic complex (Aït-Bara and Carpousis, 2015). The mycobacterial RNase E will be described in more detail at the end of this chapter.

Type IV enzymes are similar to the RNase G of *E. coli*. Consistent with this, they do not have the small domain and the non-catalytic C-terminal domain present in the RNase E of *E. coli*. Their physiological role remains to be unveiled. Although type IV enzymes are likely to play an ancillary role in RNA metabolism, for instance, in the maturation of 16S rRNA, they are highly conserved in different phyla, as the γ-proteobacteria, and could be more functional under environmental conditions that are uncommon *in vitro* (Aït-Bara and Carpousis, 2015; Aït-Bara et al., 2015).

Type V enzymes are found in the chloroplasts of plants. Due to the presence of the RP-rich stretch inside the catalytic site, they were initially classified as type II enzymes. However, deeper characterization of the RNase E in *Arabidopsis thaliana* demonstrated the presence of a specific chloroplast transit peptide, required for plant development and autotrophic growth, and placed it in a separate class (Mudd et al., 2008). Interestingly, the ability of recombinant RNase E of *A. thaliana* to form tetramers *in vitro* and its preferred substrate specificity towards monophosphate 5′ ends are suggestive of its similarity with *E. coli* RNase E, also consistent with the evolutionary origin of chloroplasts (Aït-Bara and Carpousis, 2015).

4.2 The RNase E structure

This section refers mainly to *E. coli* RNase E, which is the one best studied to date. The RNase E monomer is a large protein composed of 1061 residues with an isoelectric point ≤ 5.4, due to 86 proline residues. Proline residues are organized in clusters and mostly located between position 530 and 1061, lowering the protein binding to sodium dodecyl sulfate (SDS) and restricting the electrophoretic mobility. Although the RNase E molecular weight is 118 kDa, its unusual amino-acid composition brings the protein to migrate as if it had higher molecular weight, equal to 180 kDa (Cormack et al., 1993).

The RNase monomer can be functionally divided into two halves: the N-terminal domain (NTH; residues 1-529), exerting the endonuclease activity, and the C-terminal domain (residues 530-1061), a highly unstructured domain essential for the binding with other proteins (**Figure 14**). The NTH domain can be further subdivided into a large domain (residues 1-400), a zinc ion linker domain (Zn-link) (residues 401-414), and a small domain (residues 415-429). The large domain contains an RNA-binding S1 domain (residues 36-118); a 5'- sensor domain (residues 119-214), responsible for the preference of RNase E for 5'-phosphorylated RNA substrates; a DNase I domain (residues 401-414) and an RNase H-like subdomain (residues 1-35 and 215-278), having a putative structural function. Although the RNase H-like domain is hypothesized to carry the magnesium's binding site, which might support metallic-assisted hydrolysis, it does not show any catalytic role. On the contrary, the RNase H-like domain appears to have an inhibitory activity on the RNase E's catalytic function. The RNase H-like domain is highly acidic, and whenever charge-neutralizing mutations are introduced, a substantial enhancement in the RNase E activity is observed. Altogether these data indicate that the RNase H-like domain likely provides an autoinhibitory function to the enzyme (Bandyra et al., 2018). The Zn-link domain contains a binding site for Zn ions, which coordinates the stabilization of the RNase E dimer formation. Lastly, the small domain regulates the formation of tetramers (dimer of dimers).

The proposed model for the homotetramer formation indicated that dimers interact exclusively at the interface of the four small domains (Bandyra and Luisi, 2018). The crystal structure of the RNase E catalytic domain revealed two critical residues involved in the metal coordination of the active site. The aspartic acid (D) residues in positions 303 and 346 coordinate the binding of magnesium and/or manganese, which support RNA cleavage (Thompson et al., 2015). The N-terminal domain carries the catalytic domain and is highly conserved among different bacterial species. Nevertheless, a recent structural and biochemical study of RNase E homologs in several pathogenic bacteria identified some species-specific properties (Mardle et al., 2019). In their analysis, Mardle and colleagues compared the N-terminal domains of *Y. pestis, Francisella tularensis, Burkholderia pseudomallei,* and *Acinetobacter baumannii.* They showed that while the domain and residues involved in the tetramer formation and RNA cleavage are well conserved in all the species analyzed, the RNase E of *B. pseudomallei* and *F. tularensis* diverge in their structural and biochemical properties. These emerging differences point to hypothetical divergences in the reaction mechanism, depending on the pathogen (Mardle et al., 2019).

Figure 14. Structure of the RNase E in E. coli. ***a)*** *it is reported the primary structure of an RNase E monomer (1061 amino acids). The amino-terminal region (NTH, residues 1-549), containing the catalytic core of the enzyme, is highlighted. The NTH is further divided into a large globular domain (residues 1-400) and in a small globular domain (residues 415-529). The large and small domain contain various functional subdomains. The carboxy-terminal region (CTH) is responsible for the interaction with macromolecule and contains binding sites for several proteins. CTH interacts with the helicase RhlB in the residues 698-762, the enolase in the resides 823-846 and with the polynucleotide phosphorylase (PNPase) in the resides 1021-1061. Furthermore, the CTH residues 633-712 represents the coiled-coil domain, the residues 565-585 the segment A (the membrane-binding domain) and the two AR1 and AR2 segment represent arginine-rich domain that might play a role in the RNA binding. The RNase E, in vivo, assemblies as a tetramer formed by the interaction of two dimer. Each RNase E monomer is colored either in light or dark green (****b****) The dimer interface and the coordination of a* Zn^{2+} *ion in the Zn-link of each RNase E monomer stabilize the formation of the RNase E dimer. The tetramer is then assembled and stabilized through the interaction among the four small domains (residues 415-529). The orientation of the unstructured CTH region for each RNase E monomer is unknown and speculatively reported in the figure. In* ***c,*** *it is illustrated the crystal structure of an RNase E dimer in complex with a substrate analogue. Each domain is color-coded as in* ***a****. The grey dot in the center represents a Zn ion in the Zn-link. The second dimer is not represented and it would lie below the plane of the drawing.* ***d*** *and* ***c*** *are magnification of the 5'sensor domain and the active-site metal ion, respectively. In the 5' sensor domain magnification the residues Arg169, Thr170, Val128, Gly124 are shown. Arg169 and Thr170 contact the terminal phosphate of the substrate, Val128 stacks on the first base of the substrate and Gly124 stabilizes the side chain of Arg169. In the active-site metal ion magnification, the residues Asp303, Asp346, Phe57, Phe56 and Lys112 are highlighted. Asp303 and Asp346 chelate the metal ion and Phe57, Phe56 and Lys112 contact the substrate* (Mackie, 2013).

The C-terminal domain, considerably more variable than the N-terminal domain, is intrinsically unstructured. Despite its unstructured nature, the C-terminal domain has a critical role in regulating enzyme functionality (Kim et al., 2014). It carries an RNA recognition core region, which favors the transcript's downstream degradation by binding with the PNPase. An attractive model, built by coupling computation analysis and biophysical approaches, suggests that a highly dynamic and disordered portion of the RNase E (residues 603-850) can assume a more rigid and organized structure after binding the RhlB and enolase. Instead, the C-terminal RNA-binding domain and arginine-rich region 2 (AR2) are predicted to assume a more limited conformation to ensure the binding of RNA substrates having different shapes, sizes, and sequences (Bruce et al., 2018). As mentioned before, the C-terminal domain contains an amphipathic α-helix, known as segment A (Mackie, 2013). A more comprehensive analysis of the role of segment A will be made later on in this work

Lastly, the considerably different levels of organization of the C- and N-terminal domains result in a diverse susceptibility to proteases' action. In particular, while the C-terminal domain is

more unstable and easily cleaved by proteases, the N-terminal domain can retain its functional activity since its globular assembly determines a higher resistance to proteolysis (Mackie, 2013).

4.3 RNase E protein interactions

The RNase E homologs in different bacterial species show diverse interaction modules and partners, further enhancing the variation in the composition of the RNA degradosome and determining its functioning. The RNase E C-terminal domain of *E. coli* harbors the modules responsible for binding with the canonical components of the RNA degradosome, namely, the 5'-3' exoribonuclease PNPase, the DEAD-box helicase RhlB, and the glycolytic enzyme enolase (Bandyra and Luisi, 2018). Contrarily, in *C. crescentus*, the RNase E forms the RNA degradosome by interacting with RhlB, PNPase, the exo-RNase D, and the metabolic enzyme aconitase. Moreover, differently from *E. coli*, the S1 domain within the N-terminal domain is responsible for the interaction between the RNase E and RhlB in *C. crescentus* (Voss et al., 2014). Furthermore, in *E. coli*, the depletion of the C-terminal domain affects both the kinetics of substrate cleavage and the disassembly of the RNA degradosome (Bandyra and Luisi, 2018). Although *E. coli* mutants carrying a C-terminal truncated form of the RNase E are viable, the absence of the C-terminal region and the disassembly of the RNA degradosome could uncouple the simultaneous presence of the endonuclease, exonuclease, and unwinding activities of the enzyme participating in the complex. Hence, the RNase E, PNPase, and RhlB activity disjoining suggests a less efficient mRNA decays, which physiologically requires fast processing of the RNA intermediate products (Mackie, 2013).

The PNPase binding to the RNase E relies on a small segment at the very end of the RNase E's C-terminal domain. To initiate the cleavage of a 3' single-stranded RNA substrate, the PNPase requires magnesium as a cofactor and the presence of phosphate. PNPase can only efficiently degrade the single-stranded RNA segment, and its 3'-5’ exonuclease activity is hindered when it encounters substrate carrying secondary structure, such as large stem-loops. To overcome this limitation, bacteria add a poly(A) tails to the RNA. The added poly(A) tail provides a single-strand region, which is promptly digested by PNPase.

Furthermore, bacteria non-encoding a poly(A) polymerase exploit the synthetic rather than the degrading activity of the PNPase to add a 3' heteropolymeric tail, which will serve as a single-stranded anchor for the 3' exonucleolytic degradation (Belasco, 2010). PNPase plays a significant role in eliminating unfolded rRNA and tRNA and probably acting a chaperone for some sRNAs. This latter modulatory activity of the PNPase raised the hypothesis that the recruitment of sRNA might somehow regulate the activity of the degradosome (Bandyra et al., 2016). In *C. crescentus,* the degradosome includes a second exoribonuclease, the RNase D. RNase D belongs to

the DEDD exoribonuclease family, which also consists of the RNase T and the oligoribonuclease. Although the RNase D role in the degradosome is still not fully elucidated, it is hypothesized that the RNase D is involved in the 3' processing of tRNA, 5S RNA, and numerous small structure RNAs (Voss et al., 2014).

The presence of a DEAD-box helicase in the degradosome assembly is considered necessary to facilitate the two nucleases' action over folded RNAs (Bruce et al., 2018). For instance, in *E.* coli, the DEAD-box helicase RhlB fosters PNPase nuclease activity by remodeling protein-RNA interactions and unwinding RNA secondary structures. In other words, the concerted activity of RhlB and PNPase is necessary for efficient RNA degradation (Bruce et al., 2018). The interaction with the RNase E promotes the unwinding and remodeling activity of the RhlB. Indeed, the binding of RhlB to RNase E leads to (i) the stimulation of the unwinding and ATPase activity of the helicase, and (ii) the physical proximity of RhlB to the RNA binding sites on RNase E. Furthermore, the interaction between the RNase E and RhlB could partially inhibit the RNA-binding activity of the helicase, allowing the steering of the substrates to either processing or degradation (Chandran et al., 2007).

Interestingly, depending on the RNase E homologs and the bacteria's growth condition, different DEAD-box helicases can interact with the RNase E. For instance, in *E. coli*, it has been shown that RhlB can be functionally replaced by the DEAD-box helicase RhlE and CsdA during the *in vitro* reconstitution of the RNA degradosome. While RhlB is the only DEAD-box helicase with a known role in the degradation of the RNA *in vivo*, the role of RhlE and CsdA remains to be understood. Although immunoprecipitation experiments failed in detecting the interaction of RhlE and CsdA in optimal condition, the CsdA appears to be recruited within the formation of the degradosome upon cold shock conditions (Khemici et al., 2004). The presence of other DEAD-box helicases apart from RhlB within the degradosome formation has also been demonstrated in *C. crescentus.* In this model bacteria, immunoprecipitation experiments have been shown that in response to cold stress, RhlB is substituted by RhlE. RNase E pulldown experiments show that there is remodeled of the RNA degradosome assembly upon cold shock condition, including the transcription terminator factor Rho, a second DEAD-box helicase, and the ribosomal protein S1 (Aguirre et al., 2017).

While the nature behind the interactions of PNPase and RhlB and the RNase E is better understood, the presence of a metabolic enzyme within the degradosome remains an open question. Nevertheless, the constant association between RNases and metabolic enzymes promoted the hypothesis of this enzyme's supporting role in the RNA turnover. Several approaches have been undertaken to unveil the role of the interaction of the enolase with the RNase E. The complete depletion of enolase induces significant effects, such as suppression of the sRNA-induced RNase E-dependent degradation of the *ptsG* transcript, which encodes for a

glucose-specific transporter of the phosphotransferase system (Morita et al., 2004) and the upregulation of enzymes involved in the use and uptake of multiple carbon sources (Bernstein et al., 2004). However, these observations might be due to secondary mechanisms, unrelated to the actual enolase function played within the RNA degradosome.

Interestingly, impairment of the binding of enolase to the RNase E, by depleting its binding sequence, resulted in modest phenotype changes in *E. coli* under aerobic conditions. A more pronounced effect of the loss of the enolase-RNase E interaction was observed under anaerobic conditions, resulting in abnormal cell morphology. These changes have been attributed to the deregulation of DicF, an ncRNA that is an antisense inhibitor of *ftsZ,* encoding a critical regulator of cell division (Murashko and Lin-Chao, 2017).

Differently from *E. coli*, in *C. crescentus,* the degradosome accounts an aconitase as a metabolic enzyme. Physiologically, the aconitase catalyzes the stereo-specific isomerization of citrate to isocitrate in the Krebs cycle. The presence of an enzyme involved in energy production with the RNA degradosome suggests a constant association among the evolution of enzymes involved in the RNA and central metabolism (Hardwick et al., 2011).

4.4 RNase E substrate recognition and cleavage

The model explaining the degradation of the bacterial transcripts was outlined considering the endonuclease and 3'-exonuclease encoded in the genome of the model organism *E. coli.* In this organism, the absence of a 5'-exoribonuclease and the presence of a stem-loop at the 3'-terminal suggested that the processing of the bacterial mRNA must rely on one or more internal cleavages mediated by an endonuclease. This initial, limiting step subsequently generates two short-lived intermediates, the 5' fragments now susceptible to the 3'-degradation, and a 3' fragment hypothesized to undergo a series of endonucleolytic and 3'-exonucleolytic cleavages. This model was later confirmed by the discovery of the RNase E, the most important endoribonuclease for the RNA turnover in *E.coli* (Belasco, 2010).

Since its discovery, the RNase E cleavage activity has been implicated in several aspects of the RNA metabolism, such as the rate-limiting the step of mRNA degradation, the processing of polycistronic RNA, and the maturation of sRNA, tRNA, and rRNA (Bandyra and Luisi, 2018). Considering the essential tole of the RNase in bacterial biology, it is not surprising that the RNase E is also involved in the quality control of the RNA. Across the evolution, all the organisms have developed pathways to degrade damaged or unapt transcripts. Hence, their degradation will avoid or limit the translation of toxic proteins and free ribosomes. Three examples of RNA quality control pathways are the nonsense-mediated decay (NMD), the no-go decay, and the premature termination codon (PTC). While transcripts undergoing NMD and no-go decay pathways are

RNase E-independent and will not be treated in this section, the PTC-containing transcripts are usually quickly eliminated through the RNA degradosome. Thus, the RNase E activity in the RNA quality control appears to be limited to the PTC pathway (Belasco, 2010).

The crystallographic structure of the RNase E's N-terminal domain in association with a synthetic RNA analog demonstrated that the RNA substrate is channeled in one of the RNase E monomers of a dimer. The channel that contains the RNA substrate is formed by the S1 domain, in which Phe57, Phe67, and Lys112 are responsible for the position of phosphate undergoing to the enzymatic cleavage and for the stabilization of the transition state. The Asp303 and Asp346, positioned in the DNase I-like domain of the other RNase E monomer of the dimer, are responsible for the binding and coordinating the essential Mg^{2+} ion. These two residues are placed on the opposite side of the RNA channel, and their coordinating function over the hydrated metallic ion likely polarizes the phosphate of the cleaved bond. Indeed, it is hypothesized that the phosphate's polarization promotes the in-line attack of an activated hydroxyl group donated by the hydrate metallic ion (Callaghan et al., 2005). Finally, the transcript's cleavage results in the generation of a fragment with a 3'-OH and 5'-monophosphate termini (Mackie, 2013).

It is known that the RNase strongly prefers a single-stranded cleavage site with a marked preference for uridine at the position +2 respect to the cutting site, where a typical mapped consensus is 5' -(A/G)N↓(A/G)UU (↓indicates the site of cleavage and N any ribonucleotide). Due to the well-conserved primary sequence of the catalytic domain, it does not surprise that other bacteria, such as *Salmonella* and mycobacteria, the RNase E recognized a similar binding site (Chao et al., 2017; Taverniti et al., 2011). The RNase E consensus sequence's low specificity determines the presence of multiple RNase E binding sites over a target (Clarke et al., 2014), which, surprisingly, does not influence the RNA's lifetime. RNA lifetime can be prolonged by non-translating-dependent mechanisms, such as the action of sRNA, or by the action of proteins blocking RNase E cleavage by unknown mechanisms (Richards and Belasco, 2019). However, accumulating experimental observations demonstrate that the mRNA lifetime does not depend on the number of RNase E binding sites present on the transcript, but rather how easily the RNase E can access them (Rich ards and Belasco 2019).

One remarkable feature of the RNase E is its preference for 5'-monophosphate transcript (**Figure 15**), which has been easily explained by crystallography studies. Hence, the hydrogen bond interaction between the 5'-monophosphate group and the residues Arg169 and Thr170 in the 5' sensor domain induces an RNase E conformational changes. In other words, in the substrate's absence, the RNase E's homotetramer displays an open conformation. Still, whenever the hydrogen bond is formed, a closed conformational state boosting the enzyme activity is favored (Koslover et al., 2008). Moreover, this pocket, located at the RNA-binding channel entrance, is spatially to narrow to accommodate di- or tri-phosphate. This 5'-end dependent mode

of substrate recognition also confers 5'-3' directionality on the RNase E and contributes to enhancing the substrate-binding (Mackie, 2013). In a recent study, Richard and Belasco demonstrated that the RNase E seeks a potential cutting site after its binding to the 5'-end of a transcript. The cutting site(s) presents along the transcript can be hindered by various structural obstacles that might be critically involved in the post-transcriptional control of gene expression (Richards and Belasco, 2019). Structural obstacles responsible for the RNase E scanning activity obstruction include coaxial base pairing, bounds proteins, or ribosomes. Interestingly, these structural obstacles can alter the RNase E scanning activity only if they create a sizeable structural discontinuity. Hence, these observations add a further level of post-transcriptional control of bacterial gene expression, in which the rate of degradation of 5'-monophosphate transcript does not only depends upon the RNase E binding or on the number of cleavage site present but also structural obstacles lying on the transcript (Richards and Belasco, 2019).

A second limitation of this entry pathway is the requirement of a 5'-monophosphorylated transcript. Bacterial transcripts generally display a triphosphorylated 5' terminal, which can still be internally cleaved by the RNase E after RppH action. RppH, an RNA pyrophosphohydrolase belonging to the Nudix hydrolase family, promotes the conversion of the 5'-triphosphate end to a monophosphate one, rendering, in turn, the RNA more susceptible to the action of the RNase E (Belasco, 2010). Surprisingly, not all mRNAs are susceptible to the action of RppH, and the features determining this susceptibility are currently unknown. Presumably, single-stranded 5'-termini, the presence of a secondary loop in the proximity of the 5'-end, and a ribosomal-binding site represent two characteristics essential for RppH susceptibility (Mackie, 2013).

A second pathway employed by the RNase E to cleave the target transcripts relies on their direct entrance into the catalytic site (**Figure 15**). This pathway is known as the 5' bypass, and it is not affected by the chemical status of the 5'-end (Clarke et al., 2014). The RNase E preference for this pathway is promoted by two factors: (i) a 5' terminal stem-loop structure on the target. The presence of a stem-loop structure on the transcript generally results in a 5-10 fold increase in the stability of the RNAs, inhibiting both RppH and RNase E activity, (ii) A 'naked' RNA, which due to the outplace of ribosomes by the RNA polymerase, become highly susceptible to this degradation pathway (Mackie, 2013). Hence, the direct entry pathway could be involved in the processing of transcripts displaying complex secondary structure, which could also be favored by their possible interaction with the NTH region and the AR2 sequences in the CTH (Kaberdin et al., 2000).

Given the pivotal role of RNase in bacteria regulation of mRNA metabolism, the relevance of the pathways for its activity was investigated *in vivo.* The 5'-end or 5'-bypass pathways were deactivated either individually or in combination. Critical mutations were introduced in the phosphate-binding pocket (R169Q) to halt the two pathways individually, or the CTH region was

deleted (Garrey et al., 2009). The single deactivation of one of the two pathways resulted in still viable strains. Contrarily, their contemporary inhibition was lethal (Garrey and Mackie, 2011). These observations suggested that RNase E employs both the 5'-and 5'-bypass mechanisms to recognize the targets. Moreover, the 5'-end and 5'-bypass pathway are not mutually exclusive, and they might be working cooperatively.

Content removed for copyright

Figure 15. RNase E pathways of substrate recognition. *RNase E (in purple) can interact with the RNA target (in red) using three different pathways. The RNase E can recognize the RNA via the 5'-end sensing (top right panel), This model requires the sensing of a 5'-monophosphate group on the target, which is recognized by 5'sensing pocket (in blue). A second pathway used by the RNase E to interact with the RNA is the internal entry (middle right panel), also known as 5'-bypass. This second pathway requires the RNA fold sensing by the RNA duplex binding surface present between the RNase H, DNase I, and small domains. Depending on the fold and the alignment of the RNA on the RNase E, the RNase E can cleave the RNA both upstream and downstream the structural element. The last pathway used by the RNase E to recognize the RNA is the mixed model (bottom right panel), which combines the keys elements of both the 5'-end sensing and the 5'-bypass pathways (Bandyra, Wandzik, and Luisi 2018)*

Recent findings have added a further level of complexity in RNase E's enzymatic activity. Structural motives in the targets, like a stem-loop upstream, the cleavage site, might be necessary for the correct alignment of the single-stranded region for the cleavage (Del Campo et al., 2015). The role of these structural motives in regulating the RNase E binding to the targets has recently been further addressed by Bandyra and colleagues (Bandyra et al., 2018). They demonstrated that the 5' end sensing and 5' bypass modes act in combination, enhancing the RNase E activity.

These two modes would allow the contemporary recognition of both the stem-loop and the 5' group (**Figure 15**). Nevertheless, the synergistic effect played by these two elements would still depend upon the exact location of the 5' end, the duplex region of the stem-loop, and the single-stranded region of the targets (Bandyra et al., 2018).

Although it is well known the RNase E's prominent role in initiating RNA degradation, it is still unclear how the membrane-bound RNase E encounters the transcripts. It has been hypothesized that the RNAs can randomly undergo the RNase E attack or are actively delivering to it. Currently, two possible models are explaining the RNase E substrate access. The first model hypothesis that the RNase E meets the 5' end of an RNA released from a polysome. This model also considers that an sRNA could promote an RNase E-mediated decay of the transcript (Tsai et al., 2012). On the other hand, the second model hypothesizes that a reduced efficiency in the translation rates could promote the recognition of the RNase E binding site since the mRNA would become more expose and more likely predisposed to be degraded (Deana and Belasco, 2005).

4.5 Regulation of the RNase E activity

The essential function played by the RNase E on the bacterial cell physiology requires a complex and tight regulation of both its expression and activity, entailing several layers of regulation. Several determinants influence the activity of the RNase E, and among them, the RNase E itself, but also diverse regulatory proteins and sRNAs are implicated in its regulation (Mackie, 2013)

4.5.1 RNase E autoregulation

Bacteria use *rne* mRNA as a sensor to control the total level of the RNase E activity. Indeed, the RNase E has been reported to be a powerful self-regulator capable of modulating its mRNA level. (Diwa et al., 2000). In an initial study, Jain and Belasco demonstrated that, for instance, a 21-fold increment in the *rne* mRNA results in only a 2.8-fold increase in the RNase E protein level. The low increment in the RNase E protein levels has been associated with the faster degradation of the *rne* transcript. Contrarily, an insufficient RNase E activity determines an increase in the lifetime of the *rne* mRNA. Hence, the described RNase E self-regulatory mechanism involves modulating the longevity of *rne* mRNA (generally ~ 1 minute) depending on the variation in the RNase E activity level within the cell (Jain and Belasco, 1995).

In *E. coli,* three independent promoters (*p1*, *p2*, and *p3*) (**Figure 16**) regulate RNase E transcription. Although the *p1* alone is responsible for steady-state transcription of the *rne* mRNA

expression, both *p2* and *p3* might improve the efficiency of transcription initiation from the *p1* promoter (Ow et al., 2002). To gain a more in-depth understanding of the efficiency of transcription initiation of each promoter, in their study Ow and colleagues generated two mutant strains, namely rne*Δp2Δp3,* rne*Δp1Δp3*, and rne*Δp1Δp2*. These mutants have been used to measure the steady-state level of the *rne* mRNA, which was reduced by 0.67- and 0.33-fold, respectively, and inversely correlated with its stability. Thus, the three promoters might have diverse and inverse role respect to the half-life of the *rne* transcript (Ow et al., 2002).

Content removed for copyright

Figure 16. Sequence of the RNase E promoter*. The nucleotides are numbered using as a reference the transcriptional starting site of the promoter p1 (+1). The position of the promoters is indicated by the arrows. The promoter one, p1 is located 361 bp upstream the AUG start codon of the rne transcript, the promoter p2 and 3 are respectively positioned 34 and 141 bp upstream of the promoter p1. In the sequence the -35 and -10 consensus sequences are boxed for each promoter* (Ow et al., 2002)

Contrarily to that, the *p1*mutant did not show any difference in *rne* mRNA steady-state level respect to the wild type. However, in all *p1*, *p2,* and *p3* mutants, it has been reported a drop in the protein level of the RNase E. Altogether, these data demonstrated that the presence of all the promoters is necessary for a physiological expression of the RNase E. Although the *p1* mutant shows a steady-state level of the *rne* transcript similar to the wild-type, a drop in the protein level is still observed. One possible model proposes that the presence of a putative enhancer element upstream of the *p1* promoter and an exceptionally long 5'UTR region (361 bp) might regulate the *rne* mRNA's transcription. Indeed, the proposed model deems that while the enhancer sequence may promote the binding of the RNA polymerase (RNAP) and *rne* transcription initiation, the

5'UTR sequence may control the autocatalytic activity of the RNase E on its transcript. Since the localization of the RNAP into the body of the transcript might block the ribosome binding, the long 5'UTR might assure an efficient translation of the *rne* mRNA, not allowing the RNAP to move beyond the 5'UTR (Ow et al., 2002). Moreover, whenever an alteration in the putative enhancer element occurs, the number of translation initiation events would reduce, leading to a decrease at the protein level. Remarkably, the cell responds to this drop in the RNase E protein level, stabilizing the *rne* mRNA. Nevertheless, under these circumstances, the transcription and translation initiation events are uncoupled, the stabilized *rne* transcript would not be translatable, ultimately resulting in the accumulation of untranslated *rne* transcripts (Ow et al., 2002). In other words, the amount of RNase E within a cell is limited. Quantitatively, the pool of available RNase E can increase following a burst in its substrates' synthesis, including its mRNA. This process is only transient since the RNase E pool, after its expansion, return to the physiological level. However, the RNase E level's autoregulation cannot occur if the *rne* mRNA translation is blocked (Sousa et al., 2001).

The *rne* 5'UTR region contains six structural domains: three stem-loop structures or hairpins (hp1, hp2, and hp3) and three single-stranded segments (ss1, ss2, and ss3) (**Figure 17**). In particular, the domains hp2 and hp3 are involved in the RNase E's autoregulation, and hp2 presumably mediates this autoregulatory mechanism (Diwa et al., 2000). The hp2 stem-loop serves as a sensor of RNase E activity within the cell, and consequently, feed-back regulating the degradation of the *rne* transcript. A more in-depth analysis of hp2 showed that at the top of this stem-loop, there is a highly conserved RNA sequence of 14-bp (GCAAUGGCGUAAGA). This RNA fragment, together with two flanking nucleotides, assumes a specific structural conformation, in which a hairpin loop, a 2-bp stem, and an 8-bp internal loop are formed (Diwa et al., 2000). However, the hp2 is the more powerful modulator of the RNase E on *rne* gene expression, also the hp3 functions in some manner as a target for the RNase E. In other words, both the hp2 and hp3 independently mediate the RNase E autoregulation. Moreover, the known preference of the RNase E for single-stranded AU rich sites raised the hypothesis that the large AU-rich internal loops within hp3 might contain an RNase E cleavage site (**Figure 17**). Also, the highly structured hp2 is deemed unlikely to be targeted by the RNase. However, its binding by the RNase E, either alone or with a putative protein cofactor, might accelerate the *rne* mRNA degradation. This faster degradation of the *rne* transcript might facilitate the access of the RNase E to other endoribonucleolytic cleavage sites located elsewhere in the transcript and also overcome potential obstacles, such as ribosomes, a5'-proximal stem-loop (hp1), and a 5'-terminal triphosphate, which would protect the *rne* transcript from the RNase self-cleavage (Diwa et al., 2000; Schuck et al., 2009).

Content removed for copyright

Figure 17. Secondary structure of the RNase E 5'UTR. *Brackets denote the location of the various structural domain present in the 5' UTR of E. coli, namely hp1, ss1, hp2, ss2, hp3 and ss3. In the figure, the Shine-Dalgarno (SD) and the initiation codon are underlined* (Diwa et al., 2000)

4.5.2 Regulatory protein

Diverse proteins can also modulate the activity of the RNase E. To date, the regulator of ribonuclease activity A and B (RraA and RraB), and the 50S ribosomal protein L4 have been reported to inhibit the RNase E activity in *E. coli* (Mackie, 2013). These three proteins alter the activity of the RNase E directly binding at its C-terminal domain. More in detail, RraA binds the RNase E's C-terminal domain in two sites (AR1 and AR2), and it also interacts with the C-terminal of RhlB. RraA might negatively regulate the RNase E activity by promoting an ATP-dependent remodeling through RhlB, which would cause an alteration of the interaction between the RNase E and its RNA substrate (Górna et al., 2010).

The interaction *in vitro* between the RNase E and the ribosomal protein L4 showed that this ribosomal protein could inhibit the RNase E's endoribonucleolytic function, stabilizing both antisense regulatory RNA and mRNA usually degraded *in vivo.* Furthermore, the DNA microarray analysis of the L4-RNase E interaction showed that around 65 mRNA were deregulated, which encode not only for stress response proteins, such as HslO, Lon, CstA, YjiY, and YaeL, but also for proteins involved in carbohydrate, amino acid metabolism, transcription, translation, DNA, and RNA synthesis. The level of this pool of mRNA might be down-regulated by L4 through the impairment of their translation, thereby leading to the accumulation of ribosome-free transcripts,

which are intrinsically more susceptible to the catalytic activity of the RNase E. In other words, L4 interaction with the RNase E might modulate the activity of the endoribonuclease by altering the steady-state level and degradation of regulatory RNA and mRNA (Singh et al., 2009).

The physiological roles of RraA and RraB and how these two factors and L4 modulates the activity of the RNase E remain to be elucidated in greater detail. However, these three proteins could alter the RNase E activity under stressful conditions to reduce the degrading RNase E activity globally or toward a specific mRNA pool until the RNase E autoregulates its level (Mackie, 2013). Lastly, in *P. aeruginosa*, Dip, a phage protein, was shown to interact with the C-terminal domain, conceivably inhibiting the activity of the RNase E during phage infection (Dendooven et al., 2017).

4.5.3 sRNA-mediated regulation of the RNase E

sRNAs are a considerably diverse group of regulatory molecules, ranging from 50 to 400 nucleotides long sequence. Although sRNAs interact with their target(s) only through a short region, they can efficiently and selectively modulate at the post-transcriptional level the stability of the mRNA, either by repressing the target(s) translation or promoting its/their degradation, with the final goal of regulating gene expression in response to environmental changes (Storz et al., 2011). The post-transcriptional regulatory role of sRNAs has been studied both in model microorganism, such as *E.coli* (Waters and Storz, 2009), and in several pathogenic species (*i.e., L. monocytogenes, S. aureus, Salmonella enterica* serovar Typhimurium (*S.* Typhimurium), *Vibrio cholerae, H. pylori, Chlamydia trachomatis, P. aeruginosa,* and *M. tuberculosis*) (Arnvig and Young, 2012; Papenfort and Vogel, 2010; Quereda and Cossart, 2017). The sRNA-mediated regulation of the mRNA target(s) relies upon a variety of mechanisms. Thus, *trans*- and *cis*-acting sRNAs display different features per the molecular mechanism used to interact with the target(s).

4.5.3.1 Trans-acting sRNA and RNase E

Trans-acting sRNAs are usually 50 to 200 nucleotides long sequences that include a segment of 7 to 12 bases, referred to as the 'seed region,' which recognizes and pairs with an entirely complementary sequence of the mRNA target and is the minimal requirement for target recognition (Künne et al., 2014). Although not all *trans*-acting sRNAs contain the same structural features, in Gram-negative bacteria, they generally include a 5' seed region, an A/U-rich Hfq binding site, and a poly(U) tail at the 3', which interacts with Hfq. The Hfq possible binding with the sRNA body might organize the sRNA so that the 'seed region' is present to the transcript for

cognate base-pairing. Moreover, Hfq appears to protect the sRNAs from an early degradation (Papenfort and Vogel, 2010).

The *trans*-acting sRNA-mediated regulation of the mRNA can be the following two main pathways. A first pathway envisages the targets' indirect destabilization because of the sRNA's ability to deprive the mRNA target of ribosomes or occlude the translation starting site. The absence of bound ribosomes would then enhance the exposure of the free mRNA to the attack of endoribonucleases, such as the RNase III and the RNase E (Bandyra et al., 2012). Also, the mRNA degradation after the sRNAs pairing might be promoted by recruiting the RNase E to the Hfq-sRNA binary complex. The RNase E-Hfq-sRNAs ternary complex formation is hypothesized to guide the RNase E near the mRNA target to favor its cleavage and degradation either in a proximal or distant site sRNA pairing (Bandyra et al., 2012).

A second possible pathway hypothesizes that the sRNA/mRNA base-pairing, through specific signals, might trigger and stimulate the RNase E nuclease activity. Indirect experimental evidence supporting this model derives from the study of the sRNA MicC, which, in *E. coli*, downregulates the expression of OmpC, an outer membrane protein. As *E. coli* also in *Salmonella,* MicC, together with Hfq and RNase E, can regulate the expression of the outer membrane protein OmpD. It induces OmpD cleavages binding at codons 23-26 located far downstream of the ribosome binding site. The sRNA/mRNA base-pairing of MicC with the transcript encoding for *ompD* induces an RNase E-mediated cleavage. The final effect of this sRNA/mRNA base-pairing results in the abrogation of the transcript's translation (Pfeiffer et al., 2009).

It is well acknowledged that the RNase E nuclease activity is enhanced by the presence of a 5'-monophosphate group on the mRNA, which, from crystallography data, is known to induce structural changes that stimulate the catalytic activity of the RNase E (Callaghan et al., 2005). Hence, it has been hypothesized that the sRNA could favor an RNase E-mediated cleavage after its cognate base-pairing with its targets generating a 5'-end able to boost the RNase E activity. Hypothesis recently investigated and confirmed by Bandyra and colleagues. By repressing the action of MicC on *ompD,* they show that although the catalytic site of the RNase E is sufficient to induce the cleavage of the mRNA target, the presence of the C-terminal domain of the RNase E might be playing a critical role in the recruitment of the Hfq::sRNA complex. Indeed, the RNA binding domains present in the C-terminal region are deemed to enhance the presentation of the sRNA's seed region and assist the positioning of the target to respect the catalytic site (Bandyra et al., 2012).

sRNAs are generally used only once and degraded together with the target (Massé et al., 2003). Surprisingly, in the same study, Bandyra and colleagues showed that the sRNA and the mRNA might be eliminated in a synchronized manner. The sRNA is degraded shortly after the

cleavage of the mRNA. This evidence suggests the presence of a displacing mechanism of the sRNA from the cleaved target and that the stability of the sRNA might rely on the features of its 5'-group. Generally, the primary transcript of sRNAs shows a triphosphorylated terminus (5'PPP), which is supposed to have a protective function and is slower degradation kinetic. On the other side, the activated form of sRNA, which is rapidly degraded, displays a 5'-monophosphate group (5'P). The 5'P formation might be explained by two possible mechanisms: (i) the processing of the sRNA precursors by the RNase E or (ii) by the transformation of the 5'PPP to 5'P thanks to the action of the pyrophosphohydrolase, RppH, or by its paralogues belonging to the Nudix hydrolase family (Bandyra et al., 2012).

To sum up, all the experimental data collected so far suggest that 5' end of a *trans*-acting RNA is likely to participate in both the fidelity and the modulation of the kinetics of the response it mediates. Thus, two possible scenarios can be outlined. For instance, a 5'P sRNA, not matching or finding its target, can be rapidly cleaved by the RNase E, both in the presence or absence of Hfq. In a second possible scenario, the 5'P sRNA finds and binds its target. In this case, the sRNA guides the target degradation through its 5'P, protecting itself from the attack until the target has been degraded. This model also points out that the specificity of sRNAs' action is ensured by the turnover of activated but not paired sRNAs (Bandyra et al., 2012).

Lastly, although the sRNA's regulatory activity has been initially associated with either the inhibition of the translation or the degradation of the base-paired mRNA, recently, it has been proposed that sRNAs can also enhance the mRNA expression of their targets (Storz et al., 2011). Thus, sRNAs can activate a specific target's gene expression by blocking the RNase E binding sites on the targets (Papenfort et al., 2013). However, the regulation of the post-transcriptional activity of sRNAs mediated by RNase E has not been fully understood, and further studies are required.

4.5.3.2 Cis-acting sRNA and RNase E

During the past decade, several sRNAs have been discovered, and the majority of them are *trans*-acting sRNAs. However, the second category of sRNAs is the *cis*-acting sRNAs. Unlike the previously described *trans*-acting sRNA, the *cis*-acting or antisense sRNAs (asRNAs) are transcribed from the opposite DNA strand to their target (Waters and Storz, 2009). asRNAs regulatory activity has been associated with several fundamental cellular processes: replication, initiation, conjugation efficiency, suicide, transposition, mRNA degradation, and translation initiation. Nevertheless, the regulation of metabolic processes by asRNAs has been reported too (Brantl, 2007). asRNAs are untranslated and highly structured RNA molecules ranging from 50 to 300 nt. asRNAs generally present from one to four stem-loops, which contain a 5-8 nt GC-rich group, and are hypothesized to both prevent degradation by the RNase III. Differently from the

trans-acting sRNA, asRNAs display an extensive complementarity with their targets. The initial binding involved the formation of an unstable loop-loop interaction, known as kissing complex. This unsteady interaction is transformed in a stable inhibitory complex forming a stable asRNA-mRNA duplex the degraded by the RNase III or the RNase E.

Moreover, contrary to the *trans*-acting RNA, asRNAs can bind their target without being associated with Hfq, although other chaperones might participate in the base-pairing process (Brantl, 2007). For instance, one known *cis*-acting asRNAs activity, coupled with the RNase E's degrading function, is the FinP asRNA. FinP target is the activator of the plasmid F and R1 conjugal transfer operon, *traJ.* In F-like plasmid, the regulatory activity of FinP relies upon the action of the plasmid-encoded protein FinO. Hence, the binding of FinO to FinP protects the highly unstable FinP, sterically inhibiting the RNase E cleavage. Thus, the inhibition of RNase E's endonucleolytic activity over FinP leads to an increase in its steady-state level, resulting in the repression of *traJ* expression (Gubbins et al., 2003).

4.5.3.3 The role of RNase E in the maturation of sRNAs and sRNA interactome

Numerous sRNAs interact and recruit the RNase E to facilitate the processing of mRNAs, and complex regulation of the sRNA interactome in bacteria is emerging. The use of more sophisticated advanced technologies to investigate the RNase role in the post-transcriptional regulation of gene expression mediated by sRNAs revealed a central role of the essential RNase E in their biogenesis and functionality. Nevertheless, the complete molecular biology behind this post-transcriptional regulatory mechanism remains to be elucidated.

Accumulating experimental evidence suggests an exact role of Hfq in the base-pairing of the sRNA with its cognate targets and the subsequent RNase E-depend cleavage of the duplex. To unveil the molecular mechanism behind the RNase E and Hfq putative interplay in the sRNAs post-transcriptional regulation of mRNA, a CLASH (UV-crosslinking, ligation, and sequencing of hybrid) has been recently employed in the human pathogen enterohaemorrhagic *E. coli* (EHEC) (Dendooven et al., 2017). The CLASH approach allowed to identify, both *in vivo* and in a transcriptome-wide fashion, RNase E-mediated degradation of the sRNA-mRNA duplex. The collected data describe a model where the recruitment of RNase E to Hfq binding sites induce an RNA RNase E -mediated cleavage 13 nt downstream of its binding. Moreover, it has also been showing that the RNase E recruitment occurs with a five-base pair 3'off set and the addition of a 2- to 6- nt oligo(A) tail.

Interestingly, the RNase E-CLASH analysis revealed that sRNA-mRNA interactions have lower free energy than randomly paired RNA sequences. According to the already known *in vitro* experimental data, the identified sRNA-mRNA duplexes are predominantly found close to the start

codon. Another exciting result of the RNase E CLASH is that sRNA can interact with a variety of RNA molecules, such as ncRNA, sRNA, rRNA, and tRNA, which are deemed to act as sRNA sponges. An attractive hypothesis suggests that these interactions might temporarily stabilize in excess sRNAs and avoid non-specific binding to other mRNA substrates (Dendooven et al., 2017).

The biogenesis of the sRNA is still far to be completely understood. Currently, the several characterized sRNAs are known to be directly transcribed from the non-coding intergenic region as a primary transcript with a 5'PPP capped end. Nevertheless, new experimental evidence demonstrates some sRNAs are generated from the 3'-region of the transcript. Their biogenesis rarely depends on the presence of an internal gene promoter, and they are mostly originated following the processing of the mRNA. Considering the RNase E's role in the bacterial mRNA processing, it is not surprising that this essential endoribonuclease might be involved in the cleavage and maturation of functional 3'-generated sRNAs will ultimately act in an Hfq-dependent manner (Chao et al., 2012). In a recent study performed by Chao and colleagues, the used a transiently inactivated form of the endoribonuclease E followed by RNA-seq (TIER-seq) in *Salmonella typhimurium* profiled the role of RNase E cleavage in the biogenesis of 3' UTR-derived sRNAs and maturation of non-active sRNA from their primary transcript (Chao et al., 2017). From their analysis, RNase E-dependent biogenesis of sRNAs also involved Hfq, playing a double function. Thus, Hfq might, from one side, complexes with the RNase E to generate stable and mature sRNAs, and, from the other side, direct the base-pairing of the mature sRNAs to its target(s) (Chao et al., 2017).

4.6. RNase E cellular location

The cellular localization of RNA degradosome is one of the mechanisms contributing to regulating its activity in the bacterial cell. Importantly, by studying the primary structure of the RNase E, an amphipathic alpha-helix was identified just adjacent to the N-terminal domain (Bandyra et al., 2013). This so-called segment A (residues 565-585) is necessary and sufficient to tether the RNase E at the inner membrane (Mackie, 2013). Such binding is required for *E. coli* optimal growth, but in other species, such as *C. crescentus*, the RNase E lacks a transmembrane domain (Llopis et al., 2010).

The anchoring of RNase E and the RNA degradosome at the inner cell membrane allows its random movement across the all membrane surface. By investigating the RNase E movement and distribution through total internal reflection fluorescence, Strahl and colleagues show that fluorescently-labeled RNase E can rapidly diffuse on the inner cell membrane and form short-lived foci. Altogether these data indicate that the RNase E foci formation is highly dynamic and occurs

arbitrarily (Strahl et al., 2015). Moreover, live-cell imaging was unable to confirm past immunofluorescence observations, which proposed that RNase E exhibits a helical pattern on the *E. coli* cell periphery (Taghbalout and Rothfield, 2007).

The association of several degradosome particles presumably forms RNase E foci. They seem to share similar features with eukaryotic ribonucleoprotein (RNP) granules, a broad group of membraneless compartments, formed by liquid-liquid phase separation in cells and associated with post-transcriptional processing both under homeostatic and stressful conditions (Tejada-Arranz et al., 2020a). However, contrary to the RNP granules, the RNase E foci display a smaller size and a shorter half-life. The RNase E could form RNP granule-like foci through the unstructured C-terminal domain, promoting the RNase E's binding with RNA or other degradosome particles (Tejada-Arranz et al., 2020a). Indeed, the RNase E membrane association through segment A is hypothesized to aid the coordination of the RNase E tetramer. This and the role played by the C-terminal domain suggested that the anchoring of the RNase E to the membrane through the segment A is necessary for the formation of RNP granule-like foci and the interaction of the RNase E with other components of the degradosome (Strahl et al., 2015). Indeed, *E. coli* mutant depleted for this transmembrane domain is impaired in foci formation and shows a slowdown in the RNA turnover (Hadjeras et al., 2019).

Surprisingly, in *C. crescentus,* the RNase E is not anchored to the membrane, but it still displays a patchy foci distribution within the nucleoid-filled cytoplasm. Moreover, similarly to *E. coli*, the intrinsically disordered C-terminal region contributes to RNP granules' formation. Lastly, in *C. crescentus,* the formation of the foci is dynamic. Their disassembly concomitantly occurs with the cleavage of the RNA by the RNase E. This data suggests that within the RNP granules, the RNase E exerts its endonucleolytic activity (Al-Husini et al., 2018). Using 3D super-resolution microscopy and single-particle tracking, Bayas and colleagues found that in *C. crescentus,* the RNase E copy numbers are regulated as a function of the cell cycle, but the size of the foci remains constant. Interestingly, they also observed that the RNase E foci' localization was associated with the chromosomal loci corresponding to the highly expressed rRNA genes located on two different chromosomal positions (Bayas et al., 2018).

4.7 Mycobacterial RNase E

Mycobacteria are classified as acid-fast Gram-positive bacteria due to their lack of an outer cell membrane. They can be divided into fast-growing mycobacteria, such as *M. smegmatis*, and slow-growing ones, which include the pathogenic *M. tuberculosis.* As previously mentioned, both mycobacterial species' genome encodes for the same pool of RNases, which combine the essential

nucleases present in both Gram-positive and -negative bacteria. Thus, mycobacteria contain a functional homolog of the RNase E (Durand et al., 2015).

The mycobacterial RNase E remains a poorly characterized enzyme, even though both structural and functional experimental investigations have been only recently proving its critical and essential role in regulating mycobacterial homeostasis. Similar to *E. coli*, the mycobacterial RNase E is an essential (Forti et al., 2011) 5'-end dependent endo-RNase that recognizes an adenine/uracil (A/U)-rich binding sequence (Zeller et al., 2007). The initial biochemical studies aiming to characterize the mycobacterial RNase E showed that the mycobacterial RNase E can form both dimers and tetramers *in vitro* (Zeller et al., 2007). The assembly of the dimeric and/or tetrameric forms depends on the presence of a pair of histidine residues in the CPXCXGXG conserved domain, which is involved in coordinating a Zn^{+} ion, namely the Zn-link motif in the RNase E *E. coli.* Despite some common properties between *E. coli* and mycobacterial RNase E, both their structure and substrate specificities only partially overlap. Hence, the mycobacterial RNase E preferentially targets sequences enriched in uracil. Moreover, while in *E. coli,* the presence of a cytosine near to the RNase E cleavable bond can both inhibit or enhance the efficiency of the RNase E cleavage depending on its position, in *M. tuberculosis,* the presence of cytosine can only hinder the endonucleolytic enzyme independently of its location (Zeller et al., 2007).

Although mycobacterial RNase E displays a high similarity at the catalytic site level, structurally, it undergoes to circular permutation of its catalytic site (**Figure 18**). Thus, mycobacterial RNase E displays a relocation of the catalytic site from the N-terminal to the central position of the primary structure, flanked by both the N- and C-terminal intrinsically unstructured region. The presence of this unstructured flanking region at both the N- and C-terminal might suggest that the RNase E might interact with different proteins in mycobacteria. A first attempt to identify the RNase E protein-protein interactions was undertaken by Kovacs and colleagues (Kovacs et al., 2005), where they revealed the interaction of RNase E with DnaK, a chaperon protein known to refold and correctly assemble unfolded proteins accumulated under stress condition, with a lipoamide dehydrogenase (NADH) belonging to the 2-oxodehydrogenase and pyruvate complexes, with L1 and S2 ribosomal proteins, and with GroEL, a central cold stress-response factor (Kovacs et al., 2005). A dual proteomic and transcriptomic approach has been implemented more recently to investigate the RNase E's role in forming a putative mycobacterial degradosome and RNA metabolism (Płociński et al., 2019). Płociński and colleagues demonstrated that RNase E participates in forming a mycobacterial degradosome interacting with other known degradosome-related components, such as an orthologue of the polynucleotide phosphorylase (PNPase), the ATP-dependent RNA helicase (RhlE).

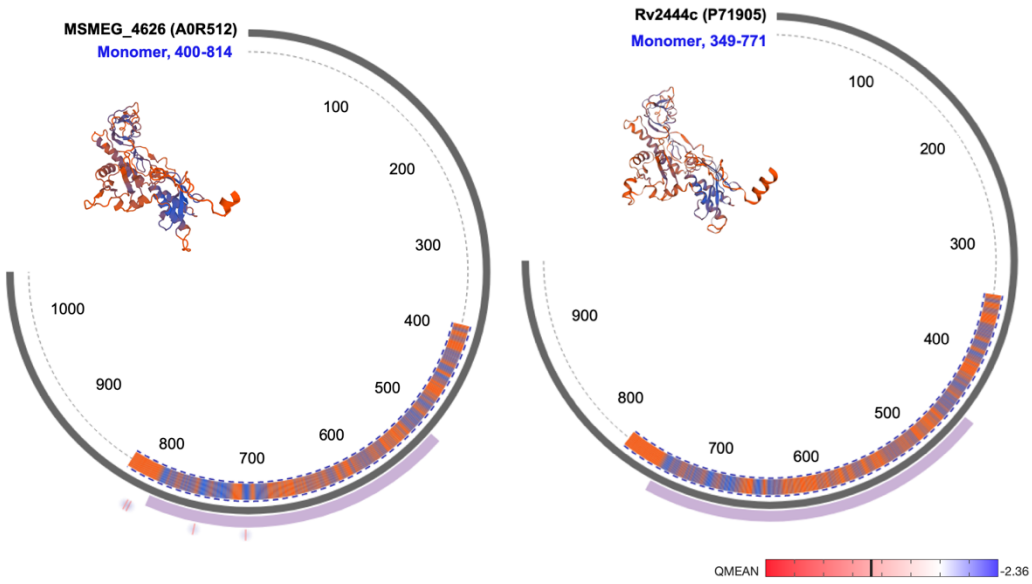

Figure 18. SWISS-Model Homology analysis of the mycobacterial RNase E. *For each model submitted, RNase E of M. smegmatis (left panel) and M. tuberculosis (right panel), the SWISS-MODEL* (Waterhouse et al., 2018) *tool selected the template with the highest quality, which has been predicted from the characteristic of the target-template alignment* (Guex et al., 2009). *The coordinates conserved between the target and the template are reported in the graph. For both mycobacterial RNase E the highly conserved catalytic domain (in purple) of the RNase E has been identified. Differently from E. coli, the catalytic site is relocated towards the central part of the primary sequence and flanked by intrinsically unstructured N- and C-terminal regions. For the RNase E of M. smegmatis three metallic binding sites, namely two Mg^{2+} (purple circle with one vertical red line) and one Zn^{2+} (purple circle with two vertical line) have been also modeled. A prediction of the tertiary structure of the RNase E in both mycobacterial species is reported (upper left for M. smegmatis and upper right for M. tuberculosis). The global and per-residue model quality had been assessed using the QMEAN scoring function* (Studer et al., 2020). *QMEAN score for MSMEG-2626= - 2.36. QMEAN score for Rv2444c = - 3.24.*

Interestingly, the pulldown of GFP-tagged RNase E showed that other proteins co-purifying with the degradosome components include two KH-domain proteins (Rv2908c, Rv3920c), included in the RNA-bound proteome, the ribonuclease J (RNase J), member of the degradosome of *B. subtilis*, and the two cold shock proteins CspA and CspB. Lastly, differently from *E. coli,* the pulldown experiment did not demonstrate the presence of enolase, data consistent with the absence of an enolase-binding site in the *M. tuberculosis* RNase E sequence. Moreover, they used the CRISPRi/Cas9 technology to modulate the RNase E level in *M. tuberculosis*. They found that its silencing massively and significantly reshapes about a quarter of the mycobacterial transcriptome. Thus, the RNase E's silencing significantly affects 26 transcripts encoding for essential transcripts, such as protein involved in cell division Rv2927c, SepF, FtsQ, RipA, FtsW, DivIVA, the response regulator MtrA, the transcription factor WhiB2, and the ATP-dependent

protease ClpX. Altogether, these findings support the critical role of the RNase E in mycobacterial physiology. Notably, the reported changes associated with the silencing of both mycobacterial RNase E and the PNPase sum up the effects derived from the activity of the two enzymes and the non-coding RNAs that they regulate (Płociński et al., 2019). Hence, like in *E. coli* and *Salmonella*, an interplay between the RNase E-mediated degradation and the sRNAs to post-transcriptional regulation of gene expression can be envisaged. Nevertheless, further studies are required.

By accounting for the similarity of the catalytic site between the RNase E of *E. coli* and the mycobacterial one, it was anticipated that this endoribonuclease might also display a similar function. Indeed, although the nuclease involved in the rRNA processing was unknown, a putative role of the RNase E in the maturation of the rRNA had already been predicted by Ji and colleagues in 1994 (Ji -e. et al., 1994). The first experimental data confirming the mycobacterial RNase's role in both the processing and degradation of RNA molecules was only published several years later (Zeller et al., 2007).

Hence, it was demonstrated that the mycobacterial RNase E could cleave both *in vitro* and *in vivo* the 9S rRNA, a precursor of the 5S rRNA. Interestingly, the *in vitro* and *in vivo* data showed a shift in the cleaved bond position, which is known to occur near the mature 5'-end of the 5S rRNA. This difference might be explained, taking into account that *in vivo,* the RNase E's endonucleolytic activity might be influenced by the presence of other auxiliary or ribosomal associated proteins (Zeller et al., 2007). A deeper understanding of the RNase E cleavage mechanism of the mycobacterial rRNA has been provided by Taverniti and colleagues (Taverniti et al., 2011). Mycobacterial *rrn* operon, which contains the genes encoding for the 16S, 23S, and 5S, is co-transcribed as a single precursor molecule. Although the *M. smegmatis* genome, differently from *M. tuberculosis*, encodes for two ribosomal operons (*rrnA* and *rrnB*), the two folded precursors show high sequence similarity. They are deemed to be processed following a similar maturation pathway. The polycistronic rRNA molecule undergoes an extensive base-pairing folding between the leader and the spacer-1 region (16S) and the spacer-1 and spacer-2 (23S and 5S) region (**Figure 19**).

The collected data suggest that the 16S rRNA maturation occurs in a two steps fashion. The first step involved RNase III ribonucleolytic cleavage at +148 and +1977/79, determining the 16S precursor's release from the 30S transcript. The second step implicates the cleavage at the position +265, carried out by an unknown nuclease, generating a shortened precursor. From this final precursor, the mature 16S rRNA 5' end is generated by subsequent cleavage of the RNase E before and then of RNase J (Taverniti et al., 2011). Although RNase E's endonucleolytic activity has also been shown in the maturation of the 23S and 5S, its role is less relevant. Indeed, the maturation of the 23S appears to be primarily driven by the nucleolytic activity of the RNase J. Regarding the maturation of the 5S rRNA; the collected data suggest the role of both the RNase E

and J in the processing of its precursor(s). However, it is plausible that the RNase E might be involved in the 5S rRNA final processing (Taverniti et al., 2011).

Content removed for copyright

Figure 19. Model of rRNAs precursors in M. smegmatis. *The nucleotide numbering has been done referring to the transcription start of the rrnB promoter as +1. The scissors indicate the cutting sites identified by primer extension, and the name of the nuclease involved in the cleavage is reported where known.* ***A*** *and* ***B*** *respectively describe the pre-16S and pre-23S secondary structure. The boxed sequences correspond to the 16S (****A****), 23S, and 5S (****B****) rRNA's mature products. The gray 12 nucleotide sequence in* ***B*** *indicates a putative rRNA sequence degraded by the 5'-3' exoribonuclease J* (Taverniti et al., 2011).

The endonucleolytic activity of the mycobacterial RNase E has also been associated with the processing of mRNA. Still, the available data are only limited to the *furA-KatG* transcript (Taverniti et al., 2011). The *furA-katG* bicistronic mRNA encodes for a Fur-like transcript repressor (*furA*) and a catalase-peroxidase (*katG*). It was previously known that the polycistronic *furA-katG* transcript was processed by an unknown nuclease in the proximity of the end of the *furA* ORF (Sala et al., 2008). Later on, it has been shown that the nuclease responsible for the maturation of the *furA-katG* mRNA is the RNase E. The RNase E cleavages occur in a single-stranded region between two putative secondary structures, located 17 nt upstream of the *furA* stop codon. The RNase E processing of the *furA-katG* mRNA generates a more stable *katG* transcript and a more labile *furA* mRNA. Although the regulatory role of FurA is still not completely understood, it is known that it negatively regulates itself acting on its transcript from

pfurA. This negative feed-back results in a sufficient amount of KatG peroxidase and low biosynthesis of the FurA repressor (Taverniti et al., 2011).

Lastly, the essentiality of the RNase E for mycobacterial and, more in general, the maintenance of bacterial homeostasis, the high conservation of its catalytic site among the different orthologs, its absence in the eukaryotic system, and the recent identification of small-molecule compounds, specifically inhibiting this enzyme (Kime et al., 2015; Mardle et al., 2020) support the role of the RNase E as a new potential drug target. Thus, RNase E begins to be considered a promising target for developing new antibiotics and targeting strategies, giving the rise and spread of drug-resistant infections caused by bacteria of clinical relevance, such as *M. tuberculosis.*

Aim of the work

Tubercular bacilli can survive in humans for long periods of time, and the diagnostic and therapeutic tools at our disposal are still suboptimal. This is mainly because the *M. tuberculosis* population is heterogeneous and can further diversify within the infection and treatment. This phenotypic heterogeneity gives rise to subpopulations that are more likely to persist in the human host, difficult to detect and treat. Although the underlying mechanisms behind phenotypic variation remain elusive, accumulating experimental observations demonstrate that this cell-to-cell diversity in gene expression might help the mycobacteria endure the harsh host environment. It is well established that single-cell phenotypic differences in the growth rate and metabolic state can influence the bacteria's fate-decision under stressful conditions (Dhar et al., 2016).

Among the putative mechanism influencing cell-to-cell phenotypic variation, we hypothesize that the influence of RNA turnover in the gene expression variation might represent one of the primary sources of bacterial phenotypic diversification (Baudrimont et al., 2019; Eldar and Elowitz, 2010). RNA decay primarily depends upon the activity of ribonucleases. Interestingly, Gram-positive and -negative bacteria own a different plethora of RNases, resulting in diverse cellular RNA degrading machinery. In Gram-negative bacteria, the RNase E serves as the structural and catalytic core of the RNA degradosome. In contrast, Gram-positive bacteria do no own an ortholog of the RNase E and display a diverse organization of the RNA degradosome, depending on the endoribonuclease encoded (Belasco, 2010; Durand et al., 2015; Mackie, 2013).

Surprisingly, mycobacterial genomes encode the main RNases of both Gram-positive and -negative bacteria, including an orthologous of RNase E. Despite the essentiality of the mycobacterial RNase E, only recently, its functional characterization has begun. To date, experimental evidence proves that the mycobacterial RNase E can assemble a degradosome-like structure and participate in the processing and maturation of differential species of RNA molecules, such as rRNA and mRNA transcript (Płociński et al., 2019; Taverniti et al., 2011).

Therefore, considering that fluctuation in RNA molecules due to their degradation by the RNases, the critical role played by the RNase E in the RNA metabolism, and that variation in the number of transcripts outlines cell-to-cell phenotypic variations; we postulated that RNase E activity might contribute to phenotypic variation and foster adaptation to stressful conditions.

Thus, within this study, we employed bulk (*i.e.,* classical genetics, conventional microbiology, and Mass Spectrometry) and single-cell approaches (*i.e.,* single-cell microscopy and

real-time microfluidic epifluorescent microscopy) to probe the role of RNase E in mycobacterial cell physiology and adaptation to stressful conditions.

Aim 1:

To investigate the temporal dynamics of the RNase E in *M. smegmatis* at the single-cell level.

For this, we coupled time-lapse microfluidic microscopy, snapshot microscopy with single-cell multiparametric analysis to determine the pattern of expression of the RNase E translation fluorescence reporter**.**

Aim 2:

To identify and validate the RNase E interactome of *M. smegmatis,* focusing on the RNase E-HupB interplay.

For this, we performed Mass Spectrometry analysis of the RNase E-6X pull-down and validated both at mRNA and protein level some short-listed putative interactor. Next, we determined the pattern of expression of RNase E and HupB, one of the strongest putative interactors of the RNase E in optimal and stress-conditions

Aim 3

In *M. tuberculosis,* to understand how RNase E and HupB interaction influences mycobacterial survival and adaptation in the presence of isoniazid (INH) and during macrophage infection.

For this, we performed time-lapse microfluidic microscopy and coupled with single-cell multiparametric analysis of RNase E and HupB double translational fluorescent reporter and of CRISPRi/dCas9 *rne* strain following INH treatment. Next, by snapshot microscopy, we studied the profile of the expression of RNase E and HupB double translational fluorescent reporter and CRISPRi/dCas9 *rne* strain during Raw 264.7 macrophage infection.

Materials and Methods

Chapter 5

5.1 Microbiology and Molecular Biology

5.1.1 Bacterial strains and growth conditions

The (sub)cloning and DNA sequencing step were performed transforming DH5α chemically competent *E. coli*. The transformed DH5α were grown in LB medium and selected by adding the appropriate antibiotics. The generated constructs obtained from the pCR2.1-TOPO plasmid, pND200^{KmR}, pGM218^{HygR}, Tweety^{KmR}, pMYC^{Hyg}, pGM256^{HygR}, and pGM309^{HygR} vectors were selected, respectively, on 100 μg/mL ampicillin; 50 μg/mL kanamycin for *E. coli*; 25 μg/mL kanamycin for *M. smegmatis* and 15 μg/mL kanamycin for *M. tuberculosis*; and 50 μg/mL hygromycin for both *E. coli* and mycobacteria.

All mycobacterial strains were cultured at 37°C in Middlebrook 7H9 broth supplemented with 0.5% BSA, 0.2% glucose, 0.085% NaCl, 0.5% glycerol, and 0.05% Tween-80. Hartman's de Bond media (HDB) (Smeulders et al., 1999) was used as minimal media**.** Complete starvation, nitrogen starvation and short-chain fatty acid media were prepared modifying carbon, nitrogen and phosphate source in the HDB medium (Smeulders et al., 1999). In the short-chain fatty acids media, glycerol, as source of carbon, was substituted with sodium propionate (2 grL^{-1}). Middlebrook 7H10 agar has been enriched with 10% OADC enrichment and 0.5% glycerol. Exponentially growing culture were started from a single colony, aliquots were enriched with 15% glycerol, stored at -80°C, and used once to start primary cultures.

RNase E-6xHis, D694R_D738R protein expression was induced in *Mycobacterium smegmatis* cultured in complete 7H9 broth containing 50 μg /mL hygromycin by adding 0.05% acetamide (Sigma).

CRISPRi_rne silencing was induced in *M. smegmatis and M. tuberculosis* cultured in complete 7H9 broth containing 150 ng /mL and 100 ng/mL anhydrotetacycline (ATC) (Sigma), respectively.

M. smegmatis and *M. tuberculosis* were grown in Middlebrook 7H9 broth at 37°C in shaking conditions to mid-log phase (OD_{600} 0.5–0.8) before bulk- and single-cell assays, unless specified otherwise. The selective antibiotic was only added for strains carrying chromosomal

integrative vectors in the primary culture and removed in the secondary culture used for the final experiments.

5.1.2 Strains construction

Translational reporter strains were constructed using stable variants of mCherry, mKate2, mCitrine, and sfGFP. An oligopeptide linker was added between the protein and the fluorescent reporter to not affect the folding of the protein. The final constructs, used for the transformation of *M. smegmatis* or *M. tuberculosis* were confirmed by restriction enzyme profiling. For chromosomal integrative vectors, the insertion was done either via the L5 phage site attB (Pena et al., 1996), for the pND200^{KmR}, pGM218^{HygR}, pGM256^{HygR}, and PLJR965, or Tweety phage attachment site attT (Pham et al., 2007) for the Tweety^{KmR} vectors. Mycobacteria were transformed with the final construct by electroporation (2,500 V; 25 µF; 1,000 Ω; 2 mm path) and plated on Middlebrook 7H10 agar containing the corresponding antibiotics.

In *M. smegmatis*, the wild-type RNase E over-expressing strain was generated by PCR-amplifying the RNase (*MSMEG_4626*) ORF. The final fragment, carrying a TEV cutting sequence, was cloned in the pMYC^{HygR} vector between the restriction site *BamHI* and *NheI.* In the final construct, the RNase E was C-tagged with a 6xHist tag. The RNase E-6xHis inducible overexpressing strain was named AGS2. The RNase E D694R_D738R over-expressing strains was generated by site-directed mutagenesis accordingly to the Q5® Site-Directed Mutagenesis Kit (NEB) and using as template the pMYC^{HygR} vector containing the RNase E wild-type. The two-point mutations were consequently introduced in the wild-type sequence, and the insertions of the mutation was confirmed by sequencing. The RNase E D694R_D738R inducible over-expressing strain was named AGS5.

In *M. smegmatis,* the RNase E fluorescent translational reporter was generated by PCR-amplifying 200 bp upstream the RNase E ORF and the RNase E ORF in-frame and fusing its C-terminus to the mKate2 ORF. The mKate2 C-tagged RNase E was cloned into the chromosomal integrative vectors pND200^{KmR} and pGM218^{Hygr}. The RNase E-merodiploid attB::RNase E-linker-mKate2 strains were named DVS2 and AGS13, respectively. To construct the DEAD (*MSMEG_5042*), RraA (*MSMEG_6439*), Obg (*MSMEG_4623*), RelA (*MSMEG_2965*), ppk (*MSMEG_2392_2391*), UvrA (*MSMEG_3808*), Lsr2 (*MSMEG_1060*), infA (*MSMEG_1519*), HupB (*MSMEG_2389*) translational reporters, each locus was PCR-amplified and fused at the C-terminus to the yellow fluorescent marker, mCitrine. The C-tagged mCitrine translational fluorescent reporters were co-transformed in AGS13 reporter strain, generating dual-translational fluorescent reporters of P*rne*-mKate2 (at the attB site) and mCitrine fluorescent reporters (at the

attT site). The final double fluorescent reporters were named: AGS15 (attB::RNase E-linker-mKate2_attT::infA-linker-mCitrine), AGS16 (attB::RNase E-linker-mKate2_attT::RraA-linker-mCitrine), AGS17 (attB::RNase E-linker-mKate2_attT::HupB-linker-mCitrine), AGS18 (attB::RNase E-linker-mKate2_attT::UvrA-linker-mCitrine), AGS19 (attB::RNase E-linker-mKate2_attT::Obg-linker-mCitrine), AGS20 (attB::RNase E-linker-mKate2_attT::DEAD-linker-mCitrine), AGS21 (attB::RNase E-linker-mKate2_attT::RelA-linker-mCitrine), AGS22 (attB:: RNase E-linker-mKate2_attT::ppk-linker-mCitrine), AGS23 (attB::RNase E-linker-mKate2_attT::Lsr2-linker-mCitrine).

To generate the P*hupB*-mCitrine over-expressing the RNase E wild-type, the AGS2 strain was co-transformed with the mCitrine C-tagged HupB construct, which was named AGS33.

For *M. tuberculosis,* the RNase E (*Rv2444c*) and HupB (*Rv2986c*) translational reporters were produced by PCR-amplifying the *rne* and *hupB* regulatory region and the *rne* and *hupB* ORF in-frame and fusing at its C-terminus to the mCherry and sfGFP ORF, respectively. The mCherry C-tagged RNase E was cloned into the chromosomal integrative vector pGM218^{HygR}, and the sfGFP C-tagged HupB was cloned into the chromosomal vector Tweety^{KmR}. To generate the dual-translational reporter, the final vector containing the P*rne*-mCherry (at the attB site) and P*hupB*-sfGFP (at the attT site) constructs were electroporated in the Erdman (Erd) wild-type strain. The final double fluorescent reporter was named GMT25.

The *rne* knock-down strains in *M. smegmatis mc²155* and *M. tuberculosis* Erdman were generated using a CRISPRi/Cas9 system (Rock et al., 2017). The sgRNA probes were designed accordingly to Rock and colleagues protocol (Rock et al., 2017), and cloned into the pGM309^{HygR} plasmid (*M. tuberculosis*) or pGM256^{HygR} plasmid (*M. smegmatis*). pGM309^{HygR} and pGM256^{Hygr} respectively correspond to the pLJR965^{KmR} and pLJR962^{KmR}, in which the kanamycin resistance cassette had been substituted with the hygromycin one. The final CRISPRi/Cas9 vectors were confirmed by both PCR amplification and sequencing. The inducible knock-down strains have been named mc²155/pGM255 and Erd/pGM309. The constructs carrying the *rne* CRISPi/Cas or the control vector (pGM255, pGM309 and pGM309) were used to co-transformed P*hupB*-mCitrine and P*hupB*-sfGFP reporters in *M. smegmatis* and *M. tuberculosis,* respectively. The strains were respectively named AGS32 (attB::CRISPRi/Cas9_*rne*_attT::HupB-linker-mCitrine), GMT27 (attB::CRISPRi/Cas9_attT::HupB-linker-sfGFP) and GMT26 (attB::CRISPRi/Cas9_*rne*_attT::HupB-linker-msGFP).

5.1.3 Growth-curve assay

Exponentially growing primary cultures were diluted to OD_{600} 0.05 in pre-warmed Middlebrook 7H9 broth and incubated at 37°C for 24 hours in the case of *M. smegmatis* and 7 and 30 days in the case of *M. tuberculosis.* The OD_{600} was measured at regular intervals.

5.2 Protein expression analysis

5.2.1 RNase E overexpression and purification

Primary cultures were obtained from single colonies of AGS2, and *M. smegmatis* wild-type transformed with $pMYC^{HygR}$ empty vector as control. The single colonies were inoculated into 7H9 selective broth and diluted to OD_{600} 0.03 until they reached OD_{600} 0.5. Secondary cultures were induced with 0.05% acetamide and incubated at 30°C for 24 hours. After 24 hours, 25 mL of culture were collected at 4 200 g for 15 minutes at 4°C. Pellets were processed under native conditions in 500 µL of protein lysis buffer (10 mM Tris-HCl pH 7.5, 150 mM NaCl, 0.5% glycerol, and 1×Protease Inhibitor Cocktail (Roche)). Cell suspensions were sonicated for 5 cycles of 30 seconds at 100% amplitude, with 45 seconds intervals on ice and then centrifuged at 10 000 g for 1 hour at 4°C. The pellet was resuspended in 250 µL of protein lysis buffer. The suspension was quantified by Bradford reagent (Sigma), and the concentration of the sample was adjusted to 1 mg/mL. 100 µg of the cellular suspension were used to perform the RNase E pull-down under native condition following the manufacturer's instruction. All the steps of the purification were performed either on ice or at 4°C. 600 µL of HisPur™ Cobalt Superflow Agarose (ThermoFisher) (ratio 1:6 v/v respect the volume of the sample) were transferred to a clean 2 mL low binding tube (Eppendorf) and equilibrated with 1.2 mL of equilibration buffer (20 mM of Na_3PO_4, 300 mM NaCl, 5 mM imidazole). The resin was sedimented by centrifugation at 700 g for 2 minutes at 4°C, and the supernatant discarded. Before adding the cellular suspension to the resin, the samples were equilibrated with 300 µL of equilibration buffer. The equilibrated samples were added to the resin and incubated for 4 hours at 4°C ensuring the resin's continuous suspension. The resin-sample suspension was centrifugated at 700 g for 2 minutes at 4°C. The supernatant was carefully removed and stored for downstream analysis. The resin was washed three times for 2 minutes in the washing buffer (20 mM Na_3PO_4, 300 mM NaCl, 15 mM imidazole). For each washing step, the supernatant was stored and used for downstream analysis. The bound RNase E-6xHist was eluted two times for 10 minutes with 0.5 ml of elution buffer (20 mM Na_3PO_4, 300 mM NaCl, 150 mM imidazole). The two elutions were pulled together and concentrate by Trichloroacetic acid

(TCA)/acetone precipitation. All the steps of the TCA/acetone precipitation were performed at 4°C, if not otherwise specified. To the pulled elutions, 1 volume of cold 40% TCA (Sigma) was added, followed by 30 min incubation and then centrifugated for 15 minutes at 14 000g. The pellet was then washed twice with 1 volume of cold acetone (Sigma), incubated for 10 minutes, and centrifugated for 10 minutes at 14 000 g. After the final washing step, the supernatant was discarded, and the samples dried. The precipitated samples were stored at 4°C before Mass Spectrometry. For each condition, 7 biological replicates have been processed.

5.2.2 RNase E pull-down Mass Spectrometry (MS)

5.2.2.1 Protein digestion

M. smegmatis bacterial lysate before the pull-down (input) and the RNase E TCA precipitated pull-down (IP) were respectively diluted 1:2 and resuspended using the denaturing buffer (100 mM NH_4HCO_3 and 8 M CH_4N_2O). Protein were subsequently reduced with 5 mM Tris(2-carboxyethyl) phosphine hydrochloride solution (TCEP, Sigma) for 30 minutes and then alkylated with 20 mM iodoacetamide (Sigma) for 1 hours in the dark. Reduced and alkylated proteins were then digested over night at 37°C with Sequencing Grade Modified Trypsin (Promega) using an enzyme: protein ration of 1:50. The digestion was stopped with 4% formic acid (FA). For the subsequent Mass Spectrometry analysis, the resulting peptides from the input and the IP were desalted with stage-tip (Rappsilber et al., 2007) using C18 Empore disc and eluted with 80% acetonitrile (ACN) and 0.1% FA. Finally, all samples were dried in a Speed-Vac and peptides were resuspended in 2 % ACN, 0.1 % FA prior to LC-MS/MS analysis.

5.2.2.2 LC-MS/MS analysis

Input: a nanochromatographic system (Proxeon EASY-nLC 1200 - Thermo Fisher Scientific) was coupled on-line to a Q Exactive™ Plus Mass Spectrometer (Thermo Fisher Scientific) using an integrated column oven (PRSO-V1 - Sonation GmbH). For each sample, peptides were loaded on a 50 cm column (EASY-Spray column, 50cm x 75 µm ID, PepMap C18, 2 µm particles, 100 A pore size - ES803 - Thermo Fisher Scientific) after an equilibration step in 100 % solvent A (H_2O, 0.1 % FA). Peptides were eluted with a multi-step gradient using 2 to 7 % solvent B (80 % ACN, 0.1 % FA) during 5 min, 7 to 23 % during 70 minutes, 23 to 45 % during 30 minutes and 45 to 95 % during 5 minutes at a flow rate of 250 nL/min over 132 minutes. Column temperature was set to 60°C.

IP: the same procedure as described above was used with an in-house packed 38 cm nano-HPLC column (75 µm inner diameter) with C18 resin (1.9 µm particles, 100 Å pore size, Reprosil-Pur Basic C18-HD resin, Dr. Maisch GmbH).

MS data were acquired using Xcalibur software using a data-dependent Top 10 method with a survey scans (300-1700 m/z) at a resolution of 70 000 and a MS/MS scans (fixed first mass 100 m/z) at a resolution of 17 500. The AGC target and maximum injection time for the survey scans and the MS/MS scans were set to 3E6, 20 ms and 1E6, 60 ms respectively. The isolation window was set to 1.6 m/z and normalized collision energy fixed to 28 for HCD fragmentation. A minimum AGC target of 1E4 was used for an intensity threshold of 1.7E5. Unassigned precursor ion charge states as well as 1, 7, 8 and >8 charged states were rejected and peptide match was disable. Exclude isotopes was enabled and selected ions were dynamically excluded for 45 seconds.

5.3 Microscopy

5.3.1 Snapshot microscopy

Phase-contrast and fluorescence snapshot imaging were acquired using an inverted DeltaVision Elite Microscope (GE Healthcare) equipped with an UPLFLN100XO2/PH3/1.30 objective (Olympus).

All the samples for the imaging were prepared dispensing 0.5 µL of batch culture between two #1.5 coverslips.

Exponential-phase AGS13 cultures were stained with 1 µM RNA Select (Invitrogen) for 1 hour. Exposure conditions : phase 100% T, 150 ms; mCherry (Ex 555/90, Em 600/675) 100% T, 600 ms ; YFP (Ex 513/17, Em 548/22) 32% T, 250 ms.

Double reporter strains AGS15, AGS16, AGS18, AGS19, AGS20, AGS21, AGS22, AGS23 cultures were split and reincubated at 37°C for 6 hours, either without stress or under HDB starvation media. Exposure conditions: phase 50% T, 150 ms; mCherry (Ex 575/25, Em 625/45) 100% T, 600 ms, and YFP (Ex 513/17, Em 548/22) 100% T, 600 ms However, for AGS15, AGS18, and AGS23 YFP (Ex 513/17, Em 548/22) was modified at 100% T, 250 ms.

AGS17 exponentially growing culture were split and then reincubated at 37°C for 6 hours, either without stress or exposed to 0.2 µg/mL MMC, 20 µg/mL Rifampicin, 64 µg/mL Chloramphenicol, 16 µg/mL C109, and 20 µg/mL Isoniazid. Exposure conditions : phase 50% T, 150 ms ; mCherry (Ex 575/25, Em 625/45) 100% T, 600 ms, and YFP (Ex 513/17, Em 548/22) 100% T, 250 ms.

AGS32 and AGS33 exponentially growing culture were split and then reincubated at 37°C for 6 hours and 24 hours, either without stress or in presence of inducer. In AGS33 the RNase E over-expression was induced adding to the media 0.05% acetamide, and in AGS32 the *rne* CRISPRi was induced adding 150 ng/mL ATC. Exposure conditions : phase 50% T, 150 ms, and YFP (Ex 513/17, Em 548/22)100% T, 250 ms.

5.3.2 Time-lapse microscopy

To eliminate clumps and assure a single-cell suspension, exponential-phase batch cultures were passed through pre-equilibrated 5 µm filters. The bacterial suspension was inoculated into a custom-made hexa-device as described (Manina et al., 2019). Syringes filled with pre-warmed 7H9 were connected to the inlet tube, and the media was pumped through the hexa-device at 10 µl/min. After the assembly, the device was installed on the microscope stage of a DeltaVision Elite Microscope (GE Healthcare). The image acquisition was set at intervals of 30 minutes for *M. smegmatis* and 3 hours for *M. tuberculosis.* A UPLFLN100XO2/PH3/1.30 objective (Olympus) and a high-speed sCMOS camera, 2,560 x 2,160 pixels, pixel size 6.5 x 6.5 µm, 15-bit, spectral range of 370–1,100 nm, were used. Exposure conditions for *M. smegmatis*: phase 100% T, 150 ms; and mCherry (Ex 575/25, Em 625/45) 100% T, 600 ms. Exposure conditions for *M. tuberculosis*: phase 100 % T, 200 ms, FITC (Ex 492/28, Em 523/23) 100% T, 200 ms; TRITC (Ex 556/25, Em 611/47) 100% T, 600 ms. Drugs were added to the medium flow when required. In separate areas of the hexa-device, different reporter strains or independent cultures of the same reporter strain were seeded, and each experimental setting was at least performed in duplicate. For each reporter strain, both technical and biological replicates individual XY fields were analyzed. Plots representing single-cell analysis were generated pooling together data obtained from independent experiments.

5.3.3 Raw macrophage infection

10^5 Raw 264.7 mouse leukemic monocyte macrophages were seeded in a 35 mm µ-Dish (Ibidi) and incubated at 37°C with 5% CO_2 for 24 hours before infection. Seeded Raw cells were infected using either MOI = 1:5 (*M. tuberculosis* OD_{600} 0.005) or MOI = 1:10 (*M. tuberculosis* OD_{600} 0.01) of an *M. tuberculosis* suspension, and after 6 hours post infection, the cells were washed extensively with DMEM (Gibco™) without phenol red. The *rne* knock-down was induced by adding 100 ng/mL of ATC in the medium. The cells were replenished with fresh medium and ATC on day 3 post infection. Infected macrophages were imagined using a 100x oil-immersion objective at day 1, 3 and 6 post infection, by z stack acquisition (6 x 1 µm). Exposure conditions : phase 32% T, 50 ms ; FITC (Ex 475/28, Em 525/48)

100% T, 200 ms ; TRITC (Ex 556/25, Em 611/47) 100% T, 600 ms. The infection was performed in triplicate and in each experiment, from 70 to 130 XT field were imagined.

5.4 Data analysis and statistic

5.4.1 Mass Spectrometry data processing for protein identification and quantification

Raw data were analyzed using MaxQuant software version 1.5.5.1 (Tyanova et al., 2016) using the Andromeda search engine (Cox et al., 2011). The MS/MS spectra were searched against the UniProt *M. smegmatis* (strain ATCC 700084 /mc²155) database containing 6 601 proteins, usual known mass spectrometry contaminants and reversed sequences of all entries. Andromeda searches were performed choosing trypsin as specific enzyme with a maximum number of two missed cleavages. Possible modifications included carbamidomethylation (Cys, fixed), oxidation (Met, variable), N-terminal acetylation (variable). The mass tolerance in MS was set to 20 ppm for the first search then 4.5 ppm for the main search and 20 ppm for the MS/MS. Maximum peptide charge was set to seven and seven amino acids were required as minimum peptide length. The "match between runs" feature was applied for samples having the same experimental condition with a maximal retention time window of 0.7 minute. One unique peptide to the protein group was required for the protein identification. A false discovery rate (FDR) cutoff of 1 % was applied at the peptide and protein levels. Quantification was performed using the XIC-based LFQ algorithm with the Fast LFQ mode as described in Cox and colleagues (Cox et al., 2014) and skip normalization was applied only for IP. Unique and razor peptides, included modified peptides, with at least 2 ratio count were accepted for quantification.

5.4.2 Single-cell analysis

ROI Manager Macro of ImageJ 1.52q software (Schneider et al., 2012) was used to perform single-cell segmentation of both snapshots and time-lapse images. The Selection Freehand line was used to cover the profile of individual cells. The thickness was set to 7 for *M. smegmatis*, and 5 for *M. tuberculosis*. The Freehand lines segmentation allowed the extraction of diverse parameters, such as the cell size and length, the total fluorescence and the intensity fluorescence profile. Both the total fluoresce and the fluorescence profile are expressed as the sum of intensity of the pixel normalized to the thickness of the line drawn across the cell. To homogenize the fluorescence, the background signal was deducted at each measurement. The cell position in the lineage and pole age were manually annotated using a binary code. Two customized scripts,

written in R (Manina et al., 2019a) and Python, allowed the post-processing of the data from the .csv and .txt files, respectively extracted from ROI Manager. Each image of the RAW 264.7 macrophage infection is derived from the projection of a stack of 6 snapshots taken on the same field of view sequentially at 1-µm z-step from each other, using the maximum intensity method (SoftWorx). The post-processing data analysis of each projection was performed using a a customized ImageJ macro.

5.4.3 Statistics

Plots and statistical analyses were generated using Prism 8.4 (GraphPad Software). Lognormal, Lorentzian and sum of two Gaussians were used to respectively examine the distribution of the populations (**Figure 20G** and **Figure 24E**). Pearson *r* correlation coefficient was computed on (x, y) data sets. Two-way ANOVA, using Turkey or Dunnett correction for multiple comparisons, were performed to evaluate statistical significance between multiple groups, unless otherwise specified. Brown-Forsythe, Welch and one-way Ordinary ANOVA tests were performed to compare the variation of a single parameter over multiple groups. Chi square test of independence was used to analyze contingency. P values < 0.05 were considered significant.

5.4.4 Mass Spectrometry Statistical Analysis

For the differential analyses, proteins identified in the reverse and contaminant databases and proteins "only identified by site" were first discarded from the list of identified proteins. Then, only proteins with at least two LFQ values in a condition were kept. After $\log_2$ transformation, LFQ values were normalized by median centering within conditions (normalizeD function of the R package DAPAR (Wieczorek et al., 2017)). Remaining proteins without any LFQ value in one of both conditions have been considered as proteins quantitatively present in a condition and absent in another. They have therefore been set aside and considered as differentially abundant proteins. Next, missing values were imputed using the imp.norm function of the R package norm (Novo, 2013). Proteins with a fold-change under 2.0 have been considered not significantly differentially abundant. Statistical testing of the remaining proteins (having a fold-change over 2.0) was conducted using a limma t-test (Smyth, 2005) thanks to the R package limma (Ritchie et al., 2015). An adaptive Benjamini-Hochberg procedure was applied on the resulting p-values thanks to the function adjust.p of R package cp4p (Giai Gianetto et al., 2016) using the robust method of (Pounds and Cheng, 2006) to estimate the proportion of true null hypotheses among the set of statistical

tests. The proteins associated to an adjusted p-value inferior to a FDR of 1% have been considered as significantly differentially abundant proteins. Finally, the proteins of interest are therefore those which emerge from this statistical analysis supplemented by those which are considered to be present from one condition and absent in another.

5.4.5 Calculation of parameters and subpopulations

The growth rate was measured by fitting an exponential curve to single-cell size measurements over the generation time (T_d) of the cell from birth to division. The systematical determinate the authenticity of single-cell localization events (foci), the intensity fluorescence profile was normalized to the cell background fluorescence and localization events were identified, for M. smegmatis, if one or more cell segments had Prne-mKate2 fluorescence values equal or greater than 500 (a.u.) after subtraction of the minimum cell fluorescence (Figure 20), and for M. tuberculosis, if one or more cell segments had Prne-mCherry and PhupB-sfGFP fluorescence values respectively equal to or greater than 150 (a.u.) and 120 (a.u.) for sfGFP after subtraction of the minimum cell fluorescence (Figure 24A-E) The focus hereditary within lineage was determined by measuring the cellular age described in (Manina et al., 2019) and segregating the mothers and the first generation offspring in the 0 and 1 foci subpopulations. Microcolony PhupB - sfGFP fluorescence (Figure 24G and Figure 25C) measured from a region of interest of constant size through the whole time-lapse image sequence and normalized to the background fluorescence. Division and lysis rates were analysis from the number of cells constituting a microcolony at the time of INH addition and scoring the division and lysis event in the following 16 days as described in (Manina et al., 2015; Wakamoto et al., 2013). Lastly, the division and lysis event were normalized by the total number of cells at the corresponding time point, generating sequential rates per hour for the same microcolony.

Results

Chapter 6

6.1 *M. smegmatis* P*rne*-mKate2 reporter strain exhibits dynamic localization events that are associated with cellular homeostasis.

We measured the levels of mRNA expression of the mycobacterial orthologs, coding for the main constituents of the RNA degradosome complex, in the non-pathogenic TB model organisms *M. smegmatis* (**Figure S1A**). We monitored the transcriptional profiles of exponentially growing cells up to stationary growth-phase, or subjected them to carbon and nitrogen starvation (Smeulders et al., 1999), and to short-chain fatty acids as a sole carbon source, aiming to mimic the host-limiting conditions. Interestingly, we observed an upregulation of all the genes that was more pronounced in stationary growth-phase and in fatty acids-enriched medium, and found to be significant for the RNase E encoding gene (**Figure S1A**). These results pointed to the possible role of RNase E in mycobacterial stress tolerance.

To monitor the effect of changes in RNase E expression to *M. smegmatis* fitness, given the alleged essentiality of *rne* (*MSMEG_4626*) (Płociński et al., 2019; Taverniti et al., 2011), we generated a strain carrying a small guide RNA targeting the *rne* catalytic site and an inducible dCas9, to silence gene expression, referred to as *rne_si*, see also **Materials and Methods**. In addition, we generated two merodiploid strains, carrying either a wild-type (WT) *rne* copy, henceforth referred to as *rne_oe*, or a mutated variant under the control of a strong inducible promoter, see also **Materials and Methods**. Given the high conservation of the RNase E catalytic site among different bacterial species (Aït-Bara and Carpousis, 2015), we focused on two point mutations formerly used to generate catalytically inactive RNase E variants in *E. coli* (Bandyra et al., 2018). By site-directed mutagenesis we introduced the two corresponding mutations in *MSMEG_4626* second copy, causing two substitutions from aspartic acid to arginine (D694R and D738R). We found that both silencing and overexpressing WT *rne*, *M. smegmatis* cells exhibited a significant growth defect, which was less pronounced by overexpressing the RNase E variant mutated in the putative active site (**Figure S1B**). Collectively these results are consistent with previous evidence suggesting the essentiality of RNase E in mycobacteria (Płociński et al., 2019; Taverniti et al., 2011).

Since changes in RNase E expression levels have a significant effect on the growth rate of *M. smegmatis* in bulk assays, and these changes are influenced by environmental stress conditions,

we asked whether RNase E expression spontaneously varied from cell to cell and if this could have an impact on single-cell physiology and stress tolerance. To monitor the native expression of the RNase E in single *M. smegmatis* cells, we reproduced the *rne* locus into the *attB* phage attachment site (Peña et al., 1996) and inserted a red fluorescent marker, to generate a C-term translational reporter of RNase E fused to mKate2 (**Figure S1C** and see also **Materials and Methods**). The reporter strain, referred to as P*rne* - mKate2, showed no growth defects and normal levels of transcription (**Figures S1D** and **S1E**).

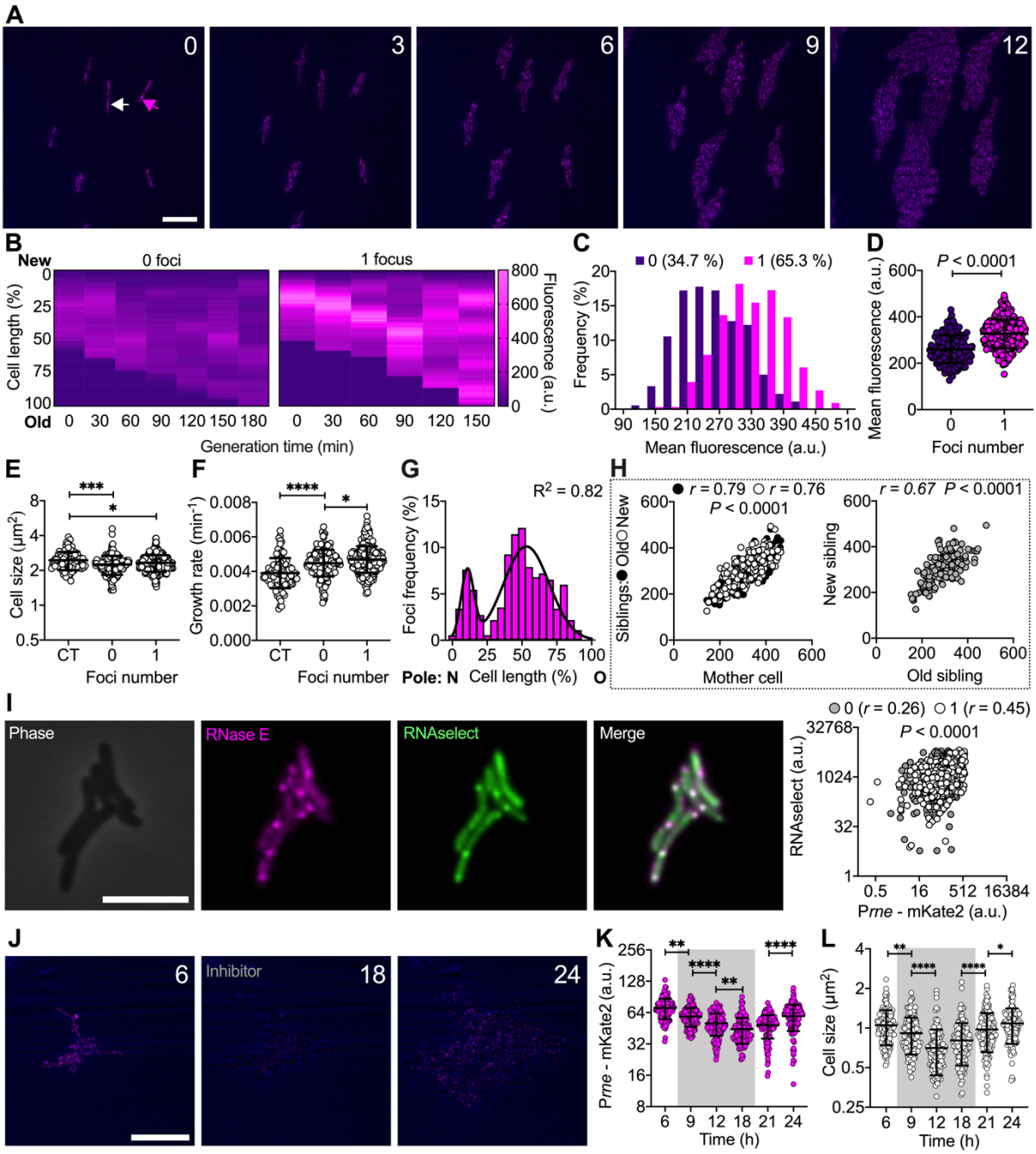

***Figure 20*. M. smegmatis Prne-mKate2 expression is dynamic and associated with cell-size and growth homeostasis.**

(A) *Representative time-lapse image series of exponentially growing M. smegmatis Prne-mKate2 reporter strain. Phase-contrast (blue) and mKate2 fluorescence (magenta) are merged. Numbers represent hours. The color-coded arrows indicate cells without (white) and with (magenta) localization events (foci), respectively. Scale bar 10 µm. See also Movie 1 (https://www.dropbox.com/sh/xkg96z82yz2zckc/AADcHvAK6HhpkMZV4tO4Esxua?dl=0).*

(B) *Representative heatmaps of Prne-mKate2 fluorescence, expressed as a function of the single-cell generation time (x-axis) and length expressed in percentage (y-axis). One cell with no RNase E localization events (left panel) and one with one localization event (right panel) are shown. RNase E localization events were identified if one or more cell segments had fluorescence values equal or greater than 500 (a.u.) after subtraction of the minimum cell fluorescence (See also Materials and Methods).*

(C) *Distribution of the Prne-mKate2 fluorescence in single cells segregated by the absence (violet, n = 330) or the presence (magenta, n = 180) of RNase E foci. The data shown are from two independent experiments.*

(D) *Prne-mKate2 fluorescence averaged over the lifetime of the cell, in subpopulations segregated by the absence (0) or presence (1) of RNase E foci (color-coded as in C). Black lines indicate mean ± SD (n = 510). Significant P value was calculated by unpaired t-test. The data shown are from two independent experiments.*

(E–F) *Single-cell cell size (**E**) and growth rate (**F**) averaged over the lifetime of the cell in the control M. smegmatis mc²155 wild type strain (CT) and in the two subpopulations identified in C and D. Black lines indicate mean ± SD (100 ≤ n ≤ 330). Asterisks denote significant difference by one-way ANOVA followed by Tukey's multiple comparison test: *P = 0.012 and 0.023; ***P = 0.0003; ****P < 0.0001.*

(G) *Histogram showing the distribution of the position of the foci expressed as a function of cell length expressed in percentage. Black line indicates fitting of the data with a sum of two Gaussians function. Old (O) and new (N) cell pole are indicated. RNase E localization events mainly occur towards the new cell pole and in the mid-cell position.*

(H) *Pearson correlation of the Prne-mKate2 fluorescence averaged over the lifetime of the cell between mothers and their old- (black) and new-pole (white) daughters (left panel), and between old- and new-pole siblings (right panel). The data shown are from 2 independent experiments (n = 170, per category).*

(I) *Representative snapshot images of the Prne-mKate2 reporter, stained for 1 hour with the RNAselect™ dye (1 µM). Phase-contrast (gray), Prne-mKate2 (magenta), and RNAselect™ (green) fluorescence are shown separately and merged, as indicated in the snapshots. Scale bar 5 µm. In the left panel, Pearson correlation of Prne-mKate2 and RNAselect™ fluorescence in single cells having none (gray circles) or one (white circles) RNase E focus. Data derive from two independent experiments (n = 145).*

(J) *Representative time-lapse image series of exponentially growing M. smegmatis Prne-mKate2 reporter strain treated with a molecule inhibiting the RNase E catalytic domain (M5, (Kime et al., 2015). Growth in standard 7H9 medium is unlabeled, and presence of the inhibitor (2.5 mM) is indicated. Phase-contrast (blue) and Prne-mKate2 (magenta) fluorescence are merged. Fluorescence images of each channel are scaled to the brightest frame. Cells were imaged at 30-*

min intervals, and numbers represent hours. Scale bar 10 µm. See also Movie 2 (https://www.dropbox.com/s/zbnnh3w049513rt/Movie2.avi?dl=0).

(K–L) *Single-cell Prne-mKate2 fluorescence (K) and cell size (L) throughout different phase of the time-lapse microscopy experiment (J). RNase E inhibitor is shown in gray, pre-growth in standard 7H9 medium and inhibitor washout correspond to the white area of the graph. Data are shown merging two independent experiments. Black lines indicate means ± SD (n = 142). Asterisks denote significance by one-way ANOVA followed by Tukey's multiple comparison test: *P < 0.038; **P < 0.004; ****P < 0.0001.*

To monitor the single-cell dynamics of the mycobacterial RNase E under optimal growth conditions, we carried out time-lapse imaging of exponential-phase P*rne* - mKate2 cells, growing inside a customized microfluidic device (Manina et al., 2019), under constant perfusion of fresh 7H9 medium (**Figure 20A**; **Move 1,** https://www.dropbox.com/sh/xkg96z82yz2zckc/AADcHvAK6HhpkMZV4tO4Esxua?dl=0). By single-cell multiparametric analysis of time-lapse image sequences, we not only found a low-intensity patchy expression of the RNase E throughout the cell, which may resemble the spatial organization of the RNA polymerase (Weng et al., 2019), but we also distinguished a fraction of the population exhibiting dynamic localization events, which we also refer to as foci (**Figure 20B**). To systematically determine the formation of RNase E foci, we analyzed the single-cell fluorescence profile over the cell generation time, and set an intensity threshold above which localization events were considered authentic, see also **Materials and Methods**. By applying this threshold value, we were able to quantify that about one third of the population displayed only low levels of patchy RNase E fluorescence and that about two thirds formed bright RNase E foci at some time during the cell lifetime, *i.e.*, between birth and division (**Figure 20C**). We confirmed that the two subpopulations were significantly different from each other (**Figure 20D**), implying that RNase E is expressed heterogeneously within a clonal *M. smegmatis* population.

Surprisingly, we measured that the P*rne* - mKate2 strain, carrying a second copy of RNase E, had slightly reduced cell size and grew at a faster rate compared to the WT (**Figures 20E** and **20F**). In particular, cells that formed foci grew significantly faster, suggesting a likely relationship between small variations in RNase E expression and growth regulation during the cell cycle (**Figure 20F**). To understand whether there was a relationship between foci formation and cell cycle, we measured the foci position relative to the cell length and generation time. Interestingly, we found that RNase E foci were mainly located towards the mid-cell position or towards the new cell-pole, but we found no significant association with the generation time and cell age (**Figures 20G, S1F** and **S1G**). Indeed, the expression of RNase E was positively correlated between one generation and the following and between siblings regardless of cell age (**Figure 20H**).

To examine the functional significance of the RNase E foci, we stained cells with RNAselect™, an RNA-specific dye. We observed that, similar to RNase E, also RNAselect™ diffused

throughout the cell body with moderate fluorescence, likely in correspondence with rRNA, and formed more intense foci, presumably associated with actively transcribed genes (**Figures 20I** and **S1H**). We also measured a significant positive correlation between the RNA dye and RNase E fluorescence, especially in cells forming foci, suggestive of preferential localization of functional RNase E clusters close to areas with active transcription (Bayas et al, 2018).

To further assess the functional relevance of the RNase E foci on mycobacterial physiology, we carried out a multi-phase time-lapse microscopy experiment. We first grew exponential P*rne*-mKate2 bacteria inside our microfluidic device for 6 hours with fresh 7H9 medium; next we treated the bacteria the with a small molecule, which specifically inhibits the catalytic site of the RNase E (Kime et al., 2015), at the minimum inhibitory concentration (1X-MIC) for 12 hours; finally we washed out the inhibitor for 12 hours (**Figure 20J; Movie 2,** https://www.dropbox.com/s/zbnnh3w049513rt/Movie2.avi?dl=0). We analyzed individual cells over time and found that RNase E foci disappeared about 8 hours following exposure to the inhibitor (**Figure 20K**), experienced a growth rate slowdown (**Movie 2,** https://www.dropbox.com/s/zbnnh3w049513rt/Movie2.avi?dl=0) and underwent reductive division (**Figure 20L**). These results confirmed not only the functional role of the RNase E fluorescent foci, but also that impairment of the RNase E activity has a detrimental effect on mycobacterial cell division and on the maintenance of the cellular homeostasis. Taken together these observations lead us to hypothesize that the phenotypic variation we found in RNase E expression may have implications in the response of single mycobacterial cells to stressful conditions.

6.2 The mycobacterial RNase E interactome includes proteins involved in RNA turnover and stress-response pathways

Aiming to identify the mycobacterial RNase E protein interactome, we induced the over-expression of the RNase E fused to a 6X-His tag in the *rne-oe M. smegmatis* strain for 24 hours, referred to as RNase E condition, and we exposed to the inducer also *M. smegmatis* carrying the empty expression vector, as a control condition (CT) (**Figure S1B**). We carried out immunoprecipitation under native conditions, using a His-Pur™ Cobalt Superflow Agarose resin against the whole-cell extracts of both the RNase E and CT conditions (**Figure S2A**), see also **Materials and Methods**. Next, we coupled the pull-down assay with mass spectrometry, to analyze the putative protein interactors of RNase E compared to CT by label-free quantification and checked samples reproducibility (**Figure S2B**). We were able to identify 224 proteins exclusively present in the RNase E pull-down and 380 proteins exclusively present in the CT pull-down. By differential analysis, we found that 301 proteins were more abundant and 36 less

abundant in the RNase E than in the CT condition (**Figure 21A**). The complete list of proteins identified in both conditions, the fold change and significance (**Supplementary table 2** https://www.dropbox.com/s/koomyyqaq3fmdph/Supplementary%20table%202.xlsx?dl=0), and the relative stoichiometry analysis computed for the interactors that resulted significant by differential analysis (**Supplementary table 4,** https://www.dropbox.com/s/r0ksjsb0hkt4asl/Supplementary%20table%204.xlsx?dl=0) are provided, see also **Materials and Methods**.

We carried out functional analysis (**Figures 21A** and **21B**), first focusing on proteins known either to be part of the canonical RNA degradosome of *E. coli* or to have functions associated with RNA turnover (Bandyra and Luisi, 2018; Belasco, 2010). Indeed, we identified 12 proteins implicated in RNA turnover that were significantly enriched in the RNase E pull-down (FDR < 0.01). In particular, we found the ribonucleoprotein MSMEG_1193 (>5-fold enriched), containing a TROVE domain that is conserved between prokaryotes and eukaryotes for RNA binding (Bateman and Kickhoefer, 2003). We also found proteins belonging to the Nudix-like RNA pyrophosphohydrolase family, responsible for removing pyrophosphate from the 5'-ends of triphosphorylated RNA transcripts, and for producing substrates that are more susceptible to the RNase E activity (Deana et al., 2008). In particular MutT2 (>2.1-fold enriched), and two non-significant proteins, namely MutT4 and MSMEG_0790. In support of the exonucleolytic activity that typically follows the endonucleolytic cleavage of RNase E, we found an enrichment in GpsI and Rph, both having 3'-5'-exoribonuclease activity similar to PNPase. Furthermore, we were able to identify several ATP-dependent helicases, which are crucial to assist RNA substrate degradation, by generating single-stranded RNA. In particular, we found two DEAD/DEAH box helicases MSMEG_1254 and MSMEG_1757 (<2-fold enriched); MSMEG_2174 (>2.2-fold enriched); HelY (>2.3-fold enriched); DeaD (>2.4-fold enriched) and HrpA (>2.5-fold enriched). Although among the non-significant proteins, the *E. coli* RhlB orthologue RhlE was also found to be poorly enriched in the RNase E fraction (>1.3 fold; $P = 0.0054$), as well as PcnA (>1.2 fold; $P = 0.34$), an RNA adenylating enzyme that could have an RNA-destabilizing role (Belasco, 2010). Interestingly, we also found a significant enrichment of RraA, which was shown to have an inhibitory effect against RNase E in *E.* coli (Lee et al., 2003), and the ribokinase MSMEG_4661 (>7.4-fold enriched) that may be implicated in mRNA recycling (Bechhofer, 2013).

In addition to a large number of proteins with unknown or predicted function, the third largest group enriched or present only in the RNase E fraction included proteins involved in transcription and its regulation (**Figures 21A** and **21B**). Enzymes responsible for different aspects of cell primary and secondary metabolism were also identified, as well as proteins implicated in signal transduction (**Figure 21B** and **Supplementary table 2** and **3**). Consistent with the role of the mycobacterial RNase E in rRNA processing and maturation (Taverniti et al.,

2011), we found several ribosomal proteins, such as RpmJ, RplB, RplA, RpmB and RpmE, not only enriched in the RNase E fraction but also ranked among the proteins that had the highest relative stoichiometric values (**Supplementary table 4).** Additionally, KsgA that demethylates two adenosines located in a hairpin closed to the 3'-end of the 16S rRNA (Dejesus et al., 2017), and the translation initiation factor InfA (González-Escalante et al., 2015) were found to be significantly enriched in the RNase E fraction (**Figure 21A** and **Supplementary table 4**).

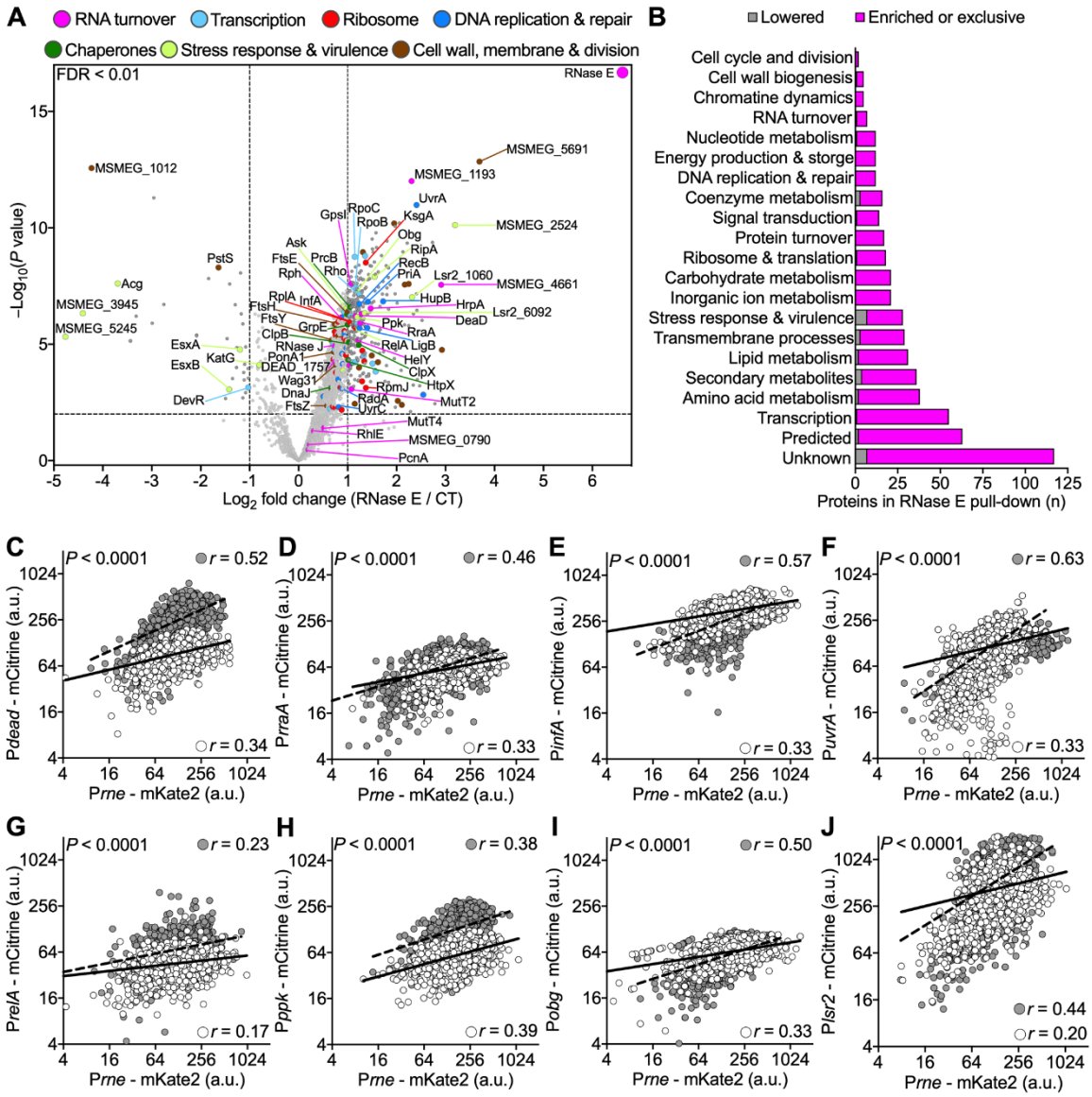

Figure 21. ***M. smegmatis RNase E pull-down coupled with mass spectrometry-based proteomic analysis reveals proteins involved in RNA turnover and stress-response pathways***

(A) *Differential analysis of the proteomics data. Proteins are ranked in a volcano plot according to their statistical P-value (y-axis), and their relative abundance ratio (log_2 fold change) between RNase E overexpressing strain (RNase E) and control (CT) (x-axis). Off-centered spots are those that vary the most between the two groups. Dashed lines on the x-axis indicates a fold change of*

2, with negative values for proteins enriched in the CT sample (or lowered in the RNase E sample) and positive values for protein enriched in the RNase E sample (or lowered in the CT sample). The dashed line on the y-axis indicates a False Discovery rate (FDR) equal to 1%. Proteins identified with a FDR < 0.01 are considered statistically significant by LIMMA t-test (dark gray), whereas proteins with a FDR > 0.01 are considered not significant (light gray). Proteins shortlisted based on functional analysis and relative stoichiometric analysis are attributed to different categories and color-coded in the legend. The corresponding protein name or gene identifier is written on the plot and connected to the relative protein by a color-coded line.

(B) *Functional analysis of the proteomics data. Number of proteins (x-axis) attributed to different functional categories (y-axis). Gray bars represent proteins lowered (n = 36) and magenta bars indicate proteins enriched (n = 301) or exclusively present (n = 224) in the RNase E pull-down from M. smegmatis overexpressing the RNase E compared to the CT strain. See also Supplementary table 4 (https://www.dropbox.com/s/r0ksjsb0hkt4asl/Supplementary%20table%204.xlsx?dl=0).*

(C–J) *Pearson's correlation between red and yellow fluorescence measured in single M. smegmatis cells (n = 150), during exponential growth-phase (white circles) and 6 h after nutrient depletion (gray circles). The data shown are from two independent experiments. On the x-axes, Prne - mKate2 reporter (C–J). On the y-axes, translational reporters of putative RNase E interactors, tagged at the C-terminal in frame with mCitrine: DeaD (C, MSMEG_5042), RraA (D, MSMEG_6439), InfA (E, MSMEG_1519), UvrA (F, MSMEG_3808), RelA (G, MSMEG_2965), Ppk (H, MSMEG_2391_2392), Obg (I, MSMEG_4623) and Lsr2 (J, MSMEG_1060). Fitting of the data with a Log-log function is shown with solid black lines for exponential growth-phase cells, and with dashed lines for nutrient depleted cells (C–J). Significant positive correlations between Prne - mKate2 and the putative interactors are suggestive of an interaction between protein pairs.*

The RNase E fraction was also significantly enriched with chaperons and proteases (**Figures 21A, 21B** and **Supplementary table 2, 3** and **4**), such as GrpE, DnaJ, ClpB, ClpX and HtpX, that ensure the maintenance of protein turnover (Müller and Weber-Ban, 2019), also consistent with former studies (Kovacs et al., 2005; Płociński et al., 2019). Surprisingly, some DNA-binding and nucleoid-associated proteins, implicated in global gene regulation and intracellular survival, such as Lsr2 and HupB (Gordon et al., 2010; Pandey et al., 2014), were enriched in the RNase E fraction and had high relative stoichiometric values, as well as proteins associated with DNA replication and repair. Consistent with these results, inhibition of RNase E activity causes a defective DNA damage response in *E. coli* (Manasherob et al., 2012).

Another category that we found particularly represented included proteins related to stress response and virulence. For instance, the peptidoglycan hydrolase RipA was enriched almost 3-fold, and MSMEG_2524, an ATP-binding ABC transporter that might uptake essential nutrients under stressful conditions, was enriched more than 9-fold. Remarkably, we also found the players of the stringent response, which causes (p)ppGpp production to slowdown bacterial metabolism and foster survival under nutrient-limiting conditions (Prusa et al., 2018; Ramisetty et al., 2016). However, some stress-response and virulence-associated proteins were also found

to be enriched in the CT fraction, such as the universal stress-response proteins MSMEG_3945 and MSMEG_5245, Acg, KatG and the sensor part of the two-component system DevR, implicated in mycobacterial metabolic adaptation to hypoxia and dormancy (Peddireddy et al., 2017). Among the most enriched proteins in the CT condition were also the phosphate ABC transporter PstS and the alkaline phosphatase MSMEG_1012.

Lastly, since a disruption of RNase E levels caused changes in mycobacterial growth (**Figures 20E, 20F, 20L** and **S1B**), we focused on proteins related to cell growth and division. Indeed, we found out several proteins implicated in cell wall remodeling and division, including FtsE, FtsH, FtsY, PonA1 and Wag31 (**Figures 21A** and **21B**). Furthermore, we found that the membrane protein with unknown function, MSMEG_5691 was not only the most enriched (>12 fold) in the RNase E fraction but also ranked among the proteins having the highest relative stoichiometric values (**Figure 21A** and **Supplementary table 4**). Importantly, disruption of MSMEG_5691 confers a growth advantage to *M. tuberculosis in vitro* (Dejesus et al., 2017).

Following the identification of the putative interactome of RNase E, we generated a shortlist that included different functional categories, to be characterized at both the RNA and protein level. We mainly focused on the RNA degradosome, rRNA, and stress response-associated proteins. We carried out gene expression quantification over an extended time span of 24 hours (equal to about 8 generation times of *M. smegmatis*), under growth conditions spanning from optimal, complete starvation, DNA damage and short-chain fatty acids as a sole carbon source (**Figure S2C**). We measured a strong positive correlation for all components of the putative degradosome tested, namely, *gpsI*, *dead* and *helY*, with the exception of a few conditions. In particular, the negative regulator encoding gene *rraA* was inversely correlated to *rne* under complete starvation, suggesting the need for starved cells to induce the endonuclease. We also measured a moderate positive correlation between the transcripts of *rne* and *infA* in all conditions. The expression of the DNA damage response genes positively correlated with *rne* mainly under optimal growth conditions and following induction of DNA damage. We also found a low to moderate positive correlation of *rne* transcripts with genes encoding the players of the stringent response (Prusa et al., 2018; Ramisetty et al., 2016) implicated in (p)ppGpp synthesis and response and protein turnover, except in the presence of fatty acids. Lastly, among the nucleoid-associated proteins involved in virulence we tested (Bartek et al., 2011; Gordon et al., 2010; Odermatt et al., 2018; Pandey et al., 2014b), *lsr2* (*MSMEG_6092*) transcripts showed the highest positive correlation values with *rne* transcripts except in the presence of fatty acids (**Figure S2C**).

Aiming to simultaneously measure the expression of the RNase E with the expression of some putative protein partners, *i.e.*, DeaD, RraA, InfA, UvrA, RelA, Ppk, Obg and Lsr2 (MSMEG_1060), at the single-cell level, we constructed an array of dual-fluorescent reporter strains of translation in the P*rne* - mKate2 background. We PCR-amplified the shortlisted loci,

cloned them in frame with the *mCitrine* fluorescent marker, and alternately inserted them into the Tweety phage attachment site (Pham et al., 2007), generating a panel of dual merodiploid strains, see also **Materials and Methods**. The strains showed no growth defects in bulk (**Figure S2D**). Next, we carried out snapshot microscopy both in exponential growth-phase and following nutrient depletion (**Figure S2E–L**). By comparing the fluorescence of each pair of reporters in single cells, we measured a moderate but significant positive correlation between RNase E and each putative partner in exponential growth-phase. The levels of correlations increased after 6 hours of starvation (**Figures 21C–J**). In particular, we found a more robust positive correlation between RNase E and DeaD and RraA (**Figures 21C** and **21D**); InfA (**Figure 21E**); UvrA (**Figure 21F**); Obg (**Figure 21I**) and Lsr2 (**Figure 21J**).

In conclusion, we were able not only to confirm some expected members of the canonical RNA degradosome (Bandyra and Luisi, 2018; Kovacs et al., 2005; Płociński et al., 2019), but also to identify new members specific to mycobacteria that can assist and complement the endonucleolytic activity of the RNase E. We also identified a number of other putative protein partners and further validated some of them, mainly associated with rRNA, stress responses and virulence. Collectively, these results imply a pleiotropic effect of RNase E on mycobacterial physiology and its role in mycobacterial adaptation to different stressful conditions, also by modulation of cell growth and division.

6.3 RNase E and HupB are molecular partners and respond jointly to stressful conditions

Our mass spectrometry analysis of proteins pulled down with RNase E revealed significant enrichment (>3 fold) of the nucleoid-associated protein HupB, which also had the highest relative stoichiometry value among all identified proteins (**Figures 21A, S2C** and **Supplementary table 4**). HupB is a widely conserved small histone-like protein that plays a major structural role in determining the nucleoid topology in both Gram-negative and -positive bacteria, including mycobacteria (Hołówka et al., 2017; Kumar et al., 2010; Oberto et al., 2009). HupB can bind both double-stranded and single-stranded DNA and has higher propensity for curved and AT-rich DNA, which is usually present at the origins of replication (*oriC*) and in regulatory regions (Dillon and Dorman, 2010; Hołówka et al., 2017). Indeed, modulation of chromosomal folding not only assists DNA replication and repair but also contributes to gene expression (Surovtsev and Jacobs-Wagner, 2018).

To investigate the possible association between HupB and RNase E in *M. smegmatis*, we generated a translational reporter strain of HupB, by inserting the *hupB* locus fused in frame with

mCitrine fluorescent marker into the Tweety phage attachment site (Pham et al., 2007), see also **Materials and Methods**. The *hupB* merodiploid showed no growth defects *in vitro* (**Figure S3A**), and the *hupB* copy fused to *mCitrine* had expression levels comparable to its native counterpart (**Figure S3B**). In order to confirm the molecular association between RNase E and HupB, we performed a reverse immunoprecipitation assay in the P*hupB* - mCitrine merodiploid strain co-transformed with the *rne*-overexpressing plasmid (*rne_oe*), using an antibody specific against the mCitrine C-terminal tag, see also **Materials and Methods**. By western blot assay, we were able to confirm the presence of the RNase E in the HupB-mCitrine immunoprecipitated fraction (**Figure S3C**).

We also analyzed the P*hupB* – mCitrine_*rne_oe* strain by single-cell snapshot imaging, after induction of *rne* expression for 6 and 24 hours, corresponding to exponential and stationary growth-phase, respectively (**Figure S3D**). We measured a moderate to marked decrease of single-cell length (**Figure S3E**), which was more pronounce after 24 hours of *rne* induction, consistent with our bulk growth kinetics results (**Figure S1B**). Moreover, we observed a significant increase of HupB fluorescence after 24 hours of *rne* overexpression (**Figure S3F**). To further verify the relationship between the two genes, we co-transformed the P*hupB* - mCitrine strain with the *rne*-silencing CRISPRi-dCas9 system (*rne_si*) (**Figure S3G**). We not only found a significant decrease of cell length 24 hours after *rne* silencing (**Figures S3H**), consistent with our bulk growth kinetics results (**Figures S1B**), but we also observed a significant and progressive decrease of HupB fluorescence shortly after *rne* depletion (**Figures S3I**). Collectively these results confirmed that variations in *rne* expression levels affect cell growth homeostasis and HupB levels, implying that *rne* and *hupB* are subject to a concerted regulation.

To further examine the association between HupB and RNase E in *M. smegmatis*, we generated the dual-merodiploid reporter strain P*rne* – mCherry_P*hupB* - mCitrine, which allowed us to simultaneously monitor the expression of both proteins in living cells (**Figures S1E, S3A** and **S3B**), see also **Materials and Methods**. We carried out snapshot imaging and quantitative analysis of individual cells in exponential growth-phase or after short treatment (two generation times) with molecules that impair different processes essential for cellular life. In particular, we used the DNA crosslinking agent mitomycin C (MMC, 2X-MIC) to impair replication; rifampicin (RIF, 2X-MIC), frontline antitubercular drug that blocks transcription; the specific RNase E inhibitor M5 (1X-MIC) (Kime et al., 2015); chloramphenicol (CAP, 2X-MIC) to inhibit translation; a specific FtsZ inhibitor (Hogan et al., 2018) to block cell division (C109, 0.5X-MIC) and isoniazid (INH, 2X-MIC), frontline drug that affects cell wall biosynthesis (**Figure 22A**).

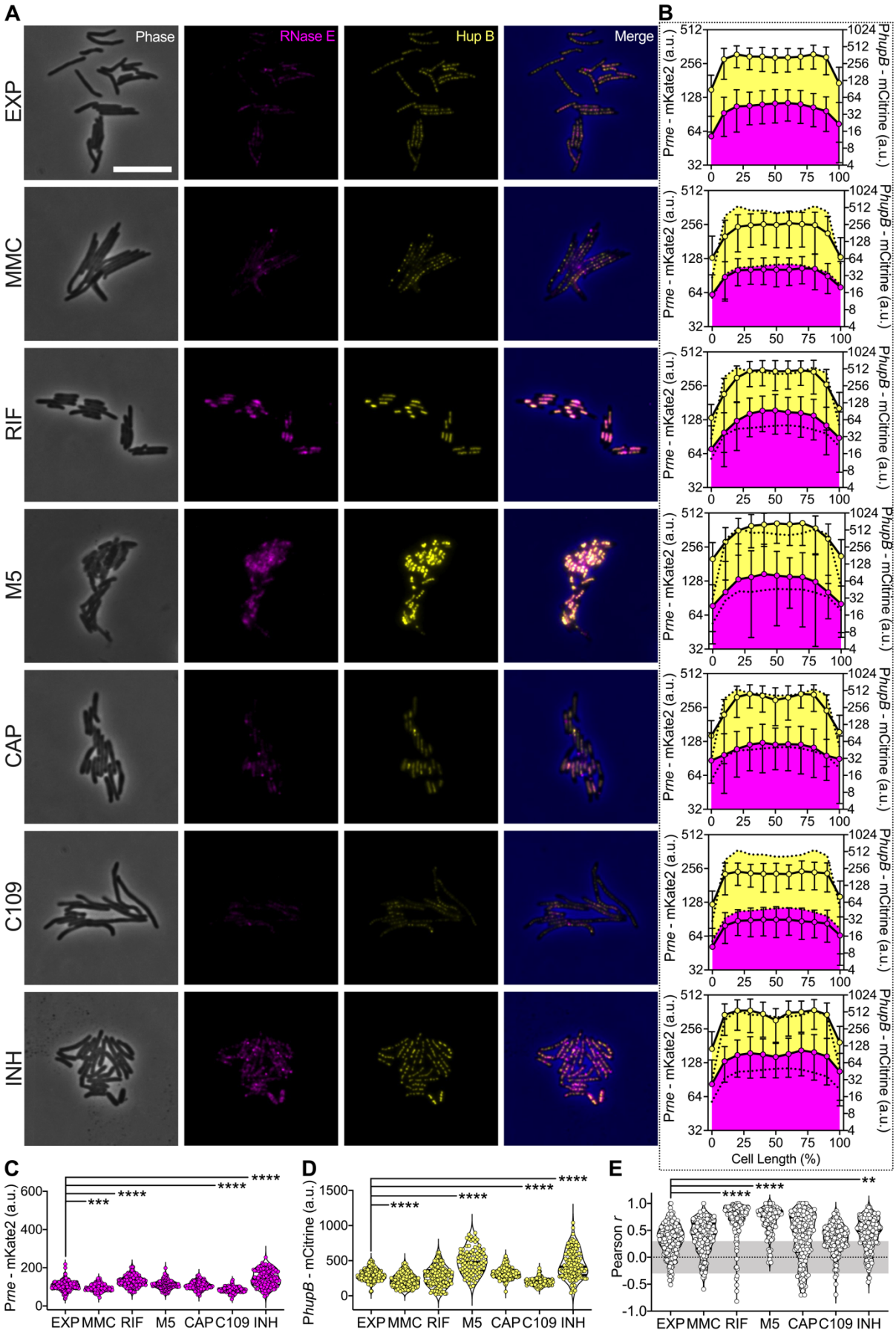
A
Phase
RNase E
Hup B
Merge
EXP
MMC
RIF
M5
CAP
C109
INH
B
Prne - mKate2 (a.u.)
PhupB - mCitrine (a.u.)
Cell Length (%)
C
Prne - mKate2 (a.u.)
D
PhupB - mCitrine (a.u.)
E
Pearson r
EXP MMC RIF M5 CAP C109 INH

Figure 22. Single-cell analysis of Prne - mKate2 and PhupB - mCitrine reveals their molecular association and joint response to stressful conditions

(A) *Representative snapshot images of Prne - mKate2_PhupB - mCitrine dual reporter in exponential growth-phase (EXP), and following 6 hours of exposure to MMC (200 ng/ml), RIF (20 μg/ml), M5 (2.5 mM), CAP (16 μg/ml), C109 (16 μg/ml) and INH (20 μg/ml). Phase contrast (gray), Prne - mKate2 (magenta), and PhupB - mCitrine (yellow) fluorescence and merged panels are shown. Fluorescence images are scaled to the brightest frame of each channel. Scale bar 10 μm.*

(B) *Single-cell fluorescence profiles as a function of the percent of cell length of the dual reporter Prne - mKate2 (magenta, left y-axes) and PhupB – mCitrine (yellow, right y-axes). Solid black lines represent mean values ± SD for each condition indicated in (A). Dotted lines represent mean values ± SD for exponential phase cells (EXP). The data shown are from 2 independent experiments (n = 150 per condition).*

(C–E) *Snapshot analysis of the dual Prne - mKate2_PhupB - mCitrine reporter in the conditions indicated in (A). Single-cell red (C) and yellow (D) fluorescence, and single-cell fluorescence correlation between the two reporters segmented over the cell length (E). Violin plots show all individual cells with medium smoothing (150 < n < 299). Asterisks denote significance by one-way ANOVA followed by Dunnett's multiple comparison test: ***P = 0.0001; ****P < 0.0001. Gray shading indicates non-significant Pearson r correlation values. The data shown are from 2 independent experiments.*

To accurately compare the cellular localization of the two fusion proteins, we analyzed their fluorescence along the major axis of individual cells and generated submicrometric maps of fluorescence as a function of cell length (**Figures S3J** and **22B**). Looking at cells in exponential growth phase, we noticed a longitudinal distribution of HupB along the nucleoid region typical of rod-shaped bacteria , resembling a string of pearls (**Figure 22A**), similar to our Lsr2 fluorescent reporter (**Figure S2L**) and confirming previous observation with HupB fluorescent fusion (Hołówka et al., 2017). Moreover, the patchy fluorescence and fluorescent foci of RNase E partly overlapped with HupB along the same nucleoid conformation (**Figure 22B-D**), corroborated by a positive correlation between the two markers at the single-cell level (**Figure 22E**).

Treatment with MMC blocks cell division following DNA damage (Manina et al., 2019), and causes cell elongation similar to inhibition of FtsZ with C190 (Hogan et al., 2018). We confirmed that both MMC and C109 caused a significant increase in cell length compared to untreated cells (**Figure S3K**), concurrent with a decrease in fluorescence of both RNase E and HupB but with no apparent relocalization (**Figures 22A–22D**), compatible with a stalled replication fork and slowdown in gene expression. In contrast, treatment with all other molecules caused a substantial relocalization of the two proteins, suggestive of condensation of the nucleoid with different morphologies (**Figure 22A**).

Indeed, cell exposure to different macromolecular synthesis inhibitors was shown to have considerable effects on chromosomal compaction in both model microorganisms and mycobacteria (Bayas et al., 2018; Cabrera et al., 2009; Scutigliani et al., 2018; Shechter et al., 2013;

Weng et al., 2019). In particular, RNA polymerase inhibition resulted in tight and homogeneous compaction of both RNase E and HupB fluorescence towards the center of the cell (**Figures 22A** and **22B**), compatible with nucleoid condensation and stalled replication and transcription. RIF exposure also caused a significant increase in fluorescence (**Figures 22C** and **22D**), confirmed by a strong positive correlation between the two markers at the single-cell level (**Figure 22E**). In contrast, the relocalization of fluorescence was less pronounced and homogeneous in cells subjected to the RNase E inhibitor, but caused a significant increase in HupB fluorescence (**Figure 22D**), suggesting a compensatory mechanism between RNase E and HupB. Lastly, inhibition of translation with CAP treatment and inhibition of cell wall biosynthesis with INH caused fluorescence condensation of both markers, with a conformation compatible with the presence of multiple copies of the chromosome (Santi et al., 2013), as if the replication process had been interrupted (**Figures 22A** and **22B**). While CAP treatment did not cause changes in the levels of fluorescence, INH treatment caused a massive induction of both RNase E and HupB and a robust positive correlation at the single cell level (**Figures 22C–E**). Surprisingly, among the different mechanisms of inhibition of cell division tested, only the inhibition of mycolic acid synthesis had a substantial effect on the relocalization and expression of both RNase E and HupB, entailing a possible association with the cellular response to INH.

Overall, our results confirmed the molecular interplay between RNase E and HupB, their association at the nucleoid level, and proved their concerted regulation under both homeostatic and stressful conditions. We showed that inhibition of fundamental cellular processes, mainly of transcription, RNA degradation and cell wall biosynthesis had a major effect on both RNase E and HupB, which is consistent with the tight interdependence between the nucleoid architecture and regulation of gene expression. This ultimately led us to hypothesize that the interaction between RNase E and HupB might be crucial for mycobacterial response to stressful conditions.

6.4 Dynamic expression of RNase E in *M. tuberculosis* positively correlates with HupB and affects the fate of individual cells stresses with isoniazid

Having discovered the molecular relationship between RNase E and HupB in the fast-growing tuberculosis model *M. smegmatis*, and that these two proteins act in concert in both optimal growth and stressful conditions to maintain the cellular homeostasis, we asked whether the same mechanism applied to the tubercular pathogen and with what functional consequences for stress tolerance.

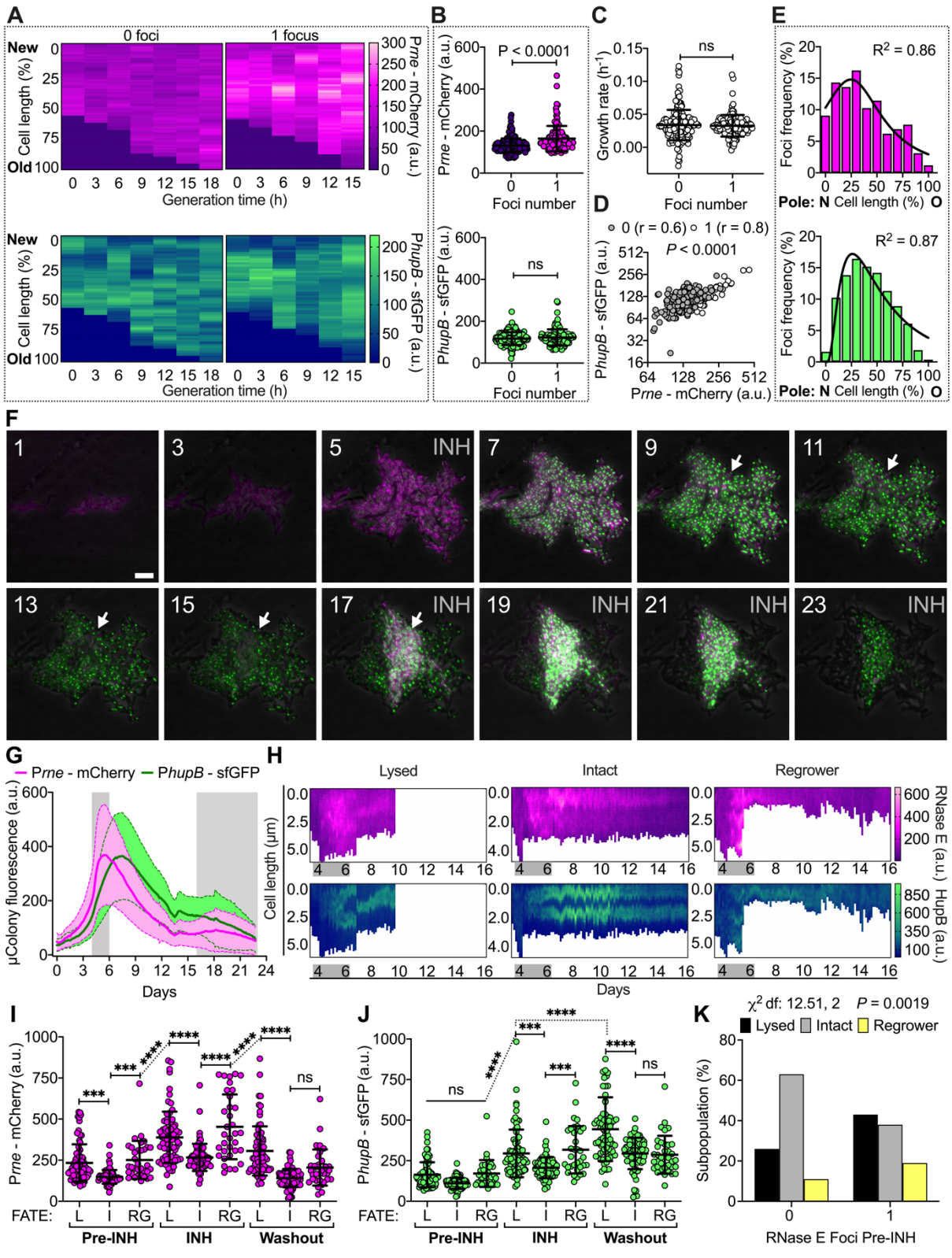
A
0 foci
1 focus
New
Old
Cell length (%)
Generation time (h)
Prne - mCherry (a.u.)
PhupB - sfGFP (a.u.)
B
P < 0.0001
ns
Foci number
C
Growth rate (h-1)
D
0 (r = 0.6) 1 (r = 0.8)
P < 0.0001
E
R2 = 0.86
R2 = 0.87
Foci frequency (%)
Pole: N Cell length (%) O
F
INH
G
Prne - mCherry
PhupB - sfGFP
µColony fluorescence (a.u.)
Days
H
Lysed
Intact
Regrower
Cell length (µm)
RNase E (a.u.)
HupB (a.u.)
I
J
FATE:
L
I
RG
Pre-INH
INH
Washout
K
χ2 df: 12.51, 2 P = 0.0019
Subpopulation (%)
RNase E Foci Pre-INH

Figure 23. ***M. tuberculosis Prne-mCherry and PhupB-sfGFP reporters are correlated both during optimal growth and isoniazid treatment***

(A) *Representative heatmaps of single-cell Prne - mCherry (upper panels) and PhupB - sfGFP (bottom panels) fluorescence, expressed as a function of the single-cell generation time (x-axes) and length expressed in percentage (y-axes). One cell with no RNase E localization events (left panel) and one with one localization event (right panel) are shown. RNase E and HupB localization events were identified if one or more cell segments had fluorescence values equal to or greater than 150 (a.u.) for mCherry and 120 (a.u.) for sfGFP after subtraction of the minimum cell fluorescence (See also Materials and Methods).*

(B) *Single-cell Prne - mCherry (upper panel) and PhupB - sfGFP (lower panel) fluorescence averaged over the lifetime of the cell in subpopulations segregated by the absence (0) or presence (1) of RNase E foci. Black lines indicate mean ± SD (n = 299). Significance by unpaired t-test: ns, not significant. The data are shown from two independent experiments.*

(C) *Single-cell growth rate of the two subpopulations identified in (C) (see also **Figure S4B**). Black lines indicate mean ± SD (120 < n < 179). Significance by unpaired t-test: ns, not significant.*

(D) *Single-cell Pearson r correlation between Prne - mCherry and PhupB - sfGFP fluorescence averaged over the lifetime cells having none (white circles) or one (gray circles) RNase E focus. The data shown are from 2 independent experiments (120 < n < 179).*

(E) *Histograms showing the distribution of the position of Prne - mCherry (upper panel) and PhupB - sfGFP (bottom panel) foci expressed as a function of cell length expressed in percentage. Black lines indicate fitting of the data with a Lorentzian and a lognormal function, respectively. Old (O) and new (N) cell poles are marked. RNase E and HupB localization events mainly occur towards the new cell pole.*

(F) *Representative time-lapse image series of the M. tuberculosis Prne - mCherry_PhupB - sfGFP dual reporter in exponential phase (see also Materials and Methods). Fresh 7H9 medium is unlabeled and INH exposure (250 ng/ml, 10X-MIC) is indicated. Phase contrast (gray), mCherry (magenta), and sfGFP (green) fluorescence are merged. Fluorescence images of each channel are scaled to the brightest frame. Cells were imaged at 3-hour intervals, and numbers represent hours. The arrows track a regrowing cell. Scale bar 5 µm. See also Movie 4 (https://www.dropbox.com/s/fomrl8vluq7lyun/Movie4.avi?dl=0)*

(G) *Microcolony Prne - mCherry (magenta) and PhupB - sfGFP (green) fluorescence, measured from a region of interest of constant size through the whole time-lapse image sequence. Fresh 7H9 medium corresponds to white background and INH exposure is indicated by gray shadings. Magenta and green continuous lines indicate mean fluorescence; magenta and green shadings represent ±SD (n = 26 microcolonies). Data from two independent replicates.*

(H) *Representative single-cell heatmaps of Prne - mCherry fluorescence (upper panels) and PhupB - sfGFP (bottom panels), expressed as a function of experimental time (x-axes) and cell length (y-axes). Cells with three different fates are shown. First INH exposure (gray shadings) and drug washout (unlabeled) are shown.*

(I, J) *Comparison of single-cell Prne - mCherry (I) and PhupB - sfGFP (J) fluorescence before (Pre-INH), during (INH) and after INH exposure (Washout) of cells that lysed (L), remained intact (I) and regrew (RG) (34 < n < 76). Black lines indicate means ± SD. Data are shown merging two independent experiments. Asterisks denote significance by one-way ANOVA followed by Tukey's multiple comparison test: ns, not significant; ***P < 0.0005; ****P < 0.0001.*

(K) *Single-cell fate as a function of the absence (0) or presence (1) of RNase E foci over the lifetime of the cell before INH exposure. Significance by Chi-square test of independence for cells that lysed (n = 57), remained intact (n = 77), and regrew (n = 24) Cells that either dye by lysis or regrow are more likely to form foci before INH exposure, in contrast, cells that remain intact are less likely to form foci.*

To this aim, we generated a dual-fluorescent reporter of both RNase E and HupB translation in *M. tuberculosis* Erdman strain. We first we duplicated the *rne* locus (*rv2444c* including a 330-ntd region upstream the translation start site), fused in frame with the *mCherry* fluorescent marker, into the L5 phage integration site (Peña et al., 1996). Then we duplicated the *hupB* locus (*rv2986c* including the whole intergenic region upstream the translation start site), fused in frame with the *sfgfp* fluorescent marker, into the Tweety phage integration site (Pham et al., 2007) (see also **Materials and Methods**). The reporter strain, referred to as P*rne* - mCherry_P*hupB* - sfGFP showed no fitness defects (**Figures S4A**).

To visualize the single-cell dynamics of RNase E and HupB in *M. tuberculosis* during optimal growth conditions, we carried out time-lapse microscopy imaging of exponential phase cells grown inside our microfluidic device (Manina et al., 2019), continuously fed with fresh 7H9 medium (**Movie 3**, https://www.dropbox.com/s/lrwf5o45g04yra3/Movie3.avi?dl=0). We generated submicrometric maps of fluorescence as a function of cell length for individual bacilli, aiming to characterize both patterns of expression during the entire generation time of the cells from birth to division (**Figure 23A**). Consistent with our findings in *M. smegmatis*, also *M. tuberculosis* exhibited low levels of RNase E background fluorescence and brighter localization foci in about 40 percent of the cells, but with an average fluorescence level reduced by about half compared to the non-pathogenic counterpart. This is also in agreement with the fact that native expression levels of mycobacterial promoters are generally lower in slow-growing than in fast-growing mycobacteria (Das Gupta et al., 1993), and consistent with our former findings related to the dynamics of *recA* expression in mycobacteria (Manina et al., 2019). In the exponential growth-phase *M. tuberculosis* expressed HupB at relatively low levels but with a distinctive string-of-pearls pattern, as with *M. smegmatis* (**Figures 23A** and **22A**). Based on the formation of RNase E foci we were able to identify two subpopulations that had significantly different levels of RNase E fluorescence and relatively homogeneous levels of HupB fluorescence (**Figures 23B** and **S4B**) and that, unlike *M. smegmatis*, showed no difference in growth rate or size at the single-cell level (**Figures 23C, S4C, 20E** and **20F**). RNase E and HupB were positively correlated between the two subpopulations, even more robustly in case of cells forming RNase E foci (**Figure 23D**). This was consistent with the fact that the highest localization levels for both RNase E and HupB were recorded towards the new pole of the cell, similar to *M. smegmatis* (**Figures 23E** and **20G**), and reminiscent of the replisome dynamics (Santi and McKinney, 2015).

Given the growing number of evidences suggesting the relevance of stochastic phenotypic variation in population fitness dynamics in both model organisms and mycobacteria (Bakkeren et al., 2020; Cadena et al., 2018; Dhar et al., 2016; Levien et al., 2020) we decided to examine the functional significance of the cell-to-cell heterogeneous expression of RNase E, in conjunction with HupB, during treatment with the frontline antitubercular INH. It is worth noting that phenotypic variation in the expression of KatG, an enzyme that activates the prodrug INH into its active form, was reported to contribute to phenotypic INH tolerance in *M. smegmatis* (Wakamoto et al., 2013). Furthermore, both RNase E and HupB can affect KatG expression levels with implications for INH activity (Niki et al., 2012; Sakatos et al., 2018; Taverniti et al., 2011; Whiteford et al., 2011).

To assess the role of RNase E and HupB on INH tolerance in single *M. tuberculosis* cells, we performed a multi-phase time-lapse microscopy experiment (**Figure 23F; Movie 4,** https://www.dropbox.com/s/fomrl8vluq7lyun/Movie4.avi?dl=0). We first grew exponential P*rne* - mCherry_P*hupB* - sfGFP bacilli inside our microfluidic device for 4 days with fresh 7H9 medium; next we treated the bacilli the with high concentration of INH (10X-MIC) for two days, and then we washed out the drug for 10 days, to monitor individual cells' responses during the recovery phase. Finally, we subjected the surviving bacilli to INH (10X-MIC) a second time, aiming to assess whether an inheritable phenotype of resistance had arisen or whether the surviving bacilli were still sensitive to the drug.

From an initial evaluation of the global fluorescence at the microcolony level, we measured a substantial increase in fluorescence of both markers following INH exposure and a strong positive correlation throughout the experiment, consistent with *M. smegmatis* snapshot analysis (**Figures 23G, S4D** and **Figure 22**). However, the fluorescence peak was reached first by RNase E and after a period of less than two days (about two replication times) by HupB, indicating a leading role of RNase E towards its molecular partner. Then we extended the analysis at the level of individual cells, to determine their fate and record their parameters at critical phases of the experiment. In particular, we distinguished three main fates following the first INH exposure, namely, cells that lysed, cells that remained intact but never resumed growth, and cells that survived and resumed growth and division during drug washout (**Figure 23H**). We confirmed the positive correlation between the two markers also in single cells, especially during pre-treatment and INH treatment. This correlation was more robust in cells that experienced lysis or survived rather than in cells that remained intact (**Figure S4E**).

Surprisingly, we found that both cells that experienced lysis and cells that survived had significantly higher RNase E levels compared with cells that remained intact after INH exposure. We observed a similar fluorescence trends for HupB, albeit not statistically significant (**Figures 23I and 23J**). Indeed, by quantifying the RNase E foci just before INH exposure and correlating them with cellular fate, we found that cells that remained intact were more likely not to form foci

compared to cells that died or survived, which had instead detectable RNase E foci prior to INH exposure (**Figure 23K**). Likewise, we observed that the induction of both fluorescent markers was significantly stronger in cells that lysed and survived compared with cells that remained intact, which weakly responded to the drug. Furthermore, only cells that experienced lysis maintained very high induction of both RNase E and HupB even after INH washout, unlike cells that survived (**Figures 23I and 23J**).

We also wondered what was the viability state of cells that remained intact but never grew back during INH washout. In contrast to survivors and in support of the fact that intact cells were likely dead, we did not observe any fluorescence induction during the second INH exposure (**Figures S4F and S4G**). Indeed, intact cells experienced a progressive decrease of fluorescence during the second phase of treatment, which was suggestive of cell mortality (**Figures S4F and S4G**). In addition, both cells dead by lysis and those that remained intact experienced a size decrease that was never restored during INH washout (**Figures S4H**). In contrast, surviving cells maintained a more homogeneous cell size throughout the experiment, indicating that adequate levels of RNase E contribute to cell-size control and maintenance of cellular homeostasis during INH stress.

Collectively these results indicate the interplay between RNase E and HupB also in *M. tuberculosis* both during normal growth and drug treatment. We found that loss of RNase E regulation is detrimental for *M. tuberculosis* survival during INH treatment. Lastly, these results suggest that pre-existing variation in RNase E and HupB may have implications for the response of single *M. tuberculosis* cells to INH, and that faulty regulation and coordination between RNase E and HupB may adversely affect the ability of *M. tuberculosis* to respond to drugs.

6.5 RNase E and HupB jointly assists *M. tuberculosis* survival during both isoniazid treatment and infection

To further verify the co-regulation between RNase E and HupB, we used the inducible CRISPRi-based transcriptional repression method to silence the *rne* expression (Rock et al., 2017). In particular we generated a vector carrying an inducible small guide RNA (sgRNA) designed against the *rv2444c* gene and an inducible dCas9 (see also **Materials and Methods)**, and integrated it into the L5 phage attachment site of the P*hupB* - sfGFP *M. tuberculosis* reporter, referred to as *si-rne* strain. As a control, we integrated the empty vector into P*hupB* - sfGFP, referred to as *wt-rne* strain. Following anhydrotetracycline (ATC) induction we were able to measure a growth-rate decrease, which was more pronounced following 7 days of *rne* silencing, in the *si-rne* strain compared to the *wt_rne* strain (**Figure S5A**). Importantly, we also measured a

significant decrease of both *rne* and *hupB* transcripts after 7 days of *rne* silencing, implying an interdependence of *hupB* from *rne* also at the transcriptional level (**Figure S5B**). After *rne* silencing we also found a significant decrease of *infA* transcripts, consistent with our proteomic findings (**Figure 21**) and with the role of RNase E in rRNA processing (Taverniti et al., 2011). Furthermore, *rne* silencing caused a significant increase of *furA*, encoding a putative KatG regulator (Taverniti et al., 2011; Zahrt et al., 2001), and a moderate increase of *katG* transcripts (**Figure S5B**), consistent with our proteomic results, in that KatG was found to be lowered in the RNase E fraction of the *rne_oe* strain (**Figure 21A**).

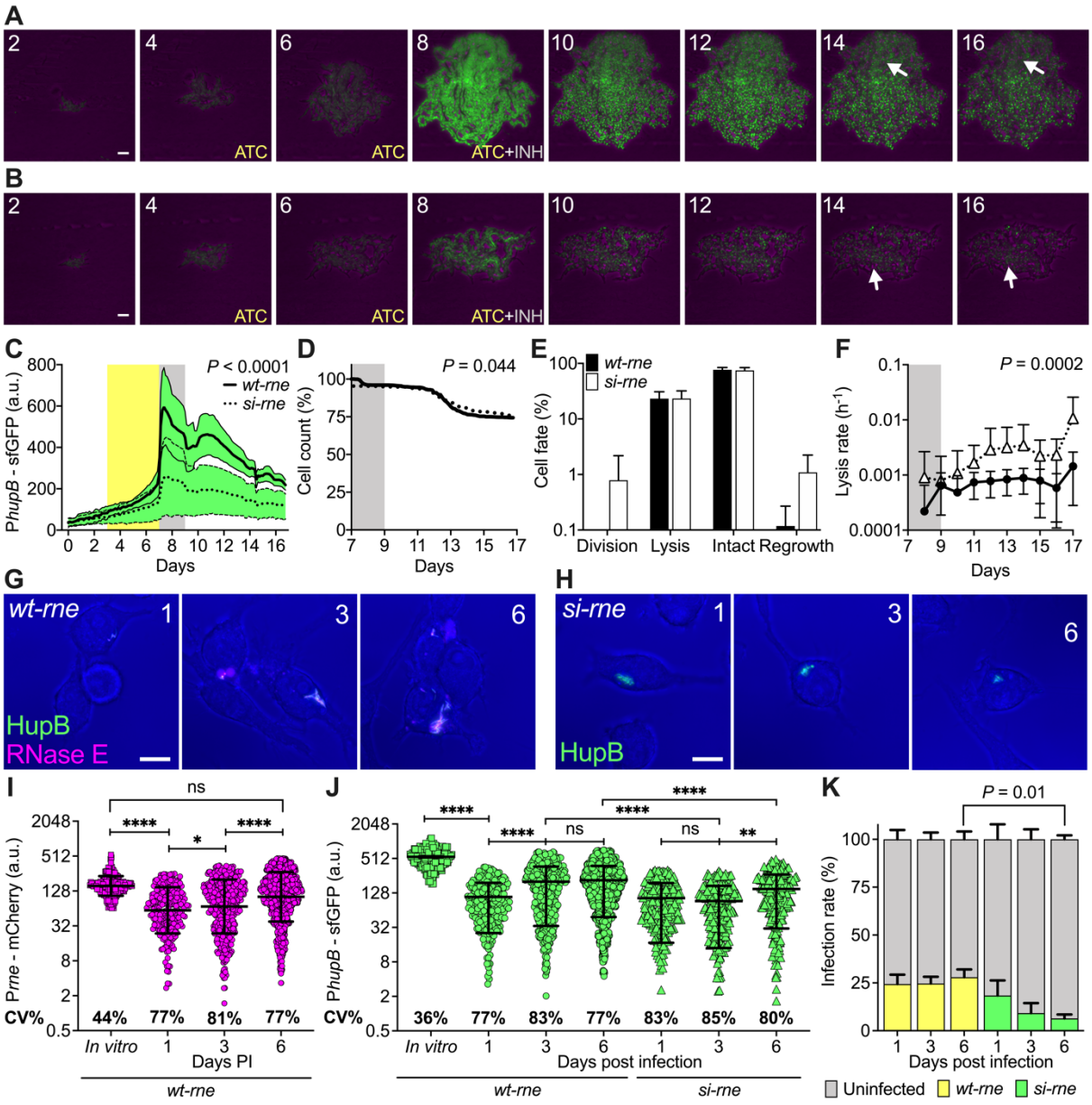

Figure 24. ***Silencing rne decreases hupB expression, and impairs M. tuberculosis survival during isoniazid treatment and macrophage infection***

(A, B) *Representative time-lapse image series of the PhupB - sfGFP reporter (wt-rne) carrying the pLJR965 vector as a control (A), or carrying the ATC-inducible CRISPRi-dCas9 system to silence rv2444c (si-rne, B) (see also Materials and Methods). Fresh 7H9 medium is unlabeled, ATC 100 ng/ml and INH 250 ng/ml are indicated. Phase-contrast (magenta) and sfGFP fluorescence (green) are merged. Fluorescence images of each channel are scaled to the brightest frame. Cells were imaged at 3-hour intervals, and numbers represent days. White arrows track cells that resumed growth during the washout phase. Scale bar 5 µm. See also Movie 5 (https://www.dropbox.com/s/rba96i3p33lcm5b/Movie5.avi?dl=0).*

(C) *Microcolony PhupB - sfGFP fluorescence measured from a region of interest of constant size through the whole time-lapse image sequence, in the wt-rne strain (solid line, mean value) and in the si-rne strain (dotted line, mean value). Green shadings represent the ±SD (10 < n < 12 microcolonies). Data are from two independent replicates. Significance by unpaired t-test.*

(D) *Number of intact cells expressed in percentage following ATC and INH exposure (gray shading) in wt-rne (solid line) and si-rne (dotted line). Data are from 2 independent experiments (3532 < n < 5814). Significance by unpaired t-test.*

(E) *Number of cells with a given fate expressed in percentage in wt-rne (black bars) and si-rne (white bars), scored as in (D). Cells that divided (8 < n < 16), died by lysis (1016 < n < 2016), remained intact (3336 < n < 5806), or regrew (8 < n < 81). Data are from 2 independent experiments.*

(F) *Rate of cell lysis following ATC and INH exposure (gray shading) in wt-rne (black line and circles) and si-rne (dotted line and white triangles) strains. The data shown are from 2 independent experiments (10 < n < 12 microcolonies) . Significance by 2-way ANOVA.*

(G, H) *Representative snapshots images of RAW264.7 macrophages infected with either Prne - mCherry_PhupB - sfGFP (wt-rne) (G) or PhupB - sfGFP_si-rne (si-rne) (H) reporter strains in the presence of ATC 100 ng/ml (See also **Figures S5C** and **S5D**). Each image is derived from the projection of a stack of 6 snapshots taken on the same field of view sequentially at 1-µm z-step from each other, using the maximum intensity method (SoftWorx). Bright field (blue) Prne-mCherry (magenta) and PhupB-sfGFP (green) fluorescence are merged (G); bright field (blue) and PhupB-sfGFP (green) fluorescence are merged (H). Numbers indicate days. Scale bars, 10 µm.*

(I) *Prne - mCherry fluorescence of wt-rne bacilli grown in vitro (square symbols) compared to intracellular bacilli and aggregates (circles) at 1, 3- and 6-days post infections (PI). Black lines indicate mean ± SD (163 < n < 1259). Coefficient of fluorescence variation expressed in percentage (CV%) is indicated. Asterisks denote significant difference by one-way ANOVA followed by Tukey's multiple comparisons test: *P = 0.014, ****P < 0.0001. Data are shown from three independent experiments.*

(J) *PhupB - sfGFP fluorescence of wt-rne bacilli grown in vitro (square symbols) compared to intracellular bacilli or aggregates of wt-rne strain (circles) and si-rne strain (triangles) at 1, 3- and 6 days PI. ATC 100 ng/ml was added at the beginning of infection to induce rne silencing (see also Materials and Methods). Black lines indicate mean ± SD (213 ≤ n ≤ 1259). CV% is indicated. Asterisks denote significance by one-way ANOVA followed by Tukey's multiple comparison test: ns = not significant; **P = 0.0017; ****P < 0.0001.*

(K) *Infection rate expressed as the percentage of infected macrophages with Prne - mCherry_PhupB - sfGFP (yellow bars) and si-rne (green bars) strains at 1, 3- and 6-days PI. ATC 100 ng/ml was added*

at the beginning of infection (see also Materials and Methods). Uninfected macrophages are indicated in gray. Data are shown merging three independent experiments. Significance by 2-way ANOVA, followed by Sidak's multiple comparisons test.

We took advantage of our ability to silence the expression of *rne* in the P*hupB* - sfGFP reporter, to gain better understanding of the implication of *rne* and *hupB* in *M. tuberculosis* response to INH treatment. We performed multi-phasic time-lapse microfluidic microscopy and single-cell analysis of both the *wt-rne* and *si-rne* strains (**Figure 24A** and **24B, Movie 5,** https://www.dropbox.com/s/rba96i3p33lcm5b/Movie5.avi?dl=0). We first pre-grew the strains in our microfluidic device with fresh 7H9 medium for three days, we added ATC for the four following days, to induce *rne* silencing, next we added INH (10X-MIC) together with the inducer for two days, and finally we eliminated both ATC and INH, in order to monitor the single-cell behavior during the recovery phase for more than one week. As expected, by measuring the total HupB fluorescence at the microcolony level following INH exposure, the *wt-rne* strain responded with about 20-fold fluorescence induction, which was more than 3-fold lower in the *si-rne* strain (**Figure 24C**).

To increase the resolution of our analysis, we quantified the number of cells during the whole time-lapse microscopy experiment, counting the events of cell division, death by lysis, as well as the number of cells that remained intact and never resumed growth, and those that restarted growing during the recovery phase. Although the total quantification of different cell fates did not show significant differences between the two strains (**Figures 24D** and **24E**), we were able to assess a significantly faster lysis rate in the *si-rne* strain compared to the *wt-rne* (**Figure 24F**), confirming that the lack of normal levels of functional RNase E is harmful to cells subject to a drug that inhibits cell wall biosynthesis, and possibly to the maintenance of balanced growth and division.

Given the essentiality of HupB for *M. tuberculosis* intracellular growth (Pandey et al., 2014), we decided to investigate the single-cell behavior of our P*rne* - mCherry_P*hupB* – sfGFP reporter, here referred to as *wt-rne*, and of the *si-rne* strain inside macrophages up to 6 days post infection (**Figures 24G, 24H, S5C** and **S5D**). Consistent with our findings in both *M. smegmatis* and *M. tuberculosis in vitro* (**Figures 22** and **23**), we measured a strong positive correlation between RNase E and HupB fluorescence at the single-cell and aggregate level both in the early and late stages of infection (**Figure S5E**), implying a concerted action of the two molecular partners also within macrophages. In particular, we observed a decrease of both HupB and RNase E fluorescence at day 1 post infection as compared with exponential-phase bacilli cultured *in vitro* and used to infect cells (**Figures 24I** and **24J**). However, as the infection progressed, we measured a significant and progressive increase of RNase E fluorescence and a significant increase of HupB

fluorescence on the third day of infection. Conversely, HupB fluorescence did not increase in the *si-rne* strain following induction of *rne* silencing at the beginning of infection, suggesting that RNase E acts as a HupB regulator, and that they are mainly implicated during late stage of macrophage infection (**Figures 24I** and **24J**). Interestingly, we also measured a doubling of the coefficient of variation of fluorescence for both HupB and RNase E, indicating an increase in phenotypic heterogeneity of *M. tuberculosis* in the host, consistent previous findings (Cadena et al., 2018; Dhar et al., 2016; Manina et al., 2015).

Lastly, we calculated a difference in macrophage infection rate between the *wt-rne* and the *si-rne* strains, particularly pronounced at late stage of the infection (**Figure 24K**), although cells that remained infected had similar characteristics regardless of the infecting strain (**Figure S5F**). Indeed, individual macrophages infected with *si-rne* strain were able to clear the infection more efficiently, implying that the coordinated activity of RNase E and HupB is crucial for *M. tuberculosis* intracellular survival.

Collectively these results not only confirm the concerted regulation of RNase E and HupB both at the RNA and protein level and their molecular association in the tubercular pathogen, but also demonstrate the contribution of these two factors in *M. tuberculosis* survival, particularly with regard to INH tolerance and intracellular persistence (**Figures 24F, 24K** and **S5G**).

Discussion

Gram-positive and -negative bacteria own diverse RNA degrading machineries, depending on the RNases present in the microorganism and on their interaction with other molecular partners (Durand et al., 2015). One of the most significant examples is the multi-enzymatic RNA degradosome complex, initially discovered in *E. coli* (Mackie, 2013). The RNase E is the core enzyme of the RNA degradosome complex, it is an essential enzyme, tightly regulated at the RNA and protein level, as well as subcellularly compartmentalized, and its deregulation is detrimental to cells (Jain and Belasco, 1995; Tejada-Arranz et al., 2020a). The combined catalytic activity of all the components of the RNA degradosome is crucial for efficient post-transcriptional regulation of gene expression in different bacterial species, where the initial endonucleolytic cleavage of the RNase E on its RNA target can be considered as the rate-limiting step (Belasco, 2010). Gram-positive bacteria lack an RNase E ortholog, but they are still capable to assemble an RNA degradosome-like complex, using as core enzyme either the RNase J or the RNase Y, which initiate the degradation of transcripts, similar to the RNase E (Cho, 2017; Tejada-Arranz et al., 2020, Galtier, et al., 2020). *M. tuberculosis* and the non-pathogenic tuberculosis model *M. smegmatis* own orthologs of both RNase E and RNase J but lack an RNase Y ortholog. However, the function and interaction of RNase E and RNase J under both homeostatic and stressful conditions, and how mycobacteria assemble an RNA degradosome complex are still open questions. A recent study, aimed to clarify the mycobacterial proteome associated with RNA, proposed that both RNase J and RNase E participate in the possible assembly of two non-mutually exclusive RNA degradosome complexes, which might coexist. Alternatively, RNase E, RNase J, PNPase, and RhlE might form a single complex that structurally excludes a direct interaction between RNase E and RNase J (Płociński et al., 2019).

Here, we focus on the mycobacterial RNase E both at the bulk- and single-cell level, probe its molecular interactions and cellular dynamics, and investigate its contribution to single-cell fitness under drug- and host-related stressful conditions.

By analyzing the RNase E-associated proteome of *M. smegmatis*, we demonstrated that the RNase E interacts not only with the key components of the canonical RNA degradosome complex, such as the PNPase ortholog GpsI and the DEAD-box helicase DeaD, which is consistent with recent findings (Płociński et al., 2019), but also with other accessory enzymes, implicated in RNA binding and RNA recycling, that may contribute to the function and regulation of the RNA degradosome. The RNase E degradosome complex typically contains an endonuclease, an

exoribonuclease, a DEAD-box helicase, and a metabolic enzyme (Bandyra et al., 2013). RNase E interactions with a PNPase-like enzyme and a DEAD-box helicase suggest that mycobacteria might primarily assemble an RNase E-based RNA degradosome complex. Although the RNA degradosome typically contains only one DEAD-box helicase, which helps unwinding or remodeling possible secondary structure in the RNA target and facilitating the endonucleolytic activity of the RNase E (Khemici et al., 2004), it was shown in both *E. coli* and *C. crescentus* that multiple helicases can participate in the activity of the RNA degradosome (Aguirre et al., 2017; Khemici et al., 2004; Redder et al., 2015). Consistent with these evidences, our functional analysis of the RNase E pull-down pointed out the presence of multiple DEAD-box ATP-dependent helicases (Redder et al., 2015), such as RhlE, DeaD, HrpA, and HelY. The identification of multiple DEAD-box helicases might suggest higher plasticity of the mycobacterial RNA degradosome. Owning a highly versatile RNA degradosome could promote mycobacterial adaptation to environmental fluctuations or to the host environment. For instance, in *C. crescentus* RhlE can substitute RhlB when bacteria are subject to cold-shock stress (Aguirre et al., 2017). Moreover, HrpA is an RNA helicase known to be essential for tick transmission to mammalian cells of *Borrelia burgdorferi* infection (Salman-Dilgimen et al., 2013).

Also, RNase J turned out to be a putative and non-robust interactor of RNase E. Unlike the RNase E, the mycobacterial RNase J can act both as a 5'-3' exoribonuclease and as an endoribonuclease, but is not essential and seems to play only a minor role in the regulation of mycobacterial mRNA metabolism (Płociński et al., 2019; Taverniti et al., 2011). It was shown that the endonuclease activity of the RNase E followed by the exoribonuclease activity of RNase J mainly regulates the maturation of rRNA precursors in *M. smegmatis* (Taverniti et al., 2011). However, the identification of RNase J in our RNase E pull-down might also reflect an accessory role of this enzyme in the mycobacterial RNA degradosome. Although a direct interaction between these two enzymes cannot be ruled out and further investigations are required, we can hypothesize the RNase E and RNase J might interact indirectly to complete the processing and/or the degradation of their targets.

Furthermore, *in vitro* analysis of the endonucleolytic activity of RNase J showed that, unlike RNase E, RNase J can bind 5'-thriphosphorylated (5'-PPP) transcripts and cleave them within the first four nucleotides (Taverniti et al., 2011). Typically, bacterial transcripts having a 5'-PPP group are protected from RNase E endoribonuclease activity, but the ability RNase J to cleave 5'-PPP mRNA suggests that this enzyme could expand the range of targets of the degradosome. While the 'sliding endoribonuclease' function of the RNase J seems to be highly sensitive to the presence of secondary structures (Taverniti et al., 2011), the RNase E endonucleolytic activity relies on a 5'-end and 5'-bypass mechanism, which assures the RNase E

recognition of targets with structural obstacles, such as 5'-stem-loops or non-5'-P ends (Bandyra et al., 2018). Hence, we can speculate that an indirect interaction and/or close proximity between RNase E and RNase J in mycobacteria might result in the process of a broader range of targets, according to the structural properties of the RNA target molecule. In the future, it will be interesting to investigate whether and how the structural properties of transcripts influence their degradation, and whether this would be specifically mediated by either RNase E or RNase J.

The catalytic domain of the RNase E is highly conserved among different species, despite some structural differences (Aït-Bara and Carpousis, 2015). For instance, by SWISS model homology analysis, we found that mycobacterial RNase E primary structure underwent circular permutation as compared to *E. coli*, causing the catalytic domain to be relocated between the middle and the C-terminal region (**Figure 19**). Despite this domains reorganization, the catalytic site of mycobacterial RNase E is conserved and preferentially cleaves non-specific A/U-rich sequences, and binds 5'- monophosphorylated RNA molecules (Zeller et al., 2007). In *E. coli*, enzymes belonging to the Nudix RNA pyrophosphohydrolase family (Nudix hydrolases) promote the conversion of the 5'-triphosphate end to 5'-monophosphate end, making the RNA accessible to the action of RNase E (Belasco, 2010).

Interestingly, in our proteomic analysis we identified different Nudix hydrolases in the RNase E pull-down, particularly MutT2 (but also MutT4 among the non-significant enriched interactors), which is a poorly characterized enzyme. Based on our findings also the mycobacterial RNase E can act on 5'-triphosphorylated ends thanks to the action of enzymes belonging to the Nudix family. Besides its hydrolytic activity, MutT2 is also responsible for removing oxidatively damaged form of guanine from DNA, contributing to DNA repair mechanisms (Dos Vultos et al., 2006). Indeed, MutT2 participates in the maintenance of an adequate intracellular pool of nucleotides. In particular, MutT2 activity seems to be crucial in mycobacterial strains carrying mutations in the β subunits of the RNA polymerase, RpoB, which is the target of rifampicin (Mokrousov, 2004). Mutations conferring rifampicin resistance occur with a fitness cost for the bacilli (Mokrousov, 2004). To compensate the fitness cost of *rpoB* mutations, *M. tuberculosis* elicits a constitutive stress response, which reduces replication fidelity by the acquisition of compensatory mutations (Bergval et al., 2007). Surprisingly from our analysis, RpoB was identified as another putative interactor of RNase E. Although further studies are required to understand the functional meaning of this interaction, it is tempting to speculate that in rifampicin-resistant *M. tuberculosis* with a higher mutation rate, the interaction between RNase E, RpoB and MutT2 might help the bacilli to degrade aberrant targets and avoid the introduction of damaged nucleotides, towards the restoration of bacterial fitness while preserving the antibiotic resistant phenotype. In sum, the hydrolytic activity of MutT2 in mycobacteria might produce

substrates that are more susceptible to the RNase E activity, while participating in the maintenance of genome integrity and generation of functional transcripts (Deana et al., 2008).

M. tuberculosis assures its long-term survival and persistence in the host by activating a wide variety of molecular mechanisms in response to the extreme conditions encountered in the host niches. The tubercular bacillus deploys diverse adaptive mechanisms, two-component and phosphorylation signaling cascades, and hundreds of transcriptional regulators (Manganelli et al., 2004) in order to endure different stresses, such as nutrients starvation (Prusa et al., 2018); iron depletion (Pandey et al., 2014b); hypoxia; ROS and NOS (Gengenbacher and Kaufmann, 2012). *M. tuberculosis* also reshapes its metabolism by favoring lipids catabolism (Ehrt et al., 2018), and upregulates pathways necessary for the maintenance of its genome integrity such as DNA recombination and repair mechanisms and mutagenesis (Dos Vultos et al., 2009; Manina et al., 2019). Furthermore a plethora of virulence factors helps this pathogen to hijack and counteract the host defenses (Zhang and Yew, 2009). Interestingly, our functional analysis of the RNase E protein interactome revealed that the RNase E not only participates in RNA turnover and ribosomal processing (Płociński et al., 2019; Taverniti et al., 2011; Zeller et al., 2007), but also exhibits a more pleiotropic function, by interacting with enzymes involved stress response and adaptive pathways.

For instance, RNase E could indirectly help preserving genome integrity by degrading aberrant transcript, which results from the activation of the SOS DNA damage response (Bergval et al., 2007). The association between RNase E and SOS response was already proposed in *E. coli,* in which inactivation of the RNase E resulted in the impairment of the initiation of a functional SOS response (Manasherob et al., 2012). Following DNA damage, the activation of the SOS regulon also brings to growth inhibition and arrest of cell division, to allow the numerous DNA repair mechanisms to restore genome integrity before chromosomal replication is completed and the next cellular generation can initiate. Among other DNA repair mechanisms, mycobacteria also own the so-called nucleotide excision repair (NER). The global SOS repressor LexA regulates also UvrA, UvrB and UvrC, which mediate the NER pathway, whose activation is crucial to recovery from the SOS response (Ni et al., 2007). Remarkably, from our proteomic analysis, we could identify a number of proteins implicated in DNA damage response, including RadA, LexA, RecA, RecX, LigB, PriA, UvrC and, among the strongest interactors, UvrA. Collectively, these data suggest that similarly to *E. coli*, the mycobacterial RNase E might participate and possibly regulate the DNA damage response.

Surprisingly, we also identified all the main players of the stringent response in the RNase E pull-down, including RelA, Ppk, Obg and Ask. Interestingly, *M. tuberculosis* RelA has two C-

terminal structural domains, i.e., the TGS domain that binds the threonyl tRNA synthetase, Obg and SpoT, and the ACT domain that binds the aspartate kinase (Ask), a chorismate mutase and the prephenate dehydrogenase TyrA (Prusa et al., 2018). Although our understanding of the stringent response in mycobacteria is still limited, its activation was proposed to enhance *M. tuberculosis* stress response mainly during nutrient starvation, long-term culture and late stage of infection (Prusa et al., 2018), but not drug tolerance (Bhaskar et al., 2018). Similarly to *E. coli*, activation of the stringent response in mycobacteria downregulates the biosynthesis of rRNA and ribosomal proteins and upregulates the biosynthesis of amino acids (Prusa et al., 2018). From our study, we were able to validate Obg as a more likely RNase E interactor in cells subject to complete nutrient starvation. Obg is a highly conserved GTPase, which was associated with (p)ppGpp production and antibiotic tolerance in Gram-negative bacteria (Verstraeten et al., 2015). Obg is also known to act at the interface of DNA and protein synthesis, and to contribute to the downregulation of cellular metabolism in Gram-positive bacteria and to promote sporulation in *B. subtilis* (Kint et al., 2014). Given the role of the RNase E in DNA integrity, processing and maturation of rRNA precursor, and its interaction with a number of ribosomal proteins, we can speculate that the RNase E might act in concert with Obg to slowdown the metabolic activity and ribosomal expression in response to nutrient depletion, fostering cellular adaptation during long-term persistence. Remarkably, we also identified the toxin MazF within the RNase E pull-down and several chaperons and proteases, which may contribute to antitoxin degradation and increased toxin levels during the stringent-response signaling cascade (Ramisetty et al., 2016). Interestingly, we recently found that *M. smegmatis* cells, experiencing lysis after INH treatment, showed a hyperaccumulation of MazF toxin and ClpP protease before death (Burgess Tornaletti and Manina, 2020). Although our present evidences support the interaction between RNase E and Obg in *M. smegmatis*, presumably to reduce the metabolic activity of cells in response to harsh environmental conditions, further investigation will be necessary to confirm the potential association between RNase E and the stringent response.

Bacteria constantly withstand selective pressure due to abrupt environmental fluctuations and need to adapt in a timely manner to ensure the survival of the population. The presence of non-genetic diverse subpopulations within an isogenic population reflects a fitness cost paid by the bacterial community to overcome detrimental circumstances without incorporating long-term alteration in the genome (Vincent and Uphoff, 2020). Indeed, phenotypic heterogeneity is an intrinsic property of all clonal bacterial populations, including mycobacterial populations. We formerly reported that clonal mycobacterial populations under optimal growth conditions exhibit broad cell-to-cell variation in the growth and metabolic state, which increases under stressful conditions (Manina et al., 2015). Indeed, *M. tuberculosis* phenotypic variation is

being increasingly associated with adaptation in response to antimicrobials and to the host (Dhar et al., 2016; Rego et al., 2017; Logsdon et al., 2017; Manina et al., 2019; Manina et al., 2015; Sakatos et al., 2018; Wakamoto et al., 2013; Zhu et al., 2018). Although the exact molecular mechanisms behind the origin of phenotypic diversification within clonal mycobacterial populations are still unclear, stochastic gene expression is among the possible causes, in conjunction with deterministic environmental factors.

Indeed, in all living organisms, phenotypic heterogeneity is influenced by a wide variety of determinants, both intrinsic and extrinsic to the organism. Among these determinants, RNA turnover is the main factor influencing variation in gene expression and, consequently, cell-to-cell phenotypic variation; conversely, protein variation tends to have a smaller influence due to the longer half-life of proteins compared to RNA (Eldar and Elowitz, 2010). Variation in RNA turnover depends not only on the rate of synthesis of the transcript but also on its rate of degradation (Baudrimont et al., 2019).

Although our understanding of RNA turnover in mycobacteria is still limited, a recent study demonstrated that mRNA degradation is associated with the energetic status of the bacteria, entailing that mRNA decay can be regulated either by protection of the transcript from RNases and/or by modulation of their activity, also depending on nutrients availability in the surrounding environment (Vargas-Blanco et al., 2019). These two factors, *i.e.,* modulation of the RNases activity and the protection of the transcript from RNases, are not mutually exclusive and both can influence mRNA decay. Although enolase, the metabolic enzyme coupled to the RNA degradosome in *E. coli*, did not appear among the mycobacterial RNase E interactors, we found out that RNase E possibly interacts with a large number of enzymes involved in diverse aspects of the bacterial metabolism, including carbohydrate, lipid, and amino acid metabolism, which might support the hypothesis of a tight association between the energetic status of the cell and the rate of mRNA decay dependent on RNase E. Therefore, cell-to-cell variation in the energetic state of the cell might bring about heterogeneous expression of RNase E, and in turn, influence single-cell gene expression variation.

Indeed, by coupling time-lapse microfluidic microscopy and fluorescent reporters of RNase E, we demonstrated that RNase E is heterogeneously expressed in both *M. smegmatis* and *M. tuberculosis* during optimal growth conditions. We monitored the behavior of RNase E fluorescent reporters over the generation time of single replicating cells and discovered that in both *M. smegmatis* and *M. tuberculosis* RNase E exhibits patchy distribution throughout the cell and forms short-lived brighter foci within the lifetime of individual cells, only in about half of the population, reminiscent of a stochastic process. Furthermore, the formation of RNase E foci was observed in a lower fraction of the *M. tuberculosis* population (40%) compared to *M. smegmatis*

(60%). While in the fast-growing model organism *M. smegmatis* the presence of RNase E foci resulted in cell-size reduction and faster growth rate, we did not observe any significant difference in growth-related parameters between *M. tuberculosis* subpopulations, based on the presence or absence of RNase E foci.

Importantly, it was reported that *M. smegmatis* and *M. tuberculosis* exhibit different mRNA half-life, which positively correlate with the growth rate, i.e., about 5 minutes in *M. smegmatis* with a generation time about 3 hours, and about 9 minutes in *M. tuberculosis* with a generation time of about 24 hours (Rustad et al., 2013). This difference of mRNA half-life between fast- and slow-growing mycobacterial species might result from diverse rates of RNase E-mediated RNA processing, whereby the subpopulation of *M. smegmatis* forming RNase E foci might not only have faster mRNA degradation rate, but also faster rRNA maturation, leading to faster growth rates. In the future it will be compelling to investigate whether these differences in RNase E expression at the single-cell level depend also on a difference in the RNA targets. In particular, whether *M. tuberculosis* transcripts are enriched in 5'-triphosphate ends, which would protect them from RNase E endonucleolytic activity.

The localization pattern of RNase E in live mycobacterial cells shares features with both *C. crescentus* and *E. coli* (Bayas et al., 2018; Strahl et al., 2015). We found that mycobacterial RNase E clusters in brighter foci that might correspond to highly transcribed loci, such as the ribosomal locus, also consistent with RNA polymerase clusters of localization identified in *E. coli* (Weng et al., 2019). Although the actual role of the RNase E foci occurrence is still unclear, they might correspond to active transcriptional hubs, consistent with their colocalization with an RNA specific dye. We can hypothesize two opposite roles for the RNase E within this clusters. On the one hand, RNase E might exert its endonucleolytic function, and on the other hand, it might be sequestered within these foci, to fine tune its function and reduce possible toxicity for the cell (Tejada-Arranz et al., 2020a). Moreover, we found that RNase E-specific chemical inhibition resulted in progressive disappearance of the foci, and also that transient inhibition of the catalytic site of RNase E is detrimental for the cells, in that cells experience reductive division events until growth arrest. These results support the hypothesis of an active role of RNase E within these localization foci. We can currently speculate on two possible scenarios. In the first scenario, the RNase E foci represent hubs of active RNA degradation, whose inhibition might alter the cellular RNA metabolism, inducing a global stress response, ultimately affecting cell replication and division. In the second scenario, the inhibition of RNase E foci might result in an uncontrolled release of the endonuclease within the intracellular environment, which might become toxic for the cell. Irrespective of which of these two scenarios is the correct one, it is clear that targeting the expression and/or the activity of RNase E considerably affects mycobacterial cell physiology, which primarily translates into a disruption of the homeostasis of growth and division. Indeed,

we found that not only major deregulation of RNase E expression levels affects the growth rate in bulk, but also that the insertion of a second copy of *rne*, expressed at native levels, moderately impacts single-cell size and growth rate under optimal growth condition, implying that even small variation in RNase E expression levels have a direct impact on cell-growth homeostasis.

The RNase E implication in cell division was proven in model microorganisms. For instance in *E. coli*, optimal levels of RNase E are required for the maintenance of a proper FtsZ/FtsA ratio, which drive cell division (Tamura et al., 2006). FtsZ downregulation usually results in bacterial cell elongation, conversely, FtsZ slight upregulation results in cell size reduction (Taheri-Araghi et al., 2015). Also nutrient deprivation, especially carbon starvation, causes reductive division. Indeed changes in the central carbon metabolism can impair cell cycle progression, lipid biosynthesis, and cell wall biogenesis (Westfall and Levin, 2018). In our proteomic analysis of the RNase E pull-down, we identified several proteins implicated in diverse aspects of metabolism, several metabolites transporters, transcriptional regulators and two-component systems, as well as some proteins directly involved in cell division. Therefore, RNase E might act as a bridge between sensing the nutrients available in the environment, adjusting the metabolic state of the cell, and altering both cell size and division, to adapt to the surrounding environment. Although maintenance of cell-size and growth homeostasis in mycobacteria is still an active subject of investigation, single-cell analysis of *M. smegmatis* dynamics of replication and division led to interpretation that mycobacteria follow neither a timer nor a sizer model of cell division but most likely an adder model (Logsdon et al., 2017; Santi et al., 2013). Indeed, mycobacterial growth is asymmetric and bipolar, with preferential incorporation of cell wall in the old pole, and results in a highly heterogeneous population, with older cells larger than their younger siblings (Santi et al., 2013; Manina et al., 2015; Priestman et al., 2017;) However, we can link spontaneous cell-to-cell variation in RNase E expression to differences in cell size and growth rate only in *M. smegmatis*, and with no relevant correlation with respect to cell age. Importantly, we found that in both *M. smegmatis* and *M. tuberculosis* RNase E foci mostly localize towards the mid-cell position or the new cell pole, similar to FtsZ septum formation in mycobacteria (Santi et al., 2013), and alike the divisome components in *C. crescentus* that relocate to the new cell-pole after cytokinesis (Laloux and Jacobs-Wagner, 2014).

In sum, we think that the role of RNase E in cell size and growth homeostasis might mainly hinge on (i) stochastic factors; (ii) direct interaction with components of the divisome; (iii) reflect the cell response to an intracellular stress, such as DNA damage, and (iv) derive from direct sensing exogenous fluctuations in nutrients availability.

Although not strictly compartmentalized like eukaryotic cells, also bacterial cells display a certain spatial organization that allows a nexus between replication and regulation of gene expression. Replicating chromosomes are usually dispersed in the cytosol and the extent of DNA compaction is closely related to the ability of ribosomal diffusion through the nucleoid and to be loaded on nascent mRNA to form polysomes and to allow translation. This process also includes RNA degrading machines that can be both sequestered at the membrane level to modulate their activity and associated with the DNA (Surovtsev & Jacobs-Wagner, 2018). Chromosomal organization and compaction is closely related to gene expression and depends on the interaction with so-called nucleoid-associated proteins (NAPs) (Dillon and Dorman, 2010). Bacteria need to fine-tune gene expression to survive in a dynamic environment, not only by means of transcription factors, but also based on the structural organization and plasticity of the nucleoid, which add an extra layer of regulation to gene expression (Dillon and Dorman, 2010). By bending, bridging, and wrapping DNA, NAPs ensure both local and global organization of the chromosome, resulting in promoting or silencing the expression of a specific gene or of a set of genes, according with the bacterial growth phase and environmental cues (Kriel et al., 2018). Interestingly, we found that RNase E interacts not only with components of the RNAP machinery, such as RpoB, RpoC and sigma factors, and with the cell division machinery, but also with more than one NAPs, such as Lsr2 and HupB. The interaction of RNase E with fundamental cell processes is suggestive of its crucial role and the pleiotropic effect of this enzyme in the maintenance the mycobacterial cell homeostasis.

Mycobacteria exhibit a unique set of NAPs that show low sequence homology to their *E. coli* counterparts and contribute to the chromosome asymmetric partitioning, regulation of gene expression and tolerance to stressful conditions (Kriel et al., 2018). Indeed, NAPs are important during mycobacterial adaptation under diverse conditions, such as nutrient starvation, heat-shock, iron limitation, and oxidative stress (Kriel et al., 2018). Differently from *E. coli*, mycobacteria only encodes seven NAPs (Datta et al., 2019), including Lsr2 and HupB (Bartek et al., 2011; Colangeli et al., 2007; Hołówka et al., 2017; Pande et al., 2014), which we identified and validated as robust interactors of RNase E. Fluorescent reporters of both Lsr2 and HupB exhibited a string-of-pearl pattern mainly located within the central region of the cell. Both Lsr2 and HupB were positively correlated with RNase E fluorescent reporter at the single-cell level, corroborating the tight association of RNase E with the nucleoid and its dynamics. We decided to focus on HupB, since it was identified with the highest stoichiometric index within the RNase E pull-down. Remarkably, HupB was associated with mycobacterial tolerance to INH, a first-line anti-tubercular drugs targeting the cell wall, (Niki et al., 2012; Sakatos et al., 2018). Although HupB is not essential, it was also shown to play a critical role in mycobacterial entry and survival into host cells (Pandey et al., 2014; Kalra et al., 2018; Yaseen et al., 2018). The question arises whether heterogeneous

expression of RNase E in conjunction with HupB could influence gene expression variation and *M. tuberculosis* adaptive responses when confronted to harsh conditions caused by drug exposure and the host cell.

Isoniazid (INH) is a highly effective first-generation drug, still used as a front-line molecule to treat tuberculosis (Pai et al., 2016). While it is particularly rapid and effective against actively growing bacilli, its antimicrobial activity is less effective against slowly/non-replicating bacilli, which endure treatment and result in a subpopulation of INH-persistent bacilli both *in vitro* and *in vivo* (Herbert et al., 1996; Vilchèze and Jacobs, 2019). INH is a prodrug that needs to be converted into its active form by the enzymatic activity of the catalase-peroxidase, KatG. Once activated, INH inhibits the biosynthesis of the cell-wall mycolic acids by targeting InhA (Katoch, 2019). In mycobacteria, *katG* expression is induced upon oxidative stress, and negatively regulated by FurA, an iron-regulated transcription factor. Interestingly, *furA* is co-transcribed with *katG* in a polycistronic mRNA (Sala et al., 2008), which is processed by the RNase E (Taverniti et al., 2011), and it downregulates its own expression by binding the 5'-UTR of *furA* (Zahrt et al., 2001). Importantly, also HupB was shown to influence the expression of *furA-katG* (Niki et al., 2012). In particular, following changes in the intracellular levels of iron, HupB binds the promoter region of the *furA-katG* locus inhibiting its expression, reducing the KatG intracellular levels, and promoting INH tolerance (Niki et al., 2012). Also, the methylation and/or acetylation of the lysine in position 86 (K86) of HupB was recently shown to induce INH tolerance (Sakatos et al., 2018). Albeit the exact molecular mechanism underlying this epigenetic induced INH tolerance remains to be elucidated, the K86 methylation and/or acetylation of HupB were shown to be heterogeneously expressed at the population level, leading to two co-existing subpopulations having different morphological and growth characteristics and diverse INH susceptibility (Sakatos et al., 2018).

In eukaryotic cells histone proteins are continuously subject to epigenetic modifications, which modulate their ability to bind nucleic acids. The reduction of positive charges, as with phosphorylation and acetylation, generally results in opening the chromatin and in initiation of transcription. Conversely, methylation usually results in repression of transcription, although some specific methylations can also result in activation of transcription (Bannister and Kouzarides, 2011). Thus, similar to eukaryotic histone protein, diverse post-translational modifications have been implicated in the ability of HupB to interact with the bacterial chromosome and influence its structure and organization, ultimately resulting in gene expression variation (Gupta et al., 2014; Sakatos et al., 2018).

Both RNase E and HupB are key determinants of the mycobacterial cell transcriptome, and we found them to act cooperatively to regulate the mycobacterial cell physiology under optimal

growth conditions. Since RNase E and HupB they regulate the expression of KatG with inverse but possibly complementary mechanisms (Taverniti et al., 2011; Niki et al., 2012; Gupta et al., 2014; Sakatos et al., 2018), we decided to monitor the single-cell expression and localization of both proteins fused to fluorescent markers also during at the transition from optimal growth to INH treatment. We were able to demonstrate that, in the presence of INH, RNase E and HupB experience correlated condensation events, and that a pre-existing cell-to-cell variation in RNase E expression can partly predict the single-cell fate of *M. tuberculosis*. Moreover, we found that single-cell survival occurred exclusively when bacilli were able to fine-tune both levels of RNase E and HupB during and after INH treatment, and that either too low or overly expression of both proteins was conducive to death in cells exposed to INH. Indeed, stressed *M. tuberculosis* cells deploy a wide range of detoxification mechanisms, including direct scavenging of reactive species, also using KatG, and enhance pathways involved in the DNA damage repair and protection turnover (Voskuil et al., 2011), which we found within the RNase E interactome.

Therefore, we think that pre-existing and/or stress-induced upregulation of RNase E might be necessary for triggering adaptive mechanisms associated to both metabolic slowdown and stress responses. However, prolonged and uncontrolled induction of RNase E turns out to be detrimental to mycobacterial single-cell physiology, consistent with the toxicity of the endonucleolytic activity of RNase E (Go et al., 2011; Mackie, 2013). Given the tight molecular association of RNase E and HupB and their increased co-localization at condensed nucleoids following drug treatment, and also considering the time-shifted upregulation of HupB compared to RNase E, we can speculate that HupB intervenes just after RNase E to counteract the endonucleolytic activity of the RNase E, by promoting chromosomal condensation and integrity, inhibiting gene expression and fostering cell survival. Collectively, our results are consistent with the association of HupB with the nucleoid (Hołówka et al., 2017), as well as with the fact that macromolecular synthesis inhibitors, such as INH, cause chromosomal condensation (Cabrera et al., 2009; Shechter et al., 2013; Bayas et al., 2018; Scutigliani et al., 2018; Weng et al., 2019). At present, we cannot rule out that HupB induction may also partly occur independently from RNase E and that a more complex mechanism might regulate mycobacterial response to INH. Nevertheless, the initial upregulation of the RNase E and its subsequent controlled regulation in conjunction with HupB appear critical for the single-cell survival of mycobacteria confronted with INH. Indeed, CRISPRi-induced downregulation of *rne* in single mycobacterial cells accelerates the rate of lysis, further confirming that the lack of normal levels of functional RNase E is harmful to INH-stressed bacilli, possibly leading to an imbalance between growth and division. In sum, too low or too high intracellular levels of RNase E negatively affect mycobacterial cell physiology, implying the need for an optimal threshold in RNase E expression, which is also dependent on

HupB-based nucleoid remodeling, for the maintenance of the mycobacterial cell homeostasis under both optimal and stressful conditions.

M. tuberculosis infection is a highly dynamic process. While the host immune system actively tries to clear the infection, the pathogen hijacks the host immune system to promote its long-term survival and dissemination (Bussi and Gutierrez, 2019). How this successful pathogen exactly subverts the host's defensive arsenal remains an open area of investigation. After mucosal cells, alveolar macrophages are essentially the first immune cells to encounter the pathogen. Nonetheless, alveolar macrophages are more permissive and slowly-responding, so that *M. tuberculosis* harness them to dictate the outcome of the infection (Upadhyay et al., 2018). Surprisingly HupB, besides its role of nucleoid organizer and gene-expression influencer, also mediates the *M. tuberculosis* adhesion to macrophages (Yaseen et al., 2018). Interestingly, macrophages can interfere with HupB-mediated adhesion utilizing an epigenetic effector, the histone H3 lysine 9 methyltransferase SUV39H1, which can relocate in the presence of the pathogen, and induce HupB trimethylation, inhibiting mycobacterial survival inside the host cell (Yaseen et al., 2018). Indeed, either the host-mediated methylation of HupB or its depletion resulted in the inability of the tubercular bacilli to survive during the infection (Kalra et al., 2018; Yaseen et al., 2018). Given the essentiality of HupB in the initiation and establishment of infection, it was also proposed as a new potent drug target, to decrease mycobacterial invasion and survival in the host cells (Kalra et al., 2018; Odermatt et al., 2018; Yaseen et al., 2018; Scutigliani et al., 2018).

Less is known about the role played by RNase E during host-cell infection with pathogenic bacteria. Its essentiality and the absence of a viable phenotype following RNase E depletion only resulted in an indirect link between the RNase and virulence in different pathogenic bacteria (Lodato et al., 2017; Sharp et al., 2019; Viegas et al., 2007; Yang et al., 2008). To the best of our knowledge, no information is currently available regarding the behavior of the RNase E during live infection. Here, we provide the first direct single-cell analysis of *M. tuberculosis* RNase E dynamics in conjunction with HupB during macrophage infection. We showed that both RNase E and HupB levels decrease at the beginning of infection, whereas their levels jointly increase as the infection progresses and in late stage of macrophage infection. Furthermore, the increased phenotypic variation of RNase E and HupB expression in single *M. tuberculosis* cells is consistent with our past observations on the increased phenotypic variation of rRNA expression during both macrophage infection and in the mouse model of infection (Manina et al., 2015). Although it is unclear whether mycobacterial phenotypic variation is directly induced by stressful conditions that interfere with vital cellular processes, or whether it results from an adaptive response that aims to foster single-cell survival, a feasible interpretation from our observations is that RNase E

and HupB might participate in enhancing bacterial cell-to-cell diversification during infection, to ultimately promote survival of at least a fraction of the population. Moreover, consistent with our *in vitro* observation of exponentially growing and drug-treated mycobacterial cells, also during single macrophage infection, RNase E and HupB exhibit a rather synchronized behavior, corroborating the tight association of these two proteins in response to a broad range of stressful conditions. However, taking into account the crucial role of HupB in promoting mycobacterial entry and survival into host cells, we cannot exclude that RNase E might be acting in a HupB-dependent fashion during infection. This would outline a scenario in which the two proteins might mutually coordinate as a function of the stress that bacilli have to cope with.

After bacterial uptake, the phagosome rapidly matures and fuses with lysosomes by inducing its acidification, iron starvation, and generating ROS in order to clear the intracellular menace. However, *M. tuberculosis* can prevent these maturation events by secreting various effectors (Upadhyay et al., 2018). The impairment of phagosome to lysosome fusion is the primary mechanism used by *M.* tuberculosis to undermine the innate immune response, and is crucial to the success of this pathogen (Bussi and Gutierrez, 2019). Among the diverse factors participating in this critical step of the infection, the 6 kDa early secretory antigenic target EsxA (ESAT-6) and the 10 kDa culture filtrate antigen EsxB (CFP10) secreted by the type VII secretion system (T7SS) play a critical role in phagosomal rupture and allows bacilli to escape into the cytosol (Martinez et al., 2018). Interestingly, in *Pseudomonas aeruginosa* and *Yersinia pseudotuberculosis*, the RNase E was reported to regulate the expression of the components of the Type III secretion system (Sharp et al., 2019; Yang et al., 2008), which in pathogenic Gram-negative bacteria represents a key virulence factor, enabling the pathogens to inject bacterial effectors into the cytoplasm of the host cell, and promoting intracellular survival (Sharp et al., 2019). Surprisingly, we found both EsxA and EsxB effectors to be lowered in the pull-down of the RNase E over-expressing strain (**Figure 2**). Hence, we can speculate that low but heterogeneous expression of RNase E in *M. tuberculosis* at the beginning of infection might contribute to differential regulation of EsxA and EsxB expression, mostly resulting in the upregulation of these effectors at the beginning of macrophage infection, consistent with early phagosomal rupture. (Bussi and Gutierrez, 2019). Considering that the RNase E most likely is involved in the late stage of the infection, it is appealing to postulate that the RNase E might be implicated in the blockage of phagosomal acidification before, and in the vacuolar breakage after. This attractive scenario might also explain our observation of increased intracellular clearance during late stage of infection in macrophages infected with bacteria in which we reduced the intracellular level of RNase E.

Despite its ancient origin, *M. tuberculosis* remains one of the deadliest pathogens of the human history, and new strategies are urgently needed to eradicate it. Within a clonal bacterial population, not all cells exhibit the same phenotype. Cell-to-cell phenotypic variation can originate from diverse sources, and noise in gene expression depending on mRNA turnover is considered one of the main drivers. Phenotypic variation helps pathogenic bacteria, such as *M. tuberculosis,* not only to endure antibiotic treatment but also to elude the host defenses. However, how mycobacterial phenotypic variation contributes to drug tolerance and infection outcome is still poorly understood, as well as the molecular mechanisms governing phenotypic variation. Here we showed that RNase E and HupB are important factors participating in both homeostasis and stress responses in the tubercular bacillus (**Figure S5G**). With this work we discovered that RNase E exhibits phenotypic variation at the single-cell level, we unveiled the interaction between RNase E and HupB and their relevance for stress tolerance, and we started to investigate the consequences of an imbalance of these two pleiotropic factors for *M. tuberculosis* fitness. In the future we envisage to further clarify the molecular mechanisms regulating these two enzymes, which we consider to be crucial for mycobacterial diversification and persistence. RNase E and HupB are also emerging as potential druggable targets (Kalra et al., 2018; Kime et al., 2015; Mardle et al., 2020; Scutigliani et al., 2018). Based on our findings, the identification of molecules altering the function of RNase E and HupB could pave the way for the development of new effective antimicrobial strategies that could help us to eradicate tuberculosis.

Movie legends

Movie 1. Time-lapse microscopy of *M. smegmatis* P*rne*-mKate2 bacteria in exponential-phase, related to Figure 20.

Representative movie in which exponential-phase bacteria seeded into a customized microfluidic device (Manina et al., 2019) and grown under a constant flow of 7h9 medium. Images were recorded at 30-minutes interval (100X objective). Magenta (P*rne*-mKate2) and blue (phase) fluorescence channel are merged. Time elapsed is indicated in hours. Selected snapshots from the movie are shown in **Figure 20A**. Scale bar 10 μm

Movie 2. Time-lapse microscopy of *M. smegmatis* P*rne*-mKate2 bacteria treated with the RNase E inhibitor M5, related to Figure 20.

Representative movie in which exponential-phase bacteria seeded into a customized microfluidic device (Manina et al., 2019) and grown under a constant flow of 7h9 medium for 6 hours. M5 (2.5 mM) was added to the flow medium for 12 hours, then followed by 12 hours of washout. Images were recorded at 30-minutes intervals (100X objective). Magenta (P*rne*-mKate2) and blue (phase) fluorescence channel are merged. Time elapsed is indicated in hours. Selected snapshots from the movie are shown in **Figure 20J**. Scale bar 5 μm

Movie 3. Time-lapse microscopy of *M. tuberculosis* P*rne*-mCherry_P*hupB*-sfGFP bacteria in exponential-phase, related to Figure 23.

Representative movie in which exponential-phase bacteria seeded into a customized microfluidic device (Manina et al., 2019) and grown under a constant flow of 7h9 medium. Images were recorded at 1-hours interval (100X objective). Magenta (P*rne*-mKate2), green (P*hupB*-sfGFP) and gray (phase) fluorescence channel are merged. Scale bar 5 μm

Movie 4. Time-lapse microscopy of isoniazid (INH) - *M. tuberculosis* P*rne*-mCherry_P*hupB*-sfGFP bacteria, related to Figure 23.

Representative movie in which exponential-phase bacteria seeded into a customized microfluidic device (Manina et al., 2019) and grown under a constant flow of 7h9 medium for 4 days. INH (250 ng/mL; 10-fold-MIC) was added to the flow medium for 2 days, then followed by 10 days of

washout. Cell were lastly subjected to a second INH (250 ng/mL; 10-fold MIC). Images were recorded at 1-hours intervals (100X objective). Magenta (P*rne*-mKate2) green (P*hupB*-sfGFP) and gray (phase) fluorescence channel are merged. Selected snapshots from the movie are shown in **Figure 23F**. Scale bar 5 µm

Movie 5. Time-lapse microscopy of isoniazid (INH) - *M. tuberculosis rne-wt* and *si-rne* bacteria, related to Figure 24.

Representative movie in which exponential-phase bacteria seeded into a customized microfluidic device (Manina et al., 2019) and grown under a constant flow of 7h9 medium for 3 days. ATC (100 ng/mL) was added for 4 following days to induced *rne* silencing. INH (250 ng/mL; 10-fold-MIC) together with the inducer was added for 2 days, followed by a wash out phase where both ATC and ING were eliminated. Images were recorded at 1-hour intervals (100X objective). Green (P*hupB*-sfGFP) and magenta (phase) fluorescence channel are merged. Selected snapshots from the movie are shown in **Figure 24A-B**. Scale bar 5 µ

Bibliography

Agarwal, N., and Tyagi, A.K. (2003). Role of 5′-TGN-3′ motif in the interaction of mycobacterial RNA polymerase with a promoter of 'extended -10' class. FEMS Microbiol. Lett. *225*, 75–83.

Aguilar, C., Vlamakis, H., Losick, R., and Kolter, R. (2007). Thinking about Bacillus subtilis as a multicellular organism. Curr. Opin. Microbiol. *10*, 638–643.

Aguirre, A.A., Vicente, A.M., Hardwick, S.W., Alvelos, D.M., Mazzon, R.R., Luisi, B.F., and Marques, M. V. (2017). Association of the cold shock DEAD-box RNA helicase RhlE to the RNA degradosome in Caulobacter crescentus. J. Bacteriol. *199*, 1–13.

Aït-Bara, S., and Carpousis, A.J. (2010). Characterization of the RNA degradosome of Pseudoalteromonas haloplanktis: Conservation of the RNase E-RhlB interaction in the gammaproteobacteria. J. Bacteriol. *192*, 5413–5423.

Aït-Bara, S., and Carpousis, A.J. (2015). RNA degradosomes in bacteria and chloroplasts: Classification, distribution and evolution of RNase E homologs. Mol. Microbiol. *97*, 1021–1035.

Aït-Bara, S., Carpousis, A.J., and Quentin, Y. (2015). RNase E in the γ-Proteobacteria: conservation of intrinsically disordered noncatalytic region and molecular evolution of microdomains. Mol. Genet. Genomics *290*, 847–862.

Al-Husini, N., Tomares, D.T., Bitar, O., Childers, W.S., and Schrader, J.M. (2018). α-Proteobacterial RNA Degradosomes Assemble Liquid-Liquid Phase-Separated RNP Bodies. Mol. Cell *71*, 1027-1039.e14.

Alderwick, L.J., Harrison, J., Lloyd, G.S., and Birch, H.L. (2015). The mycobacterial cell wall—peptidoglycan and arabinogalactan. Cold Spring Harb. Perspect. Med.

Aldridge, B.B., Fernandez-Suarez, M., Heller, D., Ambravaneswaran, V., Irimia, D., Toner, M., and Fortune, S.M. (2012). Asymmetry and aging of mycobacterial cells lead to variable growth and antibiotic susceptibility. Science (80-.).

Altink, H. (2014). "Fight TB with BCG": Mass vaccination campaigns in the British Caribbean, 1951-6. Med. Hist.

American Thoracin Society (1999). American Thoracic Society Targeted Tuberculin Testing and Treatment of Latent. Crit. Care Med.

Andersson, D.I., and Hughes, D. (2010). Antibiotic resistance and its cost: Is it possible to reverse resistance? Nat. Rev. Microbiol. *8*, 260–271.

Andrews, J.R., Noubary, F., Walensky, R.P., Cerda, R., Losina, E., and Horsburgh, C.R. (2012). Risk of progression to active tuberculosis following reinfection with Mycobacterium tuberculosis. Clin. Infect. Dis.

Andries, K., Verhasselt, P., Guillemont, J., Göhlmann, H.W.H., Neefs, J.M., Winkler, H., Van Gestel, J., Timmerman, P., Zhu, M., Lee, E., et al. (2005). A diarylquinoline drug active on the ATP synthase of Mycobacterium tuberculosis. Science (80-.).

Angerami, M., Suarez, G., Pascutti, M.F., Salomon, H., Bottasso, O., and Quiroga, M.F. (2013). Modulation of the phenotype and function of mycobacterium tuberculosis-stimulated dendritic cells by adrenal steroids. Int. Immunol. *25*, 405–411.

Antia, R., and Koella, J.C. (1994). A model of non-specific immunity. J. Theor. Biol. *168*, 141–150.

Arnvig, K.B., and Young, D.B. (2009). Identification of small RNAs in Mycobacterium tuberculosis. Mol. Microbiol.

Arnvig, K.B., and Young, D.B. (2012). Non-coding RNA and its potential role in Mycobacterium tuberculosis pathogenesis. RNA Biol.

Arnvig, K.B., Comas, I., Thomson, N.R., Houghton, J., Boshoff, H.I., Croucher, N.J., Rose, G., Perkins, T.T., Parkhill, J., Dougan, G., et al. (2011). Sequence-based analysis uncovers an abundance of non-coding RNA in the total transcriptome of Mycobacterium tuberculosis. PLoS Pathog. *7*.

Avraham, R., Haseley, N., Brown, D., Penaranda, C., Jijon, H.B., Trombetta, J.J., Satija, R., Shalek, A.K., Xavier, R.J., Regev, A.,

et al. (2015). Pathogen Cell-to-Cell Variability Drives Heterogeneity in Host Immune Responses. Cell.

B., P., and S., H. (1999). Drug-resistant and multidrug-resistant tubercle bacilli. Int. J. Antimicrob. Agents *13*, 93–97.

Babitzke, P., and Kushner, S.R. (1991). The ams (altered mRNA stability) protein and ribonuclease E are encoded by the same structural gene of Escherichia coli. Proc. Natl. Acad. Sci. U. S. A.

Bakkeren, E., Diard, M., and Hardt, W.D. (2020). Evolutionary causes and consequences of bacterial antibiotic persistence. Nat. Rev. Microbiol.

Balaban, N.Q., Merrin, J., Chait, R., Kowalik, L., and Leibler, S. (2004). Bacterial persistence as a phenotypic switch. Science (80-.). *305*, 1622–1625.

Balaban, N.Q., Gerdes, K., Lewis, K., and McKinney, J.D. (2013). A problem of persistence: Still more questions than answers? Nat. Rev. Microbiol. *11*, 587–591.

Balaban, N.Q., Helaine, S., Lewis, K., Ackermann, M., Aldridge, B., Andersson, D.I., Brynildsen, M.P., Bumann, D., Camilli, A., Collins, J.J., et al. (2019). Definitions and guidelines for research on antibiotic persistence. Nat. Rev. Microbiol. *17*, 441–448.

Bandyra, K.J., and Luisi, B.F. (2018). RNase E and the High-Fidelity Orchestration of RNA Metabolism. Regul. with RNA Bact. Archaea 1–18.

Bandyra, K.J., Said, N., Pfeiffer, V., Górna, M.W., Vogel, J., and Luisi, B.F. (2012). The Seed Region of a Small RNA Drives the Controlled Destruction of the Target mRNA by the Endoribonuclease RNase E. Mol. Cell.

Bandyra, K.J., Bouvier, M., Carpousis, A.J., and Luisi, B.F. (2013). The social fabric of the RNA degradosome. Biochim. Biophys. Acta - Gene Regul. Mech. *1829*, 514–522.

Bandyra, K.J., Sinha, D., Syrjanen, J., Luisi, B.F., and De Lay, N.R. (2016). The ribonuclease polynucleotide phosphorylase can interact with small regulatory RNAs in both protective and degradative modes. Rna *22*, 360–372.

Bandyra, K.J., Wandzik, J.M., and Luisi, B.F. (2018). Substrate Recognition and Autoinhibition in the Central Ribonuclease RNase E. Mol. Cell *72*, 275-285.e4.

Bannister, A.J., and Kouzarides, T. (2011). Regulation of chromatin by histone modifications. Cell Res.

Bansal-Mutalik, R., and Nikaido, H. (2014). Mycobacterial outer membrane is a lipid bilayer and the inner membrane is unusually rich in diacyl phosphatidylinositol dimannosides. Proc. Natl. Acad. Sci. U. S. A.

Barberis, I., Bragazzi, N.L., Galluzzo, L., and Martini, M. (2017). The history of tuberculosis: From the first historical records to the isolation of Koch's bacillus. J. Prev. Med. Hyg. *58*, E9–E12.

Barnes, P.F., and Cave, M.D. (2003). Molecular epidemiology of tuberculosis. N. Engl. J. Med. *349*, 1149–1156.

Barry, C.E. (2001). Mycobacterium smegmatis: an absurd model for tuberculosis? Trends Microbiol. *9*, 473–474.

Barry, C.E., Boshoff, H.I., Dartois, V., Dick, T., Ehrt, S., Flynn, J.A., Schnappinger, D., Wilkinson, R.J., and Young, D. (2009). The spectrum of latent tuberculosis: Rethinking the biology and intervention strategies. Nat. Rev. Microbiol. *7*, 845–855.

Bartek, I.L., Woolhiser, L.K., Baughn, A.D., Basaraba, R.J., Jacobs, W.R., Lenaerts, A.J., Voskuil, M.I., Cumming, B.M., Lamprecht, D. a, Wells, R.M., et al. (2011). Mycobacterium tuberculosis Lsr2 Is a Global Transcriptional Regulator. Front. Microbiol.

Bateman, A., and Kickhoefer, V. (2003). The TROVE module: A common element in Telomerase, Ro and Vault ribonucleoproteins. BMC Bioinformatics.

Baudrimont, A., Jaquet, V., Wallerich, S., Voegeli, S., and Becskei, A. (2019). Contribution of RNA Degradation to Intrinsic and Extrinsic Noise in Gene Expression. Cell Rep. *26*, 3752-3761.e5.

Bayas, C.A., Wang, J., Lee, M.K., Schrader, J.M., Shapiro, L., and Moerner, W.E. (2018). Spatial organization and dynamics of RNase E and ribosomes in Caulobacter crescentus. Proc. Natl. Acad. Sci. U. S. A. *115*, E3721–E3721.

Bechhofer, D.H. (2013). Nucleotide specificity in bacterial mRNA recycling. Proc. Natl. Acad. Sci. U. S. A.

Beckham, K.S.H., Staack, S., Wilmanns, M., and Parret, A.H.A. (2020). The pMy vector series: A versatile cloning platform

for the recombinant production of mycobacterial proteins in Mycobacterium smegmatis. Protein Sci.

Becskel, A., and Serrano, L. (2000). Engineering stability in gene networks by autoregulation. Nature.

Behr, M.A., Edelstein, P.H., and Ramakrishnan, L. (2018). Revisiting the timetable of tuberculosis. BMJ *362*, 1–10.

Belasco, J.G. (2010). All things must pass: Contrasts and commonalities in eukaryotic and bacterial mRNA decay. Nat. Rev. Mol. Cell Biol. *11*, 467–478.

Bercovier, H., Kafri, O., and Sela, S. (1986). Mycobacteria possess a surprisingly small number of ribosomal RNA genes in relation to the size of their genome. Biochem. Biophys. Res. Commun. *136*, 1136–1141.

van den Bergh, B., Fauvart, M., and Michiels, J. (2017). Formation, physiology, ecology, evolution and clinical importance of bacterial persisters. FEMS Microbiol. Rev. *41*, 219–251.

Bergmiller, T., Andersson, A.M.C., Tomasek, K., Balleza, E., Kiviet, D.J., Hauschild, R., Tkačik, G., and Guet, C.C. (2017). Biased partitioning of the multidrug efflux pump AcrAB-TolC underlies long-lived phenotypic heterogeneity. Science (80-.).

Bergval, I.L., Klatser, P.R., Schuitema, A.R.J., Oskam, L., and Anthony, R.M. (2007). Specific mutations in the Mycobacterium tuberculosis rpoB gene are associated with increased dnaE2 expression. FEMS Microbiol. Lett.

Bernstein, J.A., Lin, P.H., Cohen, S.N., and Lin-Chao, S. (2004). Global analysis of Escherichia coli RNA degradosome function using DNA microarrays. Proc. Natl. Acad. Sci. U. S. A. *101*, 2758–2763.

Betts, J.C., Lukey, P.T., Robb, L.C., McAdam, R.A., and Duncan, K. (2002). Evaluation of a nutrient starvation model of Mycobacterium tuberculosis persistence by gene and protein expression profiling. Mol. Microbiol.

Bhaskar, A., De Piano, C., Gelman, E., McKinney, J.D., and Dhar, N. (2018). Elucidating the role of (p)ppGpp in mycobacterial persistence against antibiotics. IUBMB Life *70*, 836–844.

Bigger, J.W. (1944). Treatment of Staphylococcal Infections With Penicillin By Intermittent Sterilisation. Lancet *244*, 497–500.

Van Boxtel, C., Van Heerden, J.H., Nordholt, N., Schmidt, P., and Bruggeman, F.J. (2017). Taking chances and making mistakes: Non-genetic phenotypic heterogeneity and its consequences for surviving in dynamic environments. J. R. Soc. Interface *14*.

Brantl, S. (2007). Regulatory mechanisms employed by cis-encoded antisense RNAs. Curr. Opin. Microbiol.

Brantl, S. (2012). Acting antisense: Plasmid- and chromosome-encoded sRNAs from Gram-positive bacteria. Future Microbiol.

Browning, D.F., and Busby, S.J.W. (2016). Local and global regulation of transcription initiation in bacteria. Nat. Rev. Microbiol.

Bruce, H.A., Du, D., Matak-Vinkovic, D., Bandyra, K.J., Broadhurst, R.W., Martin, E., Sobott, F., Shkumatov, A. V., and Luisi, B.F. (2018). Analysis of the natively unstructured RNA/protein-recognition core in the Escherichia coli RNA degradosome and its interactions with regulatory RNA/Hfq complexes. Nucleic Acids Res. *46*, 387–402.

Burgess Tornaletti, L., and Manina, G. (2020). Delving Into the Functional Meaning of Phenotypic Variation in Mycobacterial Persistence: Who Benefits the Most From Programmed Death of Individual Cells? Microbiol. Insights.

Burgos, M. V., Méndez, J.C., and Ribon, W. (2004). Molecular epidemiology of tuberculosis: methodology and applications. Biomedica.

Buskilay, A.A.A., Kannaiahy, S., and Amster-Choder, O. (2014). RNA localization in bacteria. RNA Biol. *11*, 1051–1060.

Bussi, C., and Gutierrez, M.G. (2019). Mycobacterium tuberculosis infection of host cells in space and time. FEMS Microbiol. Rev. *43*, 341–361.

Cabrera, J.E., Cagliero, C., Quan, S., Squires, C.L., and Ding, J.J. (2009). Active transcription of rRNA operons condenses the nucleoid in Escherichia coli: Examining the effect of transcription on nucleoid structure in the absence of transertion. J. Bacteriol.

Cadena, C.D., Zapata, F., and Jiménez, I. (2018). Issues and Perspectives in Species Delimitation using Phenotypic Data: Atlantean Evolution in Darwin's Finches. Syst. Biol.

Callaghan, A.J., Marcaida, M.J., Stead, J.A., McDowall, K.J., Scott, W.G., and Luisi, B.F. (2005). Structure of Escherichia coli RNase E catalytic domain and implications for RNA turnover. Nature *437*, 1187–1191.

Cambier, C.J., Takaki, K.K., Larson, R.P., Hernandez, R.E., Tobin, D.M., Urdahl, K.B., Cosma, C.L., and Ramakrishnan, L. (2014). Mycobacteria manipulate macrophage recruitment through coordinated use of membrane lipids. Nature.

Del Campo, C., Bartholomäus, A., Fedyunin, I., and Ignatova, Z. (2015). Secondary Structure across the Bacterial Transcriptome Reveals Versatile Roles in mRNA Regulation and Function. PLoS Genet.

Campos, M., and Jacobs-Wagner, C. (2013). Cellular organization of the transfer of genetic information. Curr. Opin. Microbiol.

Catanho, M., Mascarenhas, D., Degrave, W., and Miranda, A.B. de (2006). GenoMycDB: a database for comparative analysis of mycobacterial genes and genomes. Genet. Mol. Res.

Chakraborty, P., and Kumar, A. (2019). The extracellular matrix of mycobacterial biofilms: Could we shorten the treatment of mycobacterial infections? Microb. Cell *6*, 105–122.

Chandran, V., Poljak, L., Vanzo, N.F., Leroy, A., Miguel, R.N., Fernandez-Recio, J., Parkinson, J., Burns, C., Carpousis, A.J., and Luisi, B.F. (2007). Recognition and Cooperation Between the ATP-dependent RNA Helicase RhlB and Ribonuclease RNase E. J. Mol. Biol.

Chao, M.C., and Rubin, E.J. (2010). Letting sleeping dos lie: Does dormancy play a role in tuberculosis? Annu. Rev. Microbiol. *64*, 293–311.

Chao, Y., Papenfort, K., Reinhardt, R., Sharma, C.M., and Vogel, J. (2012). An atlas of Hfq-bound transcripts reveals 3′ UTRs as a genomic reservoir of regulatory small RNAs. EMBO J.

Chao, Y., Li, L., Girodat, D., Förstner, K.U., Said, N., Corcoran, C., Śmiga, M., Papenfort, K., Reinhardt, R., Wieden, H.J., et al. (2017). In Vivo Cleavage Map Illuminates the Central Role of RNase E in Coding and Non-coding RNA Pathways. Mol. Cell.

Cho, K.H. (2017). The structure and function of the gram-positive bacterial RNA degradosome. Front. Microbiol.

Chowdhury, N., Kwan, B.W., and Wood, T.K. (2016). Persistence Increases in the Absence of the Alarmone Guanosine Tetraphosphate by Reducing Cell Growth. Sci. Rep. *6*, 1–9.

Christensen, S.K., Mikkelsen, M., Pedersen, K., and Gerdes, K. (2001). RelE, a global inhibitor of translation, is activated during nutritional stress. Proc. Natl. Acad. Sci. U. S. A. *98*, 14328–14333.

Clarke, J.E., Kime, L., Romero A., D., and McDowall, K.J. (2014). Direct entry by RNase e is a major pathway for the degradation and processing of RNA in Escherichia coli. Nucleic Acids Res. *42*, 11733–11751.

Claudi, B., Spröte, P., Chirkova, A., Personnic, N., Zankl, J., Schürmann, N., Schmidt, A., and Bumann, D. (2014). Phenotypic variation of salmonella in host tissues delays eradication by antimicrobial chemotherapy. Cell.

Clemens, D.L., and Horwitz, M.A. (1996). The Mycobacterium tuberculosis phagosome interacts with early endosomes and is accessible to exogenously administered transferrin. J. Exp. Med. *184*, 1349–1355.

Cohen, N.R., Lobritz, M.A., and Collins, J.J. (2013). Microbial persistence and the road to drug resistance. Cell Host Microbe.

Colangeli, R., Helb, D., Vilchèze, C., Hazbón, M.H., Lee, C.G., Safi, H., Sayers, B., Sardone, I., Jones, M.B., Fleischmann, R.D., et al. (2007). Transcriptional regulation of multi-drug tolerance and antibiotic-induced responses by the histone-like protein Lsr2 in M. tuberculosis. PLoS Pathog. *3*, 0780–0793.

Cole, S.T., Brosch, R., Parkhill, J., Garnier, T., Churcher, C., Harris, D., Gordon, S. V., Eiglmeier, K., Gas, S., Barry, C.E., et al. (1998). Deciphering the biology of mycobacterium tuberculosis from the complete genome sequence. Nature.

Comas, I., Borrell, S., Roetzer, A., Rose, G., Malla, B., Kato-Maeda, M., Galagan, J., Niemann, S., and Gagneux, S. (2012). Whole-genome sequencing of rifampicin-resistant Mycobacterium tuberculosis strains identifies compensatory

mutations in RNA polymerase genes. Nat. Genet.

Cook, G.M., Berney, M., Gebhard, S., Heinemann, M., Cox, R.A., Danilchanka, O., and Niederweis, M. (2009). Physiology of Mycobacteria (Elsevier).

Cook, G.M., Robson, J.R., Frampton, R.A., McKenzie, J., Przybilski, R., Fineran, P.C., and Arcus, V.L. (2013). Ribonucleases in bacterial toxin-antitoxin systems. Biochim. Biophys. Acta - Gene Regul. Mech.

Cormack, R.S., Genereaux, J.L., and Mackie, G.A. (1993). RNase E activity is conferred by a single polypeptide: Overexpression, purification, and properties of the ams/rne/hmp1 gene product. Proc. Natl. Acad. Sci. U. S. A. *90*, 9006–9010.

Cortes, T., Schubert, O.T., Rose, G., Arnvig, K.B., Comas, I., Aebersold, R., and Young, D.B. (2013). Genome-wide Mapping of Transcriptional Start Sites Defines an Extensive Leaderless Transcriptome in Mycobacterium tuberculosis. Cell Rep. *5*, 1121–1131.

Cox, E., and Laessig, K. (2014). FDA approval of bedaquiline - The benefit-risk balance for drug-resistant tuberculosis. N. Engl. J. Med.

Cox, J., Neuhauser, N., Michalski, A., Scheltema, R.A., Olsen, J. V., and Mann, M. (2011). Andromeda: A peptide search engine integrated into the MaxQuant environment. J. Proteome Res.

Cox, J., Hein, M.Y., Luber, C.A., Paron, I., Nagaraj, N., and Mann, M. (2014). Accurate proteome-wide label-free quantification by delayed normalization and maximal peptide ratio extraction, termed MaxLFQ. Mol. Cell. Proteomics.

Cronan, M.R., and Tobin, D.M. (2014). Fit for consumption: Zebrafish as a model for tuberculosis. DMM Dis. Model. Mech.

Daffé, M., and Etienne, G. (1999). The capsule of Mycobacterium tuberculosis and its implications for pathogenicity. Tuber. Lung Dis.

Daniel, T.M. (2000). The origins and precolonial epidemiology of tuberculosis in the Americas: Can we figure them out? Int. J. Tuberc. Lung Dis. *4*, 395–400.

Daniel, T.M. (2005a). Robert Koch and the pathogenesis of tuberculosis. Int. J. Tuberc. Lung Dis. *9*, 1181–1182.

Daniel, T.M. (2005b). Leon Charles Albert Calmette and BCG vaccine. Int. J. Tuberc. Lung Dis. *9*, 944–945.

Daniel, T.M. (2006). The history of tuberculosis. Respir. Med. *100*, 1862–1870.

Daniel, T.M. (2011). Hermann Brehmer and the origins of tuberculosis sanatoria. Int. J. Tuberc. Lung Dis. *15*, 161–162.

Datta, C., Jha, R.K., Ahmed, W., Ganguly, S., Ghosh, S., and Nagaraja, V. (2019). Physical and functional interaction between nucleoid-associated proteins HU and Lsr2 of Mycobacterium tuberculosis: altered DNA binding and gene regulation. Mol. Microbiol.

Davies RPO, Tocque, K., Bellis, M.A., Remmington, T., and Davies PDO (1999). Historical declines in tuberculosis in England and Wales: improving social conditions or natural selection? Vesalius.

Davis, J.M., and Ramakrishnan, L. (2009). The Role of the Granuloma in Expansion and Dissemination of Early Tuberculous Infection. Cell *136*, 37–49.

Deana, A., and Belasco, J.G. (2005). Lost in translation: The influence of ribosomes on bacterial mRNA decay. Genes Dev. *19*, 2526–2533.

Deana, A., Celesnik, H., and Belasco, J.G. (2008). The bacterial enzyme RppH triggers messenger RNA degradation by 5′ pyrophosphate removal. Nature *451*, 355–358.

Dejesus, M.A., Gerrick, E.R., Xu, W., Park, S.W., Long, J.E., Boutte, C.C., Rubin, E.J., Schnappinger, D., Ehrt, S., Fortune, S.M., et al. (2017). Comprehensive essentiality analysis of the Mycobacterium tuberculosis genome via saturating transposon mutagenesis. MBio.

Delogu, G., and Goletti, D. (2014). The spectrum of tuberculosis infection: New perspectives in the era of biologics. J. Rheumatol. *41*, 11–16.

Dendooven, T., Van den Bossche, A., Hendrix, H., Ceyssens, P.J., Voet, M., Bandyra, K.J., De Maeyer, M., Aertsen, A., Noben,

J.P., Hardwick, S.W., et al. (2017). Viral interference of the bacterial RNA metabolism machinery. RNA Biol. *14*, 6–10.

Deshayes, C., Perrodou, E., Gallien, S., Euphrasie, D., Schaeffer, C., Van-Dorsselaer, A., Poch, O., Lecompte, O., and Reyrat, J.M. (2007). Interrupted coding sequences in Mycobacterium smegmatis: Authentic mutations or sequencing errors? Genome Biol.

Deutscher, M.P. (2015). Twenty years of bacterial RNases and RNA processing: How we've matured. Rna *21*, 597–600.

Dhar, N., and McKinney, J.D. (2007). Microbial phenotypic heterogeneity and antibiotic tolerance. Curr. Opin. Microbiol. *10*, 30–38.

Dhar, N., McKinney, J., and Manina, G. (2016). Phenotypic Heterogeneity in Mycobacterium tuberculosis. Microbiol. Spectr. *4*, 1–27.

Dheda, K., Gumbo, T., Gandhi, N.R., Murray, M., Theron, G., Udwadia, Z., Migliori, G.B., and Warren, R. (2014). Global control of tuberculosis: From extensively drug-resistant to untreatable tuberculosis. Lancet Respir. Med.

Dillon, S.C., and Dorman, C.J. (2010). Bacterial nucleoid-associated proteins, nucleoid structure and gene expression. Nat. Rev. Microbiol.

Diwa, A., Bricker, A.L., Jain, C., and Belasco, J.G. (2000). An evolutionarily conserved RNA stem-loop functions as a sensor that directs feedback regulation of RNase E gene expression. Genes Dev. *14*, 1249–1260.

Dockrell, H.M., and Smith, S.G. (2017). What have we learnt about BCG vaccination in the last 20 years? Front. Immunol. *8*, 1–10.

Donald, P.R., Marais, B.J., and Barry, C.E. (2010). Age and the epidemiology and pathogenesis of tuberculosis. Lancet *375*, 1852–1854.

Drain, P.K., Bajema, K.L., Dowdy, D., Dheda, K., Naidoo, K., Schumacher, S.G., Ma, S., Meermeier, E., Lewinsohn, D.M., and Sherman, D.R. (2018). Incipient and subclinical tuberculosis: A clinical review of early stages and progression of infection. Clin. Microbiol. Rev. *31*, 1–24.

Ducati, R.G., Ruffino-Netto, A., Basso, L.A., and Santos, D.S. (2006). The resumption of consumption - A review on tuberculosis. Mem. Inst. Oswaldo Cruz *101*, 697–714.

Dulberger, C.L., Rubin, E.J., and Boutte, C.C. (2020). The mycobacterial cell envelope — a moving target. Nat. Rev. Microbiol.

Durand, S., and Condon, C. (2018). RNases and Helicases in Gram-Positive Bacteria. Regul. with RNA Bact. Archaea 37–53.

Durand, S., Gilet, L., Bessières, P., Nicolas, P., and Condon, C. (2012a). Three essential ribonucleases-RNase Y, J1, and III-control the abundance of a majority of bacillus subtilis mRNAs. PLoS Genet.

Durand, S., Gilet, L., and Condon, C. (2012b). The Essential Function of B. subtilis RNase III Is to Silence Foreign Toxin Genes. PLoS Genet.

Durand, S., Tomasini, A., Braun, F., Condon, C., and Romby, P. (2015). sRNA and mRNA turnover in gram-positive bacteria. FEMS Microbiol. Rev. *39*, 316–330.

Edelmann, D., and Berghoff, B.A. (2019). Type I toxin-dependent generation of superoxide affects the persister life cycle of Escherichia coli. Sci. Rep. *9*, 1–10.

Ehrt, S., Schnappinger, D., and Rhee, K.Y. (2018). Metabolic principles of persistence and pathogenicity in Mycobacterium tuberculosis. Nat. Rev. Microbiol. *16*, 496–507.

Eldar, A., and Elowitz, M.B. (2010). Functional roles for noise in genetic circuits. Nature.

Elowitz, M.B., Levine, A.J., Siggia, E.D., and Swain, P.S. (2002). Stochastic gene expression in a single cell. Science (80-.).

van Embden, J.D.A., van Soolingen, D., Small, P.M., and Hermans, P.W.M. (1992). Genetic markers for the epidemiology of tuberculosis. Res. Microbiol. *143*, 385–391.

Erce, M.A., Low, J.K.K., and Wilkins, M.R. (2010). Analysis of the RNA degradosome complex in Vibrio angustum S14.

FEBS J. *277*, 5161–5173.

Ernst, J.D. (2012). The immunological life cycle of tuberculosis. Nat. Rev. Immunol.

Esmail, H., Barry, C.E., Young, D.B., and Wilkinson, R.J. (2014). The ongoing challenge of latent tuberculosis. Philos. Trans. R. Soc. B Biol. Sci. *369*.

Fallahi-Sichani, M., El-Kebir, M., Marino, S., Kirschner, D.E., and Linderman, J.J. (2011). Multiscale Computational Modeling Reveals a Critical Role for TNF-α Receptor 1 Dynamics in Tuberculosis Granuloma Formation. J. Immunol. *186*, 3472–3483.

Fei, J., and Sharma, C.M. (2018). RNA Localization in Bacteria. In Regulating with RNA in Bacteria and Archaea, p.

Figaro, S., Durand, S., Gilet, L., Cayet, N., Sachse, M., and Condon, C. (2013). Bacillus subtilis mutants with knockouts of the genes encoding ribonucleases RNase Y and RNase J1 are viable, with major defects in cell morphology, sporulation, and competence. J. Bacteriol.

Fisher, R.A., Gollan, B., and Helaine, S. (2017). Persistent bacterial infections and persister cells. Nat. Rev. Microbiol. *15*, 453–464.

Flentie, K., Garner, A.L., and Stallings, C.L. (2016). Mycobacterium tuberculosis transcription machinery: Ready to respond to host attacks. J. Bacteriol. *198*, 1360–1373.

Ford, C.B., Lin, P.L., Chase, M.R., Shah, R.R., Iartchouk, O., Galagan, J., Mohaideen, N., Ioerger, T.R., Sacchettini, J.C., Lipsitch, M., et al. (2011). Use of whole genome sequencing to estimate the mutation rate of Mycobacterium tuberculosis during latent infection. Nat. Genet.

Forti, F., Mauri, V., Deh, G., and Ghisotti, D. (2011). Isolation of conditional expression mutants in Mycobacterium tuberculosis by transposon mutagenesis. Tuberculosis.

Fry, S.H., Barnabas, S., and Cotton, M.F. (2019). Tuberculosis and HIV - An update on the "cursed duet" in children. Front. Pediatr. *7*, 1–12.

Gagneux, S. (2012). Host-pathogen coevolution in human tuberculosis. Philos. Trans. R. Soc. B Biol. Sci. *367*, 850–859.

Gagneux, S. (2018). Ecology and evolution of Mycobacterium tuberculosis. Nat. Rev. Microbiol.

Gagneux, S., Long, C.D., Small, P.M., Van, T., Schoolnik, G.K., and Bohannan, B.J.M. (2006). The competitive cost of antibiotic resistance in Mycobacterium tuberculosis. Science (80-.). *312*, 1944–1946.

Gandotra, S., Schnappinger, D., Monteleone, M., Hillen, W., and Ehrt, S. (2007). In vivo gene silencing identifies the Mycobacterium tuberculosis proteasome as essential for the bacteria to persist in mice. Nat. Med.

Garrey, S.M., and Mackie, G.A. (2011). Roles of the 5'-phosphate sensor domain in RNase E. Mol. Microbiol. *80*, 1613–1624.

Garrey, S.M., Blech, M., Riffell, J.L., Hankins, J.S., Stickney, L.M., Diver, M., Hsu, Y.H.R., Kunanithy, V., and Mackie, G.A. (2009). Substrate binding and active site residues in RNases E and G: Role of the 5′-sensor. J. Biol. Chem. *284*, 31843–31850.

Gengenbacher, M., and Kaufmann, S.H.E. (2012). Mycobacterium tuberculosis: Success through dormancy. FEMS Microbiol. Rev. *36*, 514–532.

Germain, E., Castro-Roa, D., Zenkin, N., and Gerdes, K. (2013). Molecular Mechanism of Bacterial Persistence by HipA. Mol. Cell *52*, 248–254.

Germain, E., Roghanian, M., Gerdes, K., and Maisonneuve, E. (2015). Stochastic induction of persister cells by HipA through (p)ppGpp-mediated activation of mRNA endonucleases. Proc. Natl. Acad. Sci. U. S. A. *112*, 5171–5176.

Gerrick, E.R., Barbier, T., Chase, M.R., Xu, R., François, J., Lin, V.H., Szucs, M.J., Rock, J.M., Ahmad, R., Tjaden, B., et al. (2018). Small RNA profiling in mycobacterium tuberculosis identifies mrsi as necessary for an anticipatory iron sparing response. Proc. Natl. Acad. Sci. U. S. A. *115*, 6464–6469.

Getahun, H., Kittikraisak, W., Heilig, C.M., Corbett, E.L., Ayles, H., Cain, K.P., Grant, A.D., Churchyard, G.J., Kimerling, M., Shah, S., et al. (2011). Development of a standardized screening rule for tuberculosis in people living with HIV in

resource-constrained settings: Individual participant data meta-analysis of observational studies. PLoS Med. *8*.

Giai Gianetto, Q., Combes, F., Ramus, C., Bruley, C., Couté, Y., and Burger, T. (2016). Calibration plot for proteomics: A graphical tool to visually check the assumptions underlying FDR control in quantitative experiments. Proteomics.

Gibson, S.E.R., Harrison, J., and Cox, J.A.G. (2018). Modelling a silent epidemic: A review of the in vitro models of latent tuberculosis. Pathogens.

Gideon, H.P., and Flynn, J.L. (2011). Latent tuberculosis: What the host "sees"? Immunol. Res. *50*, 202–212.

Glickman, M.S., and Jacobs, W.R. (2001). Microbial pathogenesis of Mycobacterium tuberculosis: Dawn of a discipline. Cell *104*, 477–485.

Go, H., Moore, C.J., Lee, M., Shin, E., Jeon, C.O., Cha, N.J., Han, S.H., Kim, S.J., Lee, S.W., Lee, Y., et al. (2011). Upregulation of RNase E activity by mutation of a site that uncompetitively interferes with RNA binding. RNA Biol.

Goeders, N., Drèze, P.L., and Van Melderen, L. (2013). Relaxed cleavage specificity within the rele toxin family. J. Bacteriol.

Golding, I., and Cox, E.C. (2004). RNA dynamics in live Escherichia coli cells. Proc. Natl. Acad. Sci. U. S. A. *101*, 11310–11315.

Gollan, B., Grabe, G., Michaux, C., and Helaine, S. (2019). Bacterial persisters and infection: Past, present, and progressing. Annu. Rev. Microbiol.

Gomes, M.G.M., Águas, R., Lopes, J.S., Nunes, M.C., Rebelo, C., Rodrigues, P., and Struchiner, C.J. (2012). How host heterogeneity governs tuberculosis reinfection? Proc. R. Soc. B Biol. Sci.

Gomez, J.E., and McKinney, J.D. (2004). M. tuberculosis persistence, latency, and drug tolerance. In Tuberculosis, p.

González-Escalante, L., Peñuelas-Urquides, K., Said-Fernández, S., Silva-Ramírez, B., and de León, M.B. (2015). Differential expression of putative drug resistance genes in Mycobacterium tuberculosis clinical isolates. FEMS Microbiol. Lett.

Gordon, B.R.G., Li, Y., Wang, L., Sintsova, A., Van Bakel, H., Tian, S., Navarre, W.W., Xia, B., and Liu, J. (2010). Lsr2 is a nucleoid-associated protein that targets AT-rich sequences and virulence genes in Mycobacterium tuberculosis. Proc. Natl. Acad. Sci. U. S. A.

Górna, M.W., Pietras, Z., Tsai, Y.I.C., Callaghan, A.J., Hernández, H., Robinson, C. V., and Luisi, B.F. (2010). The regulatory protein RraA modulates RNA-binding and helicase activities of the E. coli RNA degradosome. RNA.

Grant, S.S., and Hung, D.T. (2013). Persistent bacterial infections, antibiotic tolerance, and the oxidative stress response. Virulence *4*, 273–283.

Griesbeck, O., Baird, G.S., Campbell, R.E., Zacharias, D.A., and Tsien, R.Y. (2001). Reducing the environmental sensitivity of yellow fluorescent protein. Mechanism and applications. J. Biol. Chem.

Gubbins, M.J., Arthur, D.C., Ghetu, A.F., Glover, J.N.M., and Frost, L.S. (2003). Characterizing the structural features of RNA/RNA interactions of the F-plasmid FinOP fertility inhibition system. J. Biol. Chem. *278*, 27663–27671.

Guex, N., Peitsch, M.C., and Schwede, T. (2009). Automated comparative protein structure modeling with SWISS-MODEL and Swiss-PdbViewer: A historical perspective. Electrophoresis.

Gupta, M., Sajid, A., Sharma, K., Ghosh, S., Arora, G., Singh, R., Nagaraja, V., Tandon, V., and Singh, Y. (2014). HupB, a nucleoid-associated protein of mycobacterium tuberculosis, is modified by serine/threonine protein kinases in vivo. J. Bacteriol.

Das Gupta, S.K., Bashyam, M.D., and Tyagi, A.K. (1993). Cloning and assessment of mycobacterial promoters by using a plasmid shuttle vector. J. Bacteriol.

Hadjeras, L., Poljak, L., Bouvier, M., Morin-Ogier, Q., Canal, I., Cocaign-Bousquet, M., Girbal, L., and Carpousis, A.J. (2019). Detachment of the RNA degradosome from the inner membrane of Escherichia coli results in a global slowdown of mRNA degradation, proteolysis of RNase E and increased turnover of ribosome-free transcripts. Mol. Microbiol.

Hambraeus, G., Von Wachenfeldt, C., and Hederstedt, L. (2003). Genome-wide survey of mRNA half-lives in Bacillus

subtilis identifies extremely stable mRNAs. Mol. Genet. Genomics.

Hansen, S., Lewis, K., and Vulić, M. (2008). Role of global regulators and nucleotide metabolism in antibiotic tolerance in Escherichia coli. Antimicrob. Agents Chemother. *52*, 2718–2726.

Hansen, S., Vulić, M., Min, J., Yen, T.J., Schumacher, M.A., Brennan, R.G., and Lewis, K. (2012). Regulation of the Escherichia coli HipBA toxin-antitoxin system by proteolysis. PLoS One *7*.

Hao, W., Schlesinger, L.S., and Friedman, A. (2016). Modeling granulomas in response to infection in the lung. PLoS One.

Hardwick, S.W., Chan, V.S.Y., Broadhurst, R.W., and Luisi, B.F. (2011). An RNA degradosome assembly in Caulobacter crescentus. Nucleic Acids Res.

Harms, A., Maisonneuve, E., and Gerdes, K. (2016). Mechanisms of bacterial persistence during stress and antibiotic exposure. Science (80-.). *354*.

Harms, A., Fino, C., Sørensen, M.A., Semsey, S., and Gerdes, K. (2017a). Prophages and growth dynamics confound experimental results with antibiotic-tolerant persister cells. MBio *8*, 1–18.

Harms, A., Liesch, M., Körner, J., Québatte, M., Engel, P., and Dehio, C. (2017b). A bacterial toxin-antitoxin module is the origin of inter-bacterial and inter-kingdom effectors of Bartonella. PLoS Genet.

Hauryliuk, V., Atkinson, G.C., Murakami, K.S., Tenson, T., and Gerdes, K. (2015). Recent functional insights into the role of (p)ppGpp in bacterial physiology. Nat. Rev. Microbiol.

Hayashi, J.M., Luo, C.Y., Mayfield, J.A., Hsu, T., Fukuda, T., Walfield, A.L., Giffen, S.R., Leszyk, J.D., Baer, C.E., Bennion, O.T., et al. (2016). Spatially distinct and metabolically active membrane domain in mycobacteria. Proc. Natl. Acad. Sci. U. S. A.

Hayman, J. (1984). Mycobacterium Ulcerans: an Infection From Jurassic Time? Lancet *324*, 1015–1016.

Helaine, S., and Kugelberg, E. (2014). Bacterial persisters: Formation, eradication, and experimental systems. Trends Microbiol. *22*, 417–424.

Herbert, D., Paramasivan, C.N., Venkatesan, P., Kubendiran, G., Prabhakar, R., and Mitchison, D.A. (1996). Bactericidal action of ofloxacin, sulbactam-ampicillin, rifampin, and isoniazid on logarithmic- and stationary-phase cultures of Mycobacterium tuberculosis. Antimicrob. Agents Chemother.

Hesper Rego, E., Audette, R.E., and Rubin, E.J. (2017). Deletion of a mycobacterial divisome factor collapses single-cell phenotypic heterogeneity. Nature *546*, 153–157.

Hogan, A.M., Scoffone, V.C., Makarov, V., Gislason, A.S., Tesfu, H., Stietz, M.S., Brassinga, A.K.C., Domaratzki, M., Li, X., Azzalin, A., et al. (2018). Competitive fitness of essential gene knockdowns reveals a broad-spectrum antibacterial inhibitor of the cell division protein FtsZ. Antimicrob. Agents Chemother.

Hogg, T., Mechold, U., Malke, H., Cashel, M., and Hilgenfeld, R. (2004). Conformational antagonism between opposing active sites in a bifunctional RelA/SpoT homolog modulates (p)ppGpp metabolism during the stringent response. Cell *117*, 57–68.

Hołówka, J., Trojanowski, D., Gind, K., Wojtaś, B., Gielniewski, B., Jakimowicz, D., and Zakrzewska-Czerwińska, J. (2017). HupB is a bacterial nucleoid-associated protein with an indispensable eukaryotic-like tail. MBio.

Hör, J., Gorski, S.A., and Vogel, J. (2018). Bacterial RNA Biology on a Genome Scale. Mol. Cell *70*, 785–799.

Houben, R.M.G.J., and Dodd, P.J. (2016). The Global Burden of Latent Tuberculosis Infection: A Re-estimation Using Mathematical Modelling. PLoS Med. *13*, 1–13.

Houghton, J., Cortes, T., Schubert, O., Rose, G., Rodgers, A., De Ste Croix, M., Aebersold, R., Young, D.B., and Arnvig, K.B. (2013). A small RNA encoded in the Rv2660c locus of Mycobacterium tuberculosis is induced during starvation and infection. PLoS One *8*.

Hsieh, P.K., Richards, J., Liu, Q., and Belasco, J.G. (2013). Specificity of RppH-dependent RNA degradation in Bacillus subtilis. Proc. Natl. Acad. Sci. U. S. A. *110*, 8864–8869.

Hu, Y., Coates, A.R.M., and Mitchison, D.A. (2003). Sterilizing activities of fluoroquinolones against rifampin-tolerant

populations of Mycobacterium tuberculosis. Antimicrob. Agents Chemother. *47*, 653–657.

Hui, M.P., Foley, P.L., and Belasco, J.G. (2014). Messenger RNA degradation in bacterial cells. Annu. Rev. Genet.

Ignatov, D. V., Salina, E.G., Fursov, M. V., Skvortsov, T.A., Azhikina, T.L., and Kaprelyants, A.S. (2015). Dormant non-culturable Mycobacterium tuberculosis retains stable low-abundant mRNA. BMC Genomics.

Ihms, E.A., Urbanowski, M.E., and Bishai, W.R. (2018). Diverse Cavity Types and Evidence that Mechanical Action on the Necrotic Granuloma Drives Tuberculous Cavitation. Am. J. Pathol. *188*, 1666–1675.

Ikeda, Y., Yagi, M., Morita, T., and Aiba, H. (2011). Hfq binding at RhlB-recognition region of RNase E is crucial for the rapid degradation of target mRNAs mediated by sRNAs in Escherichia coli. Mol. Microbiol. *79*, 419–432.

Irwin, S.M., Driver, E., Lyon, E., Schrupp, C., Ryan, G., Gonzalez-Juarrero, M., Basaraba, R.J., Nuermberger, E.L., and Lenaerts, A.J. (2015). Presence of multiple lesion types with vastly different microenvironments in C3HeB/FeJ mice following aerosol infection with Mycobacterium tuberculosis. DMM Dis. Model. Mech. *8*, 591–602.

J L SEVER, G.P.Y. (1957). Enumeration of viable tubercle bacilli from the organs of nonimmunized and immunized mice. Am Rev Tuberc *76*, 616–635.

Jain, C. (2012). Novel role for RNase PH in the degradation of structured RNA. J. Bacteriol.

Jain, C., and Belasco, J.G. (1995). RNase E autoregulates its synthesis by controlling the degradation rate of its own mRNA in Escherichia coli: Unusual sensitivity of the rne transcript to RNase E activity. Genes Dev.

Javid, B., Sorrentino, F., Toosky, M., Zheng, W., Pinkham, J.T., Jain, N., Pan, M., Deighan, P., and Rubin, E.J. (2014). Mycobacterial mistranslation is necessary and sufficient for rifampicin phenotypic resistance. Proc. Natl. Acad. Sci. U. S. A. *111*, 1132–1137.

Ji -e., Y., Kempsell, K.E., Colston, M.J., and Cox, R.A. (1994). Nucleotide sequences of the spacer-1, spacer-2 and trailer regions of the rrn operons and secondary structures of precursor 23S rRNAs and precursor 5S rRNAs of slow-growing mycobacteria. Microbiology.

Kaberdin, V.R., Walsh, A.P., Jakobsen, T., McDowall, K.J., and Von Gabain, A. (2000). Enhanced cleavage of RNA mediated by an interaction between substrates and the arginine-rich domain of E. coli ribonuclease E. J. Mol. Biol. *301*, 257–264.

Kærn, M., Elston, T.C., Blake, W.J., and Collins, J.J. (2005). Stochasticity in gene expression: From theories to phenotypes. Nat. Rev. Genet.

Kaiser, P., Regoes, R.R., Dolowschiak, T., Wotzka, S.Y., Lengefeld, J., Slack, E., Grant, A.J., Ackermann, M., and Hardt, W.D. (2014). Cecum Lymph Node Dendritic Cells Harbor Slow-Growing Bacteria Phenotypically Tolerant to Antibiotic Treatment. PLoS Biol.

Kalra, P., Mishra, S.K., Kaur, S., Kumar, A., Prasad, H.K., Sharma, T.K., and Tyagi, J.S. (2018). G-Quadruplex-Forming DNA Aptamers Inhibit the DNA-Binding Function of HupB and Mycobacterium tuberculosis Entry into Host Cells. Mol. Ther. - Nucleic Acids.

Kashino, S.S., Napolitano, D.R., Skobe, Z., and Campos-Neto, A. (2008). Guinea pig model of Mycobacterium tuberculosis latent/dormant infection. Microbes Infect.

Katoch, V.M. (2019). Pathogenicity and Drug Resistance of Human Pathogens (Singapore: Springer Singapore).

Kawamoto, H., Morita, T., Shimizu, A., Inada, T., and Aiba, H. (2005). Implication of membrane localization of target mRNA in the action of a small RNA: Mechanism of post-transcriptional regulation of glucose transporter in Escherichia coli. Genes Dev.

Keiler, K.C. (2011). RNA localization in bacteria. Curr. Opin. Microbiol.

Kennell, D. (2002). Processing endoribonucleases and mRNA degradation in bacteria. J. Bacteriol.

Khan, F.Y. (2019). Review of literature on disseminated tuberculosis with emphasis on the focused diagnostic workup. J. Family Community Med.

Khemici, V., Toesca, I., Poljak, L., Vanzo, N.F., and Carpousis, A.J. (2004). The RNase E of Escherichia coli has at least two

binding sites for DEAD-box RNA helicases: Functional replacement of RhlB by RhlE. Mol. Microbiol. *54*, 1422–1430.

Khemici, V., Poljak, L., Luisi, B.F., and Carpousis, A.J. (2008). The RNase E of Escherichia coli is a membrane-binding protein. Mol. Microbiol. *70*, 799–813.

Khlebodarova, T.M., and Likhoshvai, V.A. (2018). Persister Cells – a Plausible Outcome of Neutral Coevolutionary Drift. Sci. Rep. *8*, 1–11.

Kim, J.S., and Wood, T.K. (2016). Persistent persister misperceptions. Front. Microbiol. *7*, 1–7.

Kim, D., Song, S., Lee, M., Go, H., Shin, E., Yeom, J.H., Ha, N.C., Lee, K., and Kim, Y.H. (2014). Modulation of RNase E activity by alternative RNA binding sites. PLoS One.

Kime, L., Vincent, H.A., Gendoo, D.M.A., Jourdan, S.S., Fishwick, C.W.G., Callaghan, A.J., and McDowall, K.J. (2015). The first small-molecule inhibitors of members of the ribonuclease E family. Sci. Rep.

Kint, C., Verstraeten, N., Hofkens, J., Fauvart, M., and Michiels, J. (2014). Bacterial Obg proteins: GTPases at the nexus of protein and DNA synthesis. Crit. Rev. Microbiol.

Kiran, D., Podell, B.K., Chambers, M., and Basaraba, R.J. (2016). Host-directed therapy targeting the Mycobacterium tuberculosis granuloma: a review. Semin. Immunopathol.

Komorowski, M., Miękisz, J., and Kierzek, A.M. (2009). Translational repression contributes greater noise to gene expression than transcriptional repression. Biophys. J.

Korch, S.B., Contreras, H., and Clark-Curtiss, J.E. (2009). Three Mycobacterium tuberculosis rel toxin-antitoxin modules inhibit mycobacterial growth and are expressed in infected human macrophages. J. Bacteriol. *191*, 1618–1630.

Koslover, D.J., Callaghan, A.J., Marcaida, M.J., Garman, E.F., Martick, M., Scott, W.G., and Luisi, B.F. (2008). The Crystal Structure of the Escherichia coli RNase E Apoprotein and a Mechanism for RNA Degradation. Structure *16*, 1238–1244.

Kovacs, L., Csanadi, A., Megyeri, K., Kaberdin, V.R., and Miczak, A. (2005). Mycobacterial RNase E-associated proteins. Microbiol. Immunol.

Kremer, K., Van Soolingen, D., Frothingham, R., Haas, W.H., Hermans, P.W.M., Martín, C., Palittapongarnpim, P., Plikaytis, B.B., Riley, L.W., Yakrus, M.A., et al. (1999). Comparison of methods based on different molecular epidemiological markers for typing of Mycobacterium tuberculosis complex strains: Interlaboratory study of discriminatory power and reproducibility. J. Clin. Microbiol. *37*, 2607–2618.

Kriel, A., Bittner, A.N., Kim, S.H., Liu, K., Tehranchi, A.K., Zou, W.Y., Rendon, S., Chen, R., Tu, B.P., and Wang, J.D. (2012). Direct regulation of GTP homeostasis by (p)ppGpp: A critical component of viability and stress resistance. Mol. Cell.

Kriel, N.L., Gallant, J., van Wyk, N., van Helden, P., Sampson, S.L., Warren, R.M., and Williams, M.J. (2018). Mycobacterial nucleoid associated proteins: An added dimension in gene regulation. Tuberculosis.

Kumar, A., Toledo, J.C., Patel, R.P., Lancaster, J.R., and Steyn, A.J.C. (2007). Mycobacterium tuberculosis DosS is a redox sensor and DosT is a hypoxia sensor. Proc. Natl. Acad. Sci. U. S. A. *104*, 11568–11573.

Kumar, S., Sardesai, A.A., Basu, D., Muniyappa, K., and Hasnain, S.E. (2010). DNA clasping by mycobacterial HU: The c-terminal region of HupB mediates increased specificity of DNA binding. PLoS One.

Kumar, S.K., Singh, P., and Sinha, S. (2015). Naturally produced opsonizing antibodies restrict the survival of Mycobacterium tuberculosis in human macrophages by augmenting phagosome maturation. Open Biol.

Kumar, V., Tomar, A.K., Sahu, V., Dey, S., and Yadav, S. (2017). Structural insights of Mycobacterium GTPase-Obg and anti-sigma-F factor Usfx interaction. J. Mol. Recognit. *30*, 1–8.

Künne, T., Swarts, D.C., and Brouns, S.J.J. (2014). Planting the seed: Target recognition of short guide RNAs. Trends Microbiol.

Kussell, E. (2013). Evolution in microbes. Annu. Rev. Biophys. *42*, 493–514.

Kussell, E., and Leibler, S. (2005). Ecology: Phenotypic diversity, population growth, and information in fluctuating environments. Science (80-.). *309*, 2075–2078.

De La Salmonière, Y.O.G., Li, H.M., Torrea, G., Bunschoten, A., Van Embden, J., and Gicquel, B. (1997). Evaluation of spoligotyping in a study of the transmission of Mycobacterium tuberculosis. J. Clin. Microbiol. *35*, 2210–2214.

Laalami, S., and Putzer, H. (2011). MRNA degradation and maturation in prokaryotes: The global players. Biomol. Concepts.

Laalami, S., Zig, L., and Putzer, H. (2014). Initiation of mRNA decay in bacteria. Cell. Mol. Life Sci. *71*, 1799–1828.

Lahav, G., Rosenfeld, N., Sigal, A., Geva-Zatorsky, N., Levine, A.J., Elowitz, M.B., and Alon, U. (2004). Dynamics of the p53-Mdm2 feedback loop in individual cells. Nat. Genet.

Laloux, G., and Jacobs-Wagner, C. (2014). How do bacteria localize proteins to the cell pole? J. Cell Sci.

Lambert, G., and Kussel, E. (2014). Memory and Fitness Optimization of Bacteria under Fluctuating Environments. PLoS Genet. *10*.

Lee, K., Zhan, X., Gao, J., Qiu, J., Feng, Y., Meganathan, R., Cohen, S.N., and Georgiou, G. (2003). RraA: A protein inhibitor of RNase E activity that globally modulates RNA abundance in E. coli. Cell.

Lehnik-Habrink, M., Newman, J., Rothe, F.M., Solovyova, A.S., Rodrigues, C., Herzberg, C., Commichau, F.M., Lewis, R.J., and Stülke, J. (2011). RNase Y in Bacillus subtilis: A natively disordered protein that is the functional equivalent of RNase E from Escherichia coli. J. Bacteriol.

Lenaerts, A., Barry, C.E., and Dartois, V. (2015). Heterogeneity in tuberculosis pathology, microenvironments and therapeutic responses. Immunol. Rev.

Levien, E., Kondev, J., and Amir, A. (2020). Quantifying phenotypic variability and fitness in finite microbial populations. Interface.

Lewis, K. (2010). Persister cells. Annu. Rev. Microbiol. *64*, 357–372.

Li, Y., and Altman, S. (2003). A specific endoribonuclease, RNase P, affects gene expression of polycistronic operon mRNAs. Proc. Natl. Acad. Sci. U. S. A.

Li, Z., and Deutscher, M.P. (2004). Exoribonucleases and Endoribonucleases. EcoSal Plus.

Lifescience, H. (2016). Tuberculosis … tuberculosis and its resistances. 1–4.

Lim, H.N., and Van Oudenaarden, A. (2007). A multistep epigenetic switch enables the stable inheritance of DNA methylation states. Nat. Genet. *39*, 269–275.

Lin, P.L., Ford, C.B., Coleman, M.T., Myers, A.J., Gawande, R., Ioerger, T., Sacchettini, J., Fortune, S.M., and Flynn, J.L. (2014). Sterilization of granulomas is common in active and latent tuberculosis despite within-host variability in bacterial killing. Nat. Med. *20*, 75–79.

Lin, X., Chongsuvivatwong, V., Lin, L., Geater, A., and Lijuan, R. (2008). Dose-response relationship between treatment delay of smear-positive tuberculosis patients and intra-household transmission: a cross-sectional study. Trans. R. Soc. Trop. Med. Hyg. *102*, 797–804.

Ling, D.I., Zwerling, A.A., and Pai, M. (2008). GenoType MTBDR assays for the diagnosis of multidrug-resistant tuberculosis: A meta-analysis. Eur. Respir. J. *32*, 1165–1174.

Llopis, P.M., Jackson, A.F., Sliusarenko, O., Surovtsev, I., Heinritz, J., Emonet, T., and Jacobs-Wagner, C. (2010). Spatial organization of the flow of genetic information in bacteria. Nature *466*, 77–81.

Lodato, P.B., Thuraisamy, T., Richards, J., and Belasco, J.G. (2017). Effect of RNase E deficiency on translocon protein synthesis in an RNase E-inducible strain of enterohemorrhagic Escherichia coli O157:H7. FEMS Microbiol. Lett.

Logsdon, M.M., Ho, P.Y., Papavinasasundaram, K., Richardson, K., Cokol, M., Sassetti, C.M., Amir, A., and Aldridge, B.B. (2017). A Parallel Adder Coordinates Mycobacterial Cell-Cycle Progression and Cell-Size Homeostasis in the Context of Asymmetric Growth and Organization. Curr. Biol.

Lönnroth, K., Jaramillo, E., Williams, B.G., Dye, C., and Raviglione, M. (2009). Drivers of tuberculosis epidemics: The role

of risk factors and social determinants. Soc. Sci. Med. *68*, 2240–2246.

Luca, S., and Mihaescu, T. (2013). History of BCG Vaccine. Maedica (Buchar). *8*, 53–58.

M Cristina, G., Brisse, S., Brosch, R., Fabre, M., Omaïs, B., Marmiesse, M., Supply, P., and Vincent, V. (2005). Ancient origin and gene mosaicism of the progenitor of Mycobacterium tuberculosis. PLoS Pathog. *1*, 0055–0061.

Mackie, G.A. (2013). RNase E: at the interface of bacterial RNA processing and decay. Nat. Rev. Microbiol. *11*, 45–57.

Magombedze, G., Dowdy, D., and Mulder, N. (2013). Latent Tuberculosis: Models, Computational Efforts and the Pathogen's Regulatory Mechanisms during Dormancy. Front. Bioeng. Biotechnol. *1*, 1–15.

Manabe, Y.C., Kesavan, A.K., Lopez-Molina, J., Hatem, C.L., Brooks, M., Fujiwara, R., Hochstein, K., Pitt, M.L.M., Tufariello, J.A., Chan, J., et al. (2008). The aerosol rabbit model of TB latency, reactivation and immune reconstitution inflammatory syndrome. Tuberculosis.

Manasherob, R., Miller, C., Kim, K. sun, and Cohen, S.N. (2012). Ribonuclease E modulation of the bacterial SOS response. PLoS One *7*.

Manganelli, R., Proveddi, R., Rodrigue, S., Beaucher, J., Gaudreau, L., and Smith, I. (2004). σ Factors and Global Gene Regulation in Mycobacterium tuberculosis. J. Bacteriol.

Manina, G., Dhar, N., and McKinney, J.D. (2015). Stress and host immunity amplify mycobacterium tuberculosis phenotypic heterogeneity and induce nongrowing metabolically active forms. Cell Host Microbe *17*, 32–46.

Manina, G., Griego, A., Singh, L.K.L.K., McKinney, J.D.J.D., and Dhar, N. (2019a). Preexisting variation in DNA damage response predicts the fate of single mycobacteria under stress. EMBO J. *38*, e101876.

Manina, G., Griego, A., Singh, L.K., McKinney, J.D., and Dhar, N. (2019b). Preexisting variation in DNA damage response predicts the fate of single mycobacteria under stress. EMBO J. *38*.

Marakalala, M.J., Raju, R.M., Sharma, K., Zhang, Y.J., Eugenin, E.A., Prideaux, B., Daudelin, I.B., Chen, P.Y., Booty, M.G., Kim, J.H., et al. (2016). Inflammatory signaling in human tuberculosis granulomas is spatially organized. Nat. Med.

Mardle, C.E., Shakespeare, T.J., Butt, L.E., Goddard, L.R., Gowers, D.M., Atkins, H.S., Vincent, H.A., and Callaghan, A.J. (2019). A structural and biochemical comparison of Ribonuclease E homologues from pathogenic bacteria highlights species-specific properties. Sci. Rep. *9*, 1–11.

Mardle, C.E., Goddard, L.R., Spelman, B.C., Atkins, H.S., Butt, L.E., Cox, P.A., Gowers, D.M., Vincent, H.A., and Callaghan, A.J. (2020). Identification and analysis of novel small molecule inhibitors of RNase E: Implications for antibacterial targeting and regulation of RNase E. Biochem. Biophys. Reports.

Marincola, G., Schäfer, T., Behler, J., Bernhardt, J., Ohlsen, K., Goerke, C., and Wolz, C. (2012). RNase Y of Staphylococcus aureus and its role in the activation of virulence genes. Mol. Microbiol. *85*, 817–832.

Marino, S., Sud, D., Plessner, H., Lin, P.L., Chan, J., Flynn, J.A.L., and Kirschner, D.E. (2007). Differences in reactivation of tuberculosis induced from anti-tnf treatments are based on bioavailability in granulomatous tissue. PLoS Comput. Biol. *3*, 1909–1924.

Marrakchi, H., Lanéelle, M.A., and Daffé, M. (2014). Mycolic acids: Structures, biosynthesis, and beyond. Chem. Biol.

Martinez, E., Siadous, F.A., and Bonazzi, M. (2018). Tiny architects: Biogenesis of intracellular replicative niches by bacterial pathogens. FEMS Microbiol. Rev.

Martínez, A., Torello, S., and Kolter, R. (1999). Sliding motility in mycobacteria. J. Bacteriol.

Mase, S.R., Ramsay, A., Ng, V., Henry, M., Hopewell, P.C., Cunningham, J., Urbanczik, R., Perkins, M.D., Aziz, M.A., and Pai, M. (2007). Yield of serial sputum specimen examinations in the diagnosis of pulmonary tuberculosis: A systematic review. Int. J. Tuberc. Lung Dis. *11*, 485–495.

Massé, E., Escorcia, F.E., and Gottesman, S. (2003). Coupled degradation of a small regulatory RNA and its mRNA targets in Escherichia coli. Genes Dev.

Mathy, N., Bénard, L., Pellegrini, O., Daou, R., Wen, T., and Condon, C. (2007). 5′-to-3′ Exoribonuclease Activity in Bacteria: Role of RNase J1 in rRNA Maturation and 5′ Stability of mRNA. Cell.

Mauri, P., and Dehò, G. (2008). Chapter 6 A Proteomic Approach to the Analysis of RNA Degradosome Composition in Escherichia coli (Elsevier Inc.).

Mazars, E., Lesjean, S., Banuls, A.L., Gilbert, M., Vincent, V., Gicquel, B., Tibayrenc, M., Locht, C., and Supply, P. (2001). High-resolution minisatellite-based typing as a portable approach to global analysis of Mycobacterium tuberculosis molecular epidemiology. Proc. Natl. Acad. Sci. U. S. A. *98*, 1901–1906.

Mcadams, H.H., and Arkin, A. (1997). Stochastic mechanisms in gene expression. Proc. Natl. Acad. Sci. U. S. A. *94*, 814–819.

MCCUNE, R.M., MCDERMOTT, W., and TOMPSETT, R. (1956). The fate of Mycobacterium tuberculosis in mouse tissues as determined by the microbial enumeration technique. II. The conversion of tuberculous infection to the latent state by the administration of pyrazinamide and a companion drug. J. Exp. Med. *104*, 763–802.

McKenzie, J.L., Robson, J., Berney, M., Smith, T.C., Ruthe, A., Gardner, P.P., Arcus, V.L., and Cook, G.M. (2012). A vapbc toxin-antitoxin module is a posttranscriptional regulator of metabolic flux in mycobacteria. J. Bacteriol.

Melsew, Y.A., Doan, T.N., Gambhir, M., Cheng, A.C., McBryde, E., and Trauer, J.M. (2018). Risk factors for infectiousness of patients with tuberculosis: A systematic review and meta-analysis. Epidemiol. Infect. *146*, 345–353.

Meroueh, S.O., Bencze, K.Z., Hesek, D., Lee, M., Fisher, J.F., Stemmler, T.L., and Mobashery, S. (2006). Three-dimensional structure of the bacterial cell wall peptidoglycan. Proc. Natl. Acad. Sci. U. S. A.

Miczak, A., Srivastava, R.A.K., and Apirion, O. (1991). Location of the RNA-processing enzymes RNase III, RNase E and RNase P in the Eschenchia coli cell. Mol. Microbiol.

Milstien, J.B., and Gibson, J.J. (1990). Quality control of BCG vaccine by WHO: A review of factors that may influence vaccine effectiveness and safety. Bull. World Health Organ.

Minnikin, D.E., Lee, O.Y.-C., Wu, H.H.T., Nataraj, V., Donoghue, H.D., Ridell, M., Watanabe, M., Alderwick, L., Bhatt, A., and Besra, G.S. (2015). Pathophysiological Implications of Cell Envelope Structure in Mycobacterium tuberculosis and Related Taxa. In Tuberculosis - Expanding Knowledge, p.

Mishra, R., Kohli, S., Malhotra, N., Bandyopadhyay, P., Mehta, M., Munshi, M.H., Adiga, V., Ahuja, V.K., Shandil, R.K., Rajmani, R.S., et al. (2019). Targeting redox heterogeneity to counteract drug tolerance in replicating Mycobacterium tuberculosis. Sci. Transl. Med. *11*.

Mittal, E., Skowyra, M.L., Uwase, G., Tinaztepe, E., Mehra, A., Köster, S., Hanson, P.I., and Philips, J.A. (2018). Mycobacterium tuberculosis type VII secretion system effectors differentially impact the ESCRT endomembrane damage response. MBio.

Moffitt, J.R., Pandey, S., Boettiger, A.N., Wang, S., and Zhuang, X. (2016). Spatial organization shapes the turnover of a bacterial transcriptome. Elife *5*, 1–22.

Mohanty, B.K., and Kushner, S.R. (2016). Regulation of mRNA Decay in Bacteria. Annu. Rev. Microbiol.

Mohanty, B.K., and Kushner, S.R. (2018). Enzymes Involved in Posttranscriptional RNA Metabolism in Gram-Negative Bacteria. In Regulating with RNA in Bacteria and Archaea, p.

Mok, W.W.K., and Brynildsen, M.P. (2018). Timing of DNA damage responses impacts persistence to fluoroquinolones. Proc. Natl. Acad. Sci. U. S. A. *115*, E6301–E6309.

Mokrousov, I. (2004). Multiple rpoB mutants of Mycobacterium tuberculosis second-order selection [7]. Emerg. Infect. Dis.

Monod, J., and Jacob, F. (1961). General Conclusions: Teleonomic Mechanisms in Cellular Metabolism, Growth, and Differentiation. Cold Spring Harb. Symp. Quant. Biol. *26*, 389–401.

Morgan, M., Kalantri, S., Flores, L., and Pai, M. (2005). A commercial line probe assay for the rapid detection of rifampicin resistance in Mycobacterium tuberculosis: A systemic review and meta-analysis. BMC Infect. Dis. *5*, 1–9.

Morita, T., and Aiba, H. (2011). RNase E action at a distance: Degradation of target mRNAs mediated by an Hfq-binding small RNA in bacteria. Genes Dev.

Morita, T., Kawamoto, H., Mizota, T., Inada, T., and Aiba, H. (2004). Enolase in the RNA degradosome plays a crucial role in the rapid decay of glucose transporter mRNA in the response to phosphosugar stress in Escherichia coli. Mol. Microbiol. *54*, 1063–1075.

MORSE, D., BROTHWELL, D.R., and UCKO, P.J. (1964). TUBERCULOSIS IN ANCIENT EGYPT. Am. Rev. Respir. Dis.

Mudd, E.A., Sullivan, S., Gisby, M.F., Mironov, A., Kwon, C.S., Chung, W. Il, and Day, A. (2008). A 125 kDa RNase E/G-like protein is present in plastids and is essential for chloroplast development and autotrophic growth in Arabidopsis. J. Exp. Bot. *59*, 2597–2610.

Mukamolova, G. V., Turapov, O., Malkin, J., Woltmann, G., and Barer, M.R. (2010). Resuscitation-promoting factors reveal an occult population of tubercle bacilli in sputum. Am. J. Respir. Crit. Care Med.

Müller, A.U., and Weber-Ban, E. (2019). The bacterial proteasome at the core of diverse degradation pathways. Front. Mol. Biosci.

Murashko, O.N., and Lin-Chao, S. (2017). Escherichia coli responds to environmental changes using enolasic degradosomes and stabilized DicF sRNA to alter cellular morphology. Proc. Natl. Acad. Sci. U. S. A. *114*, E8025–E8034.

Murray, J.F., Rieder, H.L., and Finley-Croswhite, A. (2016). The King's Evil and the Royal Touch: The medical history of scrofula. Int. J. Tuberc. Lung Dis. *20*, 713–716.

Nayak, S., and Acharjya, B. (2012). Mantoux test and its interpretation. Indian Dermatol. Online J.

Ndlovu, H., and Marakalala, M.J. (2016). Granulomas and inflammation: Host-directed therapies for tuberculosis. Front. Immunol. *7*.

Nevo-Dinur, K., Nussbaum-Shochat, A., Ben-Yehuda, S., and Amster-Choder, O. (2011). Translation-independent localization of mRNA in E. coli. Science (80-.). *331*, 1081–1084.

Newton-Foot, M., and Gey Van Pittius, N.C. (2013). The complex architecture of mycobacterial promoters. Tuberculosis *93*, 60–74.

Ni, M., Wang, S.Y., Li, J.K., and Ouyang, Q. (2007). Simulating the temporal modulation of inducible DNA damage response in Escherichia coli. Biophys. J.

Nielsen, J.S., Lei, L.K., Ebersbach, T., Olsen, A.S., Klitgaard, J.K., Valentin-Hansen, P., and Kallipolitis, B.H. (2009). Defining a role for Hfq in Gram-positive bacteria: Evidence for Hfq-dependent antisense regulation in Listeria monocytogenes. Nucleic Acids Res.

Nieuwenhuizen, N.E., and Kaufmann, S.H.E. (2018). Next-generation vaccines based on Bacille Calmette-Guérin. Front. Immunol.

Niki, M., Niki, M., Tateishi, Y., Ozeki, Y., Kirikae, T., Lewin, A., Inoue, Y., Matsumoto, M., Dahl, J.L., Ogura, H., et al. (2012). A novel mechanism of growth phase-dependent tolerance to isoniazid in mycobacteria. J. Biol. Chem.

Novo, A.A. (2013). Analysis of multivariate normal datasets with missing values.

Oberto, J., Nabti, S., Jooste, V., Mignot, H., and Rouviere-Yaniv, J. (2009). The HU regulon is composed of genes responding to anaerobiosis, acid stress, high osmolarity and SOS induction. PLoS One.

Odermatt, N.T., Sala, C., Benjak, A., and Cole, S.T. (2018). Essential Nucleoid Associated Protein mIHF (Rv1388) Controls Virulence and Housekeeping Genes in Mycobacterium tuberculosis. Sci. Rep.

Ohol, Y.M., Goetz, D.H., Chan, K., Shiloh, M.U., Craik, C.S., and Cox, J.S. (2010). Mycobacterium tuberculosis MycP1 Protease Plays a Dual Role in Regulation of ESX-1 Secretion and Virulence. Cell Host Microbe *7*, 210–220.

Oliva, G., Sahr, T., and Buchrieser, C. (2015). Small RNAs, 5' UTR elements and RNA-binding proteins in intracellular bacteria: Impact on metabolism and virulence. FEMS Microbiol. Rev.

Ono, M., and Kuwano, M. (1979). A conditional lethal mutation in an Escherichia coli strain with a longer chemical lifetime of messenger RNA. J. Mol. Biol.

Orman, M.A., and Brynildsen, M.P. (2013). Dormancy is not necessary or sufficient for bacterial persistence. Antimicrob.

Agents Chemother. *57*, 3230–3239.

Orme, I.M. (2015). Tuberculosis vaccine types and timings. Clin. Vaccine Immunol. *22*, 249–257.

Orme, I.M., McMurray, D.N., and Belisle, J.T. (2001). Tuberculosis vaccine development: Recent progress. Trends Microbiol. *9*, 115–118.

Osbourne, D.O., Soo, V.W.C., Konieczny, I., and Wood, T.K. (2014). Polyphosphate, cyclic AMP, guanosine tetraphosphate, and c-di-GMP reduce in vitro Lon activity. Bioengineered *5*, 264–268.

Ow, M.C., Liu, Q., Mohanty, B.K., Andrew, M.E., Maples, V.F., and Kushner, S.R. (2002). RNase E levels in Escherichia coli are controlled by a complex regulatory system that involves transcription of the rne gene from three promoters. Mol. Microbiol. *43*, 159–171.

Oxford Immunotec T-SPOT®.

Ozbudak, E.M., Thattai, M., Kurtser, I., Grossman, A.D., and Van Oudenaarden, A. (2002). Regulation of noise in the expression of a single gene. Nat. Genet. *31*, 69–73.

Page, R., and Peti, W. (2016). Toxin-antitoxin systems in bacterial growth arrest and persistence. Nat. Chem. Biol. *12*, 208–214.

Pai, M., Behr, M.A., Dowdy, D., Dheda, K., Divangahi, M., Boehme, C.C., Ginsberg, A., Swaminathan, S., Spigelman, M., Getahun, H., et al. (2016). Tuberculosis. Nat. Rev. Dis. Prim. *2*.

Pai, S.R., Actor, J.K., Sepulveda, E., Hunter, R.L., and Jagannath, C. (2000). Identification of viable and non-viable Mycobacterium tuberculosis in mouse organs by directed RT-PCR for antigen 85B mRNA. Microb. Pathog.

Pandey, D.P., and Gerdes, K. (2005). Toxin-antitoxin loci are highly abundant in free-living but lost from host-associated prokaryotes. Nucleic Acids Res. *33*, 966–976.

Pandey, S.D., Choudhury, M., and Sritharan, M. (2014a). Transcriptional regulation of mycobacterium tuberculosis hupB gene expression. Microbiol. (United Kingdom).

Pandey, S.D., Choudhury, M., Yousuf, S., Wheeler, P.R., Gordon, S. V., Ranjan, A., and Sritharan, M. (2014b). Iron-regulated protein HupB of Mycobacterium tuberculosis positively regulates siderophore biosynthesis and is essential for growth in macrophages. J. Bacteriol.

Papenfort, K., and Vogel, J. (2010). Regulatory RNA in bacterial pathogens. Cell Host Microbe.

Papenfort, K., Sun, Y., Miyakoshi, M., Vanderpool, C.K., and Vogel, J. (2013). Small RNA-mediated activation of sugar phosphatase mRNA regulates glucose homeostasis. Cell.

Peddireddy, V., Doddam, S.N., and Ahmed, N. (2017). Mycobacterial dormancy systems and host responses in tuberculosis. Front. Immunol.

Peña, C.E.A., Stoner, J.E., and Hatfull, G.F. (1996). Positions of strand exchange in mycobacteriophage L5 integration and characterization of the attB site. J. Bacteriol.

Pertzev, A. V., and Nicholson, A.W. (2006). Characterization of RNA sequence determinants and antideterminants of processing reactivity for a minimal substrate of Escherichia coli ribonuclease III. Nucleic Acids Res.

Perwez, T., and Kushner, S.R. (2006). RNase Z in Escherichia coli plays a significant role in mRNA decay. Mol. Microbiol.

Pfeiffer, V., Papenfort, K., Lucchini, S., Hinton, J.C.D., and Vogel, J. (2009). Coding sequence targeting by MicC RNA reveals bacterial mRNA silencing downstream of translational initiation. Nat. Struct. Mol. Biol. *16*, 840–846.

Pham, T.T., Jacobs-Sera, D., Pedulla, M.L., Hendrix, R.W., and Hatfull, G.F. (2007). Comparative genomic analysis of mycobacteriophage Tweety: Evolutionary insights and construction of compatible site-specific integration vectors for mycobacteria. Microbiology.

Pirquet, C. von (1909). Frequency of tuberculosis in childhood. J Am Med Assoc *52*, 675–678.

Płociński, P., MacIos, M., Houghton, J., Niemiec, E., Płocińska, R., Brzostek, A., Słomka, M., Dziadek, J., Young, D., and Dziembowski, A. (2019). Proteomic and transcriptomic experiments reveal an essential role of RNA degradosome complexes in shaping the transcriptome of Mycobacterium tuberculosis. Nucleic Acids Res. *47*, 5892–5905.

Podlesek, Z., and Žgur Bertok, D. (2020). The DNA Damage Inducible SOS Response Is a Key Player in the Generation of Bacterial Persister Cells and Population Wide Tolerance. Front. Microbiol.

Porcelli, S.A., and Jacobs, W.R. (2019). Exacting Edward Jenner's revenge: The quest for a new tuberculosis vaccine. Sci. Transl. Med.

Pounds, S., and Cheng, C. (2006). Robust estimation of the false discovery rate. Bioinformatics.

Prabowo, S.A., Painter, H., Zelmer, A., Smith, S.G., Seifert, K., Amat, M., Cardona, P.J., and Fletcher, H.A. (2019). RUTI vaccination enhances inhibition of mycobacterial growth ex vivo and induces a shift of monocyte phenotype in mice. Front. Immunol. *10*, 1–10.

Priestman, M., Thomas, P., Robertson, B.D., and Shahrezaei, V. (2017). Mycobacteria modify their cell size control under sub-optimal carbon sources. Front. Cell Dev. Biol.

Primm, T.P., Andersen, S.J., Mizrahi, V., Avarbock, D., Rubin, H., and Barry, C.E. (2000). The stringent response of Mycobacterium tuberculosis is required for long-term survival. J. Bacteriol. *182*, 4889–4898.

Prusa, J., Zhu, D.X., and Stallings, C.L. (2018). The stringent response and Mycobacterium tuberculosis pathogenesis. Pathog. Dis. *76*, 1–13.

Pu, Y., Zhao, Z., Li, Y., Zou, J., Ma, Q., Zhao, Y., Ke, Y., Zhu, Y., Chen, H., Baker, M.A.B., et al. (2016). Enhanced Efflux Activity Facilitates Drug Tolerance in Dormant Bacterial Cells. Mol. Cell *62*, 284–294.

Purusharth, R.I., Klein, F., Sulthana, S., Jäger, S., Jagannadham, M.V., Evguenieva-Hackenberg, E., Ray, M.K., and Klug, G. (2005). Exoribonuclease R interacts with endoribonuclease E and an RNA helicase in the psychrotrophic bacterium Pseudomonas syringae Lz4W. J. Biol. Chem. *280*, 14572–14578.

Quereda, J.J., and Cossart, P. (2017). Regulating Bacterial Virulence with RNA. Annu. Rev. Microbiol.

Rajaei, E., Hadadi, M., Madadi, M., Aghajani, J., Ahmad, M., Farnia, P., Ghanavi, J., Farnia, P., and Velayati, A. (2018). Outdoor air pollution affects tuberculosis development based on geographical information system modeling. Biomed. Biotechnol. Res. J.

Ramage, H.R., Connolly, L.E., and Cox, J.S. (2009). Comprehensive functional analysis of Mycobacterium tuberculosis toxin-antitoxin systems: Implications for pathogenesis, stress responses, and evolution. PLoS Genet. *5*.

Ramakrishnan, L. (2012). Revisiting the role of the granuloma in tuberculosis. Nat. Rev. Immunol. *12*, 352–366.

Ramisetty, B.C.M., Ghosh, D., Chowdhury, M.R., and Santhosh, R.S. (2016). What is the link between stringent response, endoribonuclease encoding type II toxin-antitoxin systems and persistence? Front. Microbiol.

Rando, O.J., and Verstrepen, K.J. (2007). Timescales of Genetic and Epigenetic Inheritance. Cell *128*, 655–668.

Rappsilber, J., Mann, M., and Ishihama, Y. (2007). Protocol for micro-purification, enrichment, pre-fractionation and storage of peptides for proteomics using StageTips. Nat. Protoc.

Recht, J., and Kolter, R. (2001). Glycopeptidolipid acetylation affects sliding motility and biofilm formation in Mycobacterium smegmatis. J. Bacteriol.

Redder, P. (2018). Molecular and genetic interactions of the RNA degradation machineries in Firmicute bacteria. Wiley Interdiscip. Rev. RNA *9*, 1–12.

Redder, P., Hausmann, S., Khemici, V., Yasrebi, H., and Linder, P. (2015). Bacterial versatility requires DEAD-box RNA helicases. FEMS Microbiol. Rev.

Redko, Y., Aubert, S., Stachowicz, A., Lenormand, P., Namane, A., Darfeuille, F., Thibonnier, M., and De Reuse, H. (2013). A minimal bacterial RNase J-based degradosome is associated with translating ribosomes. Nucleic Acids Res. *41*, 288–301.

Richards, J., and Belasco, J.G. (2019). Obstacles to Scanning by RNase E Govern Bacterial mRNA Lifetimes by Hindering Access to Distal Cleavage Sites. Mol. Cell *74*, 284-295.e5.

Richardson, K., Bennion, O.T., Tan, S., Hoang, A.N., Cokol, M., and Aldridge, B.B. (2016). Temporal and intrinsic factors of rifampicin tolerance in mycobacteria. Proc. Natl. Acad. Sci. U. S. A.

Ritchie, M.E., Phipson, B., Wu, D., Hu, Y., Law, C.W., Shi, W., and Smyth, G.K. (2015). Limma powers differential expression analyses for RNA-sequencing and microarray studies. Nucleic Acids Res.

Robert Kock (1890). Uber bakteriologische forschung. Verhandlungen Des X Int. Medizenischen Kongresses.

Roberts, M.E., and Stewart, P.S. (2005). Modelling protection from antimicrobial agents in biofilms through the formation of persister cells. Microbiology *151*, 75–80.

Rock, J.M., Hopkins, F.F., Chavez, A., Diallo, M., Chase, M.R., Gerrick, E.R., Pritchard, J.R., Church, G.M., Rubin, E.J., Sassetti, C.M., et al. (2017). Programmable transcriptional repression in mycobacteria using an orthogonal CRISPR interference platform. Nat. Microbiol.

Rossau, R., Traore, H., De Beenhouwer, H., Mijs, W., Jannes, G., De Rijk, P., and Portaels, F. (1997). Evaluation of the INNO-LiPA Rif. TB assay, a reverse hybridization assay for the simultaneous detection of Mycobacterium tuberculosis complex and its resistance to rifampin. Antimicrob. Agents Chemother. *41*, 2093–2098.

Rothstein, D.M. (2016). Rifamycins, alone and in combination. Cold Spring Harb. Perspect. Med.

Ruggiero, S., Pilvankar, M., and Ford Versypt, A. (2017). Mathematical Modeling of Tuberculosis Granuloma Activation. Processes *5*, 79.

Russell, D. (2017). Diversity breeds tolerance Premature lambs grown in a bag. Nature *546*, 44–45.

Russell, J.H., and Keiler, K.C. (2009). Subcellular localization of a bacterial regulatory RNA. Proc. Natl. Acad. Sci. U. S. A.

Rustad, T.R., Sherrid, A.M., Minch, K.J., and Sherman, D.R. (2009). Hypoxia: A window into Mycobacterium tuberculosis latency. Cell. Microbiol. *11*, 1151–1159.

Rustad, T.R., Minch, K.J., Brabant, W., Winkler, J.K., Reiss, D.J., Baliga, N.S., and Sherman, D.R. (2013). Global analysis of mRNA stability in Mycobacterium tuberculosis. Nucleic Acids Res. *41*, 509–517.

Sakatos, A., Babunovic, G.H., Chase, M.R., Dills, A., Leszyk, J., Rosebrock, T., Bryson, B., and Fortune, S.M. (2018). Posttranslational modification of a histone-like protein regulates phenotypic resistance to isoniazid in mycobacteria. Sci. Adv. *4*, 1–10.

Sala, A., Bordes, P., and Genevaux, P. (2014). Multiple toxin-antitoxin systems in Mycobacterium tuberculosis. Toxins (Basel). *6*, 1002–1020.

Sala, C., Forti, F., Magnoni, F., and Ghisotti, D. (2008). The katG mRNA of Mycobacterium tuberculosis and Mycobacterium smegmatis is processed at its 5′ end and is stabilized by both a polypurine sequence and translation initiation. BMC Mol. Biol.

Salman-Dilgimen, A., Hardy, P.O., Radolf, J.D., Caimano, M.J., and Chaconas, G. (2013). HrpA, an RNA Helicase Involved in RNA Processing, Is Required for Mouse Infectivity and Tick Transmission of the Lyme Disease Spirochete. PLoS Pathog.

Sander, P., Prammananan, T., and Böttger, E.C. (1996). Introducing mutations into a chromosomal rRNA gene using a genetically modifed eubacterial host with a single rRNA operon. Mol. Microbiol.

Santi, I., and McKinney, J.D. (2015). Chromosome organization and replisome dynamics in Mycobacterium smegmatis. MBio.

Santi, I., Dhar, N., Bousbaine, D., Wakamoto, Y., and McKinney, J.D. (2013). Single-cell dynamics of the chromosome replication and cell division cycles in mycobacteria. Nat. Commun. *4*, 3–8.

Santin, M., Muñoz, L., and Rigau, D. (2012). Interferon-γ release assays for the diagnosis of tuberculosis and tuberculosis infection in HIV-infected adults: A systematic review and meta-analysis. PLoS One.

dos Santos, V.T., Bisson-Filho, A.W., and Gueiros-Filho, F.J. (2012). Diviva-mediated polar localization of ComN, a posttranscriptional regulator of Bacillus subtilis. J. Bacteriol. *194*, 3661–3669.

Sasindran, S.J., Saikolappan, S., Scofield, V.L., and Dhandayuthapani, S. (2011). Biochemical and physiological characterization of the GTP-binding protein Obg of Mycobacterium tuberculosis. BMC Microbiol. *11*.

Schneider, C.A., Rasband, W.S., and Eliceiri, K.W. (2012). NIH Image to ImageJ: 25 years of image analysis. Nat. Methods.

Schnettger, L., Rodgers, A., Repnik, U., Lai, R.P., Pei, G., Verdoes, M., Wilkinson, R.J., Young, D.B., and Gutierrez, M.G. (2017). A Rab20-Dependent Membrane Trafficking Pathway Controls M. tuberculosis Replication by Regulating Phagosome Spaciousness and Integrity. Cell Host Microbe *21*, 619-628.e5.

Schuck, A., Diwa, A., and Belasco, J.G. (2009). RNase e autoregulates its synthesis in Escherichia coli by binding directly to a stem-loop in the rne 5′ untranslated region. Mol. Microbiol.

Scotto-Lavino, E., Du, G., and Frohman, M.A. (2007). 5′ end cDNA amplification using classic RACE. Nat. Protoc.

Scutigliani, E.M., Scholl, E.R., Grootemaat, A.E., Khanal, S., Kochan, J.A., Krawczyk, P.M., Reits, E.A., Garzan, A., Ngo, H.X., Green, K.D., et al. (2018). Interfering with DNA decondensation as a strategy against mycobacteria. Front. Microbiol.

Sebastian, J., Swaminath, S., Nair, R.R., Jakkala, K., Pradhan, A., and Ajitkumar, P. (2017). De novo emergence of genetically resistant mutants of Mycobacterium tuberculosis from the persistence phase cells formed against antituberculosis drugs in vitro. Antimicrob. Agents Chemother.

Shah, D., Zhang, Z., Khodursky, A., Kaldalu, N., Kurg, K., and Lewis, K. (2006). Persisters: A distinct physiological state of E. coli. BMC Microbiol. *6*, 1–9.

Shahbabian, K., Jamalli, A., Zig, L., and Putzer, H. (2009). RNase Y, a novel endoribonuclease, initiates riboswitch turnover in Bacillus subtilis. EMBO J. *28*, 3523–3533.

Sharma, V., Sharma, S., Hoener Zu Bentrup, K., McKinney, J.D., Russell, D.G., Jacobs, W.R., and Sacchettini, J.C. (2000). Structure of isocitrate lyase, a persistence factor of Mycobacterium tuberculosis. Nat. Struct. Biol. *7*, 663–668.

Sharp, J.S., Rietsch, A., and Dove, S.L. (2019). RNase E promotes expression of type III secretion system genes in pseudomonas aeruginosa. J. Bacteriol. *201*.

Shechter, N., Zaltzman, L., Weiner, A., Brumfeld, V., Shimoni, E., Fridmann-Sirkis, Y., and Minsky, A. (2013). Stress-induced condensation of bacterial genomes results in re-pairing of sister chromosomes: Implications for double strand dna break repair. J. Biol. Chem.

Singh, A.K., and Gupta, U.D. (2018). Animal models of tuberculosis: Lesson learnt. Indian J. Med. Res.

Singh, A.K., and Reyrat, J.M. (2009). Laboratory maintenance of mycobacterium smegmatis. Curr. Protoc. Microbiol.

Singh, D., Chang, S.J., Lin, P.H., Averina, O. V., Kaberdin, V.R., and Sue, L.C. (2009). Regulation of ribonuclease E activity by the L4 ribosomal protein of Escherichia coli. Proc. Natl. Acad. Sci. U. S. A. *106*, 864–869.

Singh, R., Barry, C.E., and Boshoff, H.I.M. (2010). The three RelE homologs of Mycobacterium tuberculosis have individual, drug-specific effects on bacterial antibiotic tolerance. J. Bacteriol. *192*, 1279–1291.

Slayden, R.A., Dawson, C.C., and Cummings, J.E. (2018). Toxin-antitoxin systems and regulatory mechanisms in Mycobacterium tuberculosis. Pathog. Dis.

Smeulders, M.J., Keer, J., Speight, R.A., and Williams, H.D. (1999). Adaptation of Mycobacterium smegmatis to stationary phase. J. Bacteriol.

Smith, T., Wolff, K.A., and Nguyen, L. (2013). Molecular biology of drug resistance in Mycobacterium tuberculosis. Curr. Top. Microbiol. Immunol.

Smyth, G.K. (2005). limma: Linear Models for Microarray Data. In Bioinformatics and Computational Biology Solutions Using R and Bioconductor, p.

Snapper, S.B., Melton, R.E., Mustafa, S., Kieser, T., and Jr, W.R.J. (1990). Isolation and characterization of efficient plasmid transformation mutants of Mycobacterium smegmatis. Mol. Microbiol.

Solans, L., Gonzalo-Asensio, J., Sala, C., Benjak, A., Uplekar, S., Rougemont, J., Guilhot, C., Malaga, W., Martín, C., and Cole, S.T. (2014). The PhoP-Dependent ncRNA Mcr7 Modulates the TAT Secretion System in Mycobacterium tuberculosis. PLoS Pathog. *10*.

Van Soolingen, D., Hermans, P.W.M., De Haas, P.E.W., Soll, D.R., and Van Embden, J.D.A. (1991). Occurrence and stability of insertion sequences in Mycobacterium tuberculosis complex strains: Evaluation of an insertion sequence-

dependent DNA polymorphism as a tool in the epidemiology of tuberculosis. J. Clin. Microbiol. *29*, 2578–2586.

Sousa, S., Marchand, I., and Dreyfus, M. (2001). Autoregulation allows Escherichia coli RNase E to adjust continuously its synthesis to that of its substrates. Mol. Microbiol.

Spellberg, B., Blaser, M., Guidos, R.J., Boucher, H.W., Bradley, J.S., Eisenstein, B.I., Gerding, D., Lynfield, R., Reller, L.B., Rex, J., et al. (2011). Combating antimicrobial resistance: Policy recommendations to save lives. Clin. Infect. Dis. *52*, 397–428.

Spickler, C., and Mackie, G.A. (2000). Action of RNase II and polynucleotide phosphorylase against RNAs containing stem-loops of defined structure. J. Bacteriol.

Stadthagen-Gomez, G., Helguera-Repetto, A.C., Cerna-Cortes, J.F., Goldstein, R.A., Cox, R.A., and Gonzalez-Y-Merchand, J.A. (2008). The organization of two rRNA (rrn) operons of the slow-growing pathogen Mycobacterium celatum provides key insights into mycobacterial evolution. FEMS Microbiol. Lett. *280*, 102–112.

Stek, C., Allwood, B., Walker, N.F., Wilkinson, R.J., Lynen, L., and Meintjes, G. (2018). The Immune Mechanisms of Lung Parenchymal Damage in Tuberculosis and the Role of Host-Directed Therapy. Front. Microbiol.

Stewart, E.J., Madden, R., Paul, G., and Taddei, F. (2005). Aging and death in an organism that reproduces by morphologically symmetric division. PLoS Biol. *3*, 0295–0300.

Storz, G., Vogel, J., and Wassarman, K.M. (2011). Regulation by Small RNAs in Bacteria: Expanding Frontiers. Mol. Cell *43*, 880–891.

Strahl, H., Turlan, C., Khalid, S., Bond, P.J., Kebalo, J.M., Peyron, P., Poljak, L., Bouvier, M., Hamoen, L., Luisi, B.F., et al. (2015). Membrane Recognition and Dynamics of the RNA Degradosome. PLoS Genet. *11*, 1–23.

Studer, G., Rempfer, C., Waterhouse, A.M., Gumienny, R., Haas, J., and Schwede, T. (2020). QMEANDisCo-distance constraints applied on model quality estimation. Bioinformatics.

Süel, G.M., Garcia-Ojalvo, J., Liberman, L.M., and Elowitz, M.B. (2006). An excitable gene regulatory circuit induces transient cellular differentiation. Nature *440*, 545–550.

Supply, P., Magdalena, J., Himpens, S., and Locht, C. (1997). Identification of novel intergenic repetitive units in a mycobacterial two-component system operon. Mol. Microbiol. *26*, 991–1003.

Sureka, K., Dey, S., Datta, P., Singh, A.K., Dasgupta, A., Rodrigue, S., Basu, J., and Kundu, M. (2007). Polyphosphate kinase is involved in stress-induced mprAB-sigE-rel signalling in mycobacteria. Mol. Microbiol. *65*, 261–276.

Surovtsev, I. V., and Jacobs-Wagner, C. (2018). Subcellular Organization: A Critical Feature of Bacterial Cell Replication. Cell.

Swain, P.S., Elowitz, M.B., and Siggia, E.D. (2002). Intrinsic and extrinsic contributions to stochasticity in gene expression. Proc. Natl. Acad. Sci. U. S. A. *99*, 12795–12800.

Symmons, M.F., Jones, G.H., and Luisi, B.F. (2000). A duplicated fold is the structural basis for polynucleotide phosphorylase catalytic activity, processivity, and regulation. Structure.

Taghbalout, A., and Rothfield, L. (2007). RNaseE and the other constituents of the RNA degradosome are components of the bacterial cytoskeleton. Proc. Natl. Acad. Sci. U. S. A.

Taheri-Araghi, S., Bradde, S., Sauls, J.T., Hill, N.S., Levin, P.A., Paulsson, J., Vergassola, M., and Jun, S. (2015). Cell-size control and homeostasis in bacteria. Curr. Biol.

Tait, D.R., Hatherill, M., Der Meeren, O. Van, Ginsberg, A.M., Van Brakel, E., Salaun, B., Scriba, T.J., Akite, E.J., Ayles, H.M., Bollaerts, A., et al. (2019). Final analysis of a trial of M72/AS01E vaccine to prevent tuberculosis. N. Engl. J. Med. *381*, 2429–2439.

Tamura, M., Lee, K., Miller, C.A., Moore, C.J., Shirako, Y., Kobayashi, M., and Cohen, S.N. (2006). RNase E maintenance of proper FtsZ/FtsA ratio required for nonfilamentous growth of Escherichia coli cells but not for colony-forming ability. J. Bacteriol. *188*, 5145–5152.

Taneja, S., and Dutta, T. (2019). On a stake-out: Mycobacterial small RNA identification and regulation. Non-Coding RNA

Res. *4*, 86–95.

Taraseviciene, L., Miczak, A., and Apirion, D. (1991). The gene specifying RNase E (rne) and a gene affecting mRNA stability (ams) are the same gene. Mol. Microbiol.

Taverniti, V., Forti, F., Ghisotti, D., and Putzer, H. (2011). Mycobacterium smegmatis RNase J is a 5'-3' exo-/endoribonuclease and both RNase J and RNase E are involved in ribosomal RNA maturation. Mol. Microbiol. *82*, 1260–1276.

Teimouri, H., Korkmazhan, E., Stavans, J., and Levine, E. (2017). Sub-cellular mRNA localization modulates the regulation of gene expression by small RNAs in bacteria. Phys. Biol. *14*.

Tejada-Arranz, A., de Crécy-Lagard, V., and de Reuse, H. (2020a). Bacterial RNA Degradosomes: Molecular Machines under Tight Control. Trends Biochem. Sci. *45*, 42–57.

Tejada-Arranz, A., Galtier, E., El Mortaji, L., Turlin, E., Ershov, D., and De Reuse, H. (2020b). The RNase J-Based RNA Degradosome Is Compartmentalized in the Gastric Pathogen Helicobacter pylori . MBio.

Telenti A. Iserman M (2000). Drug-resistant tuberculosis: what do we do now? Drugs *59*, 171–179.

Theodore, A., Lewis, K., and Vulić, M. (2013). Tolerance of Escherichia coli to fluoroquinolone antibiotics depends on specific components of the SOS response pathway. Genetics *195*, 1265–1276.

Theron, G., Peter, J., Richardson, M., Warren, R., Dheda, K., and Steingart, K.R. (2016). GenoType® MTBDRsl assay for resistance to second-line anti-tuberculosis drugs. Cochrane Database Syst. Rev.

Thompson, K.J., Zong, J., and Mackie, G.A. (2015). Altering the divalent metal ion preference of RNase E. J. Bacteriol. *197*, 477–482.

Tian, C., Roghanian, M., Jørgensen, M.G., Sneppen, K., Sørensen, M.A., Gerdes, K., and Mitarai, N. (2016). Rapid curtailing of the stringent response by toxin-antitoxin module-encoded mRNases. J. Bacteriol. *198*, 1918–1926.

Tobin, D.M., Vary, J.C., Ray, J.P., Walsh, G.S., Dunstan, S.J., Bang, N.D., Hagge, D.A., Khadge, S., King, M.C., Hawn, T.R., et al. (2010). The lta4h Locus Modulates Susceptibility to Mycobacterial Infection in Zebrafish and Humans. Cell.

Trauer, J.M., Dodd, P.J., Gomes, M.G.M., Gomez, G.B., Houben, R.M.G.J., McBryde, E.S., Melsew, Y.A., Menzies, N.A., Arinaminpathy, N., Shrestha, S., et al. (2019). The importance of heterogeneity to the epidemiology of tuberculosis. Clin. Infect. Dis. *69*, 159–166.

Trébucq, A., Enarson, D.A., Chiang, C.Y., Van Deun, A., Harries, A.D., Boillot, F., Detjen, A., Fujiwara, P.I., Graham, S.M., Monedero, I., et al. (2011). Xpert® MTB/RIF for national tuberculosis programmes in low-income countries: When, where and how? Int. J. Tuberc. Lung Dis.

Tsai, Y.C., Du, D., Domínguez-Malfavón, L., Dimastrogiovanni, D., Cross, J., Callaghan, A.J., García-Mena, J., and Luisi, B.F. (2012). Recognition of the 70S ribosome and polysome by the RNA degradosome in Escherichia coli. Nucleic Acids Res. *40*, 10417–10431.

Tweed, C.D., Dawson, R., Burger, D.A., Conradie, A., Crook, A.M., Mendel, C.M., Conradie, F., Diacon, A.H., Ntinginya, N.E., Everitt, D.E., et al. (2019). Bedaquiline, moxifloxacin, pretomanid, and pyrazinamide during the first 8 weeks of treatment of patients with drug-susceptible or drug-resistant pulmonary tuberculosis: a multicentre, open-label, partially randomised, phase 2b trial. Lancet Respir. Med.

Tyanova, S., Temu, T., and Cox, J. (2016). The MaxQuant computational platform for mass spectrometry-based shotgun proteomics. Nat. Protoc.

Ueno, H., Kato, Y., Tabata, K. V., and Noji, H. (2019). Revealing the Metabolic Activity of Persisters in Mycobacteria by Single-Cell D2O Raman Imaging Spectroscopy. Anal. Chem.

Upadhyay, S., Mittal, E., and Philips, J.A. (2018). Tuberculosis and the art of macrophage manipulation. Pathog. Dis.

Upton, A.M., and McKinney, J.D. (2007). Role of the methylcitrate cycle in propionate metabolism and detoxification in Mycobacterium smegmatis. Microbiology *153*, 3973–3982.

Uthman, O.A., Okwundu, C., Gbenga, K., Volmink, J., Dowdy, D., Zumla, A., and Nachega, J.B. (2015). Optimal timing of

antiretroviral therapy initiation for HIV-infected adults with newly diagnosed pulmonary tuberculosis: A systematic review and meta-analysis. Ann. Intern. Med. *163*, 32–39.

Valencia-Burton, M., McCullough, R.M., Cantor, C.R., and Broude, N.E. (2007). RNA visualization in live bacterial cells using fluorescent protein complementation. Nat. Methods.

Vargas-Blanco, D.A., Zhou, Y., Gregory Zamalloa, L., Antonelli, T., and Shell, S.S. (2019). mRNA degradation rates are coupled to metabolic status in Mycobacterium smegmatis. MBio.

Veening, J.W., Smits, W.K., and Kuipers, O.P. (2008). Bistability, epigenetics, and bet-hedging in bacteria. Annu. Rev. Microbiol. *62*, 193–210.

Velayati, A.A., Abeel, T., Shea, T., Konstantinovich Zhavnerko, G., Birren, B., Cassell, G.H., Earl, A.M., Hoffner, S., and Farnia, P. (2016). Populations of latent Mycobacterium tuberculosis lack a cell wall: Isolation, visualization, and whole-genome characterization. Int. J. Mycobacteriology.

Verstraeten, N., Knapen, W.J., Kint, C.I., Liebens, V., Van den Bergh, B., Dewachter, L., Michiels, J.E., Fu, Q., David, C.C., Fierro, A.C., et al. (2015). Obg and Membrane Depolarization Are Part of a Microbial Bet-Hedging Strategy that Leads to Antibiotic Tolerance. Mol. Cell.

Viegas, S.C., Pfeiffer, V., Sittka, A., Silva, I.J., Vogel, J., and Arraiano, C.M. (2007). Characterization of the role of ribonucleases in Salmonella small RNA decay. Nucleic Acids Res.

Vilchèze, C., and Jacobs, W.R. (2019). The Isoniazid Paradigm of Killing, Resistance, and Persistence in Mycobacterium tuberculosis. J. Mol. Biol.

Villemin, J. (1865). Cause et nature de la tuberculose. Bull. Acad. Med.

Vincent, H.A., and Deutscher, M.P. (2009). The Roles of Individual Domains of RNase R in Substrate Binding and Exoribonuclease Activity. J. Biol. Chem.

Vincent, M.S., and Uphoff, S. (2020). Bacterial phenotypic heterogeneity in DNA repair and mutagenesis. Biochem. Soc. Trans. *48*, 451–462.

Viveiros, M., Martins, M., Rodrigues, L., Machado, D., Couto, I., Ainsa, J., and Amaral, L. (2012). Inhibitors of mycobacterial efflux pumps as potential boosters for anti-tubercular drugs. Expert Rev. Anti. Infect. Ther. *10*, 983–998.

Vogwill, T., Comfort, A.C., Furió, V., and MacLean, R.C. (2016). Persistence and resistance as complementary bacterial adaptations to antibiotics. J. Evol. Biol. *29*, 1223–1233.

Voskuil, M.I., Bartek, I.L., Visconti, K., and Schoolnik, G.K. (2011). The response of Mycobacterium tuberculosis to reactive oxygen and nitrogen species. Front. Microbiol.

Voss, J.E., Luisi, B.F., and Hardwick, S.W. (2014). Molecular recognition of RhlB and RNase D in the Caulobacter crescentus RNA degradosome. Nucleic Acids Res. *42*, 13294–13305.

Dos Vultos, T., Blázquez, J., Rauzier, J., Matic, I., and Gicquel, B. (2006). Identification of nudix hydrolase family members with an antimutator role in Mycobacterium tuberculosis and Mycobacterium smegmatis. J. Bacteriol.

Dos Vultos, T., Mestre, O., Tonjum, T., and Gicquel, B. (2009). DNA repair in Mycobacterium tuberculosis revisited. In FEMS Microbiology Reviews, p.

Wakamoto, Y., Dhar, N., Chait, R., Schneider, K., Signorino-Gelo, F., Leibler, S., and McKinney, J.D. (2013). Dynamic persistence of antibiotic-stressed mycobacteria. Science (80-.).

Waman, V.P., Vedithi, S.C., Thomas, S.E., Bannerman, B.P., Munir, A., Skwark, M.J., Malhotra, S., and Blundell, T.L. (2019). Mycobacterial genomics and structural bioinformatics: opportunities and challenges in drug discovery. Emerg. Microbes Infect. *8*, 109–118.

Wang, C.C., Zhu, B., Fan, X., Gicquel, B., and Zhang, Y. (2013). Systems approach to tuberculosis vaccine development. Respirology *18*, 412–420.

Waterhouse, A., Bertoni, M., Bienert, S., Studer, G., Tauriello, G., Gumienny, R., Heer, F.T., De Beer, T.A.P., Rempfer, C., Bordoli, L., et al. (2018). SWISS-MODEL: Homology modelling of protein structures and complexes. Nucleic Acids

Res.

Waters, L.S., and Storz, G. (2009). Regulatory RNAs in Bacteria. Cell *136*, 615–628.

Wayne, L.G., and Hayes, L.G. (1996). An in vitro model for sequential study of shiftdown of Mycobacterium tuberculosis through two stages of nonreplicating persistence. Infect. Immun. *64*, 2062–2069.

Weigel, W.A., and Dersch, P. (2018). Phenotypic heterogeneity: a bacterial virulence strategy. Microbes Infect. *20*, 570–577.

van der Wel, N., Hava, D., Houben, D., Fluitsma, D., van Zon, M., Pierson, J., Brenner, M., and Peters, P.J. (2007). M. tuberculosis and M. leprae Translocate from the Phagolysosome to the Cytosol in Myeloid Cells. Cell *129*, 1287–1298.

Weng, X., Bohrer, C.H., Bettridge, K., Lagda, A.C., Cagliero, C., Jin, D.J., and Xiao, J. (2019). Spatial organization of RNA polymerase and its relationship with transcription in Escherichia coli. Proc. Natl. Acad. Sci. U. S. A.

Westfall, C.S., and Levin, P.A. (2018). Comprehensive analysis of central carbon metabolism illuminates connections between nutrient availability, growth rate, and cell morphology in Escherichia coli. PLoS Genet.

Whiteford, D.C., Klingelhoets, J.J., Bambenek, M.H., and Dahl, J.L. (2011). Deletion of the histone-like protein (Hlp) from Mycobacterium smegmatis results in increased sensitivity to UV exposure, freezing and isoniazid. Microbiology.

WHO The use of molecular line probe assays for the detection of resistance to second-line anti-tuberculosis drugs INJECTABLE.

WHO Chest Radiography in Tuberculosis. WHO Libr. Cat. Data 44.

WHO (2004). Latent tuberculosis infection.

WHO (2008). Molecular Line Probe Assays for Rapid Screening of Patients At Risk of Multidrug-Resistant Tuberculosis Policy Statement Molecular Line Probe Assays for Rapid Screening of. World Heal. Organ.

WHO (2009). Treatment of tuberculosis.

WHO (2015a). The END TB Strategy.

WHO (2015b). Policy Guidance LAQM.PG(09). 64–68.

WHO (2016). LOOP-MEDIATED ISOTHERMAL AMPLIFICATION FOR THE DETECTION OFM. TUBERCULOSIS (TB-LAMP).

WHO (2019). Global Tuberculosis Report.

Wieczorek, S., Combes, F., Lazar, C., Gianetto, Q.G., Gatto, L., Dorffer, A., Hesse, A.M., Couté, Y., Ferro, M., Bruley, C., et al. (2017). DAPAR & ProStaR: Software to perform statistical analyses in quantitative discovery proteomics. Bioinformatics.

Williams, G.T., and Williams, W.J. (1983). Granulomatous inflammation - A review. J. Clin. Pathol.

Windels, E.M., Michiels, J.E., van den Bergh, B., Fauvart, M., and Michiels, J. (2019). Antibiotics: Combatting tolerance to stop resistance. MBio *10*, 1–7.

Wolf, A.J., Desvignes, L., Linas, B., Banaiee, N., Tamura, T., Takatsu, K., and Ernst, J.D. (2008). Initiation of the adaptive immune response to Mycobacterium tuberculosis depends on antigen production in the local lymph node, not the lungs. J. Exp. Med. *205*, 105–115.

World Health Organization (1999). What is DOTS ? A Guide to Understanding the WHO-recommended TB Control Strategy Known as DOTS. Prev. Control 1–39.

World Health Organization (2011). Same-day diagnosis of tuberculosis by microscopy: policy statement. World Heal. Organ. Doc. *47*, 1–6.

World Health Organization (2016). Tuberculosis diagnostics. Automated real-time DNA amplification test for rapid and simultaneous detection of TB and rifampicin resistance. Xpert® MTB/RIF assay. Factsheet. 1–2.

Xet-Mull, A.M., Kubín, M., Príkazský, V., Harris, E.H., and Riley, L.W. (2001). DRE-PCR (Double Repetitive Element-Polymerase Chain Reaction) - A new molecular epidemiological method in tuberculosis. Epidemiol. Mikrobiol.

Imunol.

Yang, J., Jain, C., and Schesser, K. (2008). RNase E regulates the yersinia type 3 secretion system. J. Bacteriol. *190*, 3774–3778.

Yaseen, I., Choudhury, M., Sritharan, M., and Khosla, S. (2018). Histone methyltransferase SUV 39H1 participates in host defense by methylating mycobacterial histone-like protein HupB . EMBO J.

Zahrt, T.C., Song, J., Siple, J., and Deretic, V. (2001). Mycobacterial FurA is a negative regulator of catalase-peroxidase gene katG. Mol. Microbiol.

Zeller, M.E., Csanadi, A., Miczak, A., Rose, T., Bizebard, T., and Kaberdin, V.R. (2007). Quaternary structure and biochemical properties of mycobacterial RNase E/G. Biochem. J. *403*, 207–215.

Zhang, Y., and Yew, W.W. (2009). Mechanisms of drug resistance in Mycobacterium tuberculosis. Int. J. Tuberc. Lung Dis.

Zhang, H., Li, D., Zhao, L., Fleming, J., Lin, N., Wang, T., Liu, Z., Li, C., Galwey, N., Deng, J., et al. (2013). Genome sequencing of 161 Mycobacterium tuberculosis isolates from China identifies genes and intergenic regions associated with drug resistance. Nat. Genet.

Zhou, X., Rodriguez-Rivera, F.P., Lim, H.C., Bell, J.C., Bernhardt, T.G., Bertozzi, C.R., and Theriot, J.A. (2019). Sequential assembly of the septal cell envelope prior to V snapping in Corynebacterium glutamicum. Nat. Chem. Biol.

Zhu, J.H., Wang, B.W., Pan, M., Zeng, Y.N., Rego, H., and Javid, B. (2018). Rifampicin can induce antibiotic tolerance in mycobacteria via paradoxical changes in rpoB transcription. Nat. Commun. *9*.

Zumla, A., Chakaya, J., Centis, R., D'Ambrosio, L., Mwaba, P., Bates, M., Kapata, N., Nyirenda, T., Chanda, D., Mfinanga, S., et al. (2015). Tuberculosis treatment and management-an update on treatment regimens, trials, new drugs, and adjunct therapies. Lancet Respir. Med.

Zuo, Y., Wang, Y., and Steitz, T.A. (2013). The Mechanism of E. coli RNA Polymerase Regulation by ppGpp is suggested by the structure of their complex. Mol. Cell.

(2016). Murray and Nadel's Textbook of Respiratory Medicine.

Annex 1.

Supplemental Figures

Figure S1

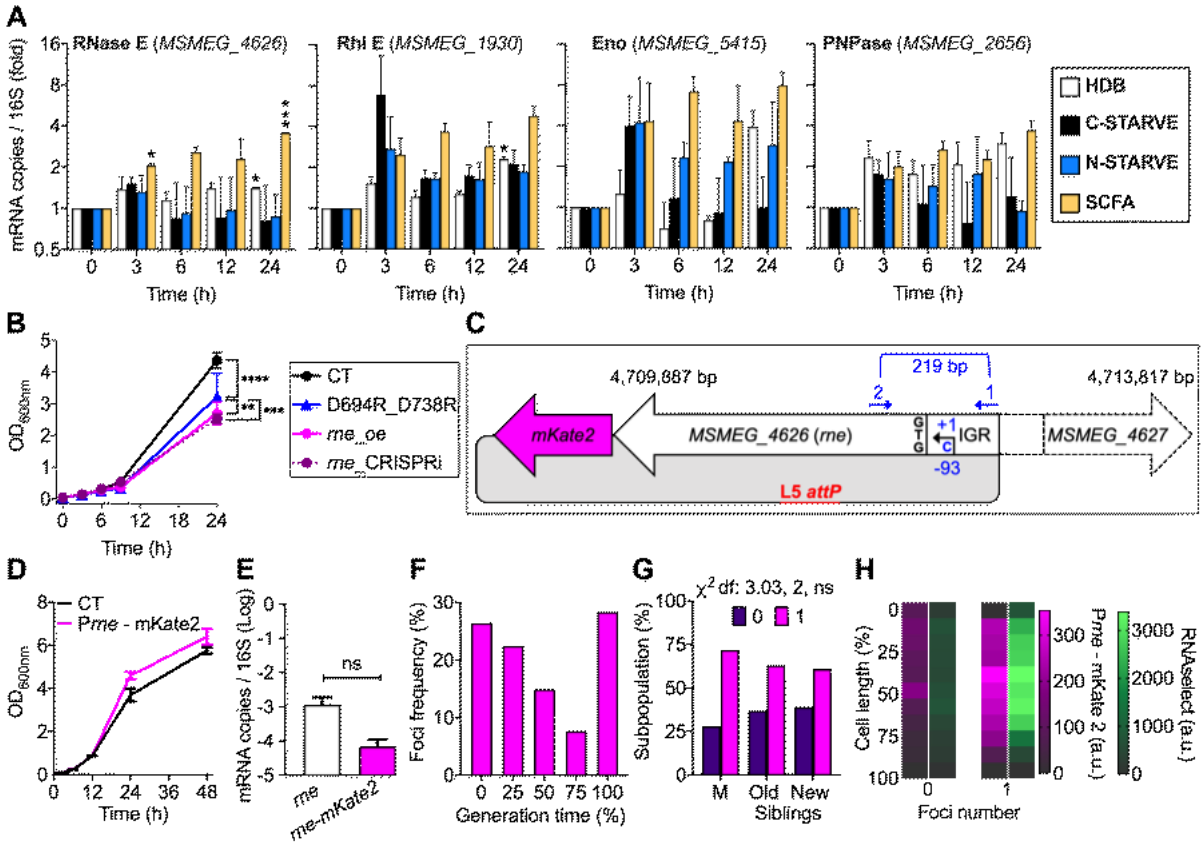

Figure S1. Bulk- and single-cell validation assays in *M. smegmatis* mc²155 wild-type (WT), fluorescent reporter and mutant strains, expressing WT and altered levels of RNase E, related to Figure 20.

(A) qRT-PCR analysis in *M. smegmatis* WT of genes encoding typical components of the RNA degradosome complex in model microorganisms. Gene expression levels are reported over a time course of *M. smegmatis* cultures grown in minimal media Hartman's de Bond Medium (HDB, white bars), complete starvation (C-STARVE, black bars), nitrogen starvation (N-STARVE, blue bars), and in short-chain fatty acid (SCFA, yellow bars). Transcripts are normalized to total RNA and 16S rRNA copies. Mean values ± SD are plotted on a Log 2 scale (n = 2). Asterisks denote significant difference by 2-way ANOVA followed by Dunnett's multiple comparisons test: *P < 0.05; ***P = 0.0009. See also Supplemental Experimental Procedures.

(B) Bulk growth kinetics of *M. smegmatis* control strain (CT); *M. smegmatis* overexpressing either a WT (*rne_oe*) or a mutated (D694R_D738R) *rne* variant, from an episomal plasmid under the control of an acetamide-inducible promoter, and *M. smegmatis* whose *rne* gene is silenced (*rne_si*) via an anhydrotetracycline-inducible CRISPRi-dCas9 system, integrated in the L5 phage attachment site. See also Materials and Methods. Mean values ± SD (n = 3). Asterisks denote significant difference by 2-way ANOVA: **P = 0.0088; ***P = 0.0004; ****P < 0.0001.

(C) Schematic of the *M. smegmatis rne* (*MSMEG_4626*) genomic locus, and of the construction of the P*rne*-mKate2 fluorescent reporter strain. The black arrow indicates the transcription start site (TSS), identified by 5' RACE-PCR, using primers 1 and 2 (blue arrows). The TSS (+1, C) is located 93 nucleotides upstream of the translation start codon (GTG). To generate the merodiploid RNase E fluorescent reporter strain, 105 nucleotides upstream the TTS and the *rne* gene, except the stop codon, were PCR-amplified and cloned together with the *mKate2* fluorescent marker into a chromosomal integrative vector, carrying the L5 phage integration site (*attP*).

(D) Bulk growth kinetics of *M. smegmatis* mc²155 (CT) and of the merodiploid P*rne*-mKate2 fluorescent reporter. Mean values ± SD (n = 3).

(E) qRT-PCR analysis comparing the *rne* gene expression levels in exponentially growing *M. smegmatis* mc²155 and of *rne* fused to *mKate2* marker in the P*rne*-mKate2 fluorescent reporter strain. Transcripts are normalized to total RNA and 16S rRNA copies. Mean values ± SD are plotted on a Log 10 scale (n = 4).

(F) Histogram showing the distribution of P*rne*-mKate2 fluorescence foci expressed as a percent of single-cell generation time. Data are shown from 2 independent experiments (n = 510 cells).

(G) Fractions of subpopulations segregated by the absence (0) or presence (1) of P*rne*-mKate2 fluorescence foci in mother cells and in new- and old-pole daughters (n = 170 per category). Significance by *Chi*-square test of independence. The data shown are from 2 independent experiments. See also **Figure 20H**.

(H) Representative heatmaps of P*rne*-mKate2 and RNAselex™ fluorescence as a function of the percent of cell length in one cell without (0) and one cell with (1) P*rne*-mKate2 foci.

Figure S2

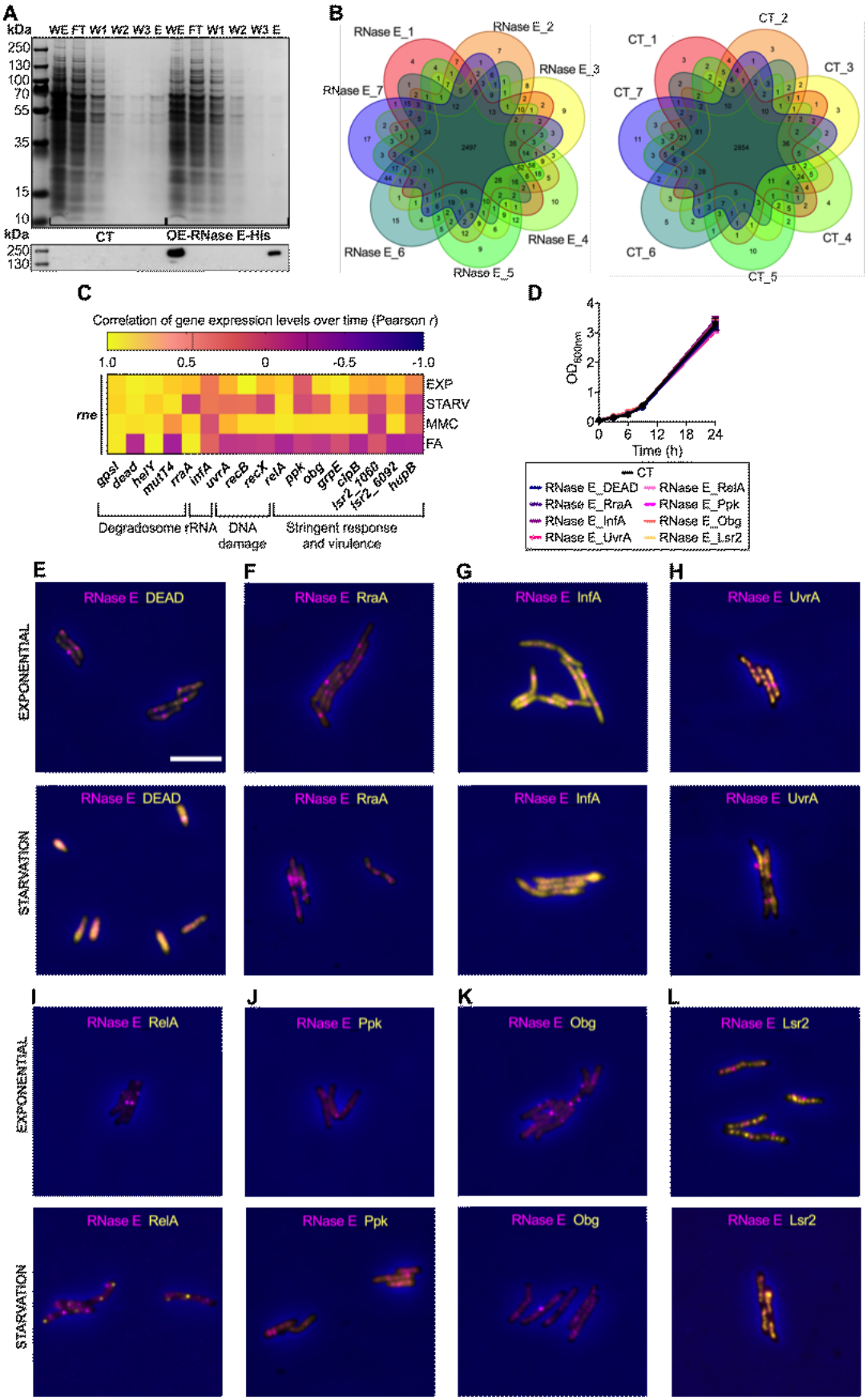
A
kDa
WE FT W1 W2 W3 E WE FT W1 W2 W3 E
250
130
100
70
55
35
15
10
kDa
CT
OE-RNase E-His
250
130
B
RNase E_1
RNase E_2
RNase E_3
RNase E_4
RNase E_5
RNase E_6
RNase E_7
CT_1
CT_2
CT_3
CT_4
CT_5
CT_6
CT_7
C
Correlation of gene expression levels over time (Pearson r)
1.0
0.5
0
-0.5
-1.0
EXP
STARV
MMC
FA
rne
gpsI dead hslV mutT4 rraA infA uvrA recB recX relA ppk obg grpE clpB lsr2_7060 lsr2_6092 hupB
Degradosome
rRNA
DNA damage
Stringent response and virulence
D
OD600nm
Time (h)
CT
RNase E_DEAD
RNase E_RraA
RNase E_InfA
RNase E_UvrA
RNase E_RelA
RNase E_Ppk
RNase E_Obg
RNase E_Lsr2
E
F
G
H
I
J
K
L
EXPONENTIAL
STARVATION
RNase E DEAD
RNase E RraA
RNase E InfA
RNase E UvrA
RNase E RelA
RNase E Ppk
RNase E Obg
RNase E Lsr2

Figure S2. Bulk- and single-cell validation of RNase E pull-down coupled with mass spectrometry-based proteomic analysis in *M. smegmatis*, related to Figure 21.

(A) Representative Coomassie-stained SDS-PAGE (upper panel) and western blot (lower panel) of whole cell extracts and immunoprecipitated RNase E pull-downs from *M. smegmatis* carrying the acetamide-inducible expression vector pMyc (Beckham et al., 2020), either empty as a control (CT) or overexpressing the His-tagged RNase E (OE-RNase E-His). RNase E overexpression was achieved using 0.05% acetamide for 24 hours. Equal volume of whole bacterial extracts (WE), flow throughs (FT), washings (W1, W2 and W3), and eluates (E) were loaded on precast 4-12% SDS-PAGE gel. The presence of the RNase E in each fraction was detected by antibody binding to the 6x-His-tag fused to the C-terminal of the RNase E. See also Materials and Methods.

(B) Venn diagrams of the number of identified proteins in the pull downs by replicates (n = 7) and conditions, after deleting reverse, contaminants and only identified by site proteins, for the RNase E overexpressing (left panel) and the CT strain (right panel).

(C) Heat map of Pearson r correlation between mRNA copies of *rne* and of genes encoding putative RNase E interactors in *M. smegmatis*. Pearson r values are computed merging different time points (0, 3, 6, 12 and 24 hours) for exponential-phase cells growing in optimal 7H9 medium (EXP) or subject to nutrient starvation (STARV), to the DNA crosslinker mitomycin C (MMC, 200 ng/ml), or transferred to a medium containing propionate (2 grL^{-1}) as a sole carbon source (FA). The genes and the conditions examined are indicated. Color gradient represents the Pearson r value for each correlation pair, averaged among different time points. Transcripts are normalized to total RNA and 16S rRNA copies (n = 3). Significance thresholds are indicated by dotted lines on the scale bar. The putative interactors were selected based on the relative stoichiometric and functional analyses, and were separated into four functional categories, *i.e.*, involvement in the degradosome complex; interaction with the rRNA, and implication in the response to DNA damage, stringent response and virulence.

(D) Bulk growth kinetics of *M. smegmatis* WT (CT) and of dual-fluorescent reporter strains generated to validate, at the single-cell protein level, a shortlist of putative RNase E interactors in the P*rne* - mKate2 background: RNase E_DEAD, RNase E_RraA, RNase E_InfA, RNase E_UvrA, RNase E_RelA, RNase E_Ppk, RNase E_Obg and RNase E_Lsr2. Mean values ± SD (n = 3).

(E-L) Representative snapshot images of P*rne* - mKate2 strain containing a second translational reporter of a putative RNase E interactor fused in frame at the C-terminus to mCitrine: DeaD (*MSMEG_5042*) (**E**), RraA (*MSMEG-6439*) (**F**), InfA (*MSMEG_1519*) (**G**), UvrA (*MSMEG_3808*) (**H**), RelA (**I**) (*MSMEG_2965*), Ppk (*MSMEG_2391_2392*) (**J**), Obg (*MSMEG_4623*) (**K**) and Lsr2 (*MSMEG_1060*) (**L**). Dual-fluorescent reporter strains were imaged in exponential growth-phase (upper panels) and after 6 hours of starvation (lower panels). Phase (blue), P*rne* - mKate2 (magenta), and mCitrine (yellow) fluorescence are merged. Scale bar 5 μm. The experiment was repeated twice.

Figure S3

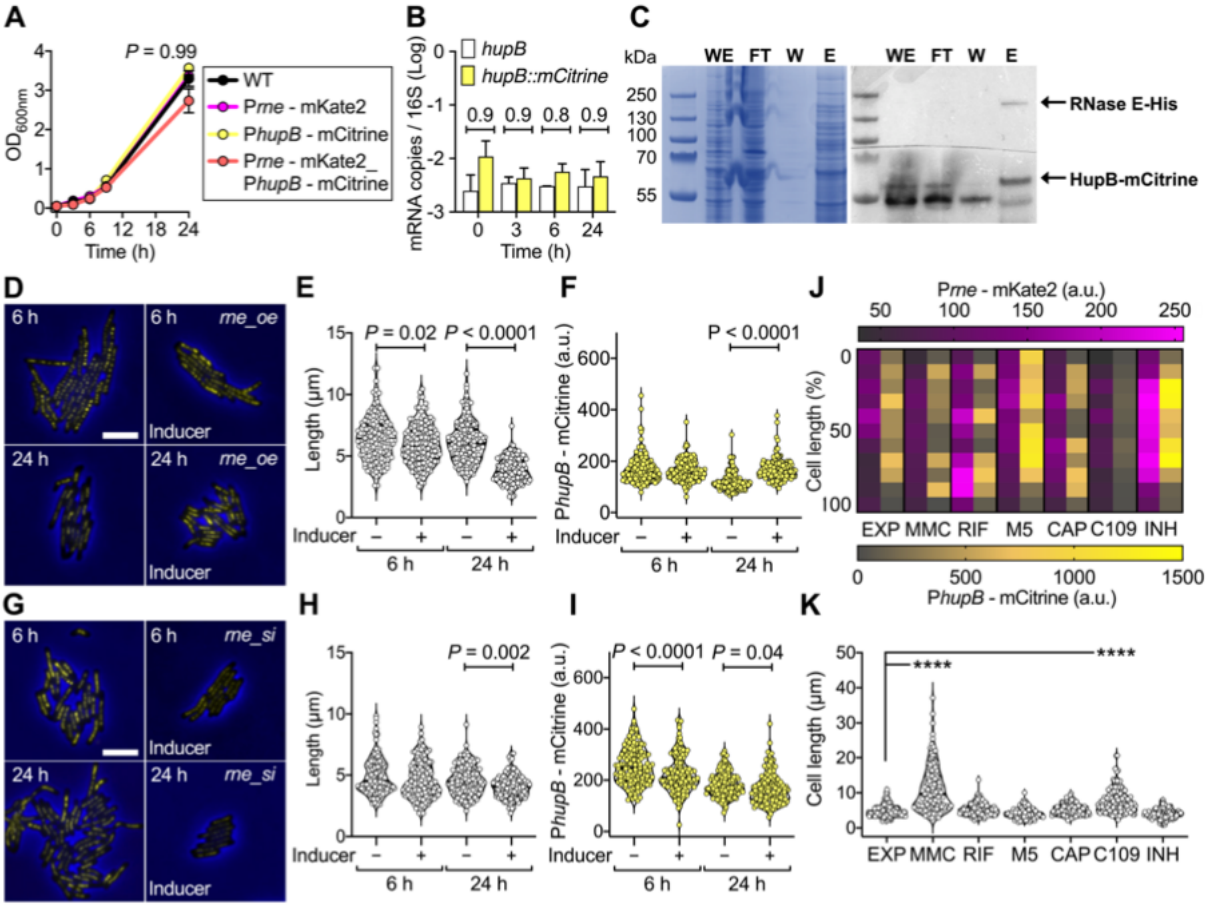
A
P = 0.99
OD600nm
Time (h)
WT
Prne - mKate2
PhupB - mCitrine
Prne - mKate2_
PhupB - mCitrine
B
hupB
hupB::mCitrine
mRNA copies / 16S (Log)
0.9 0.9 0.8 0.9
Time (h)
C
kDa
WE FT W E
WE FT W E
250
130
100
70
55
RNase E-His
HupB-mCitrine
D
6 h
6 h rne_oe
Inducer
24 h
24 h rne_oe
Inducer
E
P = 0.02 P < 0.0001
Length (µm)
Inducer
6 h
24 h
F
P < 0.0001
PhupB - mCitrine (a.u.)
Inducer
6 h
24 h
J
Prne - mKate2 (a.u.)
50 100 150 200 250
Cell length (%)
EXP MMC RIF M5 CAP C109 INH
0 500 1000 1500
PhupB - mCitrine (a.u.)
G
6 h
6 h rne_si
Inducer
24 h
24 h rne_si
Inducer
H
P = 0.002
Length (µm)
Inducer
6 h
24 h
I
P < 0.0001 P = 0.04
PhupB - mCitrine (a.u.)
Inducer
6 h
24 h
K
****
****
Cell length (µm)
EXP MMC RIF M5 CAP C109 INH

Figure S3. Characterization of *M. smegmatis* P*rne* - mKate2_P*hupB* - mCitrine dual reporter and validation of the molecular association between RNase E and HupB, related to Figure 22.

(A) Bulk growth kinetics of *M. smegmatis* WT, P*rne* - mKate2 and dual P*rne* - mKate2_P*hupB* - mCitrine fluorescent reporter strains. Mean values ± SD (n = 3). Statistics by one-way ANOVA.

(B) qRT-PCR analysis of *hupB* gene expression in *M. smegmatis* WT (white bars) and P*hupB* - mCitrine fluorescence reporter strain (yellow bars) from exponential to stationary growth-phase. To distinguish between the native copy of *hupB* and the copy fused to *mCitrine*, either *hupB*-specific or *mCitrine*-specific primers were used, respectively. Transcripts are normalized to total RNA and 16S rRNA copies. Mean values ± SD are plotted on a Log 10 scale (n = 2). Statistics by 2-way ANOVA, followed by Sidak's multiple comparisons test.

(C) Representative Coomassie-stained SDS-PAGE (left panel) and western blot (right panel) of whole-cell extract from *M. smegmatis* co-transformed with P*hupB* - mCitrine and His-tagged RNase E, used to co-immunoprecipitate HupB-mCitrine and RNase E-His using a GFP-Trap (Chromotek) against mCitrine. Whole bacterial extracts (WE), flow through (FT), pooled washing steps (W), and eluate (E) were loaded on precast 4-12% SDS-PAGE gel. The presence of the RNase E (~140 kDa) was detected by an antibody against 6X-His-tag fused to the C-terminal of the RNase E, the presence of HupB (~50 kDa) was detected by an antibody against mCitrine fused at the C-terminal of HupB, and both proteins were revealed by chemiluminescence using HRP-labelled secondary antibodies. See also Experimental Procedures.

(D, G) Representative snapshot images of *M. smegmatis* P*hupB* – mCitrine carrying either the acetamide-inducible *rne*-overexpressing plasmid (**D**), or the anhydrotetracycline-inducible *rne*-silencing CRISPRi-dCas9 system (**G**). Strains were imaged in the absence (left panels) and in the presence (right panels) of inducer, in exponential growth-phase (6 hours) and stationary growth-phase (24 hours). Phase contrast (blue) and fluorescence (yellow) are merged. Fluorescence images are scaled to the brightest frame. Scale bar 5 μm. The experiment was repeated twice.

(E, H) Snapshot analysis of single-cell length of *M. smegmatis* P*hupB* – mCitrine carrying either the acetamide-inducible *rne*-overexpressing plasmid (E), or the anhydrotetracycline-inducible *rne*-silencing CRISPRi-dCas9 system (H). The absence (–) and presence (+) of inducer and the time of induction are indicated.

(F, I) Snapshot analysis of single-cell fluorescence of *M. smegmatis* P*hupB* – mCitrine carrying either the acetamide-inducible *rne*-overexpressing plasmid (F), or the anhydrotetracycline-inducible *rne*-silencing CRISPRi-dCas9 system (I). The absence (–) and presence (+) of inducer and the time of induction are indicated.

Violin plots (E, F, H, I) show all individual cells with medium smoothing (n = 150 per condition). Significance by one-way ANOVA, followed by Sidak's multiple comparisons test. The data shown are from 2 independent experiments.

(J, K) Snapshot analysis of fluorescence (J) of single-cell length (K) of the dual P*rne* - mKate2_P*hupB* - mCitrine reporter in exponential growth-phase (EXP), and following 6 hours of exposure to MMC (200 ng/ml), rifampicin (RIF, 20 μg/ml), M5 RNase E inhibitor (2.5 mM), chloramphenicol (CAP, 16 μg/ml), FtsZ inhibitor (C109, 16 μg/ml) and isoniazid (INH, 20 μg/ml). Heat maps (J) show P*rne* - mKate2 (magenta gradient) and P*hupB* - mCitrine (yellow gradient) fluorescence as a function of the percent of cell length of one representative cells per condition. Fluorescence intensity scale bars are also reported. Violin plots (K) show all individual cells with medium

smoothing ($150 < n < 299$). Asterisks denote significance by one-way ANOVA, ****$P < 0.0001$. The data shown are from 2 independent experiments.

Figure S4

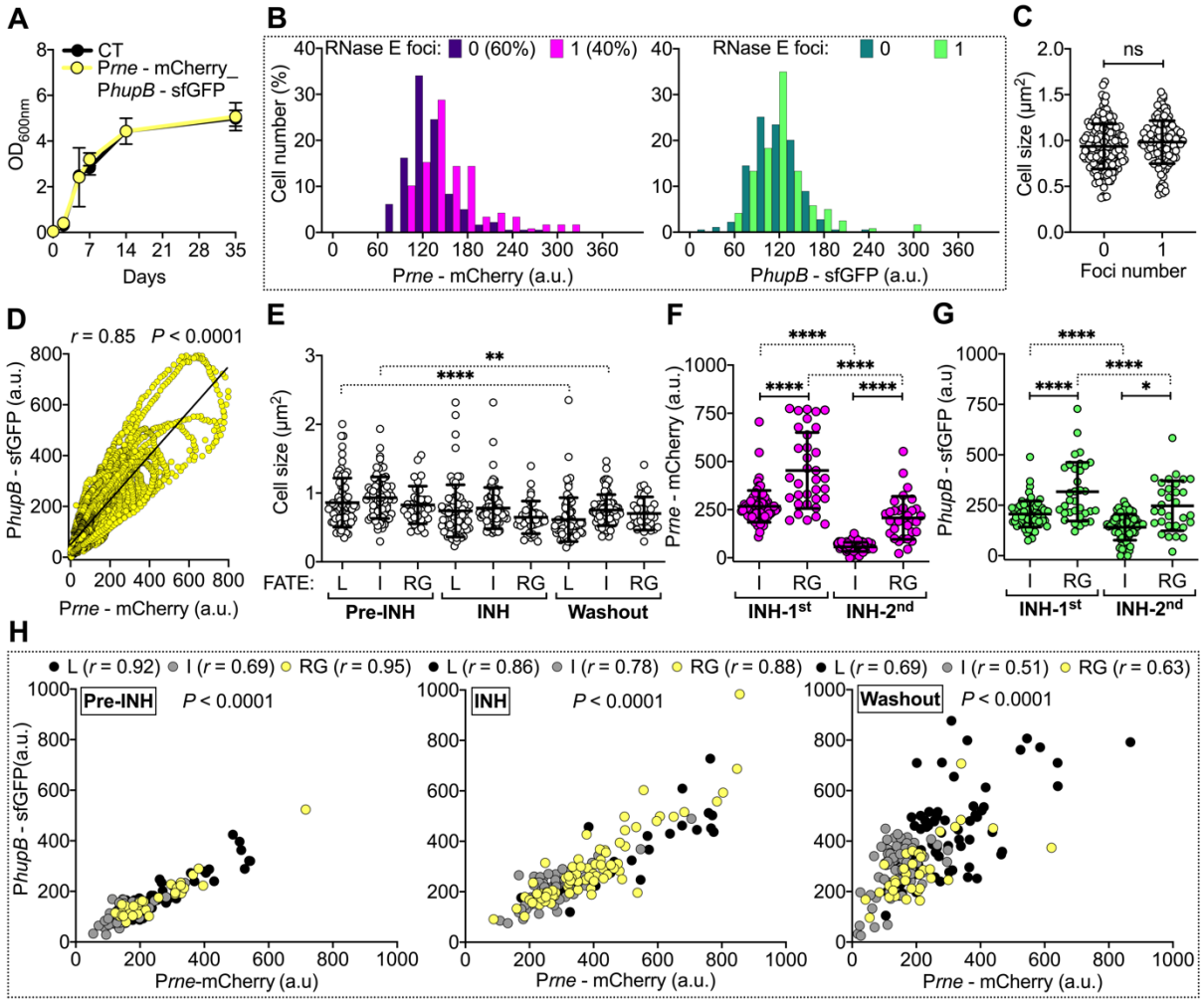
A
CT
Prne - mCherry_
PhupB - sfGFP
OD600nm
Days
B
RNase E foci: 0 (60%) 1 (40%)
Cell number (%)
Prne - mCherry (a.u.)
RNase E foci: 0 1
PhupB - sfGFP (a.u.)
C
ns
Cell size (µm2)
Foci number
D
r = 0.85 P < 0.0001
PhupB - sfGFP (a.u.)
Prne - mCherry (a.u.)
E
Cell size (µm2)
FATE: L I RG L I RG L I RG
Pre-INH
INH
Washout
F
Prne - mCherry (a.u.)
I RG I RG
INH-1st
INH-2nd
G
PhupB - sfGFP (a.u.)
I RG I RG
INH-1st
INH-2nd
H
L (r = 0.92) I (r = 0.69) RG (r = 0.95)
L (r = 0.86) I (r = 0.78) RG (r = 0.88)
L (r = 0.69) I (r = 0.51) RG (r = 0.63)
Pre-INH P < 0.0001
INH P < 0.0001
Washout P < 0.0001
PhupB - sfGFP(a.u.)
Prne-mCherry (a.u)
Prne - mCherry (a.u.)
Prne - mCherry (a.u.)

Figure S4. *M. tuberculosis* Prne - mCherry_PhupB - sfGFP dual reporter during optimal growth and isoniazid treatment, related to Figure 23

(A) Bulk growth kinetics of M. tuberculosis Erdman control strain (CT) and of the merodiploid Prne - mCherry_PhupB - sfGFP dual-fluorescent reporter. Mean values ± SD (n = 3).

(B) Distribution of the Prne - mCherry (left panel) and PhupB - sfGFP (right panel) fluorescence in single cells segregated by the absence (0) or the presence (1) of RNase E foci ($120 < n < 179$). The data shown are from two independent experiments.

(C) Single-cell cell size averaged over the lifetime of the cell in the two subpopulations defined in (B). Black lines indicate mean ± SD ($120 < n < 179$). The data shown are from two independent experiments.

(D) Pearson r correlation between the microcolony Prne - mCherry and PhupB - sfGFP fluorescence. The correlation was computed by measuring the total fluorescence values from a region of interest of constant size through the whole time-lapse image sequence (n = 26 microcolonies). The data shown are from two independent replicates.

(E) Snapshot analysis of single-cell size of the dual Prne - mCherry_PhupB - sfGFP reporter before (Pre-INH), during (INH) and after INH exposure (Washout). Columns indicate cells that lysed (L), remained intact (I) and regrew (RG). Black lines indicate mean ± SD ($34 < n < 76$). The data shown are from two independent experiments. Asterisk denote significant difference by one-way ANOVA followed by Tukey's multiple comparisons test: **P = 0.0043; ****P < 0.0001.

(F, G) Comparison of single-cell Prne - mKate2 (F) and PhupB - mCitrine (G) fluorescence of cells that remained intact (I) and regrew (RG) after the first INH treatment, monitored at the end of the first (INH-1st) and the second (INH-2nd) INH exposure period. Black lines indicate mean ± SD ($34 < n < 76$). The data shown are from two independent experiments. Asterisk denotes significant difference by one-way ANOVA followed by Tukey's multiple comparisons test: *P = 0.01; ****P < 0.0001.

(H) Pearson r correlation between single-cell Prne - mCherry and PhupB - sfGFP fluorescence of cells that lysed (L, black circles), remained intact (I, gray circles) and regrew (RG, yellow circles) at different experimental phases reported in the insets: Pre-INH (Day 4); INH (Day 5) and Washout (Day 12) ($34 < n < 76$).

Figure S5

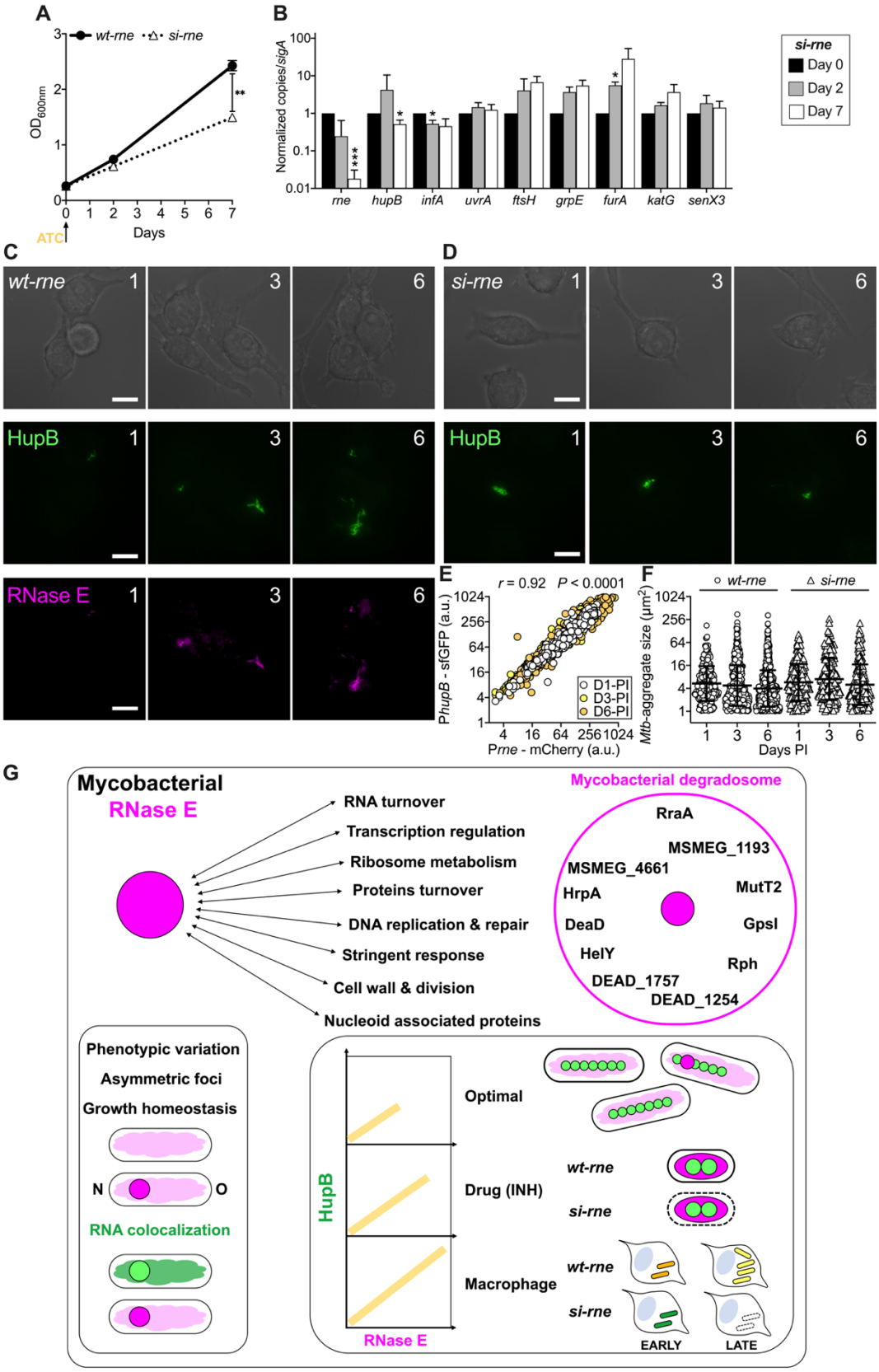
A
wt-rne
si-rne
OD600nm
Days
ATC
B
Normalized copies/sigA
si-rne
Day 0
Day 2
Day 7
rne
hupB
infA
uvrA
ftsH
grpE
furA
katG
senX3
C
wt-rne
HupB
RNase E
D
si-rne
HupB
E
r = 0.92 P < 0.0001
PhupB - sfGFP (a.u.)
Prne - mCherry (a.u.)
D1-PI
D3-PI
D6-PI
F
wt-rne
si-rne
Mtb-aggregate size (µm2)
Days PI
G
Mycobacterial
RNase E
RNA turnover
Transcription regulation
Ribosome metabolism
Proteins turnover
DNA replication & repair
Stringent response
Cell wall & division
Nucleoid associated proteins
Mycobacterial degradosome
RraA
MSMEG_1193
MSMEG_4661
HrpA
MutT2
DeaD
GpsI
HelY
Rph
DEAD_1757
DEAD_1254
Phenotypic variation
Asymmetric foci
Growth homeostasis
N
O
RNA colocalization
HupB
RNase E
Optimal
Drug (INH)
Macrophage
wt-rne
si-rne
EARLY
LATE

Figure S5. Bulk- and single-cell validation of rne silencing in *M. tuberculosis*, related to Figure 24

(A) Bulk growth kinetics of *M. tuberculosis* P*hupB* - sfGFP reporter carrying the pLJR965 vector as a control (*wt-rne*, solid line), or carrying the ATC-inducible CRISPRi-dCas9 system to silence *rv2444c* (*si-rne*, dotted line) in the L5 phage integration, see also Materials and Methods. Mean values ± SD (n = 3). Asterisks denote significant difference by 2-way ANOVA followed by Sidak's multiple comparisons test, $^{**}P = 0.0019$.

(B) qRT-PCR analysis of genes encoding putative RNase E interactors in *M. tuberculosis wt-rne* and *si-rne* strains (see also **Figure 2A**). Gene expression levels are reported at different time points after induction with ATC 100 ng/ml, as indicated in the inset. Transcripts are normalized to total RNA, *sigA* mRNA copies. Values are reported following normalization of *si-rne* against *wt-rne* strain. Mean values ± SD are plotted on a Log 10 scale (n = 2). Asterisks denote significant difference compared to day 0 by 2-way ANOVA followed by Dunnett's multiple comparisons test: $^{*}P < 0.05$; $^{***}P = 0.0001$. See also Supplemental Experimental Procedures.

(C, D) Representative snapshots images of RAW264.7 macrophages infected with either P*rne* - mCherry_P*hupB* - sfGFP (*wt-rne*) (C) or P*hupB* - sfGFP_*si-rne* (*si-rne*) (D) reporter strains in the presence of ATC 100 ng/ml. Each image is derived from the projection of a stack of 6 snapshots taken on the same field of view sequentially at 1-µm z-step from each other, using the maximum intensity method (SoftWorx). Bright field (upper panels) and green fluorescence (middle panels) are reporter for both strains. P*rne* - mCherry fluorescence is shown only for the P*rne*-mCherry_P*hupB*-sfGFP dual-fluorescent reporter (C, bottom panels). Numbers indicate days. Scale bar, 10 µm. See also Materials and Methods.

(E) Pearson correlation of P*rne* - mCherry and P*hupB* - sfGFP mean fluorescence of intracellular bacteria (both individual bacilli and aggregates) in individual macrophages at different time points post infection (PI) as specified in the inset, and after adding ATC 100 ng/ml in the cell-culture medium to induce *rne* silencing. The data shown are from 3 independent experiments ($278 < n < 2028$).

(F) Comparison of the size of intracellular *M. tuberculosis* (both individual bacilli and aggregates), P*rne* - mCherry_P*hupB* - sfGFP (*wt-rne)* and P*hupB* - sfGFP_*si-rne* (*si-rne*), at 1, 3- and 6-days PI. Black lines indicate means ± SD. The data shown are from 3 independent experiments ($216 < n < 1259$).

(G) Summary of the main findings from the mass spectrometry-based proteomic analysis of the RNase E interactome in *M. smegmatis* (top-left). Double-headed arrows indicate the main categories of putative interactors for which we characterized a shortlist. The magenta circle contains the significant proteins that were pulled down together with RNase E, and that perform functions associated with RNA turnover and are likely to contribute to the functioning of the mycobacterial RNA degradosome. Schematic of the characterization of the RNase E fluorescent reporter strain in single mycobacterial cells (bottom-left inset). Under optimal growth conditions, RNase E is expressed at a low level in all cells following a patchy distribution, while only one subpopulation exhibits brighter foci, which tend to localize towards the new cell pole, and positively correlate with a specific RNA dye. Schematic of the interaction between RNase E and HupB fluorescent reporters in single *M. tuberculosis* cells (bottom-right inset). RNase e and HupB are positively correlated under optimal growth conditions, and they are induced and their level of correlation increases during isoniazid (INH) treatment and macrophage infection.

Silencing of *rne* during INH treatment leads to faster cell lysis. Silencing of *rne* during infection improves macrophage clearance at late stage of infection.

Supplemental Experimental Procedures.

MIC evaluation by resazurin assay

Exponentially growing cultures were diluted to OD_{600} 0.005 using pre-warmed Middlebrook 7H9 broth. Each well of 96-well plate was filled with 100 µl of the diluted cell suspension. For each plate, the first row was filled with only pre-warmed 7H9 medium and used as a negative control, while the second row was filled only with the cellular suspension, no drug was added, and this row was used as a positive control. Only the first well of each row was filled with 200 µl of cell suspension. In this well, the highest concentration of drug was added and then twofold serially diluted. After 24 hours of incubation at 37°C, 10 µL/well of 0.01% resazurin was added. The plate was reincubated at 37°C for 24 h and then read out. Pink wells indicated bacterial viability, whereas wells with the unchanged blue color indicated cidality. The MIC was counted as the lowest drug concentration causing cidality.

5' RACE

12 mL of secondary exponentially growing cultures in 7H9 broth of wild type *M. smegmatis* were washed twice in 5 mL of pre-warmed HDB short-chain fatty acid enriched media. The final cellular suspension was diluted to a final OD_{600} of 0.25 and incubated for 12 hours at 37°C in short-chain fatty acid enriched media. After 12 hours, the culture wass centrifugated at 4,200 g for 15 minutes at 4°C. Cell pellet was resuspended in 700 µl of TRIzol (Sigma) and transferred into a 2 mL vials prefilled with glass beads (Precellys). The cell suspension was lysed by bead-beating two times at 4 234 g for 60 seconds, with 5 minutes intervals on ice, and centrifuged at 12 000 g for 10 minutes. The supernatant was recovered, and the RNA was precipitated with 1 volume of isopropanol enriched with 0.5% carrier (Invitrogen), washed in 70% ethanol, and resuspended in 44 µl of DEPC-treated water. Any gDNA contamination in the sample was removed performing a dual treatment with Turbo DNase (Ambion). After the DNase treatment, the sample was quantified by Nanodrop. 3 µg of the isolated RNA was used to perform reverse transcription (RT) for the cDNA, the first step of the 5'-RACE. The RT reaction was done using Transcriptase inverse Superscript™ IV and random hexamers (ThermoFisher), in agreement with the manufacturer's instruction. To remove the RNA, the cDNA was treated with RNase H (NEB) 37 °C for 20 minutes before proceeding with cDNA purification by QIAquick PCR Purification Kit (Qiagen). The second step of the 5'-RACE was a tailing step using dATP. The reaction mixture was prepared using 20 µL of purified cDNA, 10 mM of dATP, 10 U of terminal deoxynucleotidyl transferase (TdT) (NEB), 10x terminal transferase buffer and the 2.5 mM CoCl2

solution, with the final volume of 50 µL. The reaction was incubated at 37 °C for 30 minutes, and TdT was heat-inactivated at 70 °C for 10 minutes. The third step of the 5'-RACE included two PCR amplification round. The first-round PCR mixture contained 5 µl of dAtailed cDNA template, 0.15 mM MgCl2, 0.2 mM dNTPs, 200 nM of gene-specific primer 4626 (GSP_4626) (5'-ATAGGTCTTCGGTATGGGCATCTT-3') and the QT primer (5' -CCAGTGAGCAGAGTGACGAGGACTCGAGCTCAAGCTTTTTTTTTTTTTTTT-3') (Scotto-Lavino et al., 2007), 10x DreamTaq DNA polymerase and 1 U of DreamTaq DNA polymerase (ThermoFisher) with the final volume of 50 µL. The annealing step was performed at 60 °C for 30 seconds. The PCR-amplification of the fragment was executed for 40 cycles. The second-round PCR was performed with 5 µL of the first PCR product, 200 nM of GSP4626 and Qi primer (5'-GAGGACTCGAGCTCAAGC-3') (Scotto-Lavino et al., 2007). The fragment amplification was performed as of the first-round PCR. The annealing step was fixed at 65 °C for 30 seconds. The PCR-amplification of the fragment was executed for 25 cycles. The final reaction was purified by QIAquick PCR Purification Kit (Qiagen) for the sequencing of the obtained specific amplified product.

Real-time quantitative PCR

M. smegmatis and *M. tuberculosis* wild-type and fluorescent reporter strains were cultured in Middlebrook 7H9 broth until OD_{600} 0.25. The samples were split and reincubated at 37°C, either with or without stress or inducer. At regular intervals, culture volumes corresponding to OD_{600} 3.0 were taken. The collected cells were centrifugated at 4 200 g for 10 minutes at 4°C. Cell pellets were resuspended in 700 µl of TRIzol (Sigma) transferred into a 2 mL vials prefilled with glass beads (Precellys). Cell suspensions were lysed by bead-beating two times at 4 234 g for 60 seconds, with 5 min intervals on ice, and centrifuged at 12 000 g for 10 minutes. The supernatant was recovered, and the RNA was precipitated with 1 volume of isopropanol enriched with 0.5% carrier (Invitrogen), washed in 70% ethanol, and resuspended in 44 µl of DEPC-treated water.

To deplete DNA contamination, the isolated RNA was treated twice with Turbo DNase (Ambion), and cDNA was generated starting from around 250 ng of RNA using Transcriptase inverse Superscript™ IV (Invitrogen) and random hexamers (ThermoFisher), in agreement with the manufacturer's instruction. To remove the RNA contamination, the cDNA was treated with RNase H (NEB) 37 °C for 20 minutes and then inactivated for 10 minutes at 70 °C. *M. smegmatis* primers specific for *16s*, *rne, gsI, dead, hely, rraa, nudix, gpsI, recx, recb, uvra, rela, obg, ppk, mazf, pap, pks, prcb, clpb, grpe, lsr2(MSMEG_6092), lsr2(MSMEG_1060) infa, hupb, rne::mKATE2, mCitrine, and M. tuberculosis* primers specific for *rne, hupb, siga, uvra, ftsh, senX3, grpe, infa, katG, furA,* are listed in Annex 1, Table S1.

qRT–PCRs were carried out using the SYBR Green PCR Master Mix (Applied Biosystems), 0.3 µM primers, and 1 µL cDNA diluted 1:4. Absolute quantification was run on the LightCycler®480 Instrument (Roche Life Science). Standard curves were generated using serial dilutions of *M. smegmatis and M. tuberculosis* gDNA and were used to calculate transcripts copy numbers. Each biological sample was at least measured in duplicate.

Western blot assay

Western blot assays were carried out either on whole-cell extracts from the AGS2, AGS17 strains, or the pull-down of the AGS2 induced strain. Culture volumes corresponding to OD_{600} 5.0 were collected, and centrifugated at 4 200 g for 10 minutes at 4°C. Pellets were washed with 1 mL of protein lysis buffer (50 mM Tris-Cl pH 7.5, 50 mM NaCl, 5% glycerol, and 1x Protease Inhibitor Cocktail (Roche) centrifuged at 4 200 g for 10 minutes at 4°C and finally resuspended in 500 µL of protein buffer. Cell suspensions were sonicated for 5 cycles of 30 seconds at 100% amplitude, with 45 seconds intervals on ice. The cellular extracts were quantified using Bradford reagent (Sigma), and a maximum of 15 µg were used for the assay. Bis-Tris NuPAGE™ Novex™ 4 to 12% gels (ThermoFisher) were run at 100 V for 2 hours. Proteins were transferred into a PVDF membrane by wet-transfer performed at 30 V for 1 hour. The equal loading was confirmed by Ponceau S staining (Sigma). The membrane was blocked with 5% non-fat dry milk in 0.01% Tween20 (Sigma) TBS (ThermoFisher) (TBS-T) for 1 hour, incubated with primary antibody overnight at 4°C, washed three times with TBS-T for 5 min, incubated with the peroxidase-conjugated secondary antibody in TBS-T with 5% non-fat dry milk for 1 hour at RT, and washed three times with TBS-T for 5 min. Proteins were detected using the Pierce ECL Western Blotting Substrate (Thermo Scientific) and Bio-Rad ChemiDoc™ MP Imager. Primary and secondary antibodies were diluted in TBS-T, and 5% non-fat milk as follows: anti-GFP (1:5 000), anti-HSP 65 (1:5 000), anti-6xHist (1:1 000), HRP-conjugated anti-rabbit (1:2 000) and HRP-conjugated anti-mouse (1:2 000).

P*hupB*-mCitrine immunorecipitation

Single colonies of AGS33 strain were cultured in 7H9 selective broth and diluted to OD_{600} 0.01 until they reached OD600 0.5. Secondary cultures were induced with 0.05% acetamide and incubated at 37°C for 24 hours. After 24 hours of induction, 12 mL of culture were centrifugated at 4 200 g for 15 minutes at 4°C. Pellets were resuspended in 500 µL of protein lysis buffer (10 mM Tris-HCl pH 7.5, 150 mM NaCl, 0.5% glycerol, and 1×Protease Inhibitor Cocktail (Roche)). Cell

suspensions were sonicated for 5 cycles of 30 seconds at 100% amplitude, with 45 seconds intervals on ice. The cell lysates were centrifuged at 10 000 g for 1 hour at 4°C and quantified by Bradford reagent (Sigma). P*hupB-mCitrine* fraction was immunoprecipitated by using GFP-Trap® (Chromotek). The GFP-Trap® beads were equilibrated by adding 500 µl of ice-cold protein buffer and then incubated with 250 µg of protein extract for 4 hours at 4°C. Subsequently, the GFP-Trap® bead were washed initially with 500 µL of protein buffer and then with the same buffer containing 500 mM NaCl to remove non-specific bound proteins. HupB-mCitrine bound protein was dissociated by resuspending the beads in 80 µL of 2x SDS Sample Loading Buffer (Invitrogen), and boiling the suspension for 5 minutes at 95°C. 15 µL of the eluate were loaded on Bis-Tris NuPAGE™ Novex™ 4 to 12% gels for both western blot analysis and Coomassie staining

Annex 1 Table

Annex Table S1. Reagents and software used in this study. Restriction sites of oligonucleotide are bolded.

REAGENT DESCRIPTION	SOURCE	ID/NAME
Oligonucleotide		
Cloning, *linker-mKATE2*-for 5'-CT**ACTAG**GGTAGCGGTAGCGGTAGCATGCA TCAAGCTT GGTACCGA - 3'	This paper, Eurofins	#24748516
Cloning, *mKATE2*-rev 5'-GA**GATTC**TCATCTGGTGCCCCAGTTTGCT-3'	This paper, Eurofins	#24748521
Cloning, *linker-mCherry*-for 5'-TG**CCTAGG**GGTAGCGGCAGCGGTAGCGTGAG CAAGGGCGAGGAGGATAAC-3'	(Manina et al., 2019)	/
Cloning, *mCherry*-rev 5-ATGTTAACTTACTTGTACAGCTCGTCCATGCC-3'	(Manina et al., 2019)	/
Cloning, *linker-mCitrine* -for 5'-TA**ACTAGT**GGTAGCGGTAGCGGTAGCATGGTG AGCAAGGGCGAGGAG-3'	(Manina et al., 2019)	/
Cloning, *mCitrine* -rev 5'-AT**GTTAAC**TTACTTGTACAGCTCGTCCAT-3'	(Manina et al., 2019)	/
Cloning, *linker-sfGFP* -for 5'-AT**ACTAGT**GGTAGCGGTAGCGGTAGCATGCGT AAAGGCGAAGAGCTGTTC-3'	This paper, Eurofins	#23920806
Cloning, *sfGFP*-rev 5'-GA**GAATTC**TCATTTGTACAGTTCATCCAT-3'	This paper, Eurofins	#23920807
Cloning, SD-*rne-6xHist*-for 5'-AT**GGATCC**TAAGAAGGAGATATACATGTGGC CGAAGATGCCCATACC-3'	This paper, Eurofins	#23385816
Cloning, *rne*-TEV-*6xHist*-rev 5'-AT**GCTAGC**CGCTTGGAAGTACAGGTTTTCGTC GTGCGTGGGCGGCCCCGC-3'	This paper, Eurofins	#23385817
Cloning, P-M*SMEG_4626(rne)*-for 5'-AG**GTTAAC**AGACTTCGACGTGCGCGACCA-3'	This paper, Eurofins	#24171967
Cloning, P-M*SMEG_4626(rne)*-rev 5'- AT**ACTAGT**GTCGTGGCTGGGCGGCCCCGC -3'	This paper, Eurofins	#24413550
Cloning, P-*MSMEG_5042(DEAD)*-for 5'-AT**GGTACC**CACCGCACGCGCGATCTCCGG-3'	This paper, Eurofins	#26252670

Cloning, P-*MSMEG_5042(DEAD)*-rev 5'- TA**ACTAGT**CTTCACCTTCCGGTGTGGCTT-3'	This paper, Eurofins	#26252671
Cloning, P-*MSMEG_6439(RraA)*-for 5'-AT**GGTACC**GTCGTGACCGGGTACGGCCGG-3'	This paper, Eurofins	#26252672
Cloning, P-*MSMEG_6439(RraA)*-rev 5'- TA**ACTAGT**GGGGGTAACGACGACGATGCC-3'	This paper, Eurofins	#26252673
Cloning, P-*MSMEG_4623(Obg)*-for 5'-AT**GGTACC**ACGAGCATCACGGTGTCTCAG-3'	This paper, Eurofins	#26252680
Cloning, P-*MSMEG_4623(Obg)*-rev 5'-TA**ACTAGT**CGAGTCCTCTCCTCCCGATTC-3'	This paper, Eurofins	#26252681
Cloning, P-*MSMEG_2965(RelA)*-for 5'-AT**GGTACC**TCCACGGAGCGACGTACCAAT-3'	This paper, Eurofins	#26252676
Cloning, P-*MSMEG_2965(RelA)*-rev 5'-TA**ACTAGT**GGCCGCGCTGGTGACGCGGTA-3'	This paper, Eurofins	#26252677
Cloning, P-*MSMEG_2391_2392(ppk)*-for 5'-AT**TCTAGA**CACGGCCAACATCACGGTGCA-3'	This paper, Eurofins	#26252678
Cloning, P-*MSMEG_2391_2392(ppk)*-rev 5'-TA**ACTAGT**TGGCTGGCGGTGGCGTTCCAT-3'	This paper, Eurofins	#26252679
Cloning, P-*MSMEG_3808 (UvrA)*-for 5'-AT**GGTACC**CAGCAGCGTCTCGCCGGTAGA-3'	This paper, Eurofins	#26252674
Cloning, P-*MSMEG_3808 (UvrA)*-rev 5'-TA**ACTAGT**GGCGCTGACCTTGCGCCGCTT-3'	This paper, Eurofins	#26252675
Cloning, P-*MSMEG_1060 (Lsr2)*-for 5'-AT**GGTACC**ATTCGCGGCGACCGTGCATCG-3'	This paper, Eurofins	#26331636
Cloning, P-*MSMEG_1060 (Lsr2)*-rev 5'-TA**ACTAGT**CACCCTCAACTGCGAAGAGCC-3'	This paper, Eurofins	#26331637
Cloning, P-*MSMEG_1519 (InfA)*-for 5'-AT**GGTACC**CGTGTTGTCGTCTCCGGTCTC-3'	This paper, Eurofins	#26331632
Cloning, P-*MSMEG_1519 (InfA)*-rev 5'-TA**ACTAGT**CTTGTACCGGTACACGATGCG-3'	This paper, Eurofins	#26331633
Cloning, P-*MSMEG_2389 (hupB)*-for 5'-AT**GGTACC**ATCCGGGCCTTCGGCGACCCG -3'	This paper, Eurofins	#26331638
Cloning, P-*MSMEG_2389 (hupB)*-rev 5'-TA**CCTAGG**CCTGCGGCCCTTCTTGGCCGG-3'	This paper, Eurofins	#26331639
Cloning, *rne_D694R_F* 5'- GACCGTCGTC**AGG**GTCAACACCGGCAAGTTCAC-3'	This paper, Eurofins	#23385818
Cloning, *rne_D694R_R* 5' – ATGGCCTCGGTGCGGTCG – 3'	This paper, Eurofins	#23385819

Cloning, *rne_D798R_F* 5'- CGTCGTCATC**AGG**TTCATCGACATGGTCCTGGAA TCCAACCG – 3'	This paper, Eurofins	#23385820
Cloning, *rne_D798R_R* 5'- ATGCCGCCGATGTCGCGC – 3'	This paper, Eurofins	#23385821
Cloning, P-*Rv2444c (rne)*-for 5`- AT**GTTAAC**GCTCCGGGTGCGCCGATCCCG – 3`	This paper, Eurofins	#24776883
Cloning, P-*Rv2444c (rne)*-rev 5`- GC**ACTAGT**GTCTAGGCGGATTGGTGGGCC – 3'	This paper, Eurofins	#24776885
Cloning, P-*Rv2986c (hupB)*-for 5'-CA**GAATTC**AGGCGTAGAACCGGGCGAAAT-3'	This paper, Eurofins	#12CO001CST
Cloning, P-*Rv2986c (hupB)*-rev 5'-AT**CCTAGG**TTTGCGACCCCGCCGAGCGGT-3'	This paper, Eurofins	#12CO002CST
M. smegmatis qRT-PCR primers		
16s (MSMEG_3757) - for 5'-AATTCCTGGTGTAGCGGTGG-3'	This paper, Eurofins	#22543593
16s (MSMEG_3757) - rev 5'-GTTTACGGCGTGGACTACCA-3'	This paper, Eurofins	#22543594
rne (MSMEG_4626) - for 5'-GAGGTCACCGAGAAGAAGGC-3'	This paper, Eurofins	#22543590
rne (MSMEG_4626) - rev 5'-ACGGCCTCTACGTAGGAGTT-3'	This paper, Eurofins	#22543589
rne-mKATE2-for 5'-CTCGGATGAGGACGAAGAGC-3'	This paper, Eurofins	#24605411
rne-mKATE2-rev 5'-CAGCTCGCTCACCATGGTAA-3'	This paper, Eurofins	#24605412
mCitrine-for 5'-ATCATGGCCGACAAGCAGAA-3'	This paper, Eurofins	#26425097
mCitrine-rev 5'-TCTCGTTGGGGTCTTTGCTC-3'	This paper, Eurofins	#26425098
recX (MSMEG_2724) - for 5'-TGATCGACGATGAGGACTTCG-3'	This paper, Eurofins	#25823971
recX (MSMEG_2724) - rev 5'-TGACCTTGACGTCGTTTTCC -3'	This paper, Eurofins	#25823972
RraA (MSMEG_6439) - for 5'-GCTGCTGAAGTCGATCCTCTC-3'	This paper, Eurofins	#25823967
RraA (MSMEG_6439) - rev 5'-TTGATACCGACGTCGATGGTG-3'	This paper, Eurofins	#25823968

ppk-for 5'-TCGGGTTGAAGACACATTGC-3'	This paper, Eurofins	#25823983
ppk-rev 5'-TTGCGATAGGAATCCTTGCG-3'	This paper, Eurofins	#25823984
uvrA-for 5'-AGATGGGGTTCGACGTCAAC-3'	This paper, Eurofins	#25823975
uvrA-rev 5'-AAAAACGCCATGACGCCTTC-3'	This paper, Eurofins	#25823976
grpE-for 5'- GTGACCATCACCGACAAACG-3'	This paper, Eurofins	#25823999
grpE-rev 5'-TAGTTGTCGTACTCGGCCTTG-3'	This paper, Eurofins	#25824000
clpB-for 5'-ATCGCACTGGATCTCGGTTC-3'	This paper, Eurofins	#258233995
clpB-rev 5'-ATCGGCTTGATCATGTTGCC-3'	This paper, Eurofins	#258233996
recB-for 5'-TGTTGCATTCCGACTATCCG-3'	This paper, Eurofins	#258233973
recB-rev 5'-TCCAACAGCTTCGACAATGC-3'	This paper, Eurofins	#258233974
obg-for 5'-TTGCGCCCGTTGATATTTGC-3'	This paper, Eurofins	#258233981
obg-rev 5'-TCGTTGTTGAAGTCGGTCTG-3'	This paper, Eurofins	#258233982
relA-for 5'- AAGTGGTCGAGGTGTTCACC-3'	This paper, Eurofins	#258233979
relA-rev 5-ATTCATCAAGCGCTGCAACG-3'	This paper, Eurofins	#258233980
helY-for 5'-AATGCTTCTACACCACCCCG-3'	This paper, Eurofins	#258233965
helY-rev 5'-GAAGTGCACCTCGTCCATCA-3'	This paper, Eurofins	#258233966
mutT4-for 5'-TGCCGTTCATGGACTTCAAC-3'	This paper, Eurofins	#258233969
mutT4-rev 5'-TTCGTGAAGTGCAGCGATTC-3'	This paper, Eurofins	#258233970
dead-for 5'-TTCGGCCATATCACCATCCG-3'	This paper, Eurofins	#25999227
dead-rev 5'-CTTCCGGTGGTGGCTTGTACT-3'	This paper, Eurofins	#25999228

lsr2(MSMEG_6092)-for 5'-CCTCGACGGTGTGACCTATG-3'	This paper, Eurofins	#25999231
lsr2(MSMEG_6092) - rev 5'-GATCACGTCGGCAGGAATCC-3'	This paper, Eurofins	#25999232
gspI-for 5'-CAGATCCTGGGTGTCACCAC-3'	This paper, Eurofins	#25999234
gspI-rev 5'-GCGTACGGGAACTCTTCGAT-3'	This paper, Eurofins	#25999235
infA-for 5'-AGAAAGACGGTGCCATCGAG-3'	This paper, Eurofins	#26359125
infA-rev 5'-AGGTCGTACGGAGAGAGCTC-3'	This paper, Eurofins	#26359126
lsr2(MSMEG_1060) - for 5'-GCTACATCATCAAGGCCGCAAAG-3'	This paper, Eurofins	#26331636
lsr2(MSMEG_1060) -rev 5'-ACACCCTCAACTGCGAAGAG-3'	This paper, Eurofins	#26331637
hupB-for 5'-AGAACGTCGTCGACACCATC-3'	This paper, Eurofins	#26331638
hupB - rev 5'-TCTGTGCGCCAGAGATAACC-3'	This paper, Eurofins	#26331639
pnp-for 5'-CACTTCGACTTCTTCCCGCT-3'	This paper, Eurofins	#22543595
pnp-rev 5'-CCTCACGACGGAAGAACGAA-3'	This paper, Eurofins	#22543596
rhlE (MSMEG_1930) - for 5'-GACAAGGTCGAGCTGGTGAG-3'	This paper, Eurofins	#22543603
rhlE (MSMEG_1930) - rev 5'-ACTTGAGGGCTTTCTCACGG-3'	This paper, Eurofins	#22543604
Eno-for 5'-TGTCGATCGAAGATCCGCTG-3'	This paper, Eurofins	#22543599
Eno-rev 5'-GCCGATCTGGTTGACCTTCA-3'	This paper, Eurofins	#22543600
M. tuberculosis qRT-PCR primers		
sigA (Rv) – for 5'-ACGACGAAGACCACGAAGAC – 3'	This paper, Eurofins	#27779941
sigA (Rv) – rev 5' – CTTCATCCCAGACGAAATCACC – 3'	This paper, Eurofins	#27779942

rne (Rv2444c) – for *5'* – GACATGGTGCTGGAGTCCAA – 3'	This paper, Eurofins	#22543591
rne (Rv2444c) – rev 5' – ACACGATGTGGAGAACGCTT – 3'	This paper, Eurofins	#22543592
hupB (Rv2986c) – for 5' – ACGTGCTCACACAGAAATTG – 3'	This paper, Eurofins	#27779957
hupB (Rv2986c) – rev 5' – TCACCTTTACTGTCTCGCC – 3'	This paper, Eurofins	#27779958
infA (Rv3462c) – for 5' – TCCGCATTGAGCTGGAGAAC – 3'	This paper, Eurofins	#27779949
infA (Rv3462c) – rev 5' – TAGGGCGACAATTCCACCAC – 3'	This paper, Eurofins	#27779950
uvrA (Rv1638) – for 5' – GGGCTGGACTATCTGGACAA – 3'	This paper, Eurofins	#27779965
uvrA (Rv1638) – rev 5' – TTGACGTTGAACGAGAATCG – 3'	This paper, Eurofins	#27779966
ftsH (Rv3610c) – for 5' – TCATCACCAAGTACCCCACC – 3'	This paper, Eurofins	#27779969
ftsH (Rv3610c) -rev 5' – AGAACATCACGAACAGCCC – 3'	This paper, Eurofins	#27779970
grpE (Rv0351) – for 5'- ACTTCGCCAACTACCGTAAG - 3'	This paper, Eurofins	#27779911
grpE (Rv0351) – rev 5' -TCGAGATCGTCCAGTACACC - 3'	This paper, Eurofins	#27779912
furA (Rv1909c) – for 5' – CCGTCCTGGAAGCAGTGAAT – 3'	This paper, Eurofins	#28087184
furA (Rv1909c) – rev 5' – AGGGTTGGATCTTTCGCACC - 3'	This paper, Eurofins	#28087185
katG (Rv1908c) – for 5' - ACCCACCCATTACAGAAACC – 3'	This paper, Eurofins	#27779925
katG (Rv1908c) – rev 5' – GCAGTACCTTCAGATTGAGCC - 3'	This paper, Eurofins	#27779926
senX3 (Rev0490) – for 5' – GGCTACCCAATATGACCGAC – 3'	This paper, Eurofins	#27779923
senX3 (Rev0490) – rev 5' – AGGCAATCGCATTGGAAAC – 3'	This paper, Eurofins	#27779924
Q_I 5'-GAGGACTCGAGCTCAAGC-3'	This paper, Eurofins	#24948126

Q_T 5'- CCAGTGAGCAGAGTGACGAGGACTCGAGCTCAAG CTTTTTTTTTTTTTTTTT-3'	This paper, Eurofins	#24948124
GSP_4626 (Primer 2) 5'-ATAGGTCTTCGGTATGGGCATCTT-3'	This paper, Eurofins	#25442515
sgRNA_*rne*_for 5'-GGGAGTCGCCGGAGACGATCAGGCT-3	This paper, Eurofins	#26983183
sgRNA_*rne_rev* 5'-AAACAGCCTGATCGTCTCCGGCGAC-3'	This paper, Eurofins	#26983184

Plasmids		
pCR2.1-TOPO TA cloning plasmid, Amp^R, Km^R	Invitrogen	pCR2.1-TOPO
Mycobacterial expression vector, C-term 6xHist-tag pMYC	(Beckham et al., 2020)	Addgene #42192
pMV361-based integrative vector, containing L5 phage integration site, Km^R	Lab collection	pND200
pMV361-based integrative vector, containing L5 phage integration site, expressing *rne*-linker-mCherry, Hyg^R	Lab collection	pGM301
pTTP1A-based integrative vector, containing L5 phage integration site, Km^R	(Pham et al., 2007)	Addgene #91721
mCitrine-N1, containing *mEYFP* gene, Km^R	(Griesbeck et al., 2001)	Addgene #54594
pLJR962, *M. smegmatis* integrative vector (L5 phage) anhydrotetracycline inducible promoter (P_{tet}) driving catalytically-inactivated CRISPR1 *cas9* allele from *Streptococcus thermophilus*, site to integrate sgRNA and protospacer adjacent motif (PAM), Km^R	(Rock et al., 2017)	Addgene #115162
pLJR965 *M. tuberculosis* integrative vector (L5 phage), P_{tet} driving catalytically-inactivated CRISPR1 *cas9* allele from *Streptococcus thermophilus*, site to integrate sgRNA PAM, Km^R	(Rock et al., 2017)	Addgene #115163

pMYC *rne* (*MSMEG_4626*), acetamide-inducible RNase E-6xHist tag	This paper	pAG202
pMYC *rne* D694R_D738R mutant, acetamide-inducible RNase E-6xHist tag	This paper	pAG204
pND200 expressing *rne*-linker-mKate2, Km^R	This paper	pDV201
pGM218 expressing *rne*-linker-mKate2, Hyg^R	This paper	pAG212
Tweety expressing *dead*-linker-mCitrine, Km^R	This paper	pAG219
Tweety expressing *rraa*-linker-mCitrine, Km^R	This paper	pAG215
Tweety expressing *obg*-linker-mCitrine, Km^R	This paper	pAG218
Tweety expressing *relA*-linker-mCitrine, Km^R	This paper	pAG220
Tweety expressing *ppk*-linker-mCitrine, Km^R	This paper	pAG221
Tweety expressing *uvrA*-linker-mCitrine, Km^R	This paper	pAG217
Tweety expressing *lsr2*-linker-mCitrine, Km^R	This paper	pAG213
Tweety expressing *infA*-linker-mCitrine, Km^R	This paper	pAG214
Tweety expressing *hupB*-linker-mCitrine, Km^R	This paper	pAG216
pGM218 expressing *rne*-linker-mCherry, Hyg^R	This paper	pGM301
Tweety expressing *hupB*-linker-sfGFP,Km^R	This paper	pGM305
pLJR962 with Hyg^R cassette	This paper	pGM255
pLJR962 Hyg^R for *rne* (*MSMEG_4626*) CRISPRi/dCas9	This paper	pGM255
pLJR965 with Hyg^R cassette	This paper	pGM309
pLJR965 Hyg^R for *rne* (*Rv_2444c*) CRISPRi/dCas9	This paper	pGM306

Strains		
Escherichia coli DH5α	Invitrogen	Cat#12297016
Mycobacterium smegmatis mc^2155	Lab collection	ATCC®700084
ATCC®700084 - pAG202; inducible overexpressing RNase E-6x-His-tag	This paper	AGS2
ATCC®700084 - pAG204; inducible overexpressing RNase E D694R_D738R-6x-His-tag	This paper	AGS5

ATCC®700084 – pDV201; *attB::rne*-linker-mKate2	This paper	DVS2
AGS13 – pAG219, *attB::rne*-linker-mKate2_*attT::DEAD*-linker-mCitrine	This paper	AGS20
AGS13 – pAG215, *attB::rne*-linker-mKate2_*attT::rraa*-linker-mCitrine	This paper	AGS16
AGS13 – pAG218, *attB::rne*-linker-mKate2_ *attT_obg*-linker-mCitrine	This paper	AGS19
AGS13 – pAG220, *attB::rne*-linker-mKate2_ *attT::relA*-linker-mCitrine	This paper	AGS21
AGS13 – pAG221 *attB::rne-linker-mKATE2$_{wt}$*_*attT::ppk-linker-mCitrine$_{wt}$*	This paper	AGS22
AGS13 – pAG217 *attB::rne*-linker-mKate2_*attT::uvrA*-linker-mCitrine	This paper	AGS18
AGS13 – pAG213 *attB::rne*-linker-mKate2_ *attT::Lsr2*-linker-mCitrine	This paper	AGS23
AGS13 – pAG214 *attB::rne*-linker-mKate2_*attT::InfA*-linker-mCitrine	This paper	AGS15
AGS13 – pAG216 *attB::rne*-linker-mKate2_*attT::hupB*-linker- mCitrine	This paper	AGS17
ATCC®700084 – pGM255; *rne* (*MSMEG_4626*) CRISPRi/dCas9	This paper	mc^{2}155/pGM255
Mycobacterium tuberculosis Erdman	Lab collection	ATCC®35801
ATCC®35801- pGM301; *attB::rne-linker-mCherry$_{wt}$*	This paper	GMT21
GMT – pGM305 – pGM301; *attB::rne*-linker-mCherry_*attT::hupB*-linker-sfGFP	This paper	GMT25
ATCC®35801 – pGM309 ; CRISPRi/dCas9	This paper	GMT27
ATCC®35801 – pGM306 ; *rne* (*Rv_2444c*) CRISPRi/dCas9	This paper	GMT26

Antibodies		
Mouse monoclonal anti-6xHist tag (H-3)	Santa Cruz	Cat#sc-8036
Mouse monoclonal anti-HSP 65 (BDI577)	Santa Cruz	Cat#sc-57842
ECL HRP-conjugated anti-mouse m-IgGκ	Santa Cruz	Cat#sc-516102
Rabbit monoclonal anti-GFP (3E6)	Thermo Fisher	Cat#A-11120
ECL HRP-conjugated anti-rabbit	Amersham	Cat#NA934VS
GFP-Trap_A for immunoprecipitation	Chromotek	Cat#gta-20

Softwares		
Mycobrowser		https://mycobrowser.epfl.ch/
ImageJ 1.51s	(Schneider et al., 2012)	https://imagej.nih.gov/ij/
Prism Versions 8.4	GraphPad	https://www.graphpad.com/scientific-software/prism/
RStudio Version 1.1.423	RStudio, Inc	https://rstudio.com/pri
Python Version 3.8.3	Python	https://www.python.org/
Custom R script for image-analysis data post-processing	(Manina et al., 2019)	
Custom Python script for image-analysis data post-processing	This paper	NA
Custom ImageJ macros for image data analysis of intracellular bacilli	This paper	NA

Table of contents

INTRODUCTION - 1 -

AIM OF THE WORK - 125 -

MATERIALS AND METHODS - 127 -

RESULTS - 137 -

DISCUSSION - 160 -

BIBLIOGRAPHY I

ANNEX 1. XXV

Table of Figures

FIGURE 1. ESTIMATED TB INCIDENCE IN 2018. - 4 -

FIGURE 2. ESTIMATED INCIDENCE OF MDR/RR-TB[A] IN 2018. - 5 -

FIGURE 3. CIRCULAR MAP OF THE CHROMOSOME OF M. TUBERCULOSIS H37RV. - 13 -

FIGURE 4. MODEL OF THE MYCOBACTERIAL CELL ENVELOPE. - 17 -

FIGURE 5. REGULATORY SMALL RNAS (SRNAS) AND THEIR FUNCTION. - 23 -

FIGURE 6. THE LIFE CYCLE OF M. TUBERCULOSIS. - 27 -

FIGURE 7. SCHEMATIC REPRESENTATION OF THE TB GRANULOMA. - 33 -

FIGURE 8. BIPHASIC KILLING KINETICS OF A CLONAL POPULATION CONTAINING PERSISTERS. - 55 -

FIGURE 9. TOXIN ANTITOXIN (TA) MODULES PROMOTE PERSISTER FORMATION IN E. COLI K12. - 63 -

FIGURE 10. THE SPATIAL ORGANIZATION OF GENE EXPRESSION IN BACTERIA. - 83 -

FIGURE 11. THREE NONEXCLUSIVE MODELS EXPLAINING GENE EXPRESSION. - 84 -

FIGURE 12. DIVERSE LOCALIZATION OF RNA WITHIN A BACTERIAL CELL. - 85 -

FIGURE 13. SCHEMATIC SUMMARY OF KNOWN RIBONUCLEASES AND THEIR FUNCTION. - 93 -

FIGURE 14. STRUCTURE OF THE RNASE E IN E. COLI. - 103 -

FIGURE 15. RNASE E PATHWAYS OF SUBSTRATE RECOGNITION. - 109 -

FIGURE 16. SEQUENCE OF THE RNASE E PROMOTER. - 111 -

FIGURE 17. SECONDARY STRUCTURE OF THE RNASE E 5'UTR. - 113 -

FIGURE 18. SWISS-MODEL HOMOLOGY ANALYSIS OF THE MYCOBACTERIAL RNASE E. - 121 -

FIGURE 19. MODEL OF RRNAS PRECURSORS IN M. SMEGMATIS. - 123 -

FIGURE 20. M. SMEGMATIS PRNE-MKATE2 EXPRESSION IS DYNAMIC AND ASSOCIATED WITH CELL-SIZE AND GROWTH HOMEOSTASIS - - 139 -

FIGURE 21. ***M. SMEGMATIS RNASE E PULL-DOWN COUPLED WITH MASS SPECTROMETRY-BASED PROTEOMIC ANALYSIS REVEALS PROTEINS INVOLVED IN RNA TURNOVER AND STRESS-RESPONSE PATHWAYS*** - 143 -

FIGURE 22. SINGLE-CELL ANALYSIS OF PRNE - MKATE2 AND PHUPB - MCITRINE REVEALS THEIR MOLECULAR ASSOCIATION AND JOINT RESPONSE TO STRESSFUL CONDITIONS - 149 -

FIGURE 23. ***M. TUBERCULOSIS PRNE-MCHERRY AND PHUPB-SFGFP REPORTERS ARE CORRELATED BOTH DURING OPTIMAL GROWTH AND ISONIAZID TREATMENT*** - 152 -

FIGURE 24. ***SILENCING RNE DECREASES HUPB EXPRESSION, AND IMPAIRS M. TUBERCULOSIS SURVIVAL DURING ISONIAZID TREATMENT AND MACROPHAGE INFECTION*** - 157 -

Table of Table

TABLE 1. GENES RESPONSIBLE FOR GENETIC RESISTANCE TO THE PRINCIPAL DRUGS USED TO TREAT M. TUBERCULOSIS. - 80 -

Table of Equation

EQUATION 1. EMPIRIC MEASUREMENT OF THE MAGNITUDE OF NOISE IN GENE EXPRESSION. - 71 -

EQUATION 2. EMPIRICAL QUANTIFICATION OF THE TOTAL NOISE (η_{TOT}). - 73 -